DISTRIBUTED BIODYNAMIC CHARACTERISTICS OF THE HUMAN HAND-ARM SYSTEM COUPLED WITH VIBRATING HANDLES AND POWER TOOLS

Surajudeen Adedotun Adewusi

A Thesis

in

The department

of

Mechanical and Industrial Engineering

Presented in Partial Fulfillment of the Requirements
for the Degree of Doctor of Philosophy at
Concordia University
Montreal, Quebec, Canada

August, 2009

Library and Archives
Canada

Published Heritage
Branch

395 Wellington Street
Ottawa ON K1A 0N4
Canada

Bibliothèque et
Archives Canada

Direction du
Patrimoine de l'édition

395, rue Wellington
Ottawa ON K1A 0N4
Canada

Canada

ABSTRACT

DISTRIBUTED BIODYNAMIC CHARACTERISTICS OF THE HUMAN HAND-ARM SYSTEM COUPLED WITH VIBRATING HANDLES AND POWER TOOLS

Surajudeen Adedotun Adewusi, Ph.D
Concordia University, 2009

Clinical and epidemiological studies have shown that operators of hand-held power tools are prone to develop peripheral, vascular, neurological and musculoskeletal disorders collectively known as hand-arm vibration syndrome (HAVS). The reported biodynamic responses of the human hand-arm to hand-transmitted vibration exhibit considerable differences, which could be partly attributed to the complexity of the hand-arm system. Furthermore, the vast majority of the hand-arm models offer limited applicability to the tools since these lack consideration of the anthropometric, anatomical and biological properties of the hand-arm system. Experimental and analytical methods are used in this dissertation research to: (i) identify sources of discrepancies in the reported hand-arm biodynamic responses to vibration; (ii) simultaneously characterize localized vibration transmission to different segments of the human hand-arm and the driving-point mechanical impedance (DPMI) response under different hand-arm postures, hand forces, and excitation levels; (iii) develop biomechanical models corresponding to bent- and extended-arm postures on the basis of both the DPMI and vibration transmissibility responses; and (iv) characterize vibration power absorption (VPA) distribution of different components of the hand-arm for .potential injury risks assessments.

The results show that the discrepancies in the reported biodynamic responses above 500 Hz were due to acceleration measurement location, handle dynamics (handle resonant frequency and deformation) and ineffectiveness of handle inertia correction. The peaks and valleys in the DPMI magnitude correspond to resonant frequencies of the tissues/muscles and the bones/structure, respectively. On the other hand, the peaks in transmissibility magnitudes represent the resonant frequencies of both the tissues/muscles and bones/structure. Furthermore, the DPMI seems to characterize the dynamic response of the entire hand-arm system with emphasis around the driving-point, while the transmissibility responses emphasize the dynamic response of the tissues/muscles of the human hand-arm system. The VPA distributions in the forearm and upper-arm were observed to be considerably higher than those of the hand components below 100 Hz, while the VPA distribution in the fingers was greater above 100 Hz. The overall results suggest the need for two frequency-weightings for assessing the potential risks due to tools with low and high frequency vibrations.

ACKNOWLEDGEMENT

All praise and thanks are for Allah, the Almighty God, the Creator and Cherisher of the universe, the Bestower of knowledge, happiness and strength. I thank Him for making it possible to successfully complete my study. I wish to express my gratitude to my supervisors, Dr. Subhash Rakheja and Dr. Pierre Marcotte, for their guidance, encouragement, financial and moral supports during my study. Appreciation is also due to Dr. P.-E. Boileau and Mr. J. Boutin of the Institut de recherche Robert-Sauvé en santé et en sécurité du travail (IRSST), Montreal, Quebec, Canada for their assistance and support during my study.

The contributions and assistance of my committee members, Dr. P. Fazio, Dr. R. Bhat and Dr. J. Dargahi; my friends and colleagues, and the department of Mechanical and Industrial Engineering are also appreciated and acknowledged.

Finally, I thank my wife, children and other family members for their patience, support and understanding before and during my study. I appreciate everything you all did for me.

TABLE OF CONTENTS

LIST OF FIGURES

LIST OF TABLES

NOMENCLATURE

a_i	Acceleration measured at location i (m/s^2)
a_{hw}	Overall frequency-weighted root-mean-square (rms) acceleration value (m/s^2)
a_{rms}	Overall un-weighted root-mean-square acceleration value (m/s^2)
APMS	Apparent mass (ratio of force and acceleration) (kg)
ANOVA	Analysis of variance
c_i	Linear damping of component i of the simulated handle or hand-arm model (Ns/m)
C_i	Angular damping of component i of the hand-arm model (Nms/radian)
$[C]$	Damping matrix
$\{C_o\}$	Damping force vector
CTS	Carpal tunnel syndrome
D_h	Acceleration measurement direction (x_h, y_h or z_h)
DOF	Degree-of-freedom
DPMI	Driving-point mechanical impedance (ratio of force and velocity) (Ns/m)
E_{ea}	Composite error function between the model and measured biodynamic responses corresponding to elbow angle ea ($ea = 90°$ or $180°$)
f_L	Limiting frequency in Hz at which the deviation in APMS due to handle deformation is less than 5 %
f_n	Natural frequency of the handle (Hz)
f_i	Resonance frequencies ($i = 1, 2, 3...$) (Hz)
f	Excitation frequency (Hz) of excitation force (N)
f_i	Excitation force of component or substructure i (N)

F_g	Grip force (N)
F_p	Push force (N)
F_q	Dynamic force measured close to hand-handle interface (N)
F_{ea}	Excitation force of the matrix equation of motion of the hand-arm model corresponding to an elbow angle ea ($ea = 90°$ or $180°$)
h	Anthropometric height of the trunk of the body (m)
HAVS	Hand-arm vibration syndrome
HTV	Hand-transmitted vibration
ICP	Integrated circuit piezoelectric
J_i	Mass moment of inertia of component or substructure i of the human hand-arm model about the center of mass
k_i	Linear stiffness of component i of the simulated handle or hand-arm model (N/m)
K_i	Angular stiffness of component i of the hand-arm model (Nm/degree)
K	Complex dynamic stiffness (N/m)
$[K]$	Stiffness matrix
$\{K_o\}$	Stiffness force vector
l_i	Anthropometric length of component i of the hand-arm system (m)
m_i	Mass of component i of the simulated handle or the human hand-arm model (kg)
M_i	Anthropometric mass of component i of the human hand-arm system (kg)
$[M]$	Mass matrix
N	Number of frequency points considered for hand-arm model parameter identification using the error function E_{ea}

p	Statistical significance of ANOVA
P	Overall total vibration power absorption (Watts) or hand-arm posture
PSD (S_x)	Power spectral density $((m/s^2)^2/Hz)$
$P1$	Bent-arm posture with $90°$ elbow angle
$P2$	Extended arm posture with $180°$ elbow angle
P_k	Dissipated energy per second in substructure k of the hand-arm model (Watts)
P_{total}	Total dissipated energy per second in the hand-arm model (Watts)
$P_{measured}$	Total VPA of the human hand-arm system estimated from the measured DPMI and velocity (Watts)
PCB	A trademark for PCB Piezotronics Incorporation, New York USA
q_i, Q_i	Displacement and displacement magnitude of mass i of the handle model ($i = 1,2...$ or b, h) (m)
SD	Standard deviation
SPSS	Statistical product and service solutions
S_{a_i}	Auto-spectrum of acceleration measured at location i
S_{Fa_i}	Cross-spectrum of force and acceleration measured at location i ($i = b, h$)
S_k^i	Logarithmic sensitivity index of the model mass i due to a change in model parameter k
T_{l_i}	H_1 frequency response function (acceleration transmissibility) with respect to the handle vibration at location l in direction i
v	Velocity measured close to the handle-hand interface (m/s)
VWF	Vibration induced white fingers
VPA	Vibration power absorption (Watts)
x_h	Measurement along the transverse direction of the handle

X_{ea}	Hand-arm model parameters corresponding to elbow angle ea (ea = 90° or 180°)
y_h	Measurement along the longitudinal direction of the handle
y_i	Displacement of component i ($i = f, p, fa, ua$) of the human hand-arm model in the y_h-axis
y	Measurement along the y-axis of the tri-axial accelerometer
z_h	Measurement along the direction parallel to the forearm
z	Measurement along the z-axis of the tri-axial accelerometer
Z_{ji}	Impedance of system j based on acceleration measured at location i ($i = b$, h) (Ns/m)
z_i, Z_i	Displacement and displacement magnitude of component i ($i = f, p, fa, ua$) of the human hand-arm model in the z_h-axis
α_j	Weighting factors for error function between the model and measured biodynamic responses ($j = 1$ for transmissibility and $j = 2$ for DPMI)
β_j	Weighting factors for the magnitude error of the biodynamic responses ($j = 1$ for transmissibility and $j = 2$ for DPMI)
γ_j	Weighting factors for the phase error of the biodynamic responses ($j = 1$ for transmissibility and $j = 2$ for DPMI)
ζ	Damping ratio
η	Permissible variation coefficient about the nominal anthropometric masses
θ_i	Angular displacement of the human hand-arm substructure i (degree or radian)
ξ_{ea}	Generalized translational and angular displacement coordinates of the hand-arm model corresponding to an elbow angle ea (ea = 90° or 180°)
χ_{ea}^r	Response of masses of the hand-arm model corresponding to an elbow angle ea (ea = 90° or 180°) at a frequency r

ω Angular frequency of vibration (rad/s)

ω_n Natural circular/angular frequency (rad/s)

ϕ Phase angle of the biodynamic responses

Δ Changes in parameter

Ω_k Angular root-mean-square velocity across the damping element at joint k

CHAPTER 1

INTRODUCTION AND LITERATURE REVIEW

1.1 General

A number of epidemiological and clinical studies have established that operators of hand-held vibrating power tools are prone to develop peripheral, vascular, neurological or musculoskeletal disorder, collectively referred to as the hand-arm vibration syndrome (HAVS). Occupational exposure to hand-transmitted vibration (HTV) can arise from rotating and/or percussive hand-held power tools used in the manufacturing industry, quarrying, mining, construction, forestry and agriculture, public utilities and other work activities. Considerable efforts have been made to study the phenomenon of HAVS and to reduce the potential health risks of HTV. These include epidemiological studies [1 - 9, 32 - 34, 36], measurement and assessment of vibration dosage and dose-response relationship [10, 12 - 15, 18, 21, 23 - 31, 35, 37 and 41], hand-tool interactions [45, 66, 120 - 122], reduction and control of HTV [46 - 57, 87 - 91, 112, 113], and the human hand-arm biodynamic responses to HTV [52 - 86, 92 - 105, 114 - 119]. The dose-response relationship reported in ISO 5349-1 [31] relates the probability of HAVS among exposed workers directly to the magnitude of vibration at the tool handle, daily and cumulative exposure duration. Characterization and thorough understanding of the human hand-arm response to HTV is considered to be vital for deriving reliable frequency-weights for assessment of exposure, assessment of roles of various work and tool-related design factors, and development of coupled hand-tool models for design and analyses of

1

vibration attenuation mechanisms. A recent study has suggested that such responses may be applied to determine distribution of energy within the hand-arm structure, which can yield important insight into injury potential of HTV due to specific tools [128].

The human hand-arm responses to HTV, referred to as biodynamic responses, have been investigated via laboratory measurements or through mechanical-equivalent models. The biodynamic measures have been invariably expressed in the two forms: (i) force-motion relationship at the hand-tool interface expressed as apparent mass (APMS), driving-point mechanical impedance (DPMI) or dynamic compliance, and vibration power absorption (VPA); (ii) through-the-hand-arm response describing the transmission of vibration to different segments of the human hand-arm and the body such as the nail, finger, wrist, elbow, shoulder and the head. The vast majority of the studies have characterized biodynamic response in terms of the driving-point force-motion relationship, generally the DPMI, due to its relative ease of measurement. Relatively fewer studies have reported the responses in terms of vibration transmitted to the hand-arm structure. This is attributed to the complexities associated with such measurements. A number of linear mechanical-equivalent models of the hand-arm system have been developed on the basis of measured force-motion relationships at the hand-handle interface. The ranges of driving-point mechanical impedance of the hand-arm system under vibration applied along the x_h-, y_h- and z_h- direction independently have been defined in the International Standard, ISO 10068 [86].

The biodynamic responses are strongly influenced by various factors related to direction and nature of vibration, handle design, hand-handle coupling forces, hand-arm posture and individual factors (gender and anthropometry) [66, 67, 71 - 75, 78, 82, 84].

The measured responses, particularly through-the-hand-arm response, exhibit large variability. Furthermore, the measured data are also affected by the dynamics of the fixture due to requirements of relatively high frequency vibration (generally up to 1000 Hz). These differences have been partly attributed to differences in experimental conditions and measurement methods employed in the reported studies. The differences in the vibration transmissibility data reported by different investigators are even larger. Furthermore, a disagreement exists among investigators on the interpretation of the DPMI responses with regards to the resonant frequencies of the hand-arm structure. Although the DPMI and vibration transmissibility responses describe the dynamic responses of the hand-arm structure, the correlations between the two measures in terms of resonant frequencies have not been attempted. Owing to the extreme differences in the reported data, the models derived on the basis of the measured response also exhibit considerable differences. It has been suggested that the majority of the hand-arm mechanical-equivalent models that were derived from DPMI or vibration transmissibility are unsuitable for hand-tool coupled system simulation [65]. The force-motion relationship at the hand-handle interface may not fully describe the contributions due to vibration modes of the upper-arm and the whole body. The measures of vibration transmissibility of different segments of the structure may help identify various modes of vibration. It is hypothesized that the vibration transmissibility data together with the DPMI data could yield development of more reliable models of the hand-arm structure exposed to HTV. Such measures, however, are prone to errors and have been attempted only in few studies [76, 77, 79, 93].

This dissertation research is aimed at characterization of transmission of handle

3

vibration to different location of the hand-arm structure together with the DPMI for development of an anthropometry-based biodynamic model of the hand-arm. The influences of important contributing factors, such as hand-handle coupling forces, handle dynamics, excitation levels and hand-arm posture on the biodynamic responses are particularly explored. Both the DPMI and transmissibility response data are analyzed for identifying the resonance frequencies of the hand-arm structure. The significance of the two biodynamic response functions is systematically explored for identification of the model parameters for two different hand-arm postures. The dissertation research further explores the application of the hand-arm system to a percussion power tool for the characterization of vibration power absorption of different segments of the human hand-arm system.

1.2. Literature Review

1.2.1 The hand-arm vibration syndrome (HAVS)

The hand-arm vibration syndrome (HAVS) is the term used to describe the collective symptoms and disorders associated with prolonged and repeated exposure to vibration from hand-held power tools or other industrial activities in which the human hands are exposed to vibration. The major symptoms that have been identified are the vascular, neurological and musculoskeletal disorders.

Vascular disorders are the diseases associated with blood-carrying arteries and veins in the hand-arm system. The peripheral vascular symptoms commonly known as "white fingers" or vibration induced white fingers (VWF) are the most severe of the vascular disorders and have attracted most attention [3, 22, 32 - 34]. Figure 1.1 is a pictorial view of a worker's hand with evident VWF. Raynaud's phenomenon/syndrome

4

is ill-defined condition characterized by spasm of arteries in the extremities (digits) precipitated by low temperature or continued exposure to vibration leading to pain, numbness, and in severe cases, gangrene. It has been suggested that there are synergistic effects between vibration exposure and low temperature, noise, manual static work as well as emotional stress, which may contribute to the disorders [5 - 8].
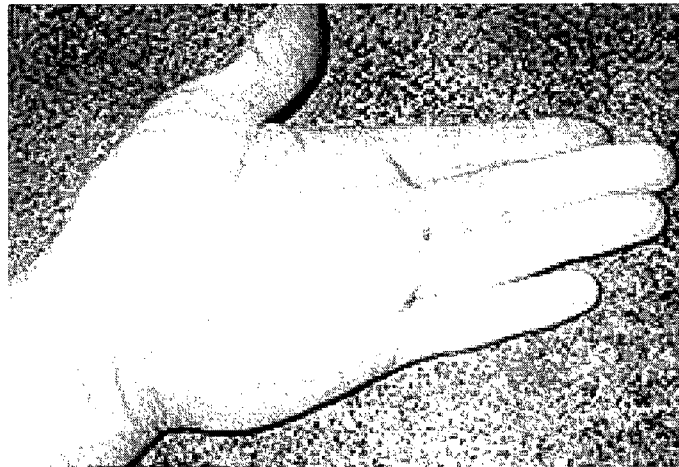
Figure 1.1: Vibration induced white fingers (VWF)

Neurological disorders, such as decrease or loss of sense of touch, decreased temperature sensitivity and neuropathy accompanied by cramp-like pains in the extremities, have been observed in workers exposed to vibration [9 - 13]. Histopathological observations conducted by Takeuchi et al. [14] on finger biopsy have shown that vibration exposure causes degeneration of sensory nerves and tactile organs. Cannon et al. [15] and Rothfleisch and Sherman [16] attributed the incidence of carpal tunnel syndrome (CTS) to the use of vibrating hand-held power tools and the position of the hand and the wrist. CTS is a painful condition caused by repetitive flexing of the wrist over a lengthy period of time, which is caused by pressure on the median nerve, and is

found mostly in workers performing repetitive hand tasks coupled with awkward hand postures.

Hassan [11] reported changes in the chemical composition of the blood in the hand and arm exposed to vibration. Muscle atrophy or muscle degeneration, reduced grip force and abnormal muscle fatigue have also been found among workers using hand-held power tools [17]. Some studies [17 – 25] have also associated bone and joint disorders to vibration exposure, while the study by Gemne and Saraste [23] suggested that bone and joint disorders are not specific to vibration exposure alone.

Up to date, very little is known about the pathological basis of HAVS [26] or the specific influences of vibration acceleration and frequency. However, the exposure-prevalence relationship between the use of hand-held power tools and the occurrence of HAVS has been established through several epidemiological studies [10, 12, 25 – 31]. Friden [27] discussed the clinical presentation of HAVS, its prognosis, length and severity of vibration exposure and the Stockholm Workshop scale for various disorders associated with HAVS. Miyashita et al. [32] reported that there is a latency period, with symptoms not appearing until after 2000 hours of vibration exposure. However, after 8000 hours of exposure, HAVS symptoms appeared in more than 50% of the forestry workers examined in the study. The period between initial exposure to vibration, the onset of symptoms and the latency period varies considerably between individuals due to differences in the type of exposure and individual susceptibility.

The International Standard Organization ISO 5349-1 [31] specifies general methods for measuring and reporting hand-transmitted vibration exposure and it provides guidance on assessment of hand-arm vibration based on frequency-weighting vibration

acceleration and dose-response relationship. The frequency-weighting tends to attenuate the vibration levels above 12.5 Hz band. However, some investigations [33 - 35] have presented results that are different from the dose-response relationship presented in ISO 5349-1. Furthermore, the validity of the frequency-weighting, particularly the attenuation at higher frequencies has been widely questioned. Lundstrom [36] indicated that exposure to high frequency vibration, above 1 kHz, could also have detrimental effect on the operators of hand-held power tools. Some investigations have shown that the impulsiveness of vibration is an additional factor in the development of HAVS [8, 37, 38], while the current weighting, which has maximum weighting factor at 12.5 Hz, generally underestimates the risk of such vibration. NIOSH [29] concluded that the use of unweighted-frequency acceleration is a better means of assessing the risk of exposure to vibration. Some investigators [39 - 41] have argued that while acceleration is a useful and convenient quantity to measure, the health risks to the human hand-arm is more likely to depend on the power absorbed/dissipated in the hand-arm system than upon the acceleration level alone. Despite the findings on the relationship between absorbed power and HAVS, the current national and international standards for the assessment of hand-arm injuries due to vibration are based on frequency-weighted acceleration.

1.2.2 Biodynamic response of the human hand-arm system

Considerable efforts have been made to quantify the responses of the human hand and arm to vibration. Such studies are considered vital for enhancing an understanding of the flow of vibration energy and to gain an insight to the potential injury mechanisms. Furthermore, such responses could yield improved frequency-weighting for assessment of potential health risks and essential basis for developing mechanical-equivalent models of

the hand-arm system. Such models are important for developing effective vibration reduction mechanism through analysis of the coupled hand-tool system. Dong et al. [64] conducted a critical review of research works on hand-transmitted vibration and concluded that although research works have contributed to advancement in understanding of hand-arm vibration responses, more gaps remain regarding the characterization of hand-transmitted vibration, injury mechanisms, tools designs and dose-response relationship. The vast majority of the studies on the human hand-arm responses to vibration have been conducted in the laboratory under controlled conditions, where the hand-arm system is excited by an electro-dynamic vibration exciter through a simulated tool handle. The exposure is mostly measured in terms of acceleration due to handle vibration, which is believed to have good correlation with the physical damage caused by HTV [29, 31].

The human hand-arm responses to vibration have been mostly studied in terms of force-motion relationship at the driving-point, namely the driving-point mechanical impedance (DPMI). Such responses have been applied to derive mechanical-equivalent of the human hand-arm system with an intent to formulate coupled hand-tool models for design of effective vibration isolators. Only a few studies, however, have attempted the modeling and analyses of hand-held power tools for identifying desirable design of the coupled hand-tool system [45, 120, 121]. This in-part may be due to unavailability of a reliable human hand-arm model. Rakheja et al. [65] evaluated the biodynamic response characteristics of various biodynamic (mechanical-equivalent) models of the human hand-arm system and concluded that the current models are not adequate for development of a mechanical hand-arm simulator for assessing the dynamic behavior of the coupled

Biodynamic coordinate system
Basicentric coordinate system
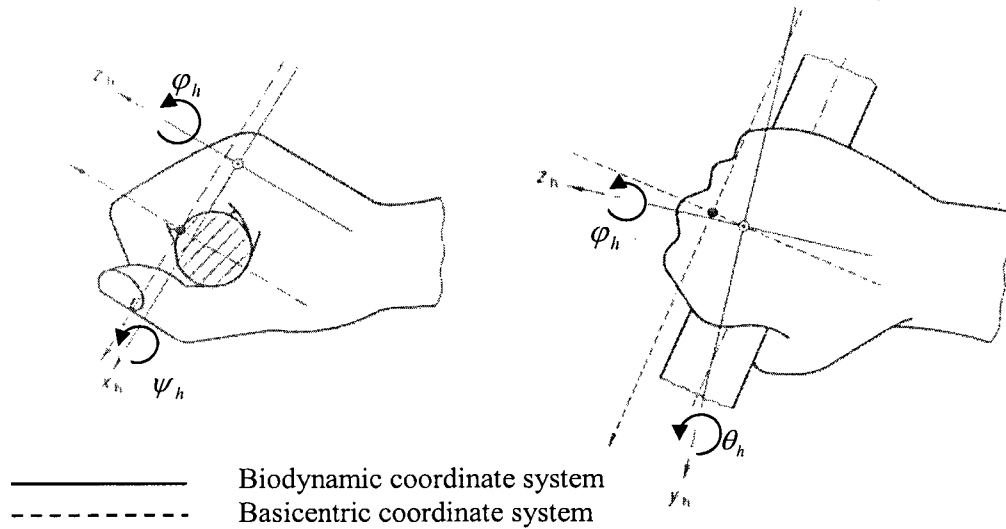
Figure 1.2: Coordinate systems for the human hand-arm

hand-tool system.

The human hand-arm is composed of complex inertial and visco-elastic properties. It exhibits six degrees-of-freedom (DOF) motions, three translational motions along x_h-, y_h-, z_h-axis, and three rotational motions along the roll (φ_h), pitch (θ_h) and yaw (ψ_h) axes, as shown in Figure 1.2. The studies thus far have been limited to vibration along the three translational axes using two standardized coordinate systems, namely the biodynamic or anatomical and basicentric (Figure 1.2). The origin of the biodynamic coordinate system is the head of the third metacarpal, while the origin of the basicentric coordinate system lies on the handle. Biodynamic response studies can be classified into three general categories: (i) force-motion relationship at the hand-tool interface expressed in terms of the apparent mass (APMS), driving-point mechanical impedance (DPMI) or dynamic compliance and vibration power absorption, also referred to as 'to-the-hand' responses; (ii) through-the-hand-arm response - describing the transmission of vibration

9

to different segments of the body such as the nail, fingers, wrist, elbow, shoulder and the head; and (iii) mechanical-equivalent analytical models.

'To-the-hand' biodynamic responses

To-the-hand biodynamic response relates the vibration in the vicinity of the hand to the force at the driving point. This may be expressed as dynamic stiffness $K(j\omega)$ (or its reciprocal - dynamic compliance), the driving-point mechanical impedance (DPMI) or apparent mass (APMS):

$$K(j\omega) = \frac{F_q(j\omega)}{q(j\omega)}, \; DPMI(j\omega) = \frac{F_q(j\omega)}{v(j\omega)}, \; APMS(j\omega) = \frac{F_q(j\omega)}{a(j\omega)} \qquad (1.1)$$

where q, v, a are displacement, velocity, and acceleration, respectively, measured at the driving-point, and $F_q(j\omega)$ is the dynamic force measured at the hand-handle interface at the excitation angular frequency ω.

The majority of studies have reported 'to-the-hand' biodynamic response, particularly the DPMI and the absorbed power, to characterize the human hand-arm response to vibration [52 - 88, 99 - 105, 114 - 119]. The reported studies have considered wide ranges of vibration types and levels, hand forces and handle sizes. Consequently, the reported data exhibit extreme differences in the responses, which are evident from the wide ranges of idealized impedance characteristics provided in ISO 10068 [86] that were established from a synthesis of reported data. Such differences in the data have been attributed to variations in intrinsic and extrinsic variables, test conditions and data analysis methodologies. While the majority of the reported DPMI magnitudes increased sharply at frequencies above 500 Hz [55, 57 - 60, 62, 68, 78 - 81, 83, 86, 99 - 105], a few studies have shown either decreasing or relatively constant magnitudes of DPMI above

10

500 Hz [67, 69, 70, 77, 82]. These differences at higher frequencies have been attributed to differences in the experimental techniques, direction of vibration, grip and push forces, vibration amplitude and individual characteristics [67 - 69, 73 - 83]. These factors are also known to influence the human hand-arm impedance at frequencies below 500 Hz. Hewitt [70], Mishoe and Suggs [72] and Reynolds et al. [76] suggested that the differences at high frequencies might be due to the handle natural frequency and the influence of the coupled hand-handle dynamics on the measurements.

Very little efforts, however, have been made to quantify the contribution of the handle and handle fixture dynamics to the hand-arm DPMI. Dong et al. [91] evaluated the potential measurement errors in vibration transmissibility of antivibration gloves introduced by dynamics of a simulated handle and a palm-held adapter. The results showed that variations in magnitude of vibration along the handle caused considerable measurement errors. Considering such measurement errors and wide variations in the reported high frequency DPMI responses, a thorough review of the fundamentals and experimental procedures used in characterization of hand-arm vibration response would be desirable for a better understanding of the influences of the handle dynamics on the hand-arm DPMI response.

The influences of various intrinsic and extrinsic factors on the DPMI responses, with the exception of the handle dynamics, have been investigated in many studies. Aldien et al. [67] studied the influences of hand-arm posture, handle size, and vibration levels on the DPMI and absorbed power responses under vibration along the z_h-axis. Burstrom [69] studied the effects of vibration direction, grip force, vibration level, hand-arm posture, subject gender and anthropometric parameters on the DPMI responses.

Cronjager and Hesse [81] studied the biodynamic response of the hand-arm to stochastic excitations and compared the response with those obtained from a hand-held tool (a percussion hammer). The results showed that the shaker experiments did not deviate much from the actual field measurements. Marcotte et al. [82] studied the effects of handle size and contact force on the DPMI responses to z_h-axis vibration. It has been established that an increase in the grip or push force yields higher DPMI magnitude and higher frequency corresponding to the peak magnitude. The grip and push force effects, however, are strongly related with those of the handle size and hand-arm posture.

The reported studies also suggest strong disagreements in interpretations of DPMI data with regards to the natural frequencies of the hand-arm system. The hand-arm is a continuous system which is expected to have several natural frequencies, but some of the reported DPMI data exhibit very few valleys and peaks [68, 72, 81]. This has been attributed to the effect of data smoothing and averaging [70]. While the majority of the studies suggest that the natural frequencies of the hand-arm correspond to the frequencies of the peak DPMI magnitude responses [67, 77, 78, 82], others relate it to the valleys in the DPMI responses [68, 72, 81]. Some studies did not attempt to relate peak DPMI responses to the natural frequencies of the hand-arm system [69, 70, 73, 80]. Further fundamental analyses of the biodynamic response data are thus vital to obtain clear interpretations of DPMI responses in view of the resonant frequencies of the hand-arm system.

The majority of the reported studies have acknowledged considerable inter-subject variations in the measured data. A standard deviation of the mean DPMI data magnitude and the mean phase angle in the order of 150 Ns/m and of $35°$ have been reported by

Burstrom [69]. Large inter-subject variations of the hand-arm impedance magnitudes have been reported in many other studies [68, 70, 72, 82, 84]. Furthermore, it has been suggested that a larger hand-arm size yields higher impedance magnitude [69]. Despite the large inter-subject variations, the mean data are invariably applied in order to quantify the role of different intrinsic and extrinsic factors. The ISO 10068 standard [86] presents the ranges of mean DPMI responses from different studies involving diverse subjects and experimental conditions.

The 'to-the-hand' biodynamic response of the hand-arm system has also been expressed in terms of the energy absorbed by the hand-arm per unit time [67, 70, 76, 77, 84]. The instantaneous total power is defined as:

$$P(t) = F_q(t) \cdot \dot{q}(t) \tag{1.2}$$

where $F_q(t)$ and $\dot{q}(t)$ are respectively the instantaneous force and velocity at the driving-point. In the frequency domain, the average vibration power absorption (VPA) is directly related to the real part of the DPMI, such that:

$$P(\omega) = \mathrm{Re}[DPMI(j\omega)] \cdot |v(j\omega)|^2 \tag{1.3}$$

where 'Re' designates the real part of the DPMI response and $|v(j\omega)|$ is the absolute value of the rms velocity measured at the hand-handle interface. The power defined in Eq. (1.3) describes the energy absorbed by the hand-arm, which is dissipated as heat due to friction within the tissues. The imaginary component of the power relates to the reactive energy stored/released within the hand-arm system [76].

From Eq. (1.3), it is evident that the VPA would also be influenced by the magnitude, frequency and direction of vibration, grip and push forces, and posture, as in the case of DPMI. Some investigators have suggested that power absorption in the hand-

arm would serve as a better measure of potential vibration injury than the currently used vibration acceleration measure [76, 130, 131]. While the reported DPMI responses do not clearly show the effects of vibration magnitude, the absorbed power can directly relate to the magnitude. The absorbed power can also be related to stress and strains in the biological materials, where stress is dependent upon the vibration level and strain relates to deformation in the tissue. It has been established that most of the vibration energy is absorbed in the low frequency region, and that the absorbed power decreases with an increase in the frequency and increases with an increase in the grip force and push force [67, 76, 77, 84]. The data reported by Hewitt [70] for the pneumatic chipping hammer and the electric grinder revealed maximum absorbed power in the bands corresponding to the operating frequencies of 35 and 200 Hz, respectively. Kihlberg [77] also reported similar results. The data reported by Aldien et al. [84] under white-noise handle vibration showed about 12 % variations in the absorbed power due to inter-subject variations.

'Through-the-hand' biodynamic responses

The 'through-the-hand' biodynamic responses describe the transmission of vibration to different segments of the hand and arm and the body, such as the nail, finger, wrist, elbow, shoulder and the head. It is expressed as the ratio of motion magnitude at a specific segment of the hand-arm to that at the handle-hand interface. This method has been widely used in the assessment of vibration attenuation performance of protective devices, such as anti-vibration gloves [87 - 91]. Only limited efforts, however, have been made on the use of 'through-the-hand' method for characterizing human hand-arm system responses to vibration. This is probably due to lack of appropriate sensors and difficulties

associated with vibration measurements on the skin, and the fact that vibration transmission magnitudes are very small above 200 Hz.

The vibration transmission characteristics of the human hand-arm have been studied in the laboratory and in the field under controlled grip conditions, different vibration excitation magnitudes and directions, and different hand-arm postures. Kihlberg [77] measured the transmission of vibration along the z_h-axis of an impact hammer and electric grinder to the finger, wrist and elbow under different grip forces. The study involved fifteen subjects with about 110° elbow angle posture. Cherian et al. [92] studied the vibration transmissibility characteristics of the human hand-arm at the finger, wrist and elbow under sinusoidal vibration in the $10 - 200$ Hz frequency range using only one subject and a constant grip force of 25 N. Reynolds and Angevine [93] measured the vibration transmitted to the finger, wrist, elbow and the shoulder under different magnitudes of palm-grip and finger-grip forces, under vibration along three independent axes (x_h, y_h, z_h). The study used subminiature piezo-resistive accelerometers that were attached to the skin near the joints by means of adhesive tape. Pyykko et al. [94] measured transmission of z_h-axis handle vibration to the wrist, elbow and the upper-arm in the $20 - 630$ Hz frequency range under different magnitudes of grip force. Aatola [95] studied vibration transmission to the wrist under different grip forces (0 - 40 N) and vibration levels in the $10 - 300$ Hz range. An accelerometer was fastened with a screw to a small acrylic plate, which was fastened very tightly against the styloid process of the ulna with the help of another piece of acrylic and a hose clamp. Measurements were performed with five subjects in sitting position with elbow bone forming an angle of about 45° upwards from the horizontal plane and with an elbow angle of about 150°.

The above studies showed a rapid decrease in transmissibility magnitude with increase in excitation frequency and the distance from the vibration source. It was suggested that vibration attenuation occurs in the tissue adjacent to the bone, and only little attenuation of vibration occurs across the joints although large relative motions across the joints could be observed. Only less than 10% of vibration magnitude at frequencies above 250 Hz is transmitted to the wrist and beyond; while the vibration at frequencies below 100 Hz is transmitted to the forearm. Vibration at frequencies below 40 Hz can be transmitted to the forearm and the upper arm. An increase in the grip force increased the resonant frequency. The reported studies invariably concluded that vibration at frequencies above 200 Hz is confined to the hand and fingers. Aatola [95] proposed linear relationships between the first three natural frequencies of the hand-arm and the grip force as:

$$f_1 = 0.7F_g + 10, \quad f_2 = 2.6F_g + 60, \quad f_3 = 2.7F_g + 120 \tag{1.4}$$

where f_i, $i = 1, 2, 3$, are the first, second and third natural frequencies of the hand-arm system in Hertz, F_g is grip force in Newton (N). The proposed relationship, however, could be considered valid only for the postural conditions considered in the study, namely, gripping the handle with grip forces up to 40 N while sitting with an elbow angle of 150°. The study also reported negligible effects of vibration magnitude on the vibration transmissibility magnitude, which increased linearly with increasing hand-grip force. The study also performed field measurements with five professional forest workers. The data revealed a decrease in vibration transmissibility with increasing frequency, similar to the trend observed in the laboratory measurements. While the second and third resonant

frequencies (f_2 and f_3) were clearly observed, the first resonant frequency could not be detected. An additional resonant frequency occurring between f_2 and f_3, however, was also observed.

Kattel and Fernandez [97] investigated the hand-transmitted vibration with ten subjects, five females and five males, operating different rivet guns. The study reported unweighted rms accelerations of transmitted vibration, while the subjects were standing erect with an elbow angle of 90°, forearm parallel to the floor and mid-pronated with three wrist postures (neutral, 1/3 maximum flexion and 1/3 maximum ulnar deviation) and imparting two applied (push) forces of 8 and 12 lb. Tri-axial accelerometers were attached to a palm-adapter held between the hand and rivet gun handle, and to the bracelets that were fastened to the wrist and the forearm of the subjects. The study concluded that the neutral wrist posture transmitted the highest vibration to the hand-arm system. The low frequency handle vibration could also be transmitted to the whole-body. Sakakibara et al. [98] measured vibration transmitted from the hand to the head under different hand-arm postures of four male subjects, using an accelerometer mounted on a bite-bar. The study showed that vibration transmitted to the head is highly dependent on the elbow angle. A straight-arm posture, with 180° elbow angle, resulted in greater vibration of the head than the bent-arm posture.

Biodynamic models of the hand-arm system

A number of mechanical-equivalent models of the hand-arm system have evolved during the past three decades for characterizing the responses of the human hand and arm to vibration. Such models are mostly developed on the basis of the measured DPMI responses. The models can be effectively used to characterize the vibration amplitude and

the power flow in the coupled hand, tool, and workpiece system; to analyze the potential performance benefits of vibration-attenuation mechanisms; and to develop test-rigs and hand-arm simulators to assess vibration transmission of different tools [45, 46, 65, 130]. The applicability of these models, however, necessitates the development of adequately validated models over a range of representative operating conditions. Owing to the excessive differences in the DPMI data reported by different investigators, the reported biodynamic models also exhibit considerable differences in their responses. The reported models include the lumped- and distributed-parameter models, although the majority is lumped-parameter model derived on the basis of measured DPMI responses.

The reported lumped-parameter models of the hand-arm system can be divided into 3 subgroups depending on the properties of the lumped elements. The first subgroup consists of models with linear stiffness and damping elements. The effects of many contributory factors, such as grip force, push force and vibration intensity on the visco-elastic properties of the hand-arm system are thus ignored. This subgroup includes: the single-.DOF models by Abram and Suggs [56] and Reynolds and Soedel [100]; 2-DOF models by Miwa et al. [51] and Mishoe and Suggs [72]; 3-DOF models by Gurram et al. [68], Mishoe and Suggs [72], ISO 10068 [86], Reynolds and Soedel [100] and Daikoku and Ishikawa [102]; and 4-DOF models by Gurram et al. [68], Reynolds and Falkenberg [79] and ISO 10068 [86]. The second subgroup comprises linear but grip force dependent element properties reported by Mishoe and Suggs [72] and Gurram et al. [103]. The third subgroup comprises 3- and 4-DOF nonlinear lumped-parameter models to characterize the nonlinear biodynamic behavior of the hand-arm system proposed by Rakheja et al. [104].

A study of relative assessments of the lumped-parameter models has concluded that the 3- and more DOF models yield impedance characteristics in the range of the idealized mean values defined in ISO 10068 [86], but they exhibit excessive static deflection even under a low-level push force [65]. These models are thus considered inadequate for simulation of a coupled hand-tool system or for developing a mechanical hand-arm simulator. Moreover, the lumped-parameters do not relate to the anatomical structure of the hand-arm system. The vibration modes of the models, therefore, cannot be related to vibration behavior of a particular substructure of the hand-arm system. Furthermore, the lumped-parameter models that were derived from only the DPMI via curve fitting are not unique since there are several sets of parameters that could yield comparable model and measured DPMI responses. Alternatively, Cherian et al. [92] proposed a 5-DOF biomechanical model of the human hand-arm system to study the vibration transmission characteristics in the 10 − 200 Hz frequency range. The masses and dimensions of the hand, forearm and the upper arm, were taken from the anthropometric data, while the visco-elastic properties of the model were estimated from the measured vibration transmissibility. Fritz [99] proposed a biomechanical model comprising four masses connected by linear springs and dampers, and damped torsion springs to represent muscle activity to study the strain in the hand-arm system during vibration. The parameters of the model were determined on the basis of the dynamic compliance reported by Reynolds and Falkenberg [79]. The vibration transmissibility responses of the model were compared with those reported in [93, 94].

Conversely, a distributed-parameter model of the hand-arm system was proposed by Wood et al. [105], which comprised homogeneous flexural members with distributed

19

mass and flexural stiffness, representing the radius, ulna and the humerus bones. The viscous effect of the tissues surrounding the bones was characterized by linear damping distributed along the bones. The beam members, representing the bones of the forearm, were coupled with the driving point by two lumped masses through visco-elastic properties of the tissue of the hand, modeled as a Kelvin visco-elastic model. The model, consisting of the hand and the forearm, was analyzed to derive its impedance response under vibration along y_h-axis alone and its parameters were determined from the DPMI data measured under 90° elbow angle and elbow supported on a molded rest. The study also reported a model of the entire hand-arm system, whose responses revealed considerable deviations from the experimental data. The models, however, would be valid under supported elbow posture, which is not likely to represent a realistic work posture. Furthermore, Rakheja et al. [65] reported some errors in the impedance formulations used in the study.

Relative evaluations of reported biodynamic models

Rakheja et al. [65] evaluated the response characteristics of twelve different biodynamic models of the human hand-arm system for applications to hand-held power tools using three criteria namely: (i) the ability of the model to characterize the DPMI of the human hand-arm system within the range of idealized values presented in ISO 10068 [86]; (ii) the magnitude of model deflection under a static feed force; and (iii) natural frequencies and damping ratios of the models. It was concluded that the majority of the models were not suitable for the development of a mechanical hand-arm simulator or for the assessment of dynamic behavior of the coupled hand-tool system. While the 3- and 4-DOF lumped mass models provided DPMI responses within the range of the idealized

values, they revealed excessive static deflection of the masses under a static feed force. On the other hand, the single-DOF lumped mass models [56, 100] and the distributed-parameter models [105] resulted in lower static deflections but poor agreement in terms of the DPMI characteristics of the hand-arm system. It has been suggested that an anatomically analogous model of the human hand-arm is vital for enhancement of its responses to vibration and to study the distribution of vibration energy for assessment of exposure [64].

1.2.3 Mechanical properties and anthropometry of the human hand and arm

The development of an effective biodynamic model of the human hand-arm necessitates knowledge of the ranges of the mechanical properties of the biological system, although the measured responses could be applied to refine these properties through curve-fitting algorithms. The reported relevant studies are briefly reviewed in an attempt to gain insight into the ranges of anthropometric and mechanical properties of the hand-arm structure.

The human hand-arm is a complex, non-homogeneous system with non-uniform geometry that basically consists of *bones, cartilage, muscles/tissues, tendon, ligament, skin* and *joints*. For simplicity, the bones and cartilage, muscles/tissues and skin could be respectively grouped in order to characterize the human hand-arm into two components: bones and muscles/tissues. *Bone* is a dynamically adaptable living calcified tissue whose form is continually undergoing subtle remodeling in order to conform to its functions [107]. The human hand-arm generally include the relatively hard and dense *cortical bone* and the relatively light-weight and spongy *trabecular or cancellous bone*. Only 15 – 25 % of the trabecular bone volume is calcified, while the rest is occupied by the blood vessels,
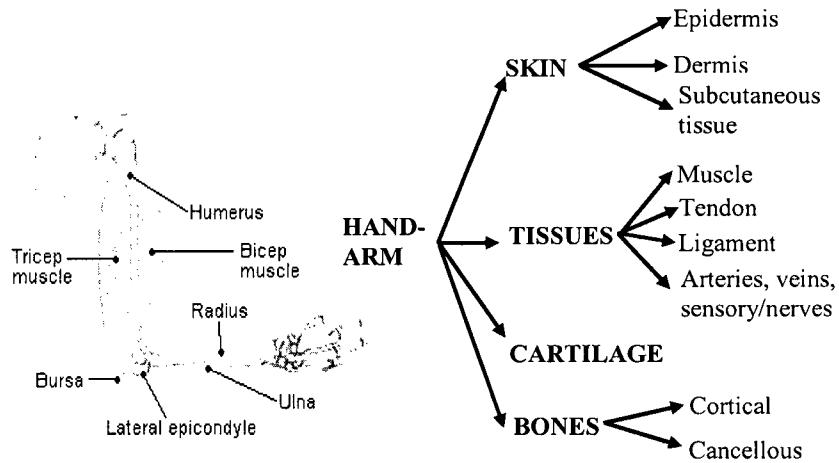
Figure 1.3: The human hand-arm system

connective tissues and bone marrows. The bones are covered with *muscles*, which is the contractile tissue which produces motion and exerts forces, and the *tendons* connecting the muscles to the bones. The biological structure also comprises *synovial joints* with no tissue between articular surfaces, *fibrous joint* with tissue bridging the joint and *cartilaginous joint* with cartilage bridging the joint [107]. A biomechanical model of the human hand-arm system may separate the mass of bones and muscles as partly demonstrated in [99, 128] instead of lumping them together as seen in most of the models.

The vast efforts on the characterization of mechanical properties of bones and muscles have invariably concluded that bones and muscles are composite materials resulting in viscoelastic and anisotropic behaviors whose properties depend on age, sex and race. Wirtz et al. [108] evaluated many reported bone properties derived from fresh untreated human femurs to determine if they were sufficient to realize anisotropic finite element model of the human femur. The bone properties were correlated with apparent density (g/cm^3) to reflect individual variables and age-dependent changes of the bone

material properties. The study evolved into power relations between the femur bone transverse and axial Young's modulus and the bone density. In a similar manner, Maganaris and Paul [109] reported the Young's modulus and stiffness properties of the human tibialis anterior (TA) tendon on the basis of *in vivo* measurements. Only limited efforts, however, have been made in characterizing the mechanical properties of the hand-arm system.

Roberts et al. [110] determined the mechanical properties of the hand-arm tissue, skin and the ulna bone from the vibration responses of the tissue and skin. The study employed a methodology referred to as the Mechanical Response Tissue Analysis (MRTA). An analytical model was developed and validated by comparing the results attained with clinical techniques, such as bone mineral density (BMD) and bone mineral content (BMC), which are used to assess the integrity of bones. Table 1.1 summarizes the results of the *in vivo* MRTA test and the model results for the skin and tissues of human forearm. The material and geometric values for the Young's modulus and density of the ulna bone, probe radius and tissue thickness were 4 MPa, 1000 kgm^{-3}, 5 mm, and 1 mm, respectively.

The weight, shape and dimensions of the human hand-arm are also known to depend on age, sex and race. Anthropometric database suggest that the masses of the hand, forearm and upper-arm are approximately 0.65 %, 1.9 % and 3.3 % of the total body mass [107]. The descriptive dimensions of the humeri and the length of the radius bones have also been reported on the basis of measurements performed on Australian aboriginal males [111]. The study suggests the mean radius and ulna bone lengths of 252.7 mm (standard deviation = 13.19 mm) and 269.9 mm (standard deviation = 12.47

Table 1.1: Properties of the skin of human hand-arm from Robert et al. [110].

Skin parameter	Units	Theoretical	Experimental
Effective mass	g	0.245	0.239
Effective damping	Ns m^{-1}	14.34	11.97
Effective stiffness	kN m^{-1}	314.2	322.5
Actual mass	g	0.079	NA

mm). The mean maximum humerus length was reported as 323.9 mm with mid shaft breadth ranging from 15.6 to 19.8 mm.

1.2.4 Hand-transmitted vibration and its control

The nature of hand-transmitted vibration from a wide range of power tools has been characterized through field measurements. These studies have shown that the magnitudes of tool vibration could exceed 2000 m/s^2 and could occur at frequencies up to 2000 Hz [112, 116]. Wasserman et al. [114] measured the vibration emission using the basicentric coordinate system and three-axis accelerometers of a group of pneumatic hand-operated grinding tools. The measured vibrations were evaluated using ANSI S3.4 [118] and ACGIH [119] hand-arm vibration exposure guidelines. The results showed that the old grinders resulted in higher vibration magnitudes in all directions than the new grinders but none of them exceeds the limits defined in ANSI S3.4 and ACGIH. The results suggested that wear and tear, and conditions of a tool influence the magnitudes of transmitted vibration. Dandanell and Engstrom [115] measured and analyzed the vibration of the percussion-type riveting hammers and bucking bar. Since the tools are characterized by relatively lower levels of acceleration at low frequencies and high levels of acceleration at higher frequencies, two different measuring systems (displacement

pickups and piezoelectric accelerometer) were used to capture both the low and high frequency responses of the tools. The results showed that percussion tools vibration exhibit high energy level above 1000 Hz, which is not covered by the ISO 5349-1. Reynolds et al. [116] performed measurements and analysis of vibration due to pneumatic chisels, chipping hammer and grinding tools. The data analyses in 1/3 -octave band in the 6.3 – 1000 Hz frequency range revealed rms acceleration levels ranging from 2000 m/s^2 to 24,000 m/s^2 for the chisels, and between 37 m/s^2 and 350 m/s^2 for the chipping hammers. The hand grinder acceleration levels ranged from 6 m/s^2 to 21 m/s^2. The study concluded that greater amount of energy is transmitted to the hand from the handles of the small chipping hammers than from the handles of the larger ones.

Owing to large magnitudes of HTV and its association with HAVS among the exposed workers, considerable efforts have been made towards protecting operators of hand-held power tools from HAVS. These include the efforts in assessment of potential risks and those aimed at reducing the magnitudes of HTV exposure. Different national and international standards [29, 31, 117-119] have evolved to provide guidelines on vibration exposure limits, the duration of exposure, and methodologies for measurement and assessment of HTV.

The efforts related to mitigation of HTV from the power tools have focused on: (i) isolation of the tool handle from the vibrating source; (ii) isolation of the hand from the handle; (iii) design of low vibration power tools; and (iv) avoidance of direct contact between the human hand-arm and the power tools by the use of automated support or the hand-arm simulator. Only limited efforts have been attempted in isolating the tool handle from the vibrating source. This is mostly due to compact designs of hand-held power

tools and extreme design complexities in implementing vibration isolation within the tool [46]. The method of isolating the hand from the tool handle is most commonly used in workplaces in the form of antivibration gloves [46 - 51]. The vibration isolation effectiveness of such gloves has been widely investigated in the laboratory through measurement of vibration transmitted to the palm of the hand, metacarpal bones and the wrist [87 - 91]. The vast majority of these studies have employed the methodology defined in ISO 10819 [117], which also defines the medium- and high-frequency vibration spectra (referred to as 'M' and 'H' spectra) for assessing the effectiveness of a glove for medium and high frequency tools. The vibration excitation corresponding to M- and H-spectra dominate in the 16 - 400 Hz and 100 – 1600 Hz, respectively. Rakheja et al. [88] compared the measured spectra of some of the hand-held power tools with the standardized M- and H- spectra. The comparisons showed that the vibration due to the pneumatic chipping hammer, nut runner and the random orbital sanders have predominant frequencies within the M-spectrum, while the magnitudes are considerably higher than that of the M-spectrum. Nut-runner and pneumatic chipping hammer vibration reveal predominant frequency in the lower frequency range (12.5 – 31.5 Hz). The rivet gun, pneumatic road breaker and chainsaw exhibit vibration within the range of H-spectrum but with lower vibration magnitudes. Some studies have shown that the gloves tend to amplify vibration in the low frequency region, and improved vibration isolation could be achieved at the expense of dexterity loss.

Cherian et al. [92] proposed the concept of energy flow divider to reduce the vibration transmitted to the human hand-arm. The energy divider, made-up of visco-elastic elements, is attached between the hand and the elbow such that part of the energy

can flow through the energy divider and be dissipated. The concept, however, showed greater vibration at the operator elbow, while the hand vibration could be reduced considerably. Golycheva et al. [122] proposed the use of a passive vibration protection system that combined the principles of vibration isolation and dynamic absorption between the hand and the handle of percussive tools. The results suggest that the system significantly reduced the HTV without significant increase in the mass of the tool. The dexterity problem introduced by the protection system was not studied or reported.

Analytical models of various tools have also been attempted for identifying potential vibration isolation methods [45, 66, 120 - 122]. The designs of low vibration emission chainsaws have been realized through such methods [50]. A few studies have focused on rotary-percussion tools that are known to produce impulsive vibration, which are believed to serve as an additional contributory factor in the development of HAVS [8, 37, 38]. The dynamic principle of a percussive- rotary hand-held tool (vibro-impact mechanism) is similar to that of the new percussive-rotary drilling technique used in petroleum exploration [125]. The complexity of the hand-held percussion tool dynamics, however, has been the primary limiting factor in models development and analyses.

Rakheja et al. [45] derived an analytical model for an electro-pneumatic percussive chipping hammer and coupled it with the 3-DOF hand-arm model defined in ISO 10068 [86] to study the hand-transmitted vibration characteristics of the tool. A comparison of the model responses with the laboratory-measured data revealed considerable disagreement, while the fundamental frequency of the model response agreed reasonably well with the experimental results. The discrepancy was attributed to the extreme softness of the standardized hand-arm model. Jahn and Hesse [66]

investigated the interactions between the human hand-arm and the tool. A mechanical model of an electro-pneumatic drilling hammer (BOSCH 11206) was derived and coupled with the 3-DOF hand-arm model. The model was also used to study the influence of the grip cushioning.

Babitsky [120] presented a general formulation and analysis of hand-held percussion machines by using methods of non-linear dynamics and optimal control. Golycheva et al. [121] refined the model proposed by Babitsky [120] by adding flexible elements to the exciting piston of the electro-pneumatic hammer to improve its excitation performance, leading to an extension of acceleration time and a reduction in the intensity of the impulses of impacts thereby relieving load on the operator. Addition of flexible elements to the piston may, in reality, make the design and fabrication of compact hand-held power tools more complicated. The reported analytical models, in general, oversimplified the thermodynamic process of the air between the piston and the striker such that it becomes redundant [45, 66, 120, 121]. Unlike the model of Rakheja et al. [45], where attempts were made to validate the model response with experimental data, the validity of models by Babitsky [120] and Golycheva et al. [121] has not been demonstrated. Research efforts towards the development of a reliable anatomical/biomechanical human hand-arm model coupled with hand-held power tool models are thus highly desirable to better understand the HTV and its mitigation at the vibration source. Efforts are also being made towards automation of various processes so as to eliminate the human operator [66, 86, 123, 124].

1.3 Scope and Objectives of the Dissertation

From the literature review, it is evident that vast majority of the studies have focused on characterization of hand-transmitted vibration (HTV), measurement of biodynamic responses and measurement of vibration attenuation performance of anti-vibration gloves. The studies on characterization of HTV have provided a significant database on the nature of vibration and for conducting exposure assessments. The efforts on characterization of biodynamic responses in terms of both 'to-the-hand' and 'through-the-hand' functions reveal extreme discrepancies among different datasets reported by different investigators, particularly at higher frequencies. A few of these studies have also investigated the contributions due to important intrinsic and extrinsic factors but only little agreements exist on the role of such factors. The discrepancies among the reported DPMI datasets have been observed to be excessive at frequencies above 500 Hz, and do not permit for generalization of the human hand-arm response to HTV. The idealized DPMI responses of the human hand-arm system in ISO 10068 [86] have thus been limited to 500 Hz. Only minimal efforts have been made to identify the sources of such discrepancies, although a few studies have attributed these to the measurement methods and handle resonant frequency. The contributions of handle dynamics and measurement location on the DPMI responses have not been quantified even though the disparities in the reported DPMI magnitudes at high frequencies have been attributed to the resonant frequencies of the handle.

Moreover, considerable disagreements exist on the identification of the natural frequencies of the hand-arm system from the DPMI responses. While the majority of studies considered natural frequencies as the frequencies corresponding to the peak DPMI

magnitude, a few have considered these to correspond to valleys in the DPMI response magnitude. Furthermore, a vast number of the reported DPMI responses do not reveal distinct magnitude peaks; which has been attributed to the effect of averaging of DPMI responses of diverse subjects. Fundamental and systematic efforts on the DPMI responses are thus needed to derive generally applicable methodologies for the identification of natural frequencies and high frequency responses of the hand-arm system.

While the DPMI measure describes the dynamic interactions of the hand at the hand-handle interface, it is hypothesized that the vibration transmitted to different segments of the hand-arm system could better describe the vibration modes. A relatively fewer number of studies, however, have attempted to characterize the 'through-the-hand-arm' biodynamic responses, most likely due to complexity of the measurement and low vibration transmission magnitudes at frequencies above 200 Hz. Moreover, only minimal efforts have been made to study the contributions due to important contributing factors, such as the push force and hand-arm posture, to the transmitted vibration. It is further hypothesized that characterization of both 'to-the-hand' and 'through-the-hand-arm' responses could provide better understanding of the hand-arm responses to vibration.

Although a number of mechanical-equivalent models of the hand-arm system have evolved, it has been suggested that none of the models are suited for applications in the coupled hand-tool analyses. This is attributed to unrealistically high static deflections of the model components, and excessive damping ratios of some modes. Moreover, the majority of the models do not consider the anatomical structure and biomechanical properties of the hand-arm system. The model parameters are merely selected to satisfy or curve-fit the DPMI dataset, which may not be unique. It is believed that the uniqueness of

the model could be enhanced by considering both 'to-the-hand' and 'through-the-hand-arm' biodynamic response functions with appropriate considerations of the hand-arm anthropometry and biomechanical properties. The model thus derived could provide the nature of vibration transmitted to different segments of the hand-arm system. Furthermore, the distribution of vibration power absorption within the hand-arm system could be estimated under vibration spectra of specific tools to assess their potential injury effects.

Development of a practically applicable hand-arm model is vital to study the power flow within the coupled hand-tool system. The studies on dynamic analysis of power tools have been severely limited due to design complexities of highly compact tools. Thus far, only three studies could be found on the analytical modeling of the coupled hand-tool system. Development of analytical models for the hand-held power tools will facilitate a better understanding of the vibration generation and mitigation phenomena in the power tools.

1.3.1 Objectives of the dissertation

The overall objective of this dissertation research is to develop biomechanical models of the human hand-arm to obtain the distribution of vibration power absorption, due to vibrating handles and power tools, in different substructures of the human hand-arm system. The specific objectives of the dissertation research are as follows:

a) Perform systematic experimental and analytical investigations for identifying the sources of deviations in the reported driving-point mechanical impedance response of the human hand-arm system under z_h-axis vibration at frequencies

31

above 500 Hz, and identify the desirable dynamic properties of the simulated handles;

b) Perform laboratory experiments to simultaneously characterize the driving-point impedance and the vibration transmitted to different segments of the hand-arm system under different excitation magnitudes, postures and hand forces;

c) Develop a biomechanical model of the human hand-arm and conduct parameter identification using the measured biodynamic responses and corresponding characteristic frequencies, and demonstrate the validity of the model;

d) Evaluate vibration power absorption distribution at different substructures of the hand-arm model due to excitation from a percussion power tool and other types of hand-held power tools for assessment of susceptibility of different segments of the hand-arm system to potential injury.

1.3.2 Organization of the dissertation

The dissertation research is divided into six chapters. Investigations on the discrepancies in the reported hand-arm DPMI at frequencies above 500 Hz are presented in Chapter 2. The contribution due to handle natural frequency, measurement location, handle deformation and the effectiveness of handle mass cancellation are systematically explored through development and analysis of the handle model coupled with the 3-DOF hand-arm model reported in ISO 10068.

Chapter 3 presents the methodology for simultaneous measurements of 'to-the-hand' and 'through-the-hand-arm' responses together with the data analysis. The effects of different hand forces, vibration level, measurement location and hand-arm posture on hand-transmitted vibration are particularly discussed together with the identification of

hand-arm resonance frequencies. Statistical analysis of variance (ANOVA) using SPSS software was performed on the experimental data to investigate the significance of the main factors on the DPMI and transmissibility responses.

In Chapter 4, the experimental data obtained in Chapter 3 were used to realize a biomechanical/anatomical model of the human hand-arm system. The human hand-arm anthropometric parameters, biodynamic responses and characteristic frequencies were considered in deriving two models corresponding to the bent-arm and the extended arm postures.

The vibration power absorption distribution at different substructures of the hand-arm model due to vibration from a percussion tool and other hand-held power tools is presented in Chapter 5 to investigate susceptibility of different segments of the hand-arm to potential injury.

Finally, the highlights of the dissertation research, major conclusions drawn and recommendations for future work are presented in Chapter 6.

CHAPTER 2

ANALYSES OF DISCREPANCIES IN THE HAND-ARM IMPEDANCE DATA

2.1 Introduction

Biodynamic response analysis of the hand-arm system exposed to hand-transmitted vibration (HTV) is among the most fundamental aspects for understanding the potential vibration-induced disorders. The biodynamic responses of the human hand–arm have thus been widely characterized in terms of the driving-point mechanical impedance (DPMI) [67 – 78, 80 – 83]. The responses reported by different investigators, however, exhibit considerable discrepancies, particularly above 500 Hz, which have been attributed to an array of factors involving differences in handle geometry and size, excitation magnitude, hand-arm posture, hand-handle coupling forces, subjects employed, and measurement system and methods.

While the majority of the studies show sharp increase in DPMI magnitude at frequencies above 500 Hz [68, 78, 79, 81], a few studies have shown either decreasing or relatively steady DPMI magnitudes above 500 Hz [67, 70, 77, 82]. Other studies have shown that the hand forces, and hand-arm posture affect the human hand-arm impedance at frequencies below 500 Hz [67, 69, 73, 82]. A few early investigators had suggested that the differences in DPMI at higher frequencies may be caused by handle natural frequency, while a quantitative analysis was not attempted [70, 72, 76]. Handles with sufficiently high natural frequency are thus generally recommended for laboratory

characterization of DPMI, which is a difficult task considering that the vibration due to various tools may comprise components at frequencies up to 2000 Hz. A recent study evaluated the contribution of handle dynamics to measurement errors in laboratory-based performance assessment of anti-vibration gloves, and concluded that distribution of vibration along the handle span due to handle bending, and palm-adapter misalignment can cause considerable measurement errors [91].

The relatively large discrepancy in the reported data is also attributed to extremely low apparent mass of the hand-arm system at higher frequencies. At frequencies near 1000 Hz, the apparent mass of the hand-arm system could approach as low as 25 g [67]. This small apparent mass in relation to relatively large mass of the handle and its supporting fixture could yield considerable measurement errors, when mass cancellation is performed. A handle design with low effective mass comprising force sensors in the immediate vicinity of the driving-point has been proposed to reduce such errors [127]. Furthermore, this handle design allows for measurement of the biodynamic force either from the fingers or from the palm side of the hand. The instrumented handle employed in such studies [67, 127] requires the measurement of the total biodynamic force, apart from the grip and push forces, which tends to increase the effective mass of the handle.

A systematic and thorough examination of the measurement and data analysis techniques employed for characterizing biodynamic responses is vital for identifying essential sources of errors and thus the discrepancies among the reported data, particularly at higher frequencies. The influences of handle dynamics and measurement locations on the measured responses could also be quantified. In this chapter, the reported biodynamic responses are reviewed in an attempt to identify various sources of variability

in the high frequency region. The influences of measurement location, handle and supporting fixture resonant frequencies, type and geometry of handle, and mass cancellation methods, are particularly investigated using experimental and analytical techniques. The results are used to propose design guidelines for the instrumented handles.

2.2 Comparison of the Reported Hand-arm Impedance Responses

The DPMI responses of the human hand-arm system exposed to HTV have been mostly characterized in the laboratory using instrumented handles. The driving-point responses have been measured at different locations of the handle and its supporting structure, depending upon handle and fixture design and convenience of installation of the sensor, assuming negligible contributions due to structure dynamics. Depending upon the dynamic behavior of the handle and the measurement location, the measured force and velocity actually describe the transfer impedance properties of the coupled handle-fixture-hand-arm system. This can perhaps be illustrated through a review of the different handle designs and measurement locations employed in various studies.

The reported studies [67, 68, 73, 79, 80, 82, 84] have employed handles supported at the extreme ends and at the mid-span, and the column designs as shown in Figure 2.1. The dynamic properties of these handles would differ depending upon the support conditions. Furthermore, split handle designs are invariably employed for the measurement of grip force using either strain gages or force sensors. The biodynamic force developed by the hand-arm system is mostly measured by introducing force sensors between the handle and its supports, as seen in Figure 2.1(a) and Figure 2.1(c), or between the handle fixture and the exciter, as seen in Figures 2.1(d), 2.1(e), and 2.1(f)).
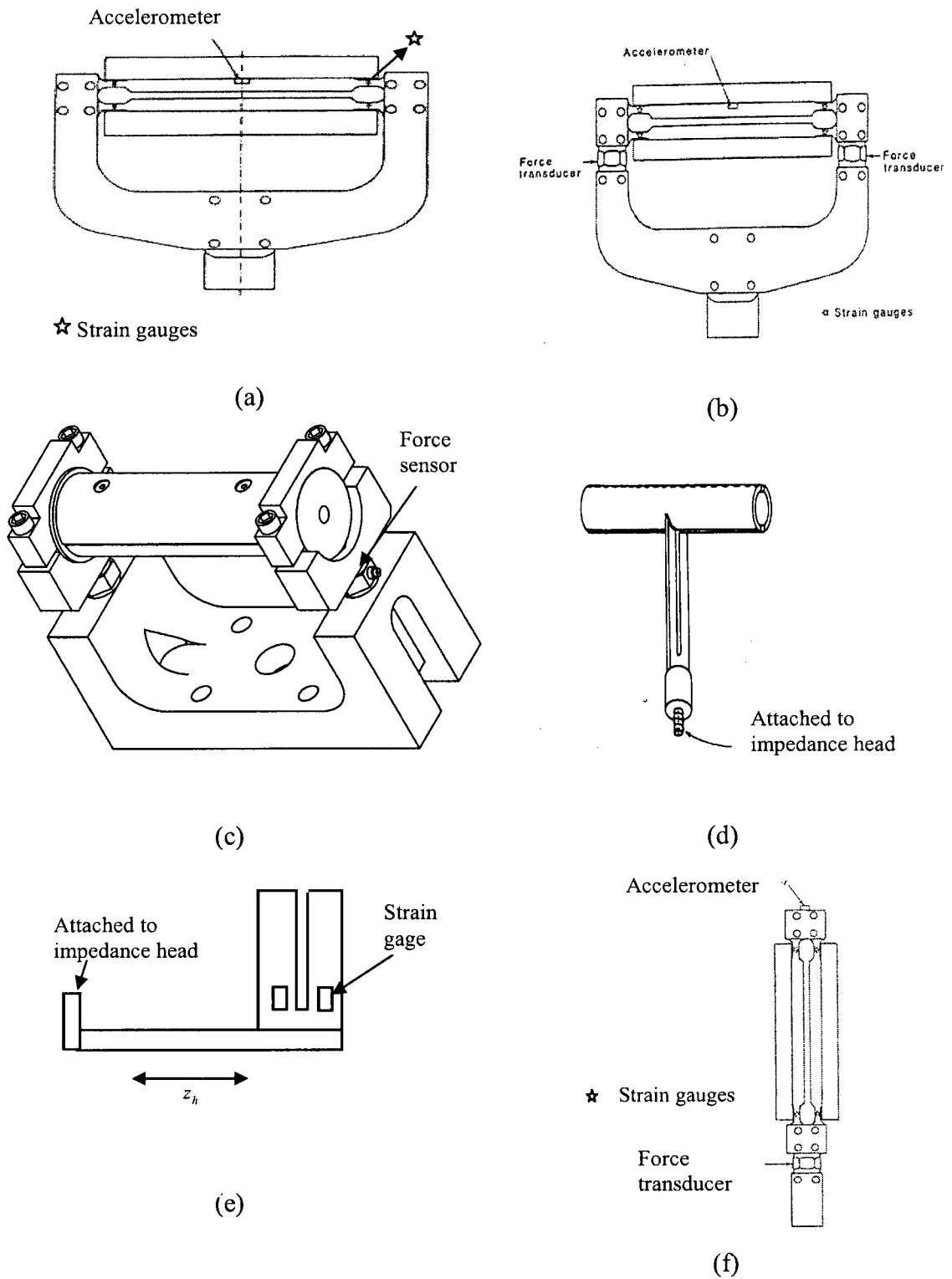
Figure 2.1: Schematics of different handles used for biodynamic studies: (a) Lundstrom and Burstrom [80]; (b) Burstrom [73]; (c) Aldien et al. [67, 84] and Marcotte et al. [82]; (d) Reynolds and Falkenberg [79]; (e) Gurram et al. [68]; (f) Burstrom [73].

The signal from these force sensors also provides a measure of the hand push force. An accelerometer is installed either within the handle, or at the supporting fixture to measure the motion. It is evident that the column (Figure 2.1(f)) and center-supported (Figure 2.1(d)) designs do not provide measures at the driving-point, while the end-supported handles can yield measurements of force and acceleration very close to the driving-point. The effective handle mass supported by the force sensors in all these cases, however, tends to be relatively large.

Tables 2.1 and 2.2 summarize the conditions employed in a number of studies on hand-arm biodynamics that are grouped on the basis of elbow angle used, close to 90° and 180°, respectively. The tables summarize the nature of excitation, hand-arm posture, hand forces, and handle size and design, together with the location of force and acceleration measurement systems. The force was measured either within the handle (designated by 'h') or between the handle and its support ('s') or between the handle support and the exciter ('b'). The accelerometer, on the other hand, is mounted either in the handle ('h') or at its base near the exciter ('b'). Different dataset reported for each posture can be grouped in two categories on the bases of measurement system location: (i) those with force and acceleration measurements close to handle fixture base [68, 78, 79, 81]; and (ii) those with acceleration measurement within the handle and total biodynamic force within or near the handle support [67, 69, 70, 73, 77, 80].

Figures 2.2(a) and 2.2(b) compare the mean DPMI magnitude responses reported in selected studies with elbow angles close to 90° and 180°, respectively, together with the mean values reported in ISO 10068 [86]. Owing to the limited frequency range of

Table 2.1: Experimental conditions employed in selected studies with elbow angle close to 90°

Investigator	Measurement Location		Excitation		Hand Forces		Freq. Range (Hz)	Elbow Angle	Handle Diameter
	Force	Acc.	Type	Magnitude	Grip (N)	Push (N)			
ISO 10068 [86]	+	+	+	≤ 50 m/s^2	25 - 50	≤ 50	10 - 500	60° -165°	19 - 45 mm
Reynold & Falkenberg [79]	b	b	Sine	NR	25.4	NR	5-1000	NR	38 mm cylindrical
Guram et al. [68]	b	b	Sine	0.2 m/s^2 rms	25	NR	10 - 1000	90°	38.1 mm tubular
Kihlberg [77]	h	h	Random	10 m/s^2	50	50	10 - 1000	110°	NR
Burstrom [73]	s	h	Random	13 mm/s	25	20	2.1000	90°	31x42 mm Elliptical
Jandak [78]	b	b	Random	8mm/s	25	60	8 – 800	90°	NR
Aldien et al. [67]	s	h	Random	2.5 m/s^2 rms weighted	30	50	10 -1000	90°	40 mm cylindrical
Hewitt [70]	s	h	Random	3 m/s^2 rms weighted	50	NR	5 - 1000	120°	31x42 mm Elliptical

Keys: NR - Not reported; Acc. - Acceleration; Freq. – Frequency, b – between handle fixture and exciter; h- handle; s-between handle and its support, + - Synthesis of data involving all experimental conditions.

Table 2.2: Experimental conditions employed in selected studies with elbow angle close to 180°

Investigator	Measurement Location		Excitation		Hand Forces		Freq. Range (Hz)	Elbow Angle	Handle Diameter
	Force	Acc.	Type	Magnitude	Grip (N)	Push (N)			
Reynold & Falkenberg [79]	b	b	Sine	NR	25.4	NR	5-1000	NR	38 mm cylindrical
Lundstrom and Burstrom [80]	h	h	Sine	22 mm/s	50	NR	20-1500	180°	31x42 mm Elliptical
Burstrom [69]	s	h	Sine	14 mm/s	50	NR	2.1000	180°	31x42 mm Elliptical
Cronjager and Hesse [81]	b	b	Random	10 m/s^2	30	30	3 - 1000	180°	45 mm cylindrical
Burstrom [73]	s	h	Random	6.5 mm/s	25	20	2.1000	180°	31x42 mm Elliptical
Aldien et al. [67]	s	h	Random	2.5 m/s^2 rms weighted	30	50	10 -1000	180°	40 mm cylindrical
Hesse [83]	b	b	Random	9.8 m/s^2 rms weighted	30	30	3 -1000	180°	45 mm cylindrical

Keys: NR - Not reported; Acc. - Acceleration; Freq. – Frequency, b – between handle fixture and exciter; h- handle; s-between handle and its support.
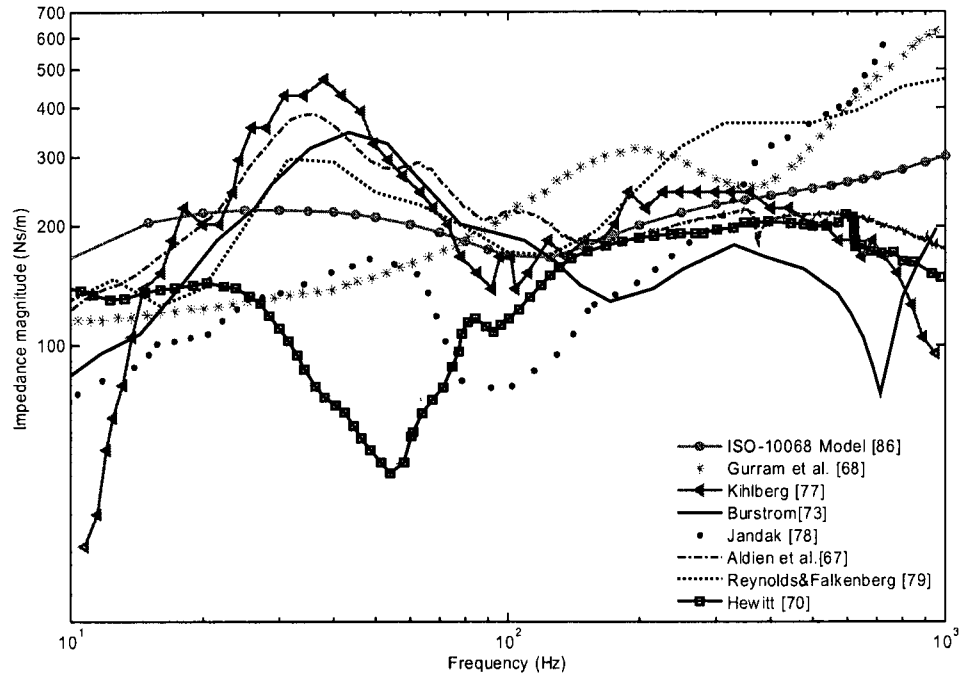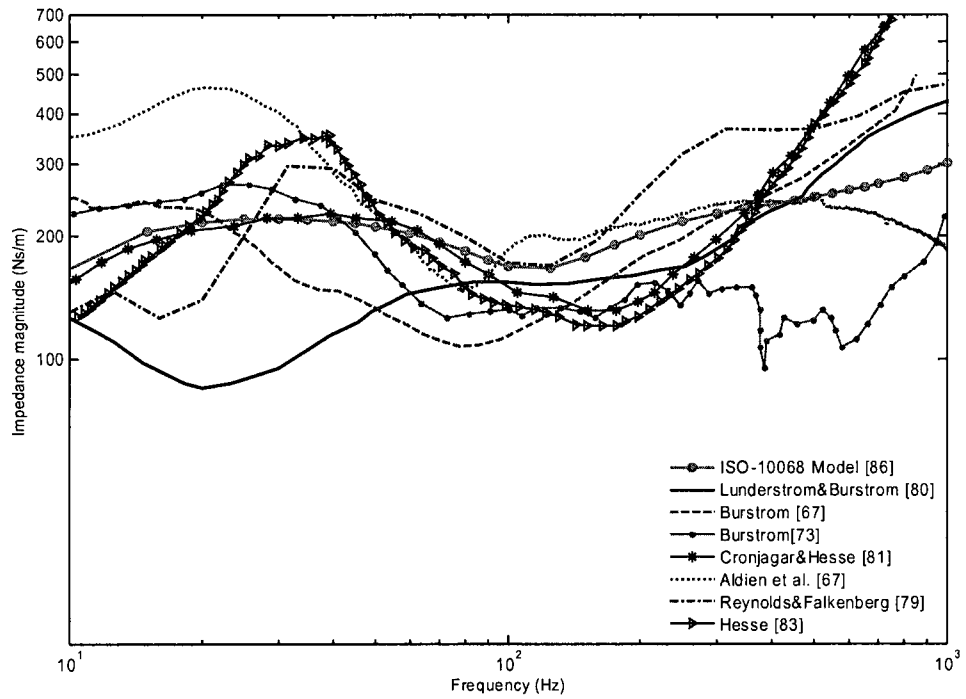
Figure 2.2: (a) Comparisons of hand-arm impedance magnitudes reported in selected studies involving: (a) elbow angle close to 90°; and (b) elbow angle close to 180°.

standardized values, the three-DOF hand-arm model formulated on the basis of mean DPMI values was used to determine DPMI response in the 10 − 1000 Hz frequency range. The scatter among the datasets tends to be greater at frequencies above 500 Hz, irrespective of the hand-arm posture. While some of the datasets reveal increasing magnitude at high frequencies, others show decreasing trend. A closer look at the associated experimental designs suggests that the studies [68, 78, 79, 81] involving acceleration measurements near the base of the handle support ('b') yield increasing magnitudes at higher frequencies, with no exception. The force measurement in all these studies was also taken at the base of the handle supports. The studies [67, 79, 83] involving acceleration measurement within or close to the handle yield either a decreasing or relatively steady magnitudes at higher frequencies, with the exception for the data reported by Burstrom [69], and Lundstrom and Burstrom [80]. These two studies employed an identical handle design comprising a strain-gage based force sensing member within the handle, as shown in Figure 2.1(a). The increasing magnitude trend in these studies is perhaps caused by the resonance of the force sensing member. The authors claimed good agreements between their data and those reported by Mishoe and Suggs [72], who used a center-supported handle with acceleration measurement near the exciter. Another study by the same author of [69] employed handle-support mounted force sensors, as shown in Figure 2.1(b), which resulted in significantly lower magnitudes in the 200 − 600 Hz frequency range and increasing trend at higher frequencies [73]. The results suggest that the measurement location could significantly affect the DPMI magnitude response of the hand-arm system, particularly at higher frequencies. The discrepancies observed below 500 Hz, however, have been attributed to

42

a range of factors, namely hand forces, excitation magnitude, handle size and inter-subject variability [67, 73, 82].

2.3 Methodology

2.3.1 Experimental method

Owing to the complex contributions of the handle dynamics and measurement locations, as observed from the reported data, an experimental and analytical study is undertaken to examine the effects of these parameters. The experiments involved four adult male subjects and four different handle designs: two instrumented cylindrical aluminum handles (40 and 50 mm diameters), shown in Figure 2.1(c); a tubular 40 mm diameter aluminum handle with 7.5 mm wall thickness; and a 40 mm diameter solid aluminum handle. All the handles were installed on an electro-dynamic vibration shaker using the support fixture shown in Figure 2.1(c), which comprised two force sensors for measurement of hand push and total dynamic force developed by the hand and handle fixture. Each handle was oriented to generate vibration along the z_h-axis of the hand-arm system. The acceleration due to vibration of the 40 and 50 mm instrumented handles was measured using a PCB SEN026 tri-axial accelerometer installed within the handle, while the acceleration of the tubular handle was measured using a miniature Bruel & Kjaer accelerometer (B&K 4393) fastened inside the handle at the mid-span. For the solid 40 mm handle, the same accelerometer was attached to the exterior surface at the mid-span using wax.

The instrumented handles integrated two force sensors for the measurement of grip force. The measured grip and push forces were low-pass filtered at a rate of 4 samples per second and displayed to the subject on a computer monitor. The subjects

were advised to maintain the desired hand forces (30 N grip and 50 N push) within ±2 N by monitoring the displayed forces, while gripping the handle with an elbow angle of 90°. For the tubular and solid handles, it was not possible to measure the grip force; subjects were however advised to maintain a grip similar to that used for the instrumented handles.

The handles were subject to broadband random vibration in the 2.5 to 3000 Hz frequency range, with constant power spectral density (PSD) and frequency-weighted overall rms acceleration of 5.25 m/s^2. The flexural deformation of the 40 mm instrumented handle was initially evaluated through measurement of acceleration along half the span of the handle. The acceleration at the handle surface was measured at four different locations, including the mid-position (Pos 1) and the support (Pos 4), as shown in Fig, 2.3(a). The measured acceleration was normalized with respect to that measured at
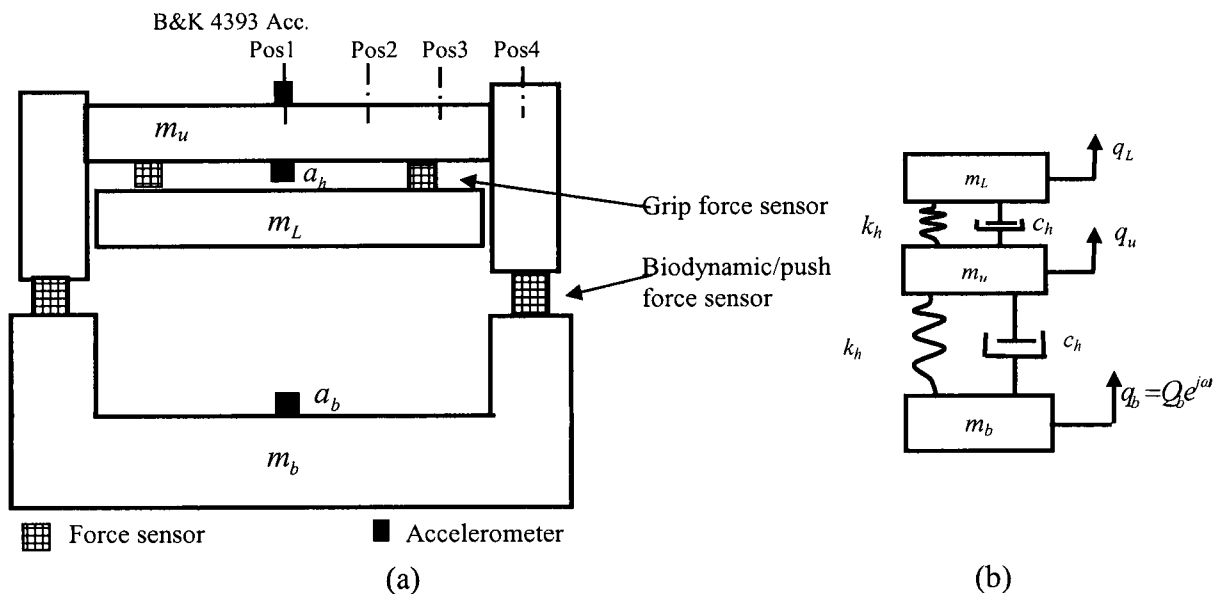
Figure 2.3: (a) Experimental setup for measurement of handle vibration at various locations; and (b) base-excited 2.DOF model of the handle.

the inside center of the handle (a_h). An additional single-axis accelerometer (a_b) was also installed at the base of the handle fixture as shown in Figure 2.3(a). The resonant frequencies and the apparent mass of each handle were also derived from the measured force and acceleration responses. For this purpose, the signals from the base-mounted (a_b) and the handle-mounted (a_h) accelerometers, and the fixture-mounted force sensors were acquired in a multi-channel Pulse data analyzer. The data were analyzed to derive acceleration transmissibility, the ratio of handle acceleration to the base acceleration, and the apparent mass of each handle. The handle apparent mass characteristics were computed using both the handle and base acceleration, such that:

$$APMS_b(j\omega) = \frac{S_{Fa_b}(j\omega)}{S_{a_b}(j\omega)}$$

$$APMS_h(j\omega) = \frac{S_{Fa_h}(j\omega)}{S_{a_h}(j\omega)}$$

(2.1)

where $APMS_b$ and $APMS_h$ are complex apparent mass responses of the handle derived on the basis of base and handle acceleration, respectively. $S_{a_i}(j\omega)$ and $S_{Fa_i}(j\omega)$ are the auto-spectrum of acceleration measured at location i ($i = b$, h), and cross-spectrum of force and acceleration corresponding to excitation angular frequency ω.

Subsequently, experiments were performed to measure the driving-point impedance properties of the hand and arm of four adult male participants. Each participant was advised to maintain the desired hand forces (30 N grip and 50 N push) with an elbow angle of 90° and 0° shoulder abduction. Each measurement was performed three times, and the measured force and acceleration data were analyzed to determine the driving-point impedance of the coupled hand-handle system. The impedance magnitude and phase responses of the hand-arm system were obtained by applying appropriate

inertial correction for the handle effective mass. The results attained for the three trials were averaged to determine mean responses based upon both handle and base accelerations, as described in Eq. (2.1).

Relative analysis of the two apparent mass (APMS) responses could provide considerable insight into the effects of handle deformations and measurement location. The measured APMS responses of the handle were analyzed in an attempt to identify a limiting frequency, f_L, such that the APMS response can be considered reliable within 5% for $f \leq f_L$. The percentage deviation in the APMS magnitude was computed with reference to that measured at 10 Hz in order to determine the limiting frequency f_L. The reference value at 10 Hz was chosen since the flexural deformations are not expected to occur at such a low frequency. The acceleration data acquired at different locations were further analyzed to derive acceleration transmissibility and identify the natural frequencies of each handle.

2.3.2 Analytical method

The contributions due to handle dynamics and acceleration measurement location could also be estimated through the development and analysis of a simple model of the handle. A coupled hand-handle system model could be further realized to study the effects of handle dynamics and measurement location. The instrumented handle used in this study, schematically shown in Figure 2.1(c), can be modeled as a base-excited two-degree-of-freedom (DOF) dynamical system, as shown in Figure 2.3(b), assuming negligible contribution due to the bending mode. The grip force sensing cap is represented by a lumped mass m_L, while the handle is represented by mass m_u, which is coupled to the fixture/base of mass m_b through effective stiffness k_h and damping c_h

properties of the handle and the push/biodynamic force sensors. Masses m_L and m_u are also coupled through the effective stiffness and damping properties of the grip force sensors and the sensing cap. The mass parameters of the 40 mm instrumented handle were measured as $m_b = 1.0$ kg, $m_u = 0.52$ kg and $m_L = 0.20$ kg.

The equation of motion for the 2.DOF linear model of the handle can be written as:

$$[M]\{\ddot{q}\} + [C]\{\dot{q}\} + [K]\{q\} = \{C_o\}\dot{q}_b + \{K_o\}q_b \qquad (2.2)$$

where $[M]$, $[C]$ and $[K]$ are (2×2) mass, damping and stiffness matrices, respectively, $\{C_o\}$ and $\{K_o\}$ are (2×1) forcing damping and stiffness vectors, $\{q\}$ is (2×1) displacement vector and q_b is the displacement of the fixture base.

The above equation is solved to compute the apparent mass of the handle and its support fixture in the frequency domain on the basis of acceleration responses at the base and in the vicinity of the hand, such that:

$$APMS_{fb}(j\omega) = \frac{(k_h + j\omega c_h)}{-\omega^2}\left(1 - \frac{Q_u}{Q_b}(j\omega)\right) \qquad (2.3)$$

$$APMS_{fh}(j\omega) = \frac{(k_h + j\omega c_h)}{-\omega^2}\left(\frac{Q_b}{Q_L}(j\omega) - \frac{Q_u}{Q_L}(j\omega)\right) \qquad (2.4)$$

where $Q_u(j\omega)$, $Q_L(j\omega)$ and $Q_b(j\omega)$ are the Fourier transforms of $q_u(t)$, $q_L(t)$ and $q_b(t)$, respectively. The impedance of the handle and its support on the basis of base and handle velocities can be expressed as:

$$Z_{fb}(j\omega) = j\omega\, APMS_{fb} \qquad (2.5)$$

47

$$Z_{fh}(j\omega) = j\omega\,APMS_{fh} \qquad\qquad (2.6)$$

Considering that the fundamental mode vibration is of primary concern, the damping c_h

and stiffness k_h properties of the structure and force sensors corresponding to the first

mode were identified. An eigenvalue problem was formulated and solved to determine

the fundamental natural frequency ω_n and the corresponding damping ratio ζ. The

equation of motion was then manipulated to express k_h and c_h as functions of masses,

ω_n and ζ, in the following manner:

$$k_h = \frac{2m_L m_u \omega_n^2}{(2m_L + m_u) - \sqrt{(2m_L + m_u)^2 + 4m_L m_u}} \qquad\qquad (2.7)$$

$$c_h = 2(m_L + m_u)\omega_n \zeta \qquad\qquad (2.8)$$

Owing to the very light damping of the handle structure, the handle natural frequency

was taken as the frequency corresponding to the peak in the measured acceleration

transmissibility of the 40 mm instrumented handle (a_h/a_b). The identified frequency was

subsequently applied in the above equations to estimate the values of c_h and k_h

corresponding to the first mode. The damping ratio ζ was selected to attain good

agreement between the peak impedance magnitude responses (Z_{fb} and Z_{fh}) of the model,

derived from Equations (2.5) and (2.6) and the peak measured impedance responses. A

damping ratio of 0.009 was found to yield reasonably good agreements between the

model and the measured impedance responses. The values of c_h and k_h are found to be

105.09 Ns/m and 52120 kN/m, respectively for handle natural frequency of 1305 Hz,

while the parameters of the 3-DOF hand-arm model reported in ISO 10068 [86] are: $m_1 =$

2.9 kg, $m_2 = 0.662$ kg, $m_3 = 0.03$ kg, $c_1 = 30.3$ Ns/m, $c_2 = 380.6$ Ns/m, $c_3 = 227.5$ Ns/m,

$k_1 = 2.495$ kN/m, $k_2 = 299.4$ kN/m and $k_3 = 5.335$ kN/m. The resulting model was then

applied to study the influence of handle resonance frequency on the dynamic

characteristics of the hand-arm system by varying the stiffness coefficient k_h.

Subsequent to the development of a handle model, a 5-DOF model of the coupled

hand-arm-handle system is formulated by integrating the 3-DOF z_h-axis hand-arm system

model, defined in ISO 10068 [86], with the 2-DOF handle model, as shown in Figure

2.4(a). The equation of motion for the coupled model in the matrix form can be expressed

by Eq. (2.2), which is solved to compute the impedance responses of the hand-arm model

on the basis of both the base and handle accelerations, represented by $\ddot{q}_b$ and $\ddot{q}_L = \ddot{q}_3$,

respectively. The handle acceleration is taken as $\ddot{q}_L$ rather than $\ddot{q}_u$, since the relative

dynamic deflection across the grip sensors, when hand grip force is applied, is very small.

The total impedance of the coupled model is computed using the total dynamic force,

which is subsequently corrected for the impedance of the handle alone such that:

$$Z_{hi}(j\omega) = Z_{ci}(j\omega) - Z_{fi}(j\omega) \qquad (2.9)$$

where Z_{hi} is the hand-arm impedance on the basis of acceleration measured at location i,

$(i = h, b)$, Z_{ci} is the impedance of the coupled hand-arm-handle system model (Figure

2.4(a)), which is derived as:

$$Z_{ci}(j\omega) = \frac{(k_h + j\omega c_h)[(Q_b(j\omega) - Q_u(j\omega))]}{j\omega Q_i(j\omega)} \qquad (2.10)$$

The impedance based on the handle acceleration, $Z_{hh}(j\omega)$, can also be computed directly

from the decoupled force-excited 3-DOF hand-arm system, shown in Figure 2.4(b) [68, 72]:

$$Z_{hh}(j\omega) = \frac{-\omega^2 m_3 + (k_3 + j\omega c_3)}{j\omega}\left(1 - \frac{Q_2}{Q_3}(j\omega)\right) \qquad (2.11)$$

Equation (2.11) represents the impedance response of the uncoupled hand-arm system that can be achieved only via analytical means. Such decoupling of the hand-arm from the handle in experimental characterization is attained through inertia cancellation, which may introduce errors in the impedance properties of the hand-arm system.
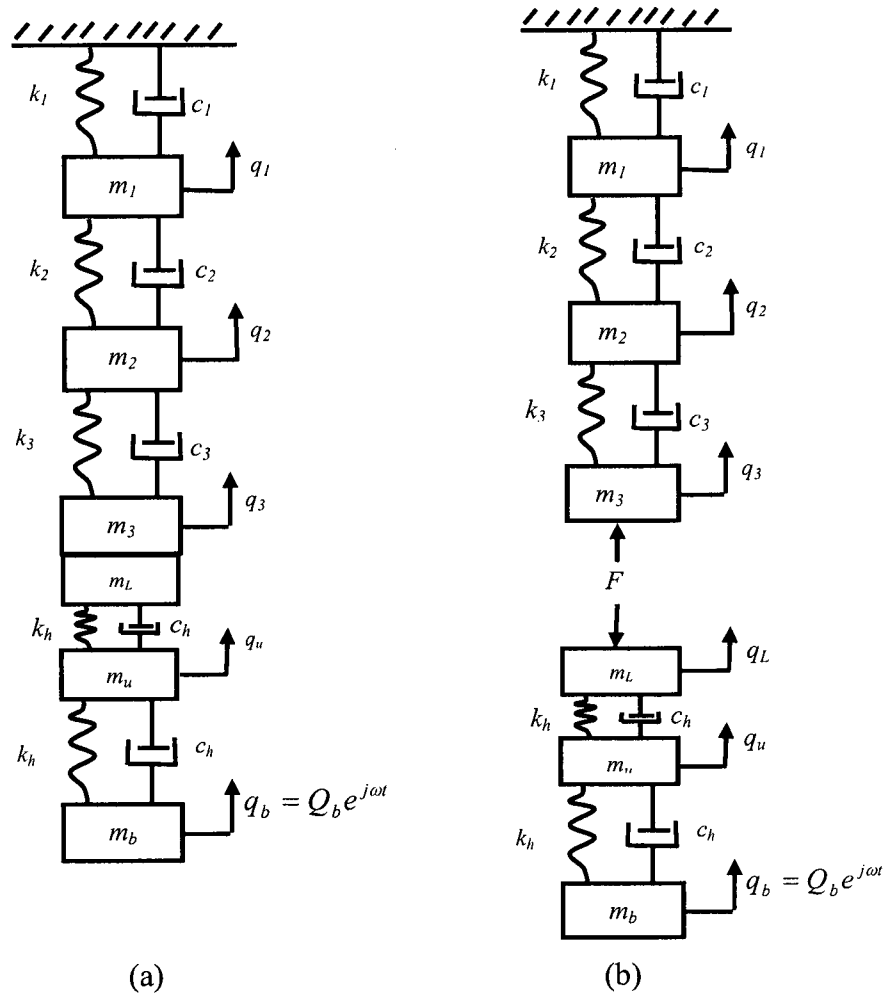
Figure 2.4: Mechanical equivalent models of: (a) the coupled hand-arm-handle system; and (b) the decoupled hand-arm and handle

2.4 Effects of Handle Dynamics and Measurement Location on Impedance Response

Figure 2.5(a) shows the measured acceleration transmissibility magnitude responses (a_h/a_b) of the four handles considered in the study under broadband random excitation in the 2.5 to 3000 Hz frequency range. The responses show large magnitude peaks at frequencies considered to be the fundamental mode resonant frequency of the handle, although some of the handles also show secondary peaks at higher frequencies. The observed resonant frequencies of the handles are summarized in Table 2.3. The results show that the tubular 40 mm handle yields the highest fundamental frequency of 1769 Hz due to its lower mass and area moment of inertia. The fundamental frequency of the solid handle with higher mass and area moment of inertia is lower than the tubular handle while both the instrumented handles yield the lowest frequencies due to their split design.

Table 2.3: Natural frequencies of test handles, identified from the measured data

Handle type	Diameter	Primary frequency
Tubular	40 mm	1769 Hz
Instrumented	40 mm	1305 Hz
Instrumented	50 mm	1240 Hz
Solid	40 mm	1534 Hz

The measured impedance response magnitudes of all the handles, on the basis of base and handle acceleration, are shown in Figure 2.5(b). The results show that the impedance magnitudes based on the base motion exhibit sharp peaks occurring at the identified resonant frequencies. The impedance magnitudes based on the handle motion, does not show distinct peaks in the 2.5 – 3000 Hz frequency range, the magnitude tends to either settle down or decrease at frequencies above 1000 Hz. The reported DPMI

51
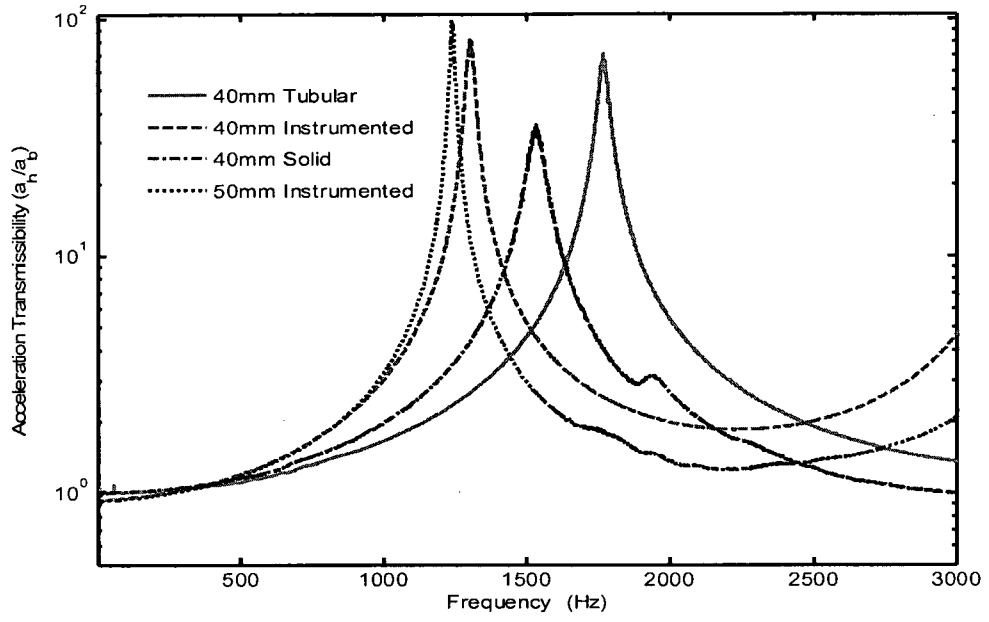
(a)
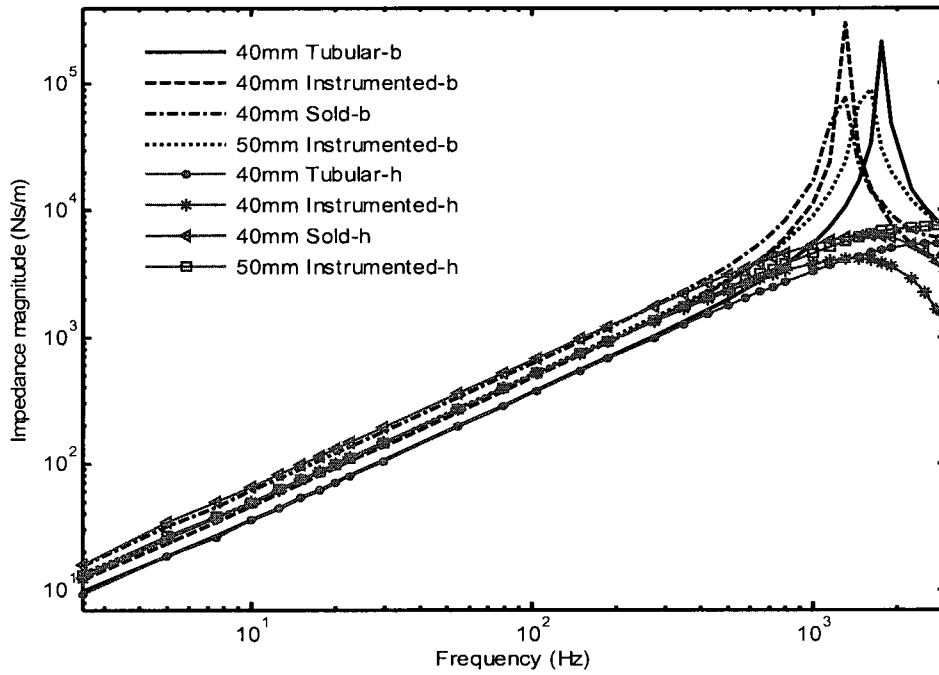
(b)

Figure 2.5: Comparison of experimental frequency response characteristics of the test handles; (a) acceleration transmissibility; and (b) Impedance magnitude.

responses of the hand-arm system exhibit both the trends, increasing or decreasing/settling, in the magnitude. These results thus confirm the earlier observation, shown in Figure 2.2, that the data based on acceleration measurement at the base would yield increasing magnitude at higher frequencies, while those based on the handle acceleration would exhibit decreasing or settling magnitude at higher frequencies.

The measured impedance magnitude responses of the 40 mm instrumented handle are further compared with those derived from the 2-DOF model in Figure 2.6. Measurements based on the base and handle acceleration are identified with 'b' and 'h', respectively. The results show reasonably good agreements between the model and experimental results, particularly for impedance based on base motion (see Fig. 2.6). Good agreement between the model and experimental results are also observed in impedance based on handle acceleration up to 1000 Hz. The observed discrepancies
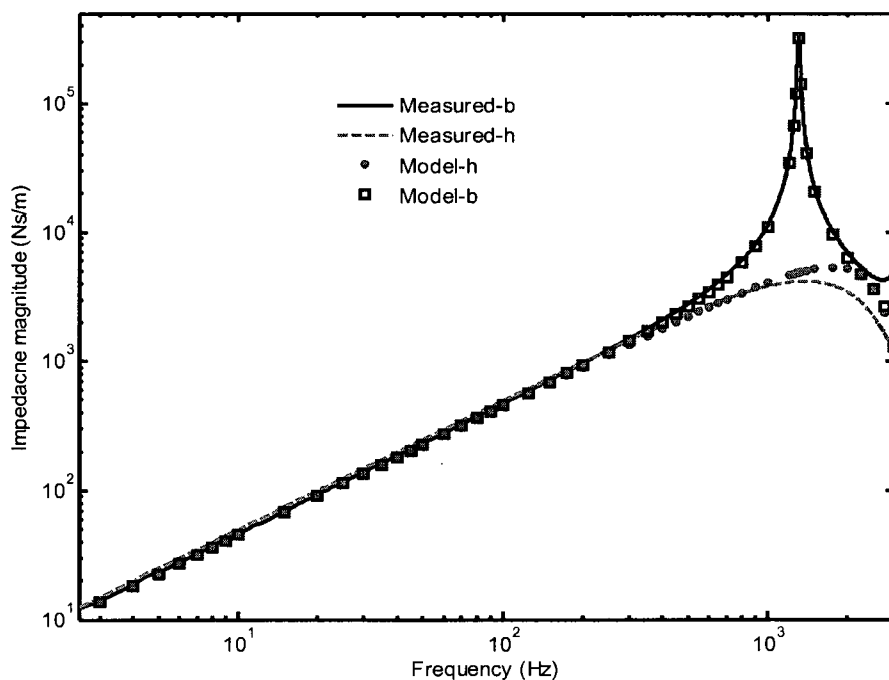
Figure 2.6: Comparisons of measured impedance magnitude responses of the 40 mm instrumented handle with the model results ('b'- base, 'h'- handle).

between the two results above 1000 Hz may be attributed to lack of consideration of the handle flexural bending in the model. The results, however, suggest that the proposed 2-DOF handle model can adequately simulate the handle dynamics.

Figure 2.7(a) shows the mean impedance responses of the hand and arm, measured on the basis of base and handle accelerations (Z_{hb} and Z_{hh}), attained for the four subjects grasping different handles. The measured mean responses were derived upon inertial correction using Eq. (2.9). The figure also illustrates the impedance response of the 3-DOF hand-arm model described in ISO 10068 [86]. The results show that the frequencies corresponding to peak magnitudes observed in Z_{hb} are quite close to the respective natural frequencies of the handles identified from the measured acceleration transmissibility (Table 2.3). Apart from the handle (with natural frequency of 1305 Hz) considered for modeling, the influence of handle resonance frequency on the impedance magnitudes are also obtained by varying the natural frequency of the 2-DOF handle model from 900 to 4000 Hz. Figure 2.7(b) presents the impedance response characteristics of the hand-arm model based upon the base and handle motions (Z_{hb} and Z_{hh}) obtained using Eqs. (2.9) - (2.11) together with the mean impedance data and hand-arm model response reported in 1SO 10068 standard. Simulation results also reveal peak magnitudes in Z_{hb} near the chosen natural frequencies. The appearance of peaks that are close to the natural frequencies of the handles in Figure 2.7 suggests that the mass cancellation did not completely remove the contributions due to handle dynamics, particularly at higher frequencies.

The measured DPMI magnitude responses based upon handle acceleration (Z_{hh}) invariably do not show peaks near the handle resonant frequencies. The magnitude
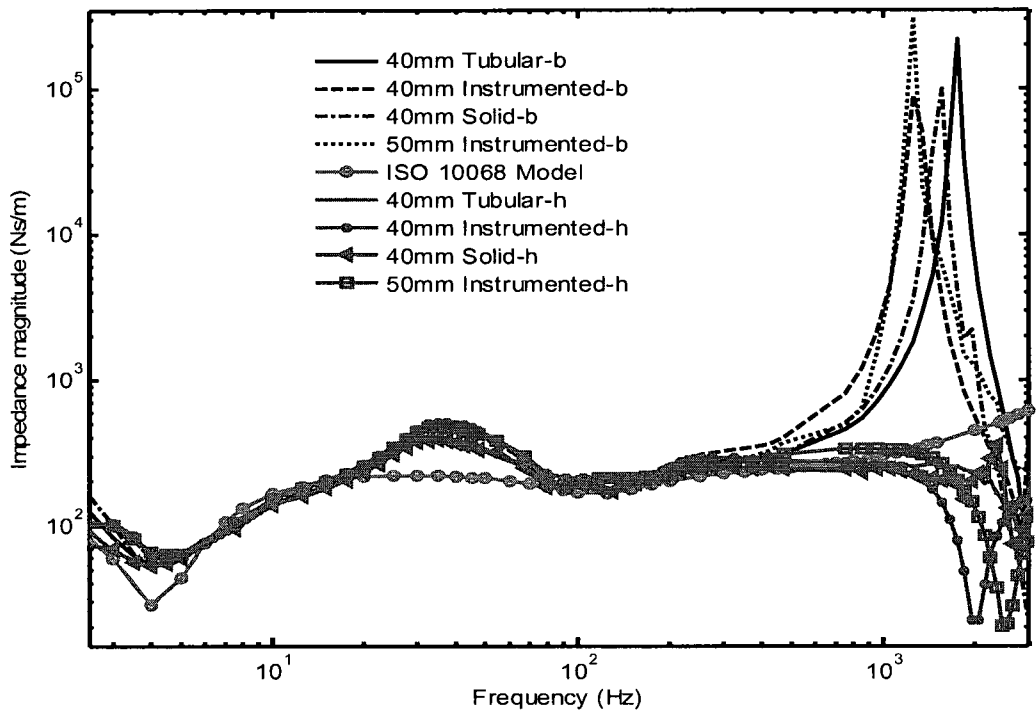
(a)
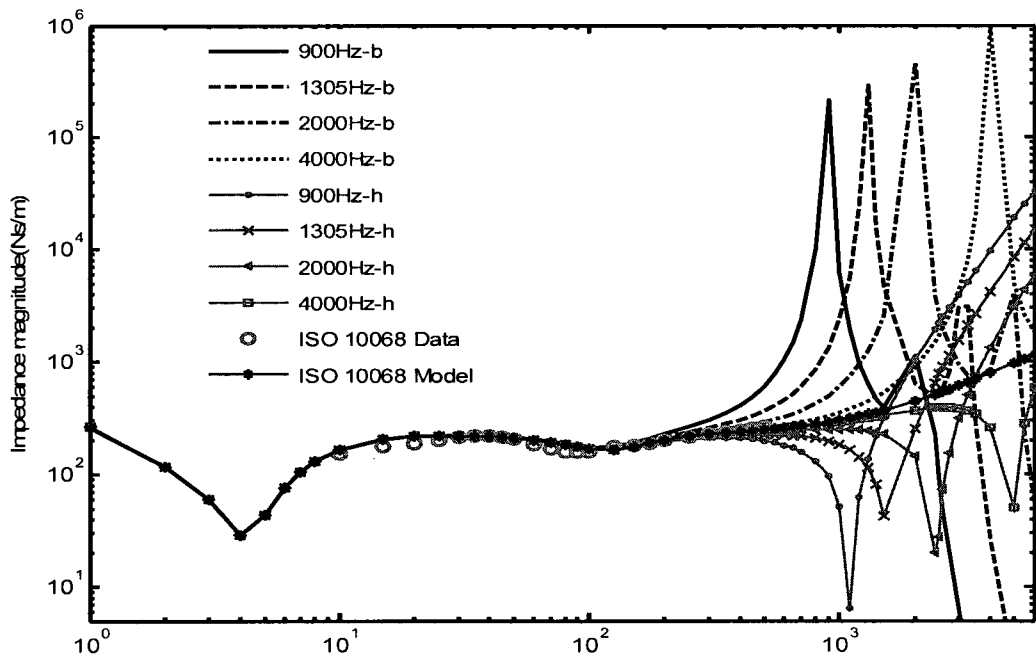
(b)

Figure 2.7: Effects of handle natural frequency and measurement location on the hand-arm impedance response: (a) mean measured; and (b) model results.

responses, however, show valleys at frequencies greater than the natural frequencies of the handles. These trends are similar to those observed in the reported DPMI presented in Figure 2.2, and in the measured and computed handle responses presented in Figures 2.5(b) and 2.6. The results clearly show most significant effect of measurement location. The magnitude responses obtained with the base acceleration, Z_{hb}, clearly show rapidly increasing magnitude at higher frequencies up to the handle resonant frequency, while the Z_{hh} magnitude exhibits either a settling or decreasing magnitude to form a valley at a frequency greater than the handle resonant frequency for all the handles. Such a valley is also evident in impedance response reported by Burstrom [73], as shown in Figure 2.2. This suggests relatively lower natural frequency of the handle used in the study. From the results, it can thus be deduced that the different trends and discrepancies in high frequency impedance of the hand-arm system are in-part attributable to location of measurement and the handle resonant frequency.

The results further show that the higher is the natural frequency of the handle, the closer is the responses attained to the impedance response of the model reported in ISO 10068 at higher frequencies. It should be noted that the ISO hand-arm model was derived from mean impedance data in the 10 – 500 Hz range; hence it is not expected to show contributions due to handle resonance. From the results, it can be further deduced that the model can predict the hand-arm system impedance responses below 10 Hz, although the majority have reported data above 10 Hz. The DPMI magnitude response of the model reveals a valley around 4 Hz, similar to that observed in the experimental data obtained in this study, although the model was derived using the mean data in the 10 - 500 Hz range.

A closer examination of the mean measured impedance responses, presented in

Figure 2.7(a), shows that the mean magnitudes obtained with all the handles are quite comparable up to about 250 Hz, irrespective of the measurement location. This observation can be attributed to negligible deformations of the handles at frequencies below 250 Hz. Furthermore, the Z_{hh} magnitude begins to deviate considerably from the
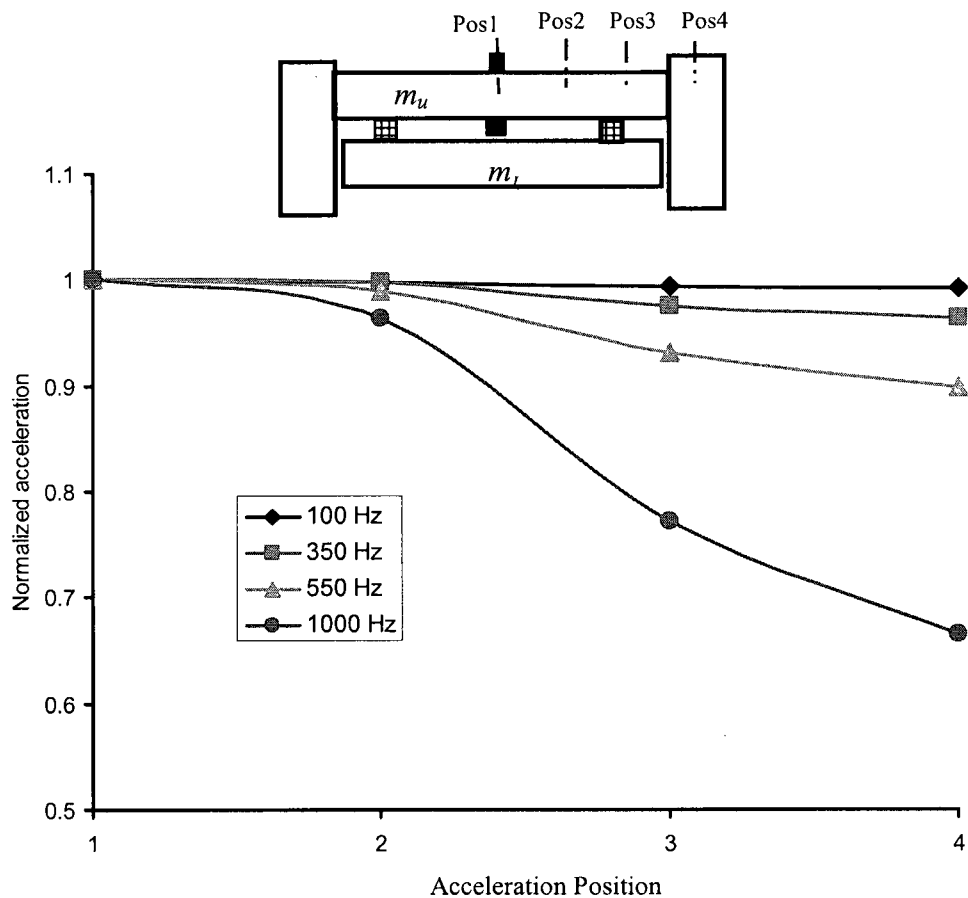
Figure 2.8: Distribution of normalized acceleration magnitude along half-span of the 40 mm instrumented handle at different excitation frequencies.

ISO 10068 model response at frequencies close to or above 1000 Hz, while the deviation of Z_{hb} could be observed at frequencies above 300 Hz. The impedance response measured on the basis of handle acceleration Z_{hh} can thus be considered more reliable to a relatively higher frequency than that based on the fixture or base acceleration Z_{hb}.

Figure 2.8 presents the variations in acceleration magnitudes measured along the span of the 40 mm instrumented handle at four different excitation frequencies in the 100 - 1000 Hz range. The figure shows magnitudes of accelerations measured at the four locations normalized with respect to that at the mid-span (Pos 1). The results clearly show notable handle deformation at frequencies above 350 Hz. Such flexural bending of the handle has also been reported by Dong et al. [91]. The handle used in this study, however, revealed relatively lower natural frequency than that used in [91], which is attributed to additional force sensors installed between the handle support and the fixture for simultaneous measurement of grip, push and total biodynamic forces.

2.5 Measurement Reliability and Handle Design Guidelines

The results suggest that laboratory characterization of the human hand-arm responses to vibration would necessitate: (i) design of high natural frequency handle and the fixture; (ii) provisions for measurements of acceleration and force in close proximity of the hand-handle interface, similar to those used in [67, 73, 84, 87, 91]. The measurement errors attributed to handle dynamics could be estimated from deviations in the apparent mass of the handle and its support fixture [70]. Figure 2.9(a) illustrates the measured apparent masses based on base and handle acceleration, $APMS_b$ and $APMS_h$, of the four handles used in this study, while Figure 2.9(b) shows the corresponding magnitudes ($APMS_{fb}$ and $APMS_{fh}$) derived from the 2-DOF handle model. Similar to the trend observed in Figures 2.5(b), 2.6 and 2.7, the $APMS$ magnitude obtained on the basis of base acceleration increases at frequencies above 400 Hz, while that based on handle acceleration decreases above 500 Hz.

The limiting frequency f_L of each handle is estimated as the frequency at which

the percentage deviation in the handle *APMS* magnitude (Figure 2.9(a)) exceeds 5% of its value at 10 Hz. An impedance measurement may thus be considered reliable for $f < f_L$. Table 2.4 summarizes the limiting frequencies derived from the results attained with each handle on the basis of both the handle as well as base acceleration together with the handle natural frequencies. The ratio of natural frequency f_n to the limiting frequency f_L varies from 4.43 for the 50 mm instrumented handle to 5.93 for the 40 mm solid handle, when $APMS_b$ response is considered. This ratio ranges from 1.95 to 3.3 for the measurements based on handle acceleration. The f_n/f_L ratio may be used as a guideline in the design of instrumented handle for laboratory characterization of the human hand-arm biodynamic responses. The mean results suggest that the handle natural frequency should generally be 5.4 times the highest frequency of interest, when measurement is performed using the base acceleration. This ratio reduces to 2.6, when measurement utilizes the handle acceleration. These results suggest that an accurate measurement of the impedance (error ≤ 5%) of the hand-arm system up to 1000 Hz would require the handle natural frequency in the order of 5400 Hz and 2600 Hz, for measurements based upon the base and handle accelerations, respectively. This relationship between f_n and f_L appears to be

Table 2.4: Reliability of measurement from the measured APMS responses of the handles

Handle type and diameter	f_n (Hz)	Frequency at which APMS deviation is within ± 5 %			
		Measurement at Base		Measurement at Handle	
		f_L (Hz)	f_n/f_L	f_L (Hz)	f_n/f_L
40 mm Tube	1769	300	5.90	805	2.19
40 mm Instrumented	1305	250	5.22	395	3.30
40 mm Solid	1539	260	5.92	790	1.95
50 mm Instrumented	1240	280	4.43	420	2.95
Average			5.37		2.60
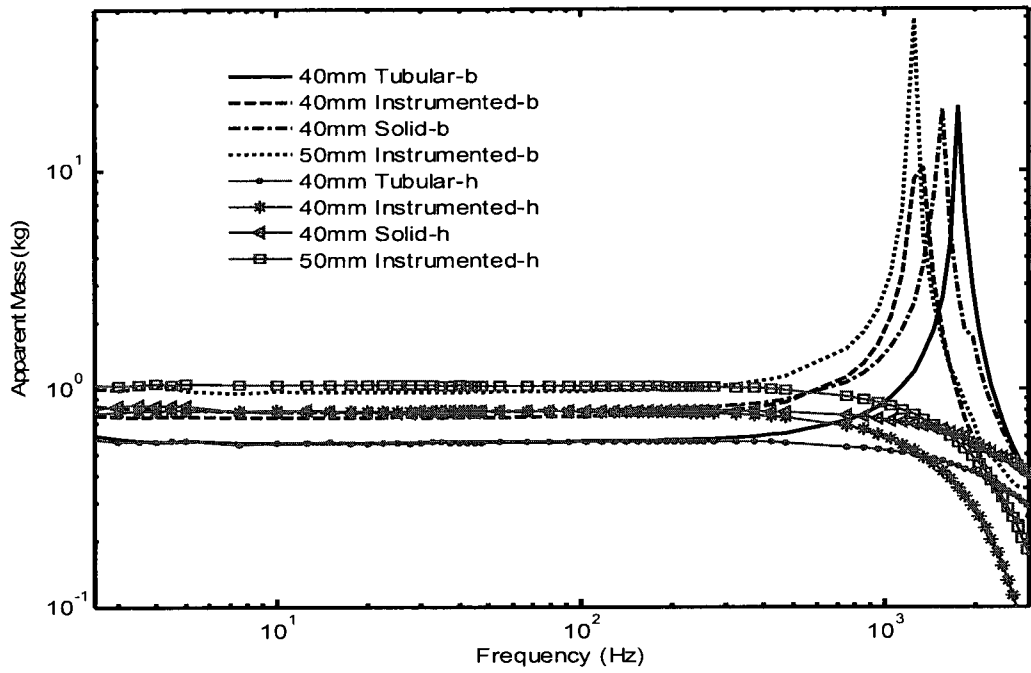
(a)
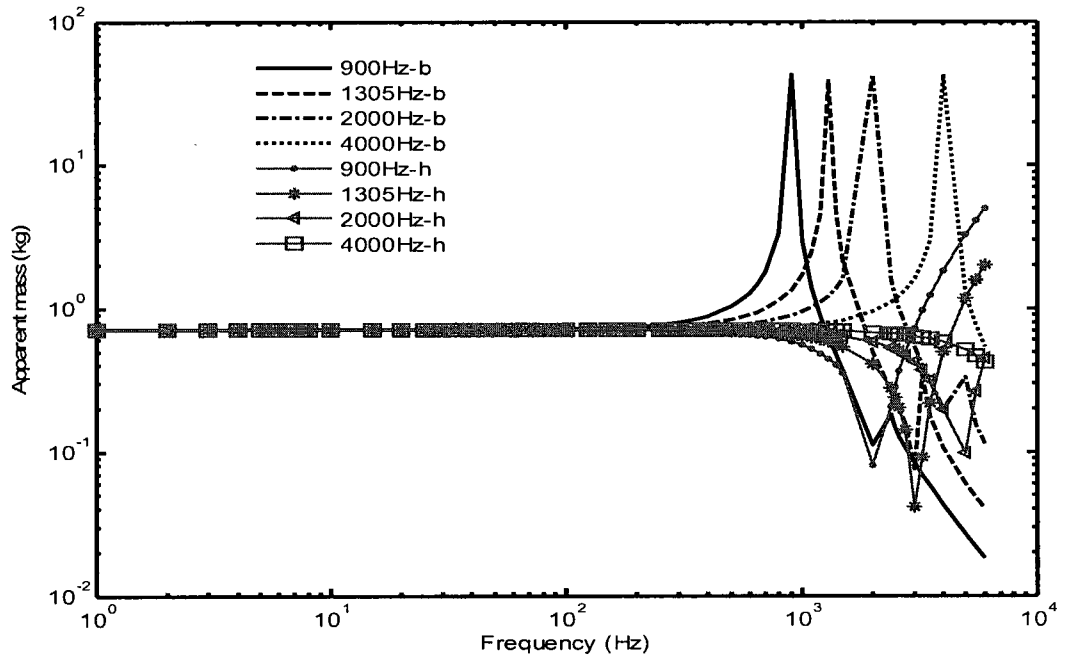
(b)

Figure 2.9: Apparent mass responses of different handles on the basis of base (b) and handle (h) accelerations: (a) measured; and (b) model results.

consistent with the measurements obtained with the handles in this study (Figure 2.7), where Z_{hb} and Z_{hh} magnitudes tend to deviate from the 3-DOF ISO 10068 model response at frequencies above 250 Hz and 400 Hz, respectively, depending on the handle.

The observed relationship between f_n and f_L was further explored using the handle model with four different natural frequencies (900, 1305, 2000 and 4000 Hz). The limiting frequencies, estimated from the model responses in terms of $APMS_{fb}$ and $APMS_{fh}$, are presented in Figure 2.10 as a function of the handle natural frequency. The results suggest a linear relationship between f_n and f_L, with $f_n \approx 4.5 f_L$ and $f_n \approx 1.9 f_L$, when base and handle accelerations are applied, respectively. The differences between f_n and f_L that were derived from the experimental and the model response data are most likely attributed to lack of consideration of handle flexural deformations in the lumped-mass model.

The measured acceleration transmissibility (a_h/a_b) of the 40 mm instrumented handle, shown in Figure 2.5(a), is applied to $APMS_b$ response of the handle, shown in Figure 2.9(a), to obtain an estimate of the $APMS_h$ ($APMS_h = APMS_b /(a_h/a_b)$). The estimated response is identical to the measured $APMS_h$ as it is evident from the comparison shown in Figure 2.11. The results could be used to explain the decreasing trend in $APMS_h$ magnitude at higher frequencies. It can be seen that the magnitude of acceleration transmissibility is nearly unity at frequencies up to about 250 Hz, which would yield identical magnitudes of $APMS_h$ and $APMS_b$. However, at frequencies above 250 Hz, the acceleration transmissibility and $APMS_b$ magnitudes rapidly increase to their peak values near the resonant frequency of 1305 Hz. The peak acceleration
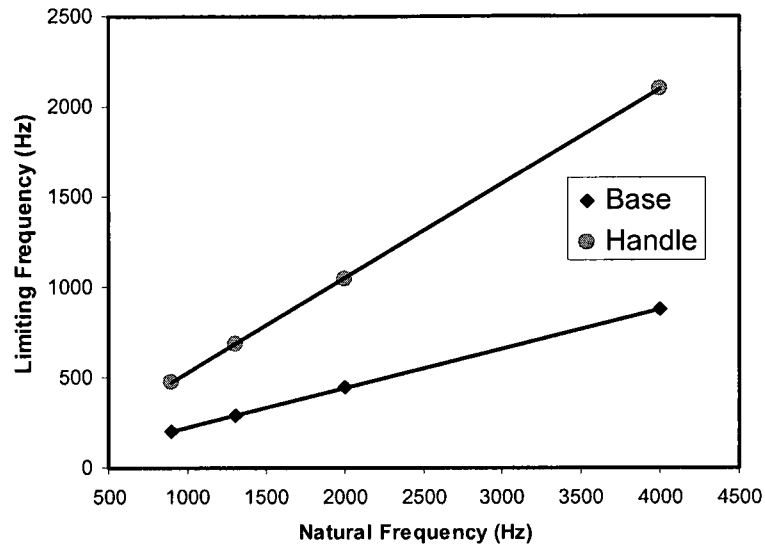
Figure 2.10: Relationship between handle resonant frequency and the limiting frequency derived from deviation in APMS magnitude response of the model.
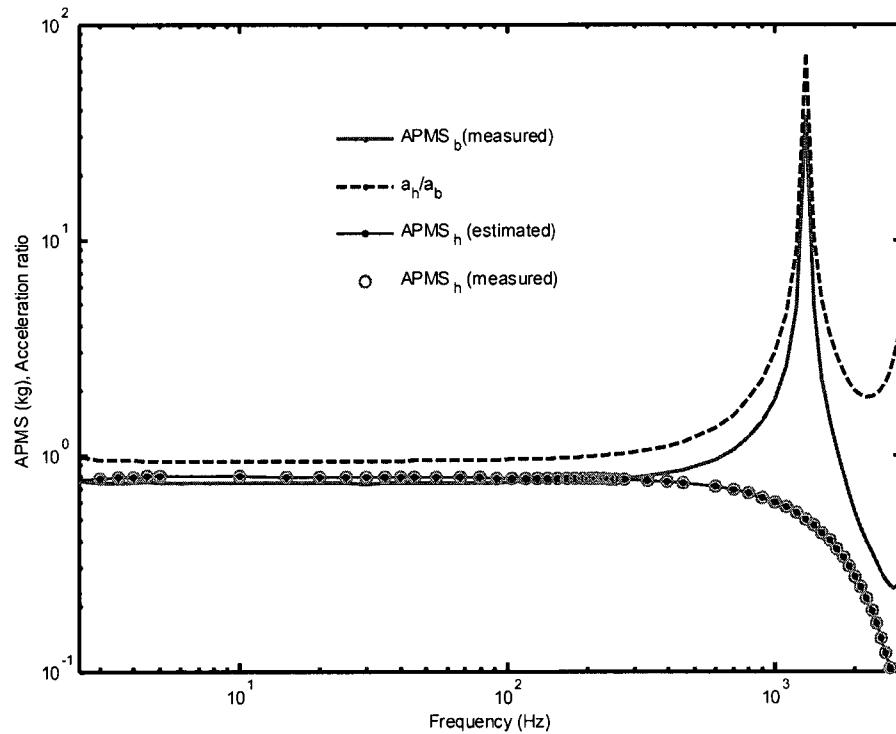
Figure 2.11: Relationship between APMS of the 40 mm instrumented handle at different measurement locations and its acceleration transmissibility.

transmissibility is greater than the peak $APMS_b$ magnitude; the ratio of $APMS_b$ to acceleration transmissibility ($APMS_h$) thus yields a value lower than the constant APMS observed at frequencies below 250 Hz.

The validity of this limiting frequency for reliable measurement of DPMI responses of the human hand-arm system, however, cannot be established due to coupling between the hand and handle, and lack of reference impedance data. An analyses of error in the hand-arm impedance magnitude corresponding to f_L, however, is attempted using the measured data for the four handles and the model simulation results with a range of natural frequencies. The deviation between the impedance magnitude of the hand-arm system measured with a particular handle at its f_L from the mean value of all the datasets acquired with different handles at the same frequency is evaluated and summarized in Table 2.5 for both measurement locations. The results suggest that impedance error corresponding to f_L of each handle ranges from 0.8 to 12.2 %. The 40 mm tubular handle with the highest natural frequency yields the least deviation.

The deviations are also computed from the model simulation with respect to mean value at each f_L by considering different natural frequencies, and the results are summarized in Table 2.6. The table shows that the handle model yields larger deviation when its natural frequency is much larger than the baseline value of 1305 Hz. The deviations and percentage error obtained from the model results are greater than those from the experimental results. Despite the limitations of the linear models, it is interesting to note that the mean impedance magnitudes derived for both locations are quite close. The percentage deviations between the experimental and simulation results are in the orders of 1.6 % and 2.5 %, respectively, for measurements at the base and the handle.

Table 2.5: Hand-arm impedance magnitudes at the limiting frequency of different handles from the measured data.

Handle type and diameter	Impedance at Limiting/Reliable Frequency					
	Measurement at Base			Measurement at Handle		
	f_L (Hz)	Impedance (Ns/m)	% Error	f_L (Hz)	Impedance (Ns/m)	% Error
40 mm Tube	300	280.3	0.8	800	261.3	2.4
40 mm Instrumented	250	308.0	10.8	395	285.0	6.5
40 mm Solid	260	256.5	7.8	790	235.0	12.2
50 mm Instrumented	280	267.4	3.8	420	289.1	8.0
Mean		278.1			267.6	
Standard deviation		22.2			24.9	

Table 2.6: Hand-arm impedance magnitude at the limiting frequency of handle models

Natural Frequency of handle model	Impedance at Limiting/Reliable Frequency (Ns/m)					
	Measurement at Base			Measurement at Handle		
	f_L (Hz)	Impedance (Ns/m)	% Error	f_L (Hz)	Impedance (Ns/m)	% Error
4000 Hz	875	328.5	20.2	2100	375.0	43.7
2000 Hz	445	277.4	1.5	1045	250.2	4.1
1305 Hz	290	259.0	5.2	685	218.0	16.5
900 Hz	200	228.5	16.4	475	200.6	23.1
Mean		273.4			261.0	
Standard deviation		41.9			78.8	

This suggests that the handle model yields reasonably good prediction of impedance magnitude around f_L, and that the error in impedance response may be estimated from deviation in the handle apparent mass as suggested in [70].

2.6 Mass Cancellation and Handle Dynamics

The magnitude of apparent mass of the hand-arm system approaches a very low value at high frequencies compared to that of the handle and its support. The mass cancellation of the measured impedance data at such frequencies could thus lead to some errors. The measured impedance magnitudes of the handle alone and the coupled hand-arm-handle system for the 40 mm instrumented handle, on the basis of both the handle
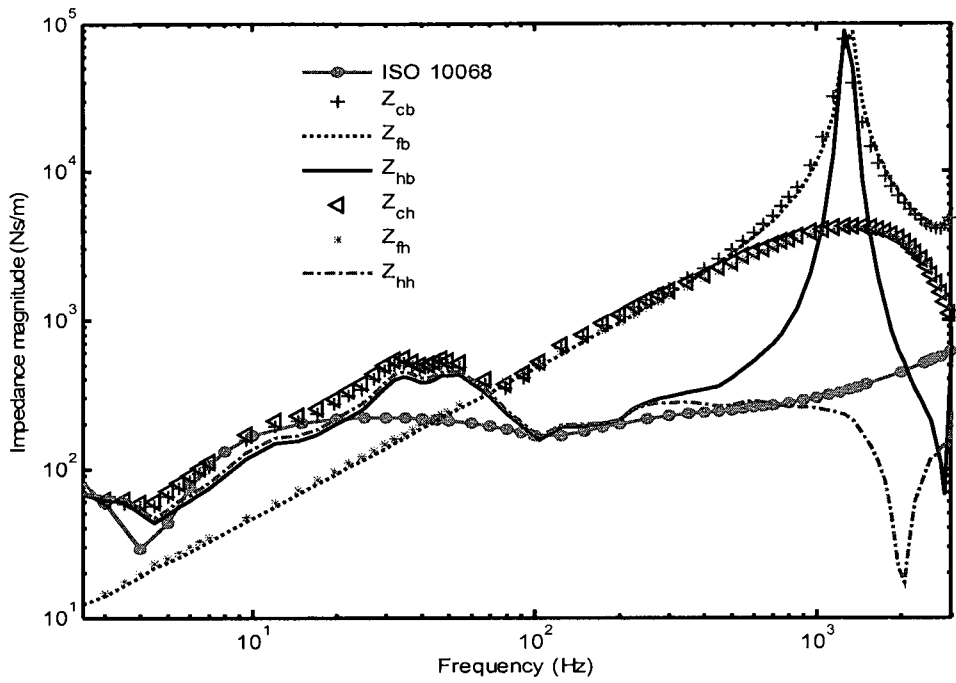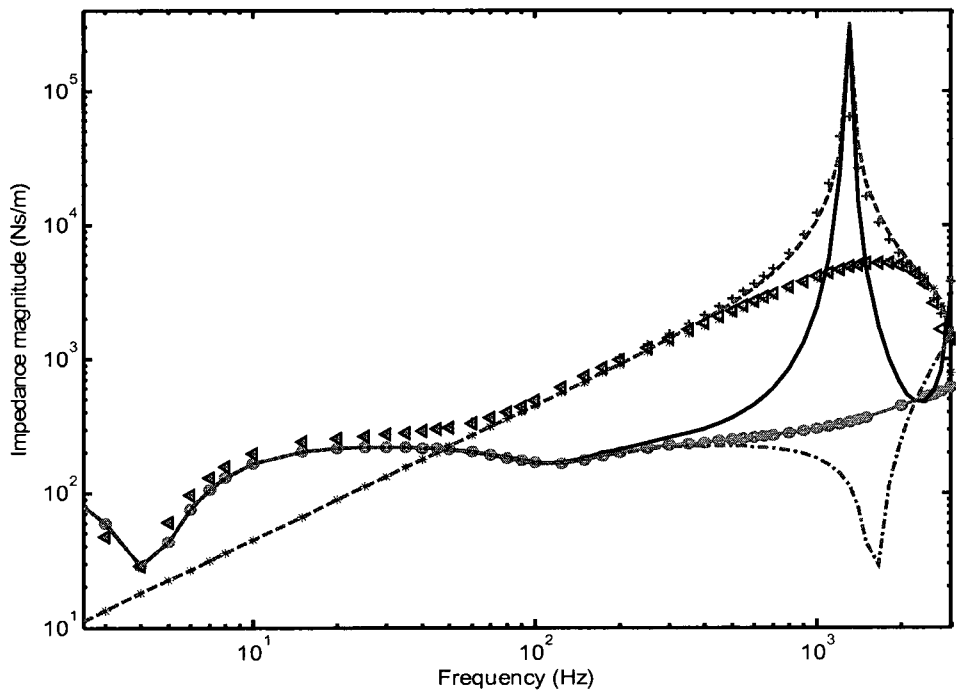
Figure 2.12: Comparisons of impedance magnitude responses of the handle, hand-arm and coupled handle-hand-arm systems obtained with the 40 mm instrumented handle:(a) experimental measurements; and (b) simulation results.

and base accelerations, are presented in Figure 2.12(a). The figure also present the impedance magnitudes attained after mass cancellation together with the ISO 10068 model results. Figure 2.12(b) illustrates the same responses obtained from the models, which show trends identical to those of the measured data. In the figure, Z_{cb}, Z_{fb}, Z_{hb} are the impedance magnitudes, on the basis of base acceleration, for coupled hand-arm-handle, handle alone and hand-arm alone, respectively; while Z_{ch}, Z_{fh}, Z_{hh} represent impedance magnitudes on the basis of handle acceleration. The impedance response of the handle increases linearly with frequency, until the handle deformation and resonant frequency distort its mass-like behavior, irrespective of the acceleration measurement location. The impedance magnitudes of the coupled hand-arm-handle system and the handle alone are nearly the same in the 75-500 Hz frequency range. The differences at frequencies below 75 Hz are attributed to dynamics of the hand-arm system, while those at frequencies above 500 Hz are partly due to the handle dynamics. The experimental and analytical results suggest that the contributions due to handle dynamics at higher frequencies are not entirely eliminated by mass cancellation. This can be attributed to relatively small apparent mass of the human hand-arm in relation to that of the handle at higher frequencies and the lack of knowledge of the handle dynamic properties in the presence of coupling with the hand and arm. The contributions of the latter is also evident from the measured data, which shows a slightly lower resonant frequency and lower peak magnitude of the coupled hand-arm-handle system when compared to that of the handle alone. Further efforts would be necessary to seek alternate methods for compensating for the handle dynamics.

2.6 Summary

Comparisons of the selected human hand-arm impedance datasets in the z_h-direction revealed extreme variabilities at frequencies above 500 Hz. From the systematic analysis of the dynamic responses of the handle, hand-arm, the coupled handle-hand-arm systems, it was concluded that discrepancies in the high frequency DPMI magnitudes are attributable to measurement location, handle natural frequency and ineffectiveness of handle mass cancellation. The impedance responses derived on the basis of measurements at the fixture base revealed sharp increase in the impedance magnitude near the handle resonance, while those based upon measurements close to the hand-handle interface resulted in either decreasing or steady magnitude at higher frequencies, and a valley at a frequency greater than the handle natural frequency. The results were subsequently used to recommend handle design guidelines to ensure measurement errors within ± 5%. The results suggest that an accurate measurement of the impedance of the hand-arm system up to 1000 Hz would require the handle natural frequency in the order of 5400 Hz and 2600 Hz, for measurements based upon the base and handle accelerations, respectively. Comparison of the measured response and the response of the 3-DOF hand-arm model, described in ISO 10068 (1998) on the basis of mean responses in the 10 - 500 Hz range, showed that the model can reasonably predict impedance responses below 10 Hz. It is suggested that researchers report the apparent mass response of the handle used during laboratory measurements up to about 2000 Hz. This can help in identifying the influence of handle dynamics on the reported impedance values and the frequency at which the reported data could be considered reliable.

CHAPTER 3

CHARACTERIZATION OF IMPEDANCE AND TRANSMITTED VIBRATION RESPONSES

3.1 Introduction

The vast majority of studies on biodynamic responses of the human hand-arm system to vibration employed 'to-the-hand' response in which the DPMI is widely reported. Only limited efforts, however, have been made on the use of 'through-the-hand-arm' method to characterize the human hand-arm system. This is mostly due to lack of appropriate sensors, difficulties associated with vibration measurement on the skin, and very small magnitudes of transmitted vibration above 200 Hz. Only a few studies on 'through-the-hand-arm' response could be found in the critical literature review on hand-transmitted vibration [64], and only one study attempted simultaneous measurement of DPMI and transmissibility responses of the hand-arm system subject to vibration from an impact hammer and a grinder [77]. Moreover, very little agreement exists among the few reported data on vibration transmission through the hand and arm, investigators also differed on the methods for the identification of resonance frequencies of the hand-arm from transmissibility magnitudes.

While the DPMI emphasizes the hand-arm interaction with the handle at the driving-point, the characterization of the vibration transmitted to different segments of the hand-arm system could provide considerable insight into the vibration modes of the structure. It is expected, therefore, that mechanical-equivalent models derived from

combined DPMI and transmissibility responses would yield a more reliable distribution of vibration power absorption in the substructures of the hand-arm system than models derived solely on either DPMI or transmissibility response. Vibration power absorption (VPA) distribution within the hand-arm system is vital for the assessment of potential injury risks of different segments of the hand-arm structure exposed to vibration. Furthermore, simultaneous characterization of both the DPMI and transmitted vibration could help identify important natural frequencies of the hand-arm system.

In this chapter, laboratory experiments were performed to simultaneously measure the DPMI and vibration transmitted to the wrist, elbow and shoulder, when the hand-arm is subjected to vibration along the z_h-axis under different hand forces, excitation magnitudes and two different postures. Natural frequencies of the hand-arm system are determined from both biodynamic responses. The mean measured data were subsequently analyzed to investigate the influence of main factors, namely the grip and push forces, hand-arm posture and excitation magnitudes, on the DPMI and transmissibility responses, using single- and multi- factor ANOVA.

3.2 A Discussion on the Reported Vibration Transmissibility Characteristics

The few studies on characterization of the human hand-arm vibration transmissibility have employed a wide range of experimental conditions, which are summarized in Table 3.1. The studies also used different techniques to attach accelerometer on the hand-arm, while the reference acceleration used to compute transmissibility was either measured at the fixture base or close to hand-handle interface.

Table 3.1: Experimental conditions employed in the selected studies on hand-arm vibration transmissibility

| Investigator | Acceleration Measurement | | Excitation | | | Grip force | Elbow angle | Handle Diameter |
	Locations	Method	Type and direction	Magnitude	Frequency range (Hz)			
Kihlberg [77]	Finger, wrist and elbow Reference	Accelerometers mounted on plastic sheet and taped to locations Handle	Grinder vibration z_h	NR	20 - 1000	50 N	110°	NR[a]
Kattel and Fernandez[97]	Wrist, elbow and shoulder Reference	Accelerometers on hand adapter and bracelets Handle	Rivet gun z_h	NR	NR	18 N 26 N	90°	NR
Reynolds & Angevine [93]	Finger, wrist, elbow and shoulder Reference	Accelerometer attached to skin using adhesive tape Handle base	Sinusoidal x_h, y_h, z_h	NR	5 – 1000	9 N 18 N	NR	19mm
Pyykko et al. [94]	Wrist, elbow and upper arm[b] Reference	Accelerometer mounted on plexiglass attached to location by a metal clamp with screws. Handle.	Sinusoidal z_h	1g, 3g and 10g rms	20 – 630	10 N 20 N 40 N	120°	25 mm
Cherian et al. [92]	Finger and elbow Reference	Accelerometer attached on a ring for the middle finger; and on an aluminum strip held by an elbow pad. Handle base	Sinusoidal z_h	0.5g peak	10 - 200	25 N	90°	38 mm
Aatola [95]	Wrist Reference	Accelerometer attached on acrylic plate held tight by hose clamp. Handle	Sinusoidal z_h	2.5, 7.9 and 25 ms^{-2}	10 - 300	10 to 40 N	150°	26 mm
Sakakibara et al. [98]	Head Reference	Accelerometer attached on bite-bar. Handle	Sinusoidal x_h	3.15, 10.1, 31.5 ms^{-2}	8 - 200	5 kg (pulling)	180°	NR

a -Not reported; b - in the vicinity of the elbow, medial epicondylus

The reported data exhibit considerable differences in the measured magnitudes, which are evident from the comparisons shown in Figure 3.1(a) for the wrist and in Figure 3.1(b) for the elbow. The studies reported by Kattel and Fernandez [97] and Sakakibara [98] are not included in Figure 3.1 for comparison since this study [97] reported only the weighted root-mean-square acceleration values and study [98] reported only transmissibility response of the head. The reported transmissibility response magnitudes are presented in both linear and logarithmic scales in order to clearly show the responses in the low as well as high frequency regions. Furthermore, the comparisons are limited to magnitude alone since the vast majority of the studied did not report the phase response.

(a)   (b)
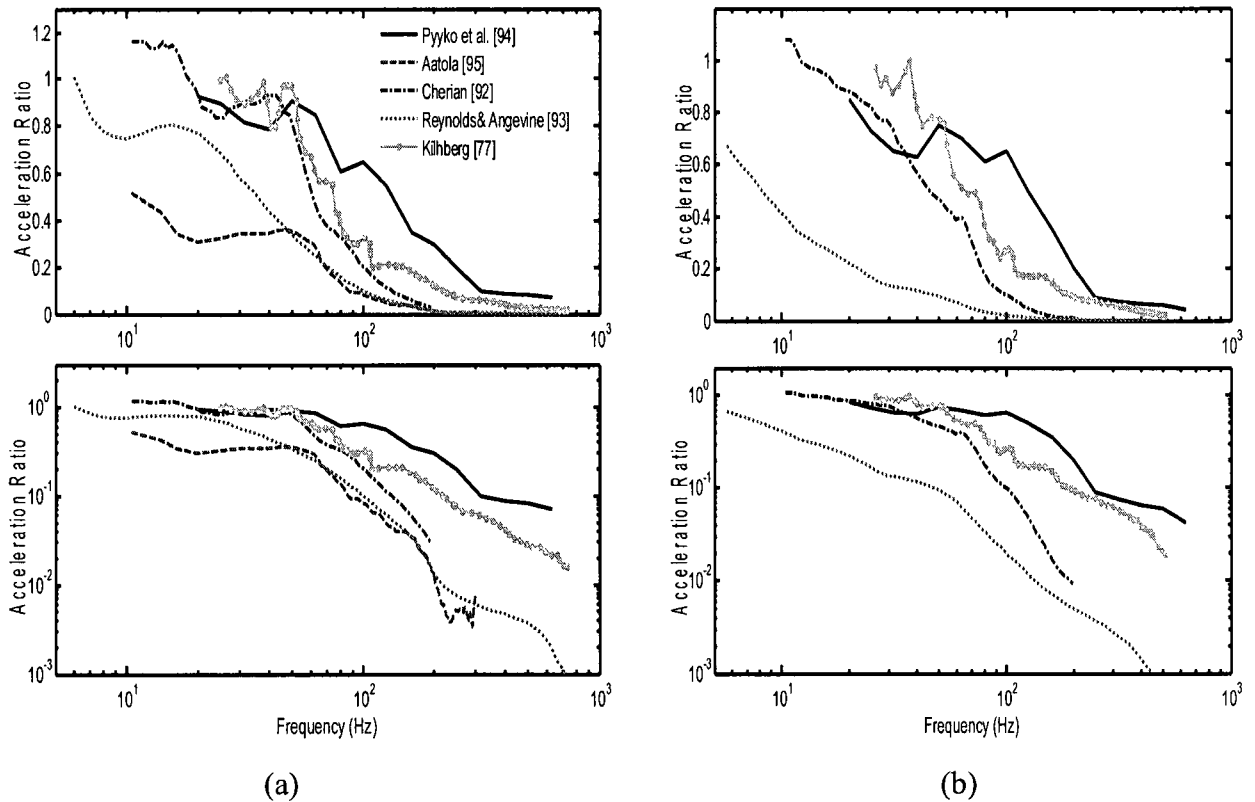
Figure 3.1: Comparisons of transmissibility magnitudes reported in selected studies:
(a) wrist; and (b) elbow.

The comparisons show wide variations in the transmissibility magnitudes, which could be mostly attributed to differences in the experimental conditions, human subjects, measurement and analysis methods, and methods of fixing accelerometers to the hand and arm. All of the reported data, however, consistently shows peaks and a rapid attenuation in the transmissibility magnitudes with increase in frequency. Furthermore, the studies have considered reference acceleration measured either directly at the handle or the base of the handle fixture, which may also contribute to the differences that may arise from the dynamic behavior of the handle and fixture. These have also resulted in many contradictory conclusions. For example, a negligible effect of handle vibration level on the transmitted vibration was reported in [95], while other studies have shown higher transmitted vibration under higher levels of vibration [94, 98].

The studies also differ on the method of identification of resonant frequencies of the hand-arm system from transmissibility magnitudes, although the majority did not attempt to identify the resonance frequencies due to lack of conspicuous magnitude peaks since transmissibility magnitudes were presented in logarithmic scale. In one study, the frequencies corresponding to the valleys in the magnitude response were reported as the resonant frequencies [94], while in another study, those corresponding to peaks in the imaginary component of the transmissibility function were reported as resonant frequency [95]. However, the conventional technique of identifying resonance (characteristic) frequencies is the frequencies corresponding to the peaks in the frequency response function or transmissibility magnitudes [130]. The data however exhibit peaks in the magnitudes within comparable frequency bands. The characteristic frequencies of the human hand-arm, identified from Figure 3.1, are summarized in Table 3.2, which can

Table 3.2: Characteristic frequencies identified from reported transmissibility magnitudes shown in Figure 3.1

Investigator	Characteristic frequencies (Hz)			Frequency range (Hz)
	Wrist	**Elbow**	**Shoulder**	
Kihlberg [77]	32, 50, 74, 105, 152	33, 51, 101,146, 306	-	20 - 1000
Cherian et al. [92]	16, 40, 80	16, 30, 65	-	10 - 200
Reynolds & Angevine [93]	10, 65, 130, 410	7, 138, 484	12, 200	5 – 1000
Pyykko et al. [94]	50, 102, 200	50, 102	-	20 – 630
Aatola [95]*	25, 50, 96, 154	-	-	10 - 300

* 31, 138 and 201 Hz are obtained from the formulae in reference [95] for 30 N grip force

be grouped into five different bands: 7 – 16 Hz, 30 – 50 Hz, 65 – 80 Hz, 90 – 140 Hz, 150 – 200 Hz. Some of these characteristic frequency bands compare reasonably well with those estimated from the impedance responses.

Furthermore, the likelihood of considerable errors existed in some of the earlier studies where the data were directly plotted on the graph papers [93, 94]. Moreover, the effect of push force on the transmitted vibration has not been investigated, which is known to have notable effect on the low frequency DPMI responses [82]. The above discrepancies suggest the need for further systematic measurements of the vibration transmissibility responses of the hand-arm system under a range of important influencing factors, namely the grip force, push force, posture and the vibration level. The resulting data on the localized vibration responses could help derive more reliable models capable of predicting distributed VPA and localized deformations for assessment of potential exposure injury risks.

3.3 Dynamic Characteristics of the Hand-arm Model reported in ISO 10068.

The driving-point mechanical impedance and transmissibility responses of the idealized mechanical equivalent models of the human hand-arm system are critically investigated in order to enhance understanding and interpretations of the experimental data. The 3-DOF hand-arm model in the z_h-axis reported in ISO 10068 [86] is considered for the analysis, since it has been shown that the response of the 3-DOF models yield good agreement with the measured DPMI [65]. The hand-arm model is coupled with the 2-DOF handle model developed in Chapter 2, as shown in Figure 2.4(a). The hand-arm model may be excited by force $f(t)$ or motion $q(t)$, as shown in Figures 3.2(a), 3.2(b) and 3.2(c). The dynamic characteristics of the model shown in Figure 3.2(c) is different from those of Figure 3.2(a), it is used just to illustrate the influence of configuration and excitation type on biodynamic responses. The motion excitation, however, reduces the DOF of the hand-arm model shown in Figure 3.2(b) to two [126]. Although the model masses do not relate to the anatomical structure of the hand-arm system, the vibration transmissibility of individual masses (m_1, m_2 and m_3) are evaluated with respect to the handle base motion q_b (Q_1/Q_b, Q_2/Q_b, Q_3/Q_b), and the motion in the vicinity of the handle-hand interface q_3 (Q_1/Q_3, Q_2/Q_3), as shown in Figures 3.3 and 3.4, to gain a better understanding on transmissibility responses and identification of resonant frequencies. The transmissibility responses of the 3-DOF force- and 2-DOF motion-excited hand-arm system models are similar to those of the coupled handle-hand-arm model with respect to q_3 but different from those of the 3-DOF motion-excited transmissibility responses, as shown in Figure 3.4.

74
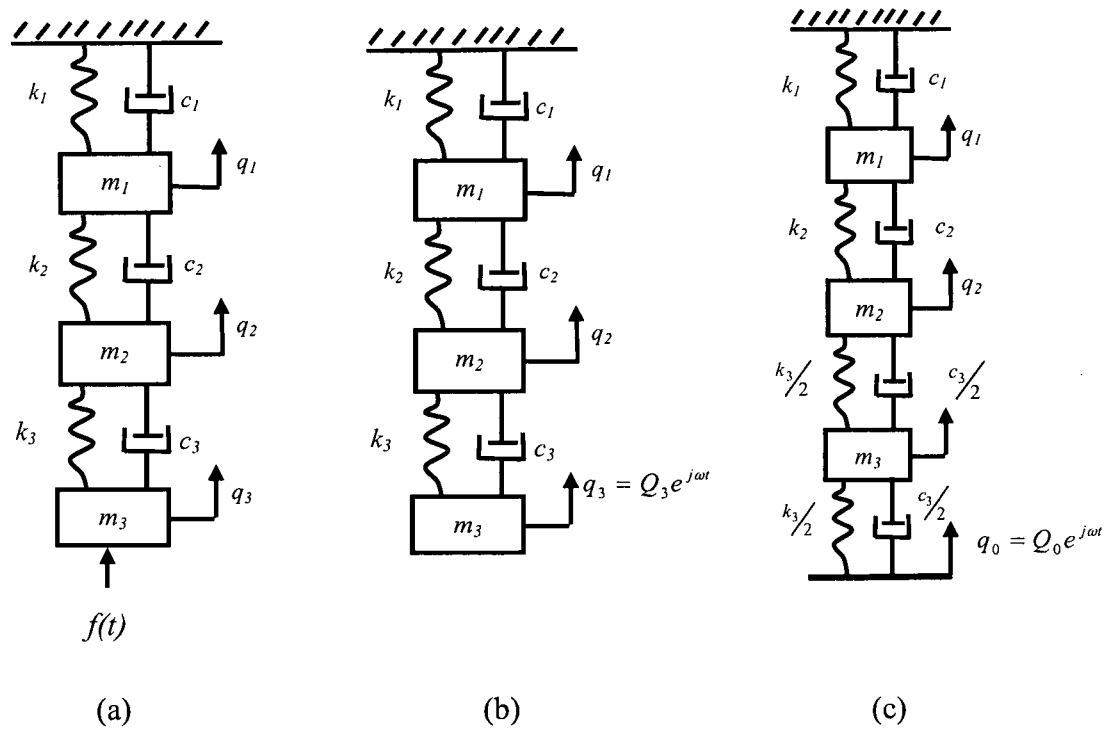
Figure 3.2: Different configurations of the 3-DOF hand-arm model: (a) 3-DOF force-excited; (b) 2-DOF motion-excited; and (c) 3-DOF motion-excited.
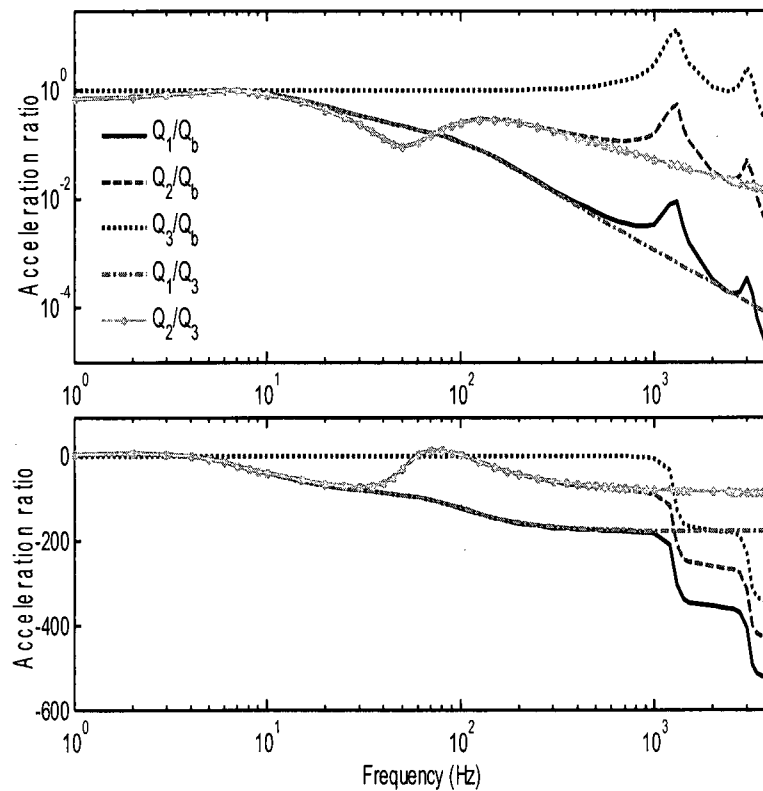
Figure 3.3: Transmissibility magnitudes of the coupled handle-hand-arm model.
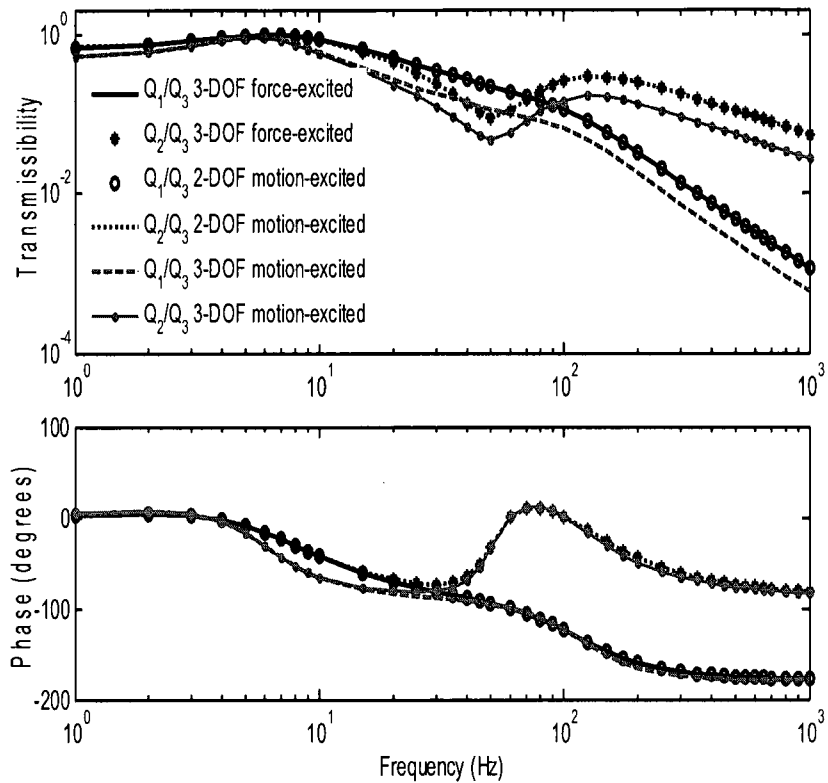
Figure 3.4: Comparisons of transmissibility responses of models shown in Figure 3.2.

The responses with respect to q_b could be related to experimental data based on the base acceleration [92 and 93], while those computed with respect to q_3 could be related to data derived on the basis of handle acceleration [77, 94, 95]. The responses with respect to the base motion (Q_1/Q_b, Q_2/Q_b, Q_3/Q_b) exhibit peaks around 1265 and 3065 Hz, which are close to the first two natural frequencies of the handle, in addition to peaks near 6.5 and 125 Hz. The responses with respect to q_3, however, show only lower frequency peaks, which suggests that the transmissibility responses relative to the hand-handle interface acceleration, q_3, are insensitive to dynamics of the handle. The response magnitudes of masses m_1 and m_2 with respect to q_b and q_3 are quite similar if the peaks corresponding

to the handle resonant frequencies are ignored. The transmissibility phase of the responses of the masses m_1 and m_2, derived on the basis of base and handle motions, are also comparable up to approximately 500 Hz. The phase responses, however, differ considerably above 500 Hz, which is attributable to the influence of damping and differences in the effective number of degree-of-freedom (DOF).

The modal parameters of the models presented in Figures 2.4(a) and 3.2 were obtained through eigen-analysis and are summarized in Table 3.3 for comparison with the characteristic frequencies obtained from transmissibility responses of the models. The natural frequencies of the uncoupled masses (for example, $\omega_{m_1} = \sqrt{k_1/m_1}$) in the standardized 3-DOF model [86] were also determined as 4.7, 107 and 67 Hz corresponding to masses m_1, m_2 and m_3, respectively. The results show that the natural frequencies associated with the hand-arm model masses (7.84 and 119.34 Hz) in the

Table 3.3: Natural frequencies of different configurations of the hand-arm model

Model	Natural Frequency (Hz)	Damping Ratio	Damped Frequency (Hz)
5-DOF coupled handle-hand-arm	7.84	0.77	4.81
	119.34	0.67	87.32
	1266.00	0.04	1264.10
	3069.60	0.03	3065.70
3-DOF force-excited	4.19	0.16	4.14
	66.82	9.22	-
	119.66	0.47	102.83
2-DOF motion-excited	7.84	0.77	4.81
	119.34	0.67	87.32
3-DOF motion-excited	5.21	0.37	4.84
	67.04	9.05	-
	119.07	0.52	100.95

coupled 5-DOF model are similar to those of the motion-excited 2-DOF model. These natural frequencies, however, differ from those of 3-DOF force- and motion-excited hand-arm vibration models, which are comparable. The differences may be due to the exclusion of mass m_3 from equations of motion of the 2-DOF motion-excited hand-arm model.

Furthermore, the two characteristics frequencies (6.5 and 125 Hz) from the transmissibility responses of the 5-DOF, 2-DOF and the 3-DOF force-excited models are considerably greater than the corresponding damped frequencies (4.81 and 87.32 Hz) of the 5-DOF and 2-DOF models, and (4.14 and 102.83 Hz) for the 3-DOF force-excited model. However, the characteristic frequencies from transmissibility responses of the 3-DOF motion-excited model are comparable with the damped frequencies obtained from eigen-analysis. It has been shown that some of the peaks in outputs only transmissibility responses, (e.g. Q_1/Q_3 from the coupled 5-DOF model) may not correspond to the mode frequencies of a system, while peaks in frequency response function (FRF), transmissibility based on output-input ratio, always yield the mode frequencies of a system [130]. This reason coupled with the very high damping of the 66.82 Hz mode may explain the observed differences.

Conversely, the two damped mode frequencies (4.14 and 102.83 Hz) from eigen-analysis, however, correspond well with the two prominent valleys in the DPMI responses of the models, as shown in Figure 3.5. The figure shows the prominent valleys in the DPMI magnitude and phase responses of the models in Figure 3.2 together with the ISO 10068 mean impedance data, similar results are obtained with APMS. The DPMI and APMS responses of the 5-DOF, 2-DOF motion- excited and 3-DOF force-excited
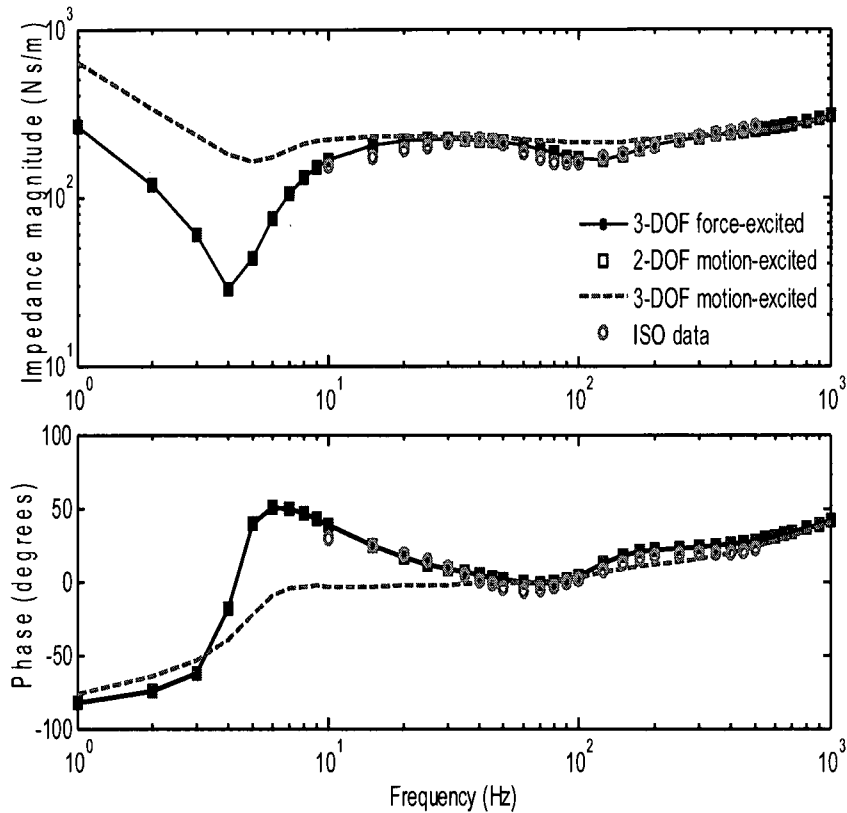
Figure 3.5: Comparison of the DPMI responses of the models shown in Figure 3.2.

models are identical and comparable with ISO mean values, while those of the 3-DOF motion-excited model differ. The results show that the characteristic frequencies corresponding to the valleys in the DPMI and APMS magnitudes of the models are identical to the damped frequencies derived from eigen-analysis. The biodynamic responses of the 5-DOF and 2-DOF motion-excited, and the 3-DOF force-excited models are similar but their eigen-frequencies are different, while the eigen-frequencies of the 3-DOF force- and motion-excited models are comparable but their biodynamic responses are different. These observations suggest that the dynamic characteristics of a system are affected by the system configuration and the type of excitation.

The relationship between resonant frequencies associated with the valleys and peaks in the DPMI magnitude and the resonant frequencies derived from eigen-analysis is further explored by considering two different idealized models of a mechanical system with two masses: a motion-excited unrestrained model and a force-excited restrained system with fixed upper mass, as shown in Figure 3.6. The models are selected based on the established fundamental principles that a restrained system at the upper end is usually excited with a force while an unrestrained system is usually excited at the base with a motion since excitation with a force will yield a semi-definite system, in which one of the natural frequencies will be zero [131]. The analogous electrical model of the force-excited mechanical system [132] is also considered. All the models are essentially a single-DOF system even though the mechanical models have two masses.
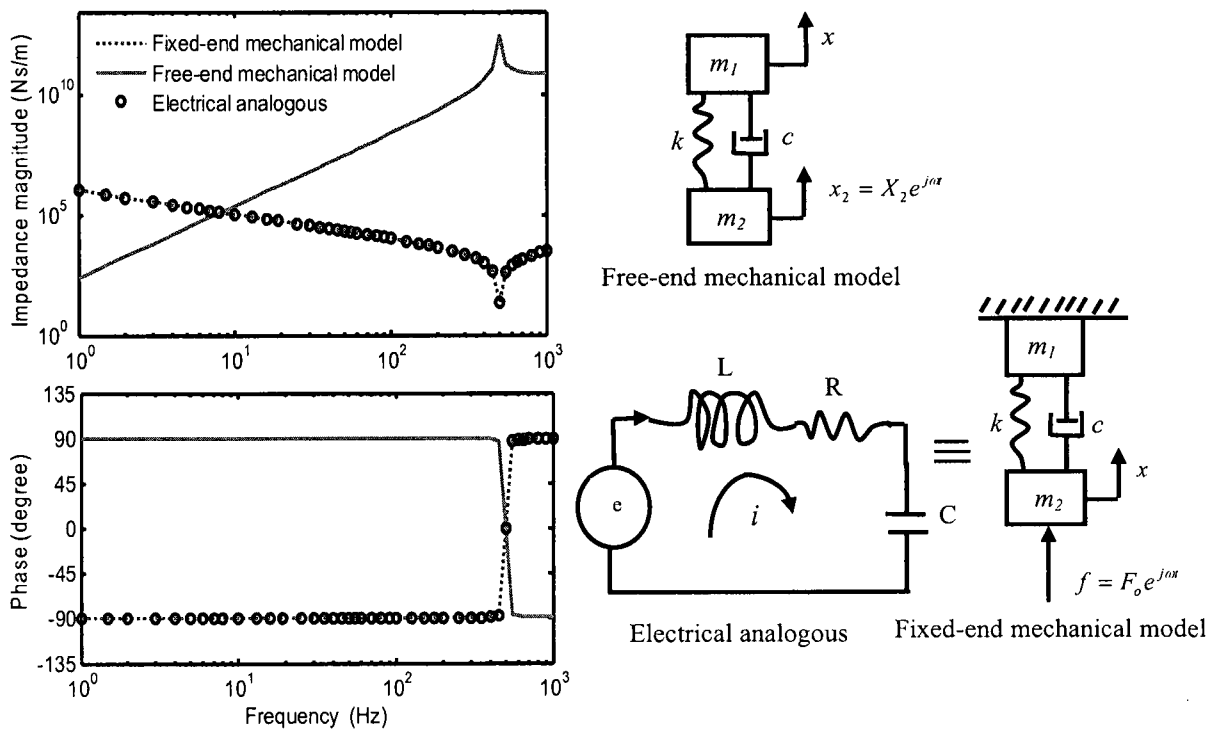
Figure 3.6: DPMI response of simple mechanical and analogous electrical systems.

The mechanical models yield considerably different impedance responses. The natural frequency of the free-end model and the fixed-end mechanical and its electrical analogous models correspond to the peak and valley, respectively. It should be noted that the biodynamic models of the hand-arm system are mostly restrained, while those of the seated body exposed to whole-body vibration are motion-excited free-end system models. The whole-body vibration models consistently show good agreements in the characteristic frequencies derived from either APMS/DPMI or transmissibility peaks with those computed from the eigen-analysis [113]. Although the reported hand-arm vibration models are mostly force-excited restrained models, with the exception of that reported by Mishoe and Suggs [71], the resonant frequencies have been generally identified as those corresponding to peaks in the measured DPMI responses [65, 67, 77, 82]. A few investigators, however, have associated these to valleys in the DPMI magnitude [71, 81].

The results attained from the analysis of biodynamic models of the hand-arm system strongly suggest that the biodynamic responses depend on the model configuration (free-free or fixed-free system) and the type of excitation, which greatly affect the identification of characteristic frequencies from the responses. It seems that the bones and tissue/muscle of the human hand-arm system form different equivalent-mechanical systems when subjected to vibration. Therefore, it is hypothesized that the peaks in the DPMI magnitude correspond to the resonant frequencies of the tissues/muscles, while the valleys correspond to resonant frequencies of the bones/structure of the human hand-arm system.

3.4 Laboratory Measurements of Biodynamic Responses of the Hand-arm System

3.4.1 Experimental set-up and methods

Laboratory experiments were performed to simultaneously measure the driving-point mechanical impedance (DPMI) and vibration transmitted to the wrist, elbow and shoulder of six male subjects while grasping a 40 mm diameter handle excited along the z_h-axis. The experiments were performed using two hand-arm postures ($P1$ – bent-arm with $90°$ elbow angle; and $P2$ – extended arm with $180°$ elbow angle), nine different combinations of hand forces (10, 30 and 50 N grip and 25, 50, 75 N push forces), and two levels of broad-band random excitation (frequency-weighted rms acceleration a_{hw}= 2.65 and 5.25 m/s^2) in the 2.5 - 2500 Hz frequency range. Tables 3.4 and 3.5 summarize the anthropometric parameters of the subjects and the test matrix, respectively. A 40 mm diameter cylindrical aluminum handle with integrated two force sensors to measure the grip force was used in the study. Additional two force sensors were mounted between the

Table 3.4: Anthropometric data of six subjects.

Parameters	Range	Mean	Standard deviation
Age (years)	26 - 53	36.50	11.33
Height (m)	1.71 - 1.80	1.74	0.02
Weight (kg)	61 - 86	72.17	9.87
BMI	20.4 - 28.7	23.82	3.13
Hand length (cm)	17 - 20.5	18.42	1.20
Hand breath at thumb (cm)	9.5 - 12.0	10.92	0.86
Hand breath at metacarpal (cm)	7.0 - 8.5	7.50	0.63
Hand thickness (cm)	2.0 - 3.7	2.87	0.55
Wrist diameter (cm)	16.0 - 18.5	17.25	1.04
Forearm diameter (cm)	25 - 32	28.00	2.53
Elbow diameter (cm)	24.4 - 30.5	26.42	2.22
Forearm length (cm)	24.0 - 28.5	26.00	1.58
Upper arm diameter (cm)	28 - 33	29.25	3.13
Upper arm length (cm)	18 - 24	20.50	2.35

Table 3.5: Test matrix

Number of subjects:	6 males
Excitation:	
Type	Broad-band random
Axis	z_h
Magnitudes (Frequency-weighted) (a_{hw})	2.65 and 5.25 m/s^2
Frequency range:	2.5 – 2500 Hz
Hand Forces:	
Grip (F_g)	10, 30, 50 N
Push (F_p)	25, 50, 75N
Posture:	
P1	Elbow angle of 90°
P2	Elbow angle of 180°

handle supports and the base fixture for measurement of the push and total dynamic forces. The handle with its base was attached to an electro-dynamic exciter. The measured grip and push forces were low-pass filtered and displayed to the subjects at a rate of 4 samples/s to serve as a feedback to the subjects, who were advised to maintain the desired hand forces within ± 2 N by monitoring the displayed forces on a flat screen monitor. The handle acceleration was measured with a PCB SEN026 tri-axial accelerometer installed inside the handle but acceleration in the z_h-axis alone was considered. This also served as the feedback control signal for the vibration exciter controller. Figure 3.7(a) illustrates the schematic diagram of the experimental set-up.

Vibration transmitted to four different locations on the hand-arm was measured using tri-axial PCB accelerometers attached on Velcro strips, which were tightly fastened near the joints to minimize the contributions due to skin artifacts, while the correction for the skin deformation was not attempted. The responses at the wrist and shoulder were measured along the y_h- and z_h-axis, while those around the elbow were measured in the three axes. Vibration transmission measurements near the elbow were performed on the
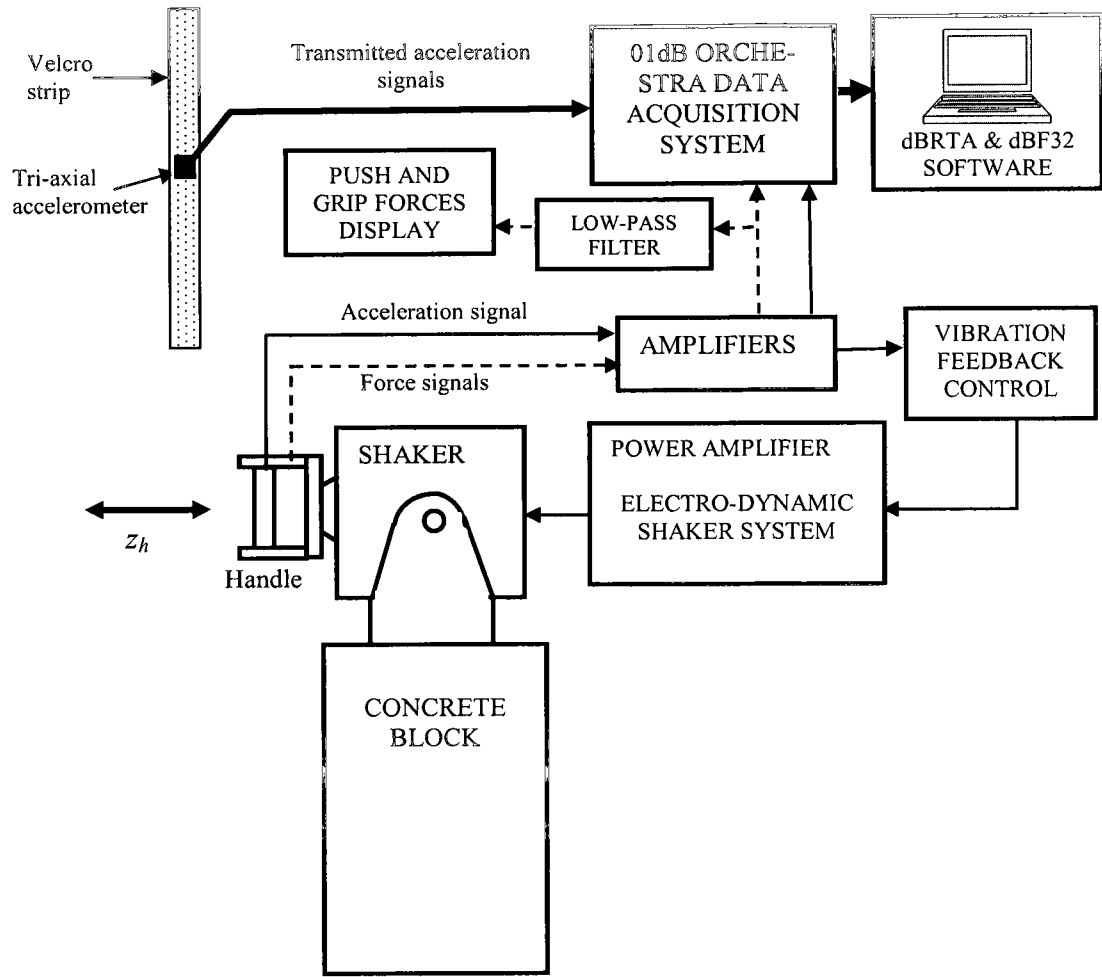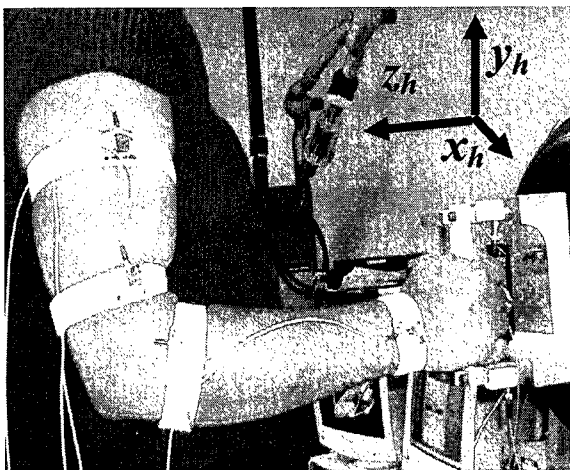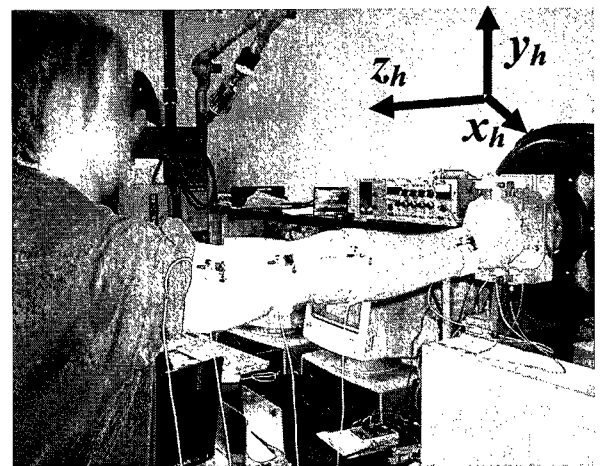
Figure 3.7: Experimental set-up: (a) schematic diagram of the measurement set-up; (b) measurement locations for *P1* posture; (c) measurement locations for *P2* posture

forearm and upper-arm sides, referred to as "Elbow 1" and "Elbow 2", respectively, as shown in Figure 3.7 (b) and (c). The measured data were analyzed to derive DPMI at the hand-handle interface, which was subsequently corrected for the handle inertia effect. The vibration transmissibility at the four different segments of the hand-arm system relative to the z_h-axis handle acceleration using the H_1 frequency response estimator was obtained, such that:

$$T_{W_i}(j\omega) = \frac{S_{a_{Wi},a_h}(j\omega)}{S_{a_h}(j\omega)}; \qquad i = y_h, \ z_h \tag{3.1}$$

$$T_{E_{ji}}(j\omega) = \frac{S_{a_{Eij},a_h}(j\omega)}{S_{a_h}(j\omega)}; \qquad i = x_h, y_h, \ z_h; \ j = 1, \ 2 \tag{3.2}$$

$$T_{S_i}(j\omega) = \frac{S_{a_{Si},a_h}(j\omega)}{S_{a_h}(j\omega)}; \qquad i = y_h, \ z_h \tag{3.3}$$

where T_{W_i}, $T_{E_{1i}}$, $T_{E_{2i}}$ and T_{S_i} are the acceleration transmissibility responses measured at the wrist, elbow 1, elbow 2 and the shoulder, respectively, along direction i ($i = x_h$, y_h, z_h). S_{a_h} is the auto-spectrum of the handle acceleration and S_{q,a_h} is the cross-spectrum of a response acceleration q with the handle acceleration. The coherence of the DPMI and transmissibility was also monitored during experiments to ensure reliability of the data. Measurements were acquired and analyzed using Orchestra 01dB multi-channel data acquisition and analysis system.

The measurements of vibration at the skin surface are known to be sensitive to relative motions of the skin. The Velcro strips containing the accelerometers were thus fastened sufficiently tight to minimize the skin artifacts, while the subjects comfort was also ensured. Repeatability of the measurements was also ensured by repeating each trial

three times. The reproducibility of the measurement method was also examined with two subjects. For this purpose, repeated measurements were performed with the two subjects gripping the handle with 30 N grip and 50 N push forces assuming $P1$ posture under 5.25 m/s^2 excitation. The Velcro strips were removed and re-fastened between consecutive measurements. The reproducibility of the data was evaluated in terms of peak standard deviation of the mean data and the corresponding frequency at which it occurred.

The inter-subject variability in the measurements was analyzed from the mean measured data of six subjects corresponding to the condition used for the reproducibility test. The acceleration transmissibility magnitudes were evaluated in both linear and logarithmic scales for a better understanding of responses in the low and high frequency regions. The characteristic frequencies corresponding to peaks and valleys in the mean impedance responses of subjects, and the peaks in the vibration transmissibility responses were obtained and compared to identify resonant frequencies of the human hand-arm system. Effects of all the main factors (grip and push forces, posture and excitation level) on impedance and transmissibility responses were analyzed through observed trends in the responses and through statistical analyses, as described in the following sub-section.

3.4.2 Statistical analysis of the data

The influences of different factors on the human hand-arm biodynamic responses were often studied from the mean of measured responses of different subjects with diverse anthropometry parameters. In such approach, the effect of inter-subject variations may affect the results. Statistical analysis of variance (ANOVA) is now widely used to study and quantify the influences of the main contributing factors on biodynamic responses [67, 97, 128].

In this study, the effects of main factors on the DPMI and transmissibility magnitude responses are evaluated through ANOVA using the Statistical Product and Service Solutions (SPSS) software. Two different study designs were used for the analysis of data obtained with subjects who were available for all the experimental conditions in order to attain balanced ANOVA designs. The purpose of the first design was to study the effect of all the main factors on the responses. This involves a factorial design of two levels of posture (P), two levels of excitation magnitudes (a_{hw}), three levels of grip force (F_g) and three levels of push force (F_p), as shown in Table 3.6(a). The second design involved the effects of grip and push forces, and excitation magnitude on the responses for each posture considered separately (Table 3.6(b)). The response magnitudes were obtained at eleven different frequencies that were selected around the characteristic frequencies obtained from both the DPMI and transmissibility responses.

Table 3.6: ANOVA designs for DPMI response: (a) 2x2x3x3 factorial design; and (a) 2x3x3 factorial design for DPMI response magnitudes for each posture.

(a)

Posture (P)	Excitation (a_{hw})	Grip Force (F_g)	Push Force (F_p)	DPMI
$1 = 90°$	$1 = $ high (5.25 m/s^2)	$1 = 10$ N	$1 = 25$ N	Subject 1
$2 = 180°$	$2 = $ low (2.75 m/s^2)	$2 = 30$ N	$2 = 50$ N	Subject 2
		$3 = 50$ N	$3 = 75$ N	Subject 3
				Subject 4

(b)

Excitation (a_{hw})	Grip Force (F_g)	Push Force (F_p)	DPMI
$1 = $ high (5.25 m/s^2)	$1 = 10$ N	$1 = 25$ N	Subject 1
$2 = $ low (2.75 m/s^2)	$2 = 30$ N	$2 = 50$ N	Subject 2
	$3 = 50$ N	$3 = 75$ N	Subject 3
			Subject 4

The univariate General Linear Model (GLM) ANOVA in SPSS software was used to analyze the two ANOVA designs for DPMI magnitudes. The transmissibility magnitudes at the four measurement locations, wrist, elbow 1, elbow 2 and shoulder, were each considered as dependent variables hence multivariate GLM was used for the analysis of the two designs for transmissibility magnitudes. The measurement direction was considered as an additional main factor in the first design for transmissibility responses, while the second design was also analyzed in the z_h- and y_h-axis for each posture.

3.5 Repeatability and Reproducibility of Measurements

The repeatability and reproducibility of the measured data corresponding to 90° elbow angle posture, 30 N grip and 50 N push hand forces and weighted acceleration level of 5.25 m/s^2 were analyzed. The selected hand forces are identical to those recommended in ISO 10819 [117] for the assessment of anti-vibration gloves. Moreover, this hand forces combination was judged as the most comfortable, easily controllable and could be maintained for relatively long period of time by all the subjects. Comparisons of the repeated measurements revealed reasonably good agreements for all subjects. As an example: Figure 3.8 shows comparisons of measured responses over three trials with one subject. The responses are presented in terms of impedance magnitude, impedance phase and coherence. The measurements revealed peak standard deviation in DPMI magnitudes of 48.8 Ns/m at 33.6 Hz, where the mean was in the order of 347.3 Ns/m. The coherence of the force and velocity signals was also observed to be nearly unity throughout the frequency range. Figures 3.9 and 3.10 further show comparisons of transmissibility magnitudes, phase and the corresponding coherence measured at the wrist and the shoulder in the z_h- and y_h-axis, respectively, over the three trials. The repeatability of
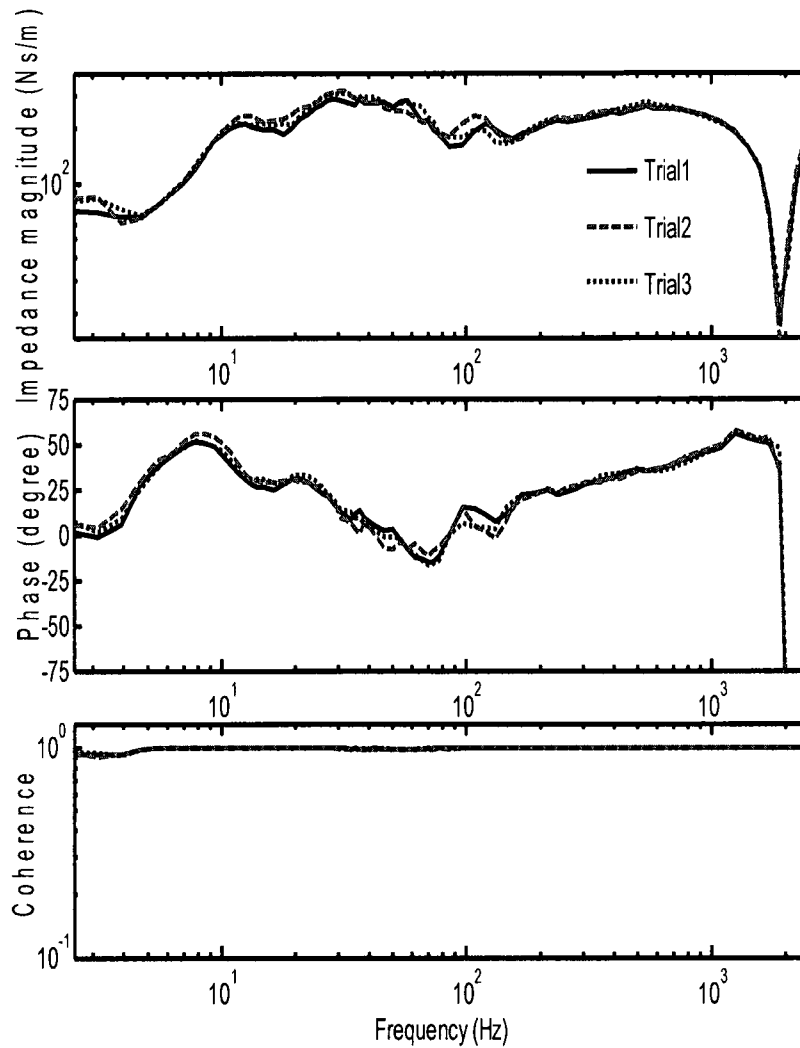
Figure 3.8: Comparisons of impedance of one subject measured during the three trials ($P1$ posture, $F_g = 30$ N, $F_p = 50$ N, $a_{hw} = 5.25$ m/s^2).

transmissibility is also reasonably good and it revealed peak standard deviation (SD) in the z_h-axis transmissibility magnitude at the wrist of 0.37 near 39 Hz, where the mean value was in the order of 1.41. The coherence in the z_h-axis measurements (Figure 3.9 (a)) was nearly unity at frequencies below 200 Hz but becomes considerably lower at 250, 300 and 400 Hz. The y_h-axis transmissibility data also revealed lower coherence at
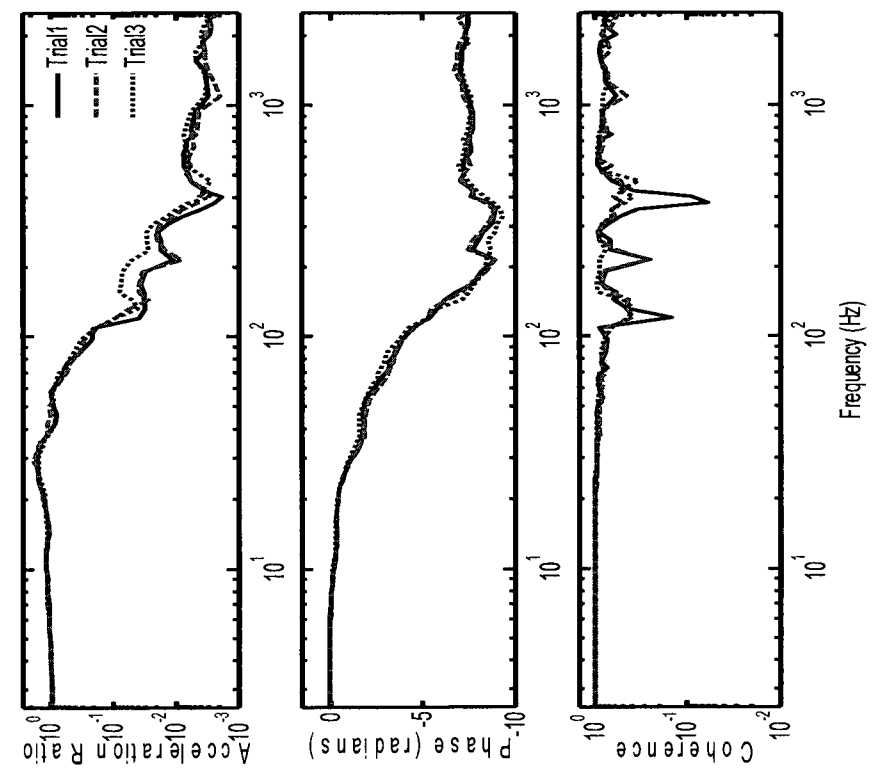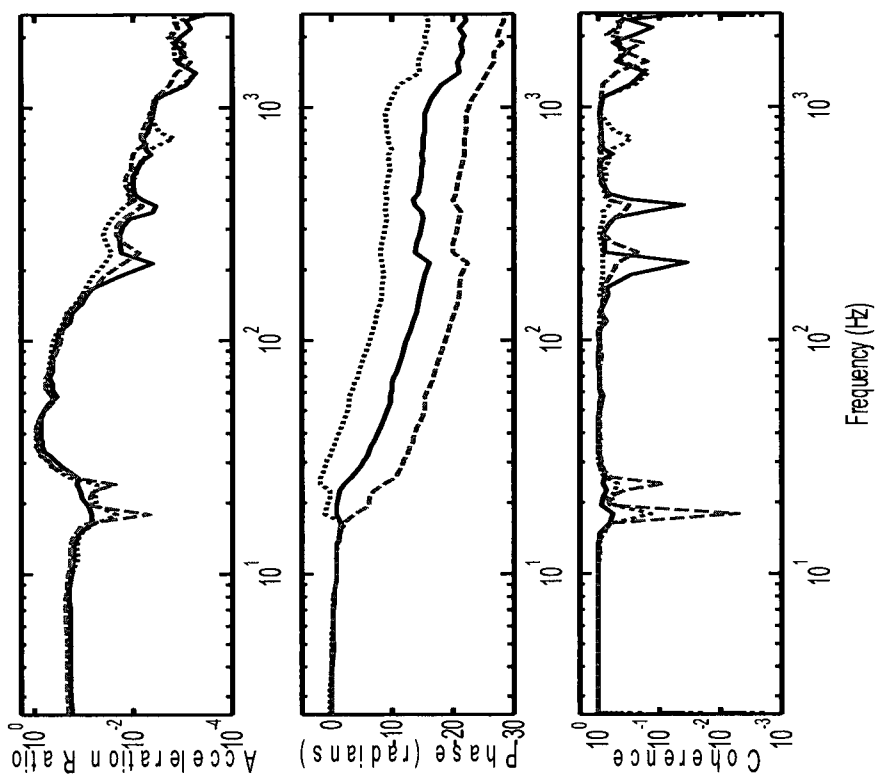
Figure 3.9: Comparisons of acceleration transmissibility of one subject measured at the wrist during three trials (*P1* posture, $F_g = 30$ N, $F_p = 50$ N, $a_{hw} = 5.25$ m/s^2): (a) z_h–axis; (b) y_h–axis.
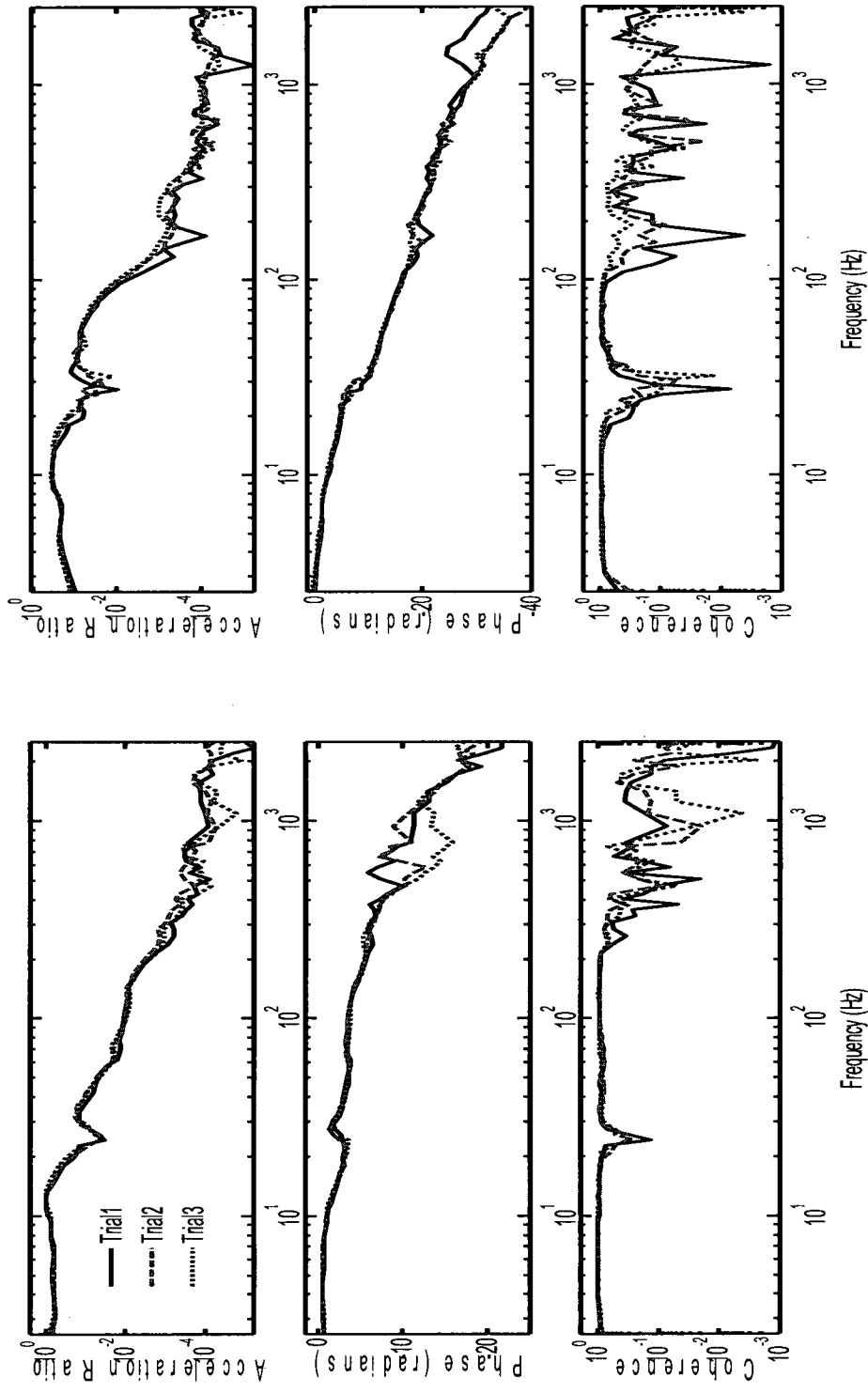
Figure 3.10: Comparisons of acceleration transmissibility of one subject measured at the shoulder during the three trials (*P1* posture, F_g = 30 N, F_p = 50 N, a_{hw} = 5.25 m/s^2): (a) z_h-axis; (b) y_h-axis.

(a)

(b)
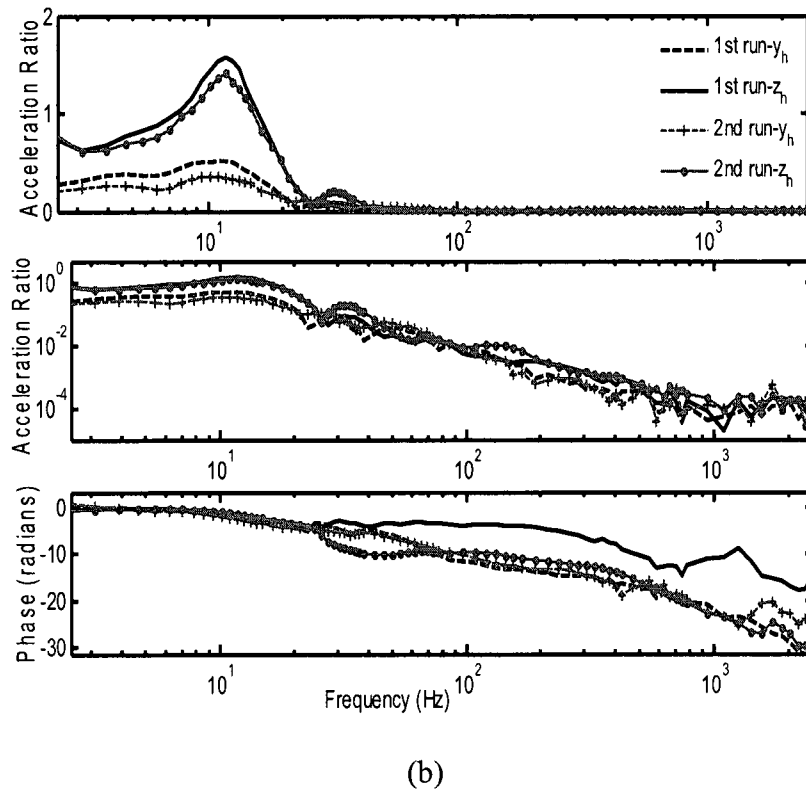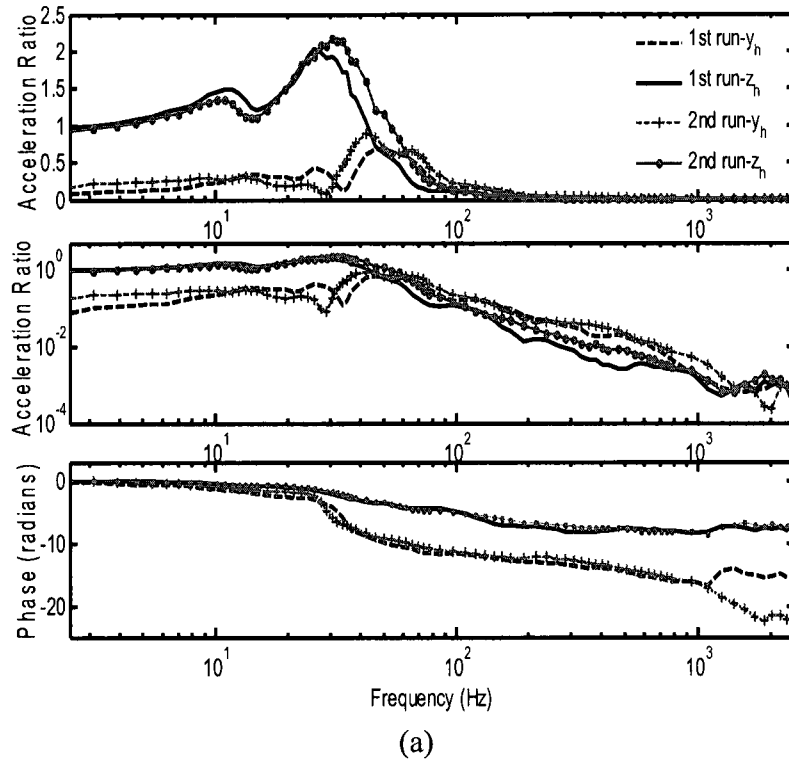
Figure 3.11: Comparisons of acceleration transmissibility of one subject during the two runs (*P1* posture, $F_g = 30$ N, $F_p = 50$ N, $a_{hw} = 5.25$ m/s^2): (a) wrist; and (b) shoulder.

frequencies above 500 Hz. Similar degree of repeatability was observed in the data acquired with most of the subjects under different conditions.

The reproducibility of the transmissibility measurements was evaluated through analysis of data acquired with two subjects. The comparisons of means and SD of two runs involving removal and installation of Velcro strips at different locations revealed reasonably good agreement, irrespective of the measurement location. Figure 3.11 illustrates comparisons of the mean transmissibility response of one subject measured at the wrist and the shoulder during the two runs. The peak SD of the mean z_h-axis transmissibility magnitudes ranged from 0.26 to 0.37 and 0.24 to 0.26 in the 35 - 39 Hz band for the two subjects. These values of standard deviations are quite comparable, which suggest that the Velcro strap-mounted accelerometer could yield reproducible measurements despite the possible variations in the tightness and orientation of the accelerometers. Considering the extremely low transmissibility magnitudes above 500 Hz and predominance of handle dynamics above 500 Hz, as illustrated in Chapter 2, the subsequent analysis of data were limited to 2.5 – 500 Hz range.

3.6 Inter-subject Variability

The mean responses attained for six male subjects revealed considerable variations. As examples, Figure 3.12 illustrates the mean DPMI response acquired with *P1* posture together with the SD, while Figures 3.13 – 3.15 show the mean transmissibility responses at the wrist, elbow 2 and shoulder, respectively. These results were obtained under F_g = 30 N, F_p = 50 N and a_{hw} = 5.25 m/s^2. The DPMI and transmissibility responses of the six subjects in the direction of excitation, z_h-axis, generally revealed comparable trends but higher deviations were observed around the

magnitude peaks. This may be associated with differences in biodynamic and anthropometric properties of the subjects. The transmissibility responses in the y_h-axis revealed relatively larger variations and lower magnitudes. The dispersions in the x_h-axis transmissibility magnitudes around the elbow were observed to be very large, as shown in Figure 3.16, while the magnitudes are comparable with those in the y_h-axis. The phase responses revealed larger deviations at frequencies above 200 Hz.
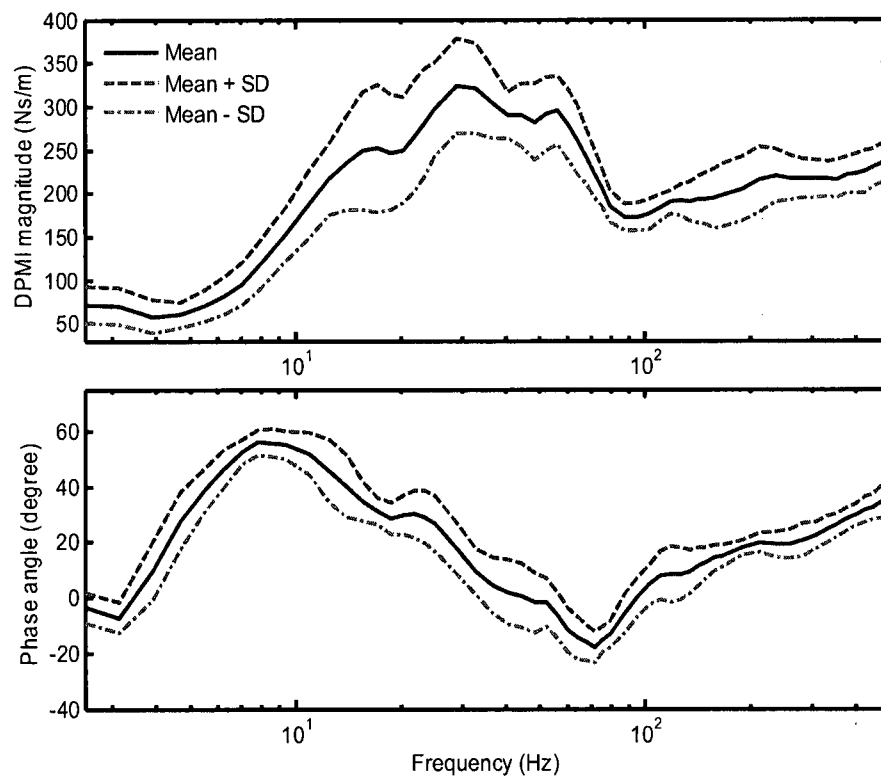
Figure 3.12: Mean and standard deviation (SD) of mean DPMI ($P1$ posture, F_g = 30 N, F_p = 50 N and a_{hw} = 5.25 m/s^2)

The observed variabilities in the magnitude and phase data acquired with six subjects appear to be considerably lower than those reported in [95, 97]. These studies reported substantial scatter in the subjects' transmissibility responses even though no
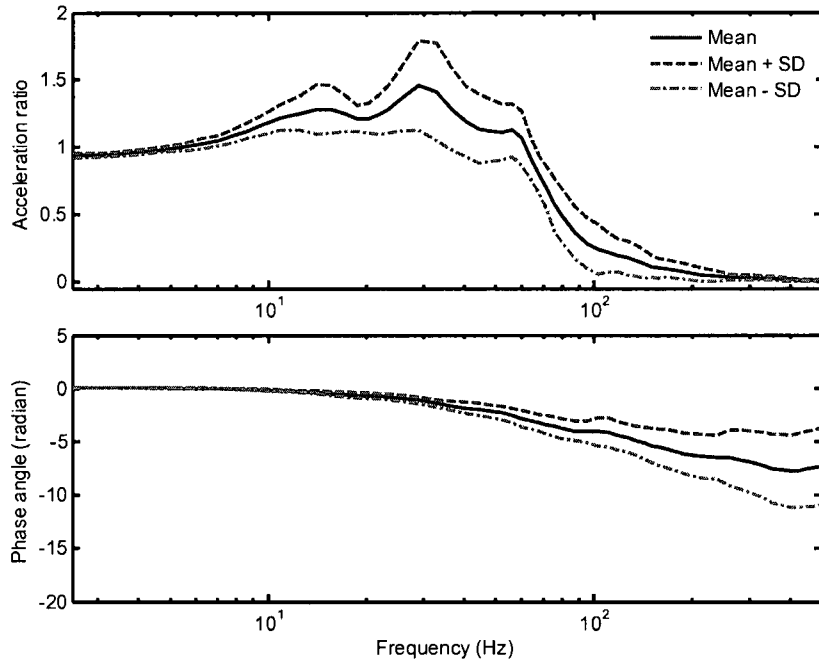
(a)
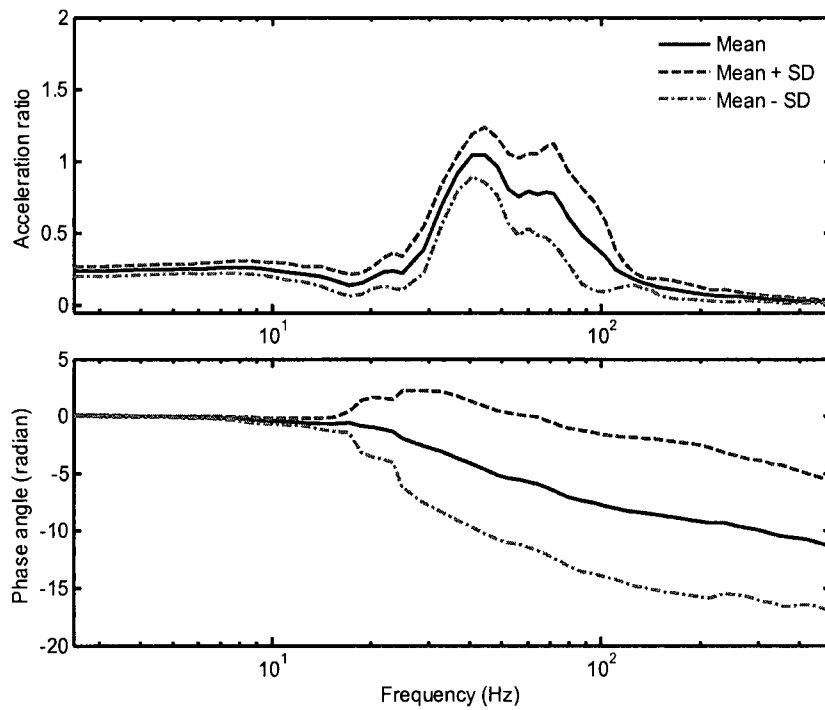
(b)

Figure 3.13: Mean and standard deviation (SD) of mean vibration transmissibility measured at the wrist ($P1$ posture, F_g = 30 N, F_p = 50 N and a_{hw} = 5.25 m/s^2): (a) z_h-axis; (b) y_h-axis.
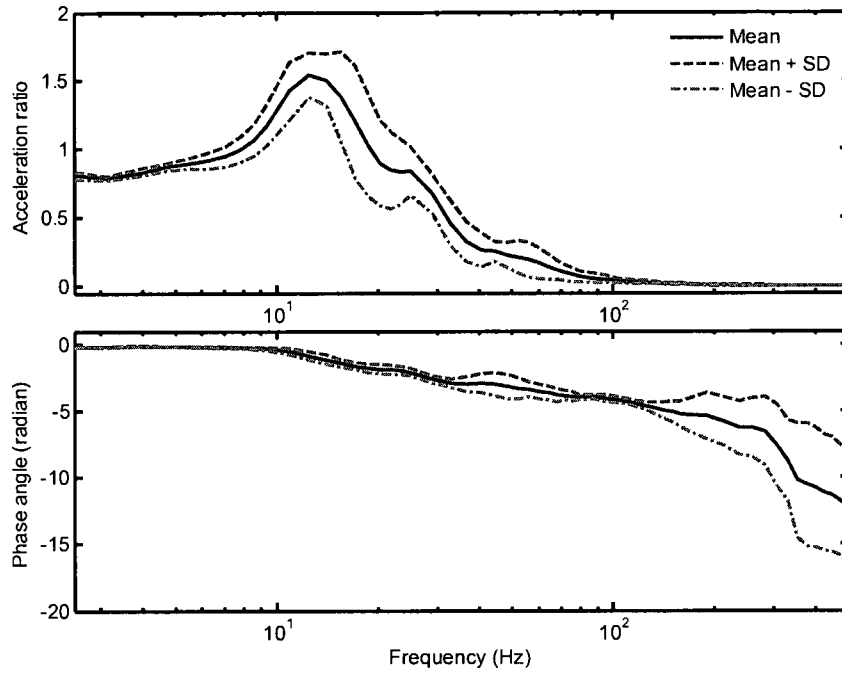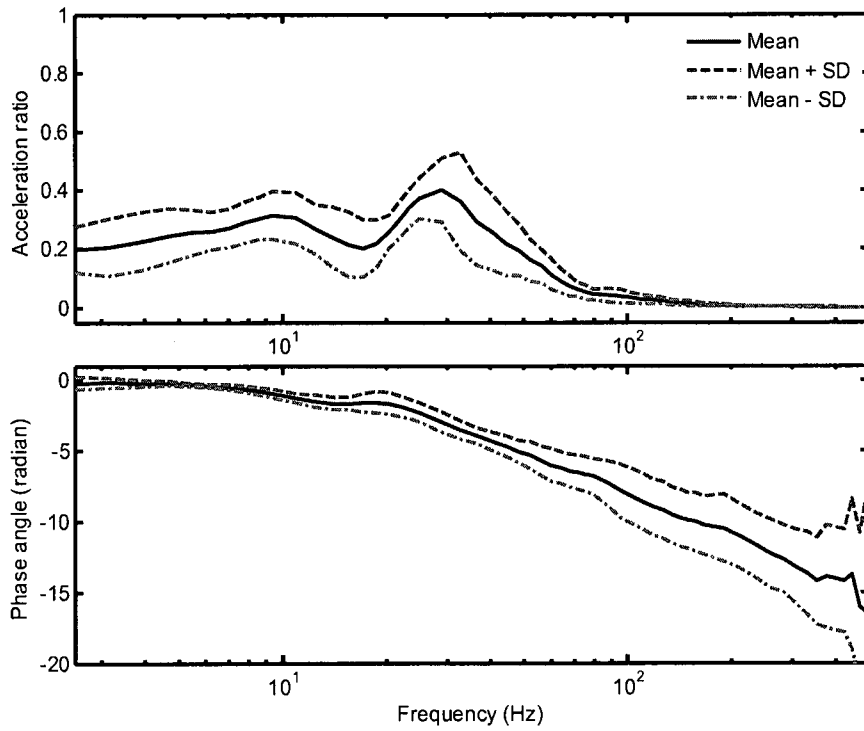
Figure 3.14: Mean and standard deviation (SD) of mean vibration transmissibility measured at elbow 2 (*P1* posture, $F_g = 30$ N, $F_p = 50$ N and $a_{hw} = 5.25$ m/s^2): (a) z_h-axis; (b) y_h-axis.
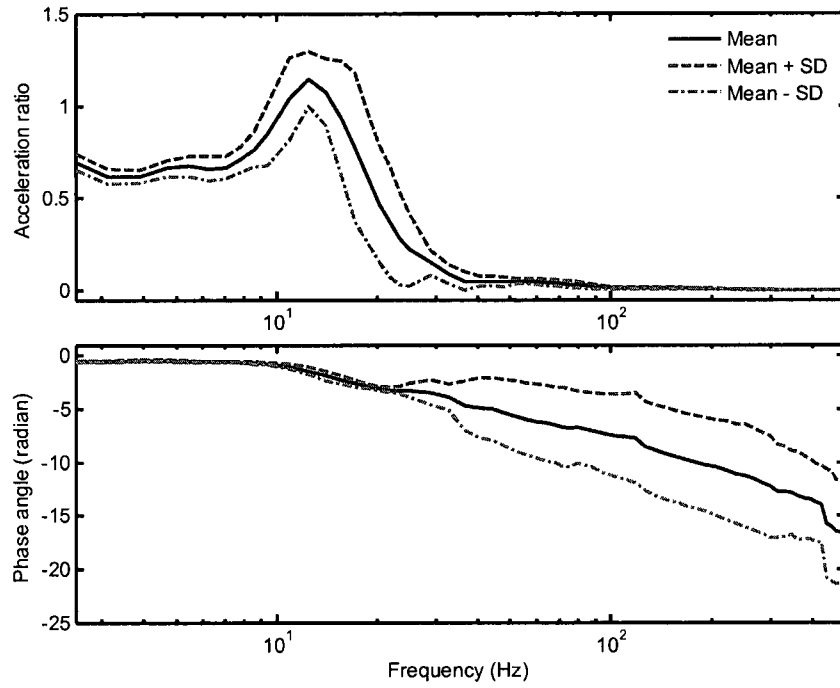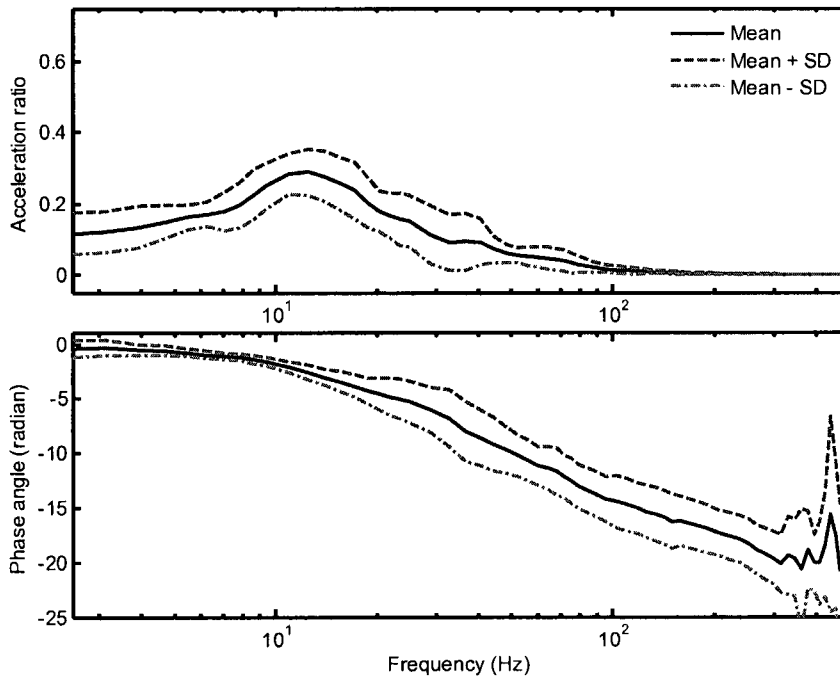
Figure 3.15: Mean and standard deviation (SD) of mean vibration transmissibility measured at the shoulder (PI posture, $F_g = 30$ N, $F_p = 50$ N and $a_{hw} = 5.25$ m/s^2): (a) z_h-axis; (b) y_h-axis.
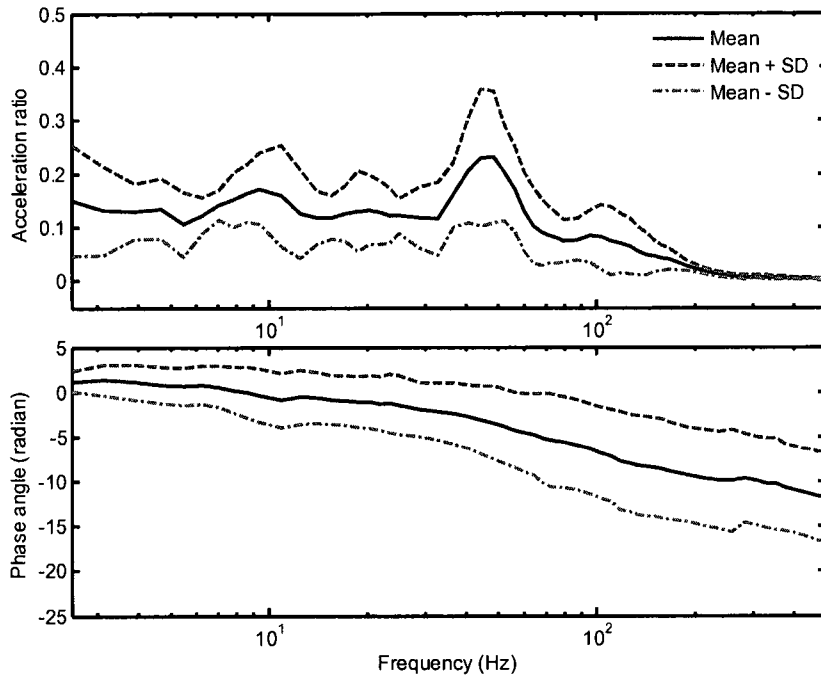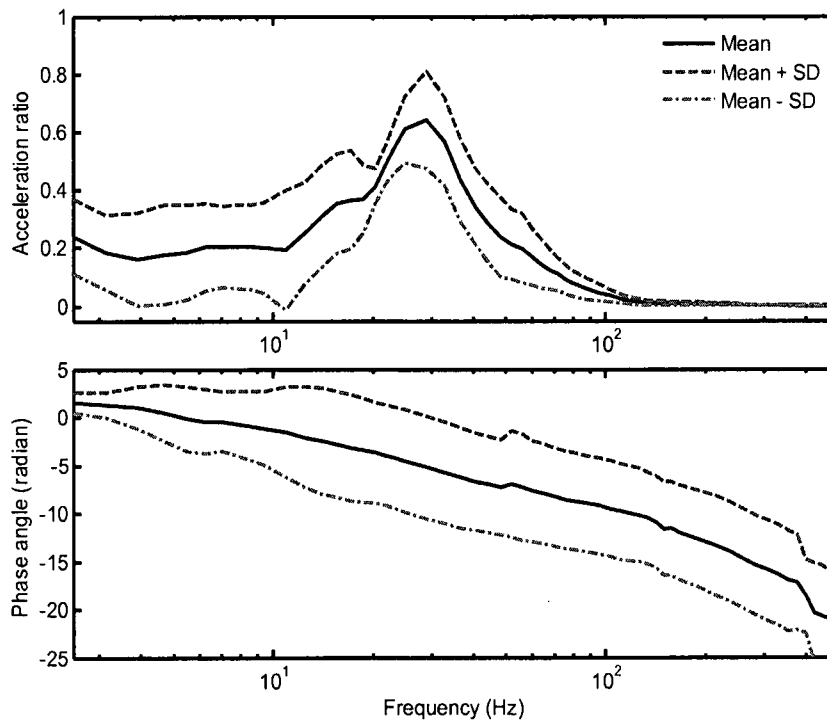
Figure 3.16: Mean and standard deviation (SD) of mean x_h-axis vibration transmissibility (*P1* posture, $F_g = 30$ N, $F_p = 50$ N and $a_{hw} = 5.25$ m/s^2) measured at: (a) elbow 1; (b) elbow 2.

analysis was performed to quantify the variations. The observed high inter-subject variability was attributed to changes in the hand-grip force during the test [95]. The factors responsible for inter-subject variability in this study include uneven tightness of Velcro strips on the hand-arm, variations in grip and push forces, randomness of the excitation, and difference in the biodynamic and anthropometric parameters of the subjects. The peak inter-subject variability/deviation (SD) is thus expected to be greater than the peak SD observed in reproducibility test, which in turn should be greater than that of repeatability test. Table 3.7 summarizes the peak SD and the corresponding frequencies in impedance and transmissibility data due to inter-subject variability. The results show peak deviations in DPMI of 73.9 Ns/m and the z_h-axis transmissibility magnitude of 0.41 at elbow 2 and the shoulder occurring at 17.2 Hz, which are higher than those obtained for the data acquired during repeatability and reproducibility tests. The peak SD in the DPMI magnitude is far less than the 150 Ns/m reported in [69]. The

Table 3.7: Maximum standard deviation of the mean measured responses ($P1$ posture, F_g = 30 N, F_p = 50 N and a_{hw} = 5.25 m/s^2).

Biodynamic measure	Measurement location_axis	Peak standard deviation	Mean	Corresponding frequency (Hz)
DPMI	Driving-point	73.94	251.77	17.19
	Wrist_y_h	0.35	0.59	82.03
	Wrist_z_h	0.37	1.41	32.81
	Elbow1_x_h	0.13	0.23	47.66
	Elbow1_y_h	0.15	0.18	14.84
Transmi-ssibility	Elbow1_z_h	0.26	1.40	28.91
	Elbow2_x_h	0.21	0.20	10.94
	Elbow2_y_h	0.17	0.34	33.59
	Elbow2_z_h	**0.41**	1.20	17.19
	Shoulder_y_h	0.09	0.09	34.38
	Shoulder_z_h	**0.41**	0.77	17.19

observed maximum deviation in the transmissibility responses at elbow 2 may be attributed to greater variations in the diameter of the upper arm of the subjects near elbow 2, as seen in Table 3.4.

3.7 Mean Measured Biodynamic Responses

3.7.1 Driving-point mechanical impedance (DPMI)

The mean measured impedance responses are compared with those attained in an earlier study conducted in the same laboratory [67], and ranges of standardized data and the standardized 3-DOF model responses reported in ISO 10068 [86]. Figure 3.17(a) compares the DPMI responses for the *P1* posture, while those for the *P1* and *P2* postures are shown in Figure 3.17(b). The mean measured data falls within the limits defined in ISO 10068 in the 10 – 500 Hz range. It should be noted that the standard defines the mean and ranges of DPMI in the 10 – 500 Hz frequency range, and the corresponding model can be considered valid only in that frequency range. Both the model and the mean measured data, however, exhibit considerably lower magnitude and phase at frequencies below 10 Hz. Furthermore, both responses exhibit a valley near 4 Hz. The mean measured data are also comparable with those reported in [67], although some deviations are evident at frequencies below 30 Hz. This may be attributed to differences in the biological and anthropometric properties of the subjects employed in the two studies. Although the reported data [67] was acquired in the same laboratory, it employed a different data acquisition and analysis system (Pulse). The differences in the two sets of response, particularly the phase below 10 Hz, may thus in-part be caused by the differences in the two data analysis systems.

Figure 3.17(b) compares the mean measured DPMI responses obtained for the
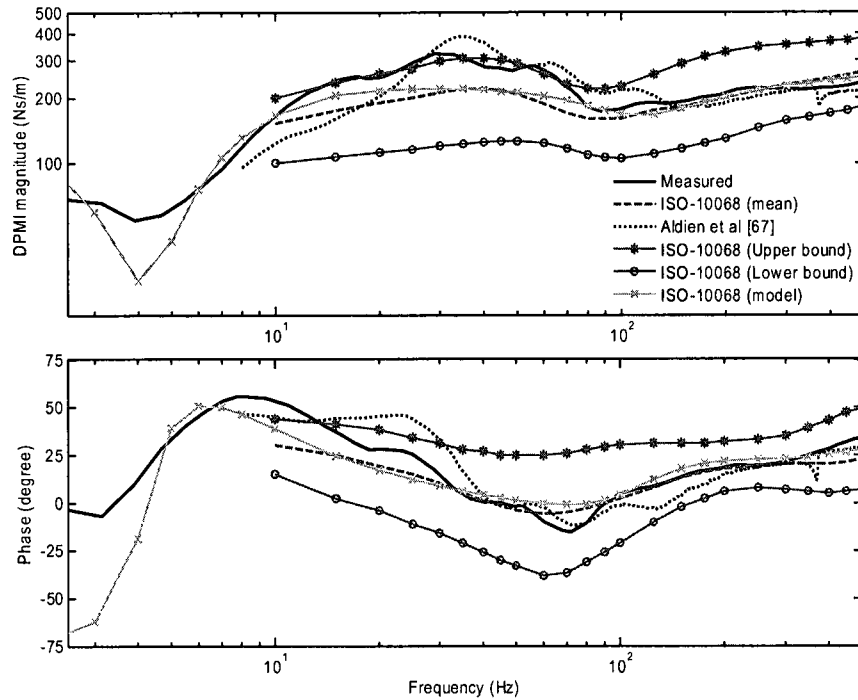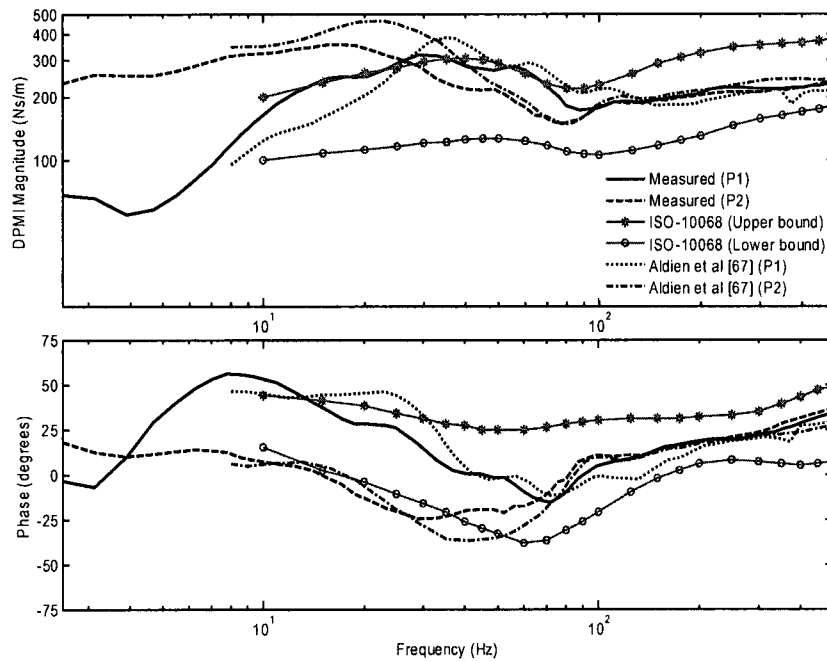
Figure 3.17: Comparison of the mean measured impedance with the reported and standardized data ($F_g = 30$ N, $F_p = 50$ N and $a_{hw} = 5.25$ m/s^2): (a) *P1* posture; (b) *P1* and *P2* postures.

two postures with the limits and those reported in [67]. The difference in the impedance

magnitudes due to posture effect is very significant below 25 Hz. The mean DPMI

magnitude corresponding to *P2* is about 258 Ns/m at 2.5 Hz, while that for *P1* is around

70 Ns/m. The difference in the DPMI magnitudes gradually decreases as frequency

increases up to 25 Hz, where the DPMI magnitude corresponding to *P1* posture exceeds

that of the *P2* posture up to around 100 Hz. The difference in the DPMI magnitudes of

the two postures, however, is relatively small above 100 Hz. Similar postural effect are

also evident in reported data [67], while the limits defined in ISO 10068 are applicable

only for the *P1* posture.

The impedance responses of the handle alone obtained from the two data analyses

systems (Pulse and 01dB) are compared in Figure 3.18. The results show comparable
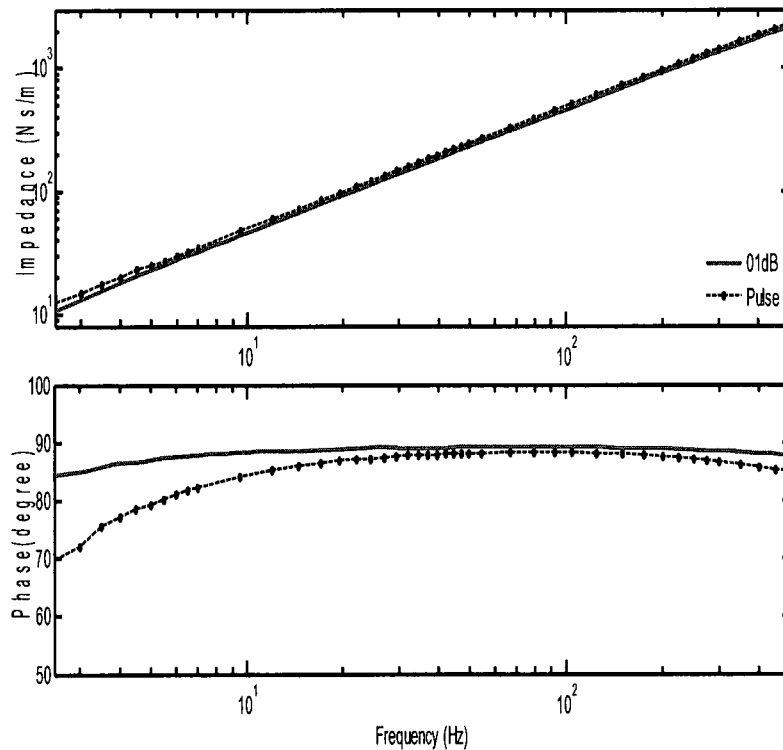
Figure 3.18: Comparisons of DPMI responses of the simulated handle obtained using the
Pulse and 01dB data acquisition and analyses systems.

magnitude response from the two systems but considerable deviation in the phase response below 10 Hz. It was noted that the Pulse system directly provides the DPMI response through integration of the handle acceleration signal, while the 01dB does not integrate the acceleration and yield only apparent mass. The DPMI response was thus evaluated by multiplying the apparent mass by $j\omega$. It was concluded that the signal integration in the Pulse system can cause considerable error in the phase response at lower frequencies.

3.7.2 Vibration transmissibility

The mean z_h-axis transmissibility responses at the four measurement locations for the bent-arm (*P1*) posture are shown in Figure 3.19(a), while Figure 3.19(b) presents the responses for the extended arm (*P2*) posture. The responses in the y_h- and x_h- axis for the two postures are illustrated in Figures 3.20 and 3.21, respectively. The z_h-axis transmissibility magnitude for the *P1* posture generally decreases from the wrist to the shoulder, although the magnitude at the elbow 1 is higher than that of the wrist in the 2.5 - 20 Hz frequency range. The transmissibility data reported in [93] showed a similar trend. The observed exception in the 2.5 - 20 Hz frequency range may be due to the high concentration of muscles/tissues around the elbow on the forearm side. The highest transmissibility magnitude occurred around 12.5 Hz in the responses of elbow 1 and 2 (Figure 3.19(a)). The frequency-weightings defined in ISO 5349-1 [31] also has the highest weight near 12.5 Hz. In the y_h-axis above 30 Hz, the magnitudes of the response at the wrist is higher than those measured at other locations. The trend above 30 Hz is similar in both the z_h-axis and y_h-axis, the response decreases from the wrist to the shoulder.

Unlike the bent-arm posture, the z_h-axis transmissibility magnitude responses with the extended arm posture generally remain above unity from the wrist to the shoulder at frequencies below 20 Hz, with the response at elbow 2 having the highest magnitude around 8.5 Hz. This is evident only in the linear scale presentation of the data, as shown in Figure 3.19. Such differences, however, are not evident from the logarithmic scale presentation of the responses, which has been widely used for the published research on vibration transmissibility responses. In the y_h-axis (Figure 3.20(b)), the response at the shoulder has the largest magnitude in the low frequency region, while that at the wrist is the lowest, suggesting greater amplification of low frequency vibration along the y_h-axis. Above 20 Hz, the magnitude decreases from the wrist to the shoulder, as observed for the *P1* posture, in both the z_h-axis and y_h-axis above 30 Hz. The transmissibility responses in the x_h-axis for the *P2* posture around the elbow are similar, while those for the *P1* posture differ in the entire frequency range, as seen in Figure 3.21. The *P1* posture yields a significant peak in the x_h-axis transmissibility at elbow 2 near 28 Hz.

The difference in the transmissibility magnitudes between the *P1* and *P2* postures in the z_h-axis in the low frequency region at the wrist is relatively small, but quite considerable at the shoulder. The z_h-axis wrist and elbow vibration magnitudes for the *P1* posture are generally greater than those for the *P2* posture above 30 Hz. These trends are evident in Figures 3.23 to 3.25. This trend is also evident in the shoulder response above 80 Hz. Transmissibility magnitudes in the y_h-and x_h-axis are generally considerably lower than those in the z_h-axis, which is attributable to source vibration along the z_h-axis. The differences in the magnitudes, however, are strongly dependent on the posture. For the *P1*
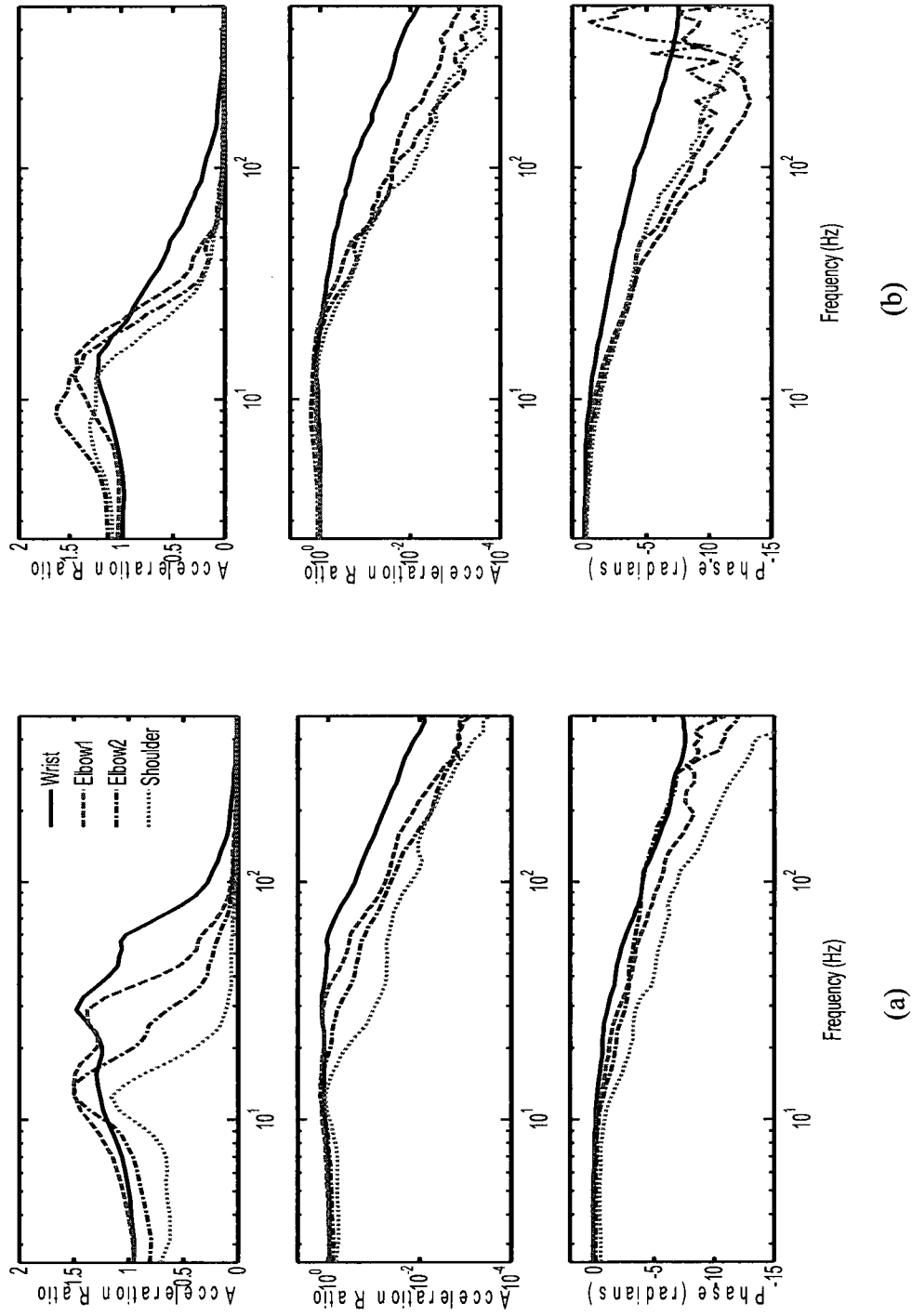
Figure 3.19: Comparisons of z_h-axis mean transmissibility responses measured at different locations ($F_g = 30$ N, $F_p = 50$ N and $a_{hw} = 5.25$ m/s^2): (a) $P1$ posture; (b) $P2$ posture.

105
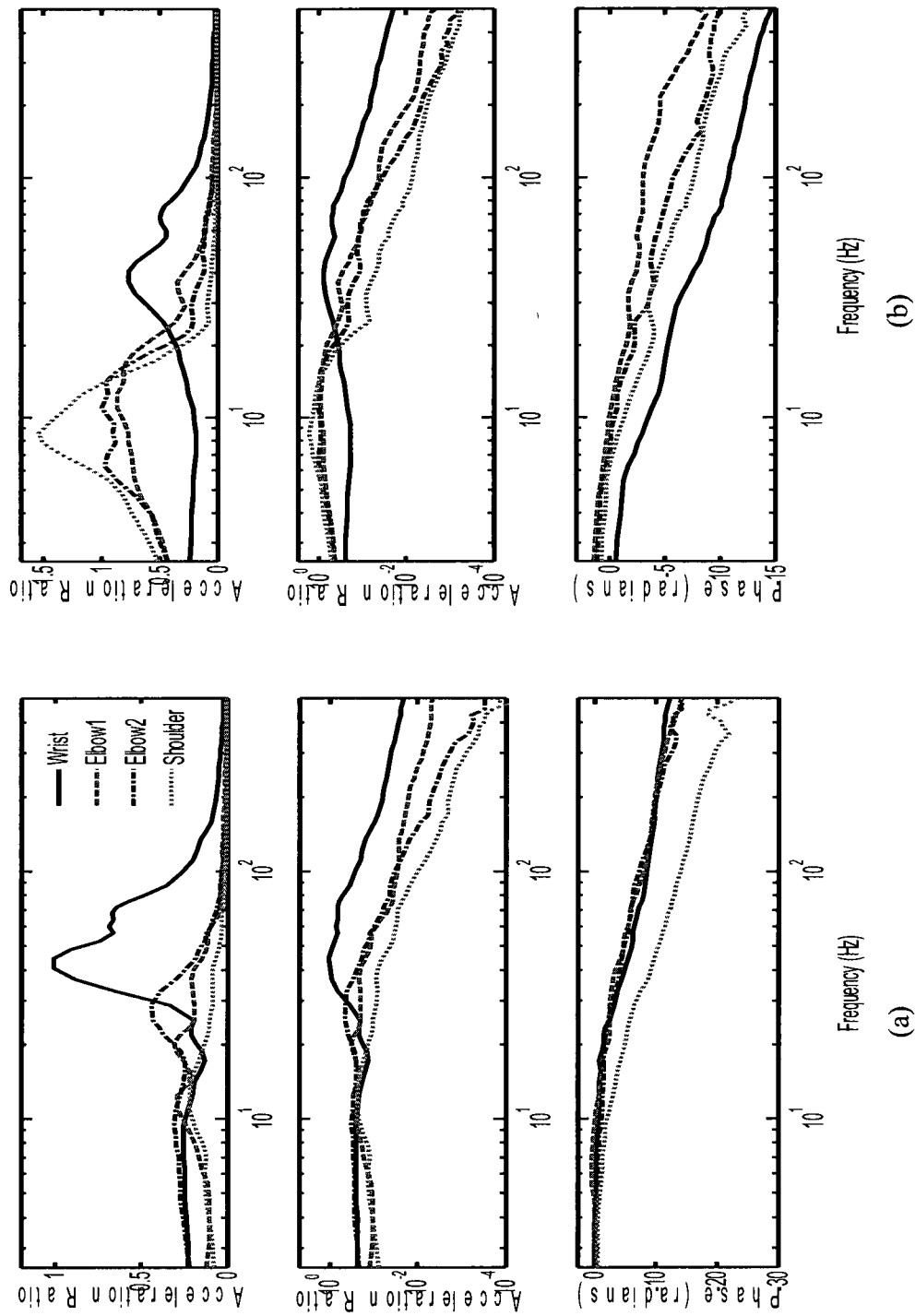
Figure 3.20: Comparisons of y_h-axis mean transmissibility responses measured at different locations (F_g = 30 N, F_p = 50 N and a_{hw} = 5.25 m/s²): (a) P1 posture; (b) P2 posture.
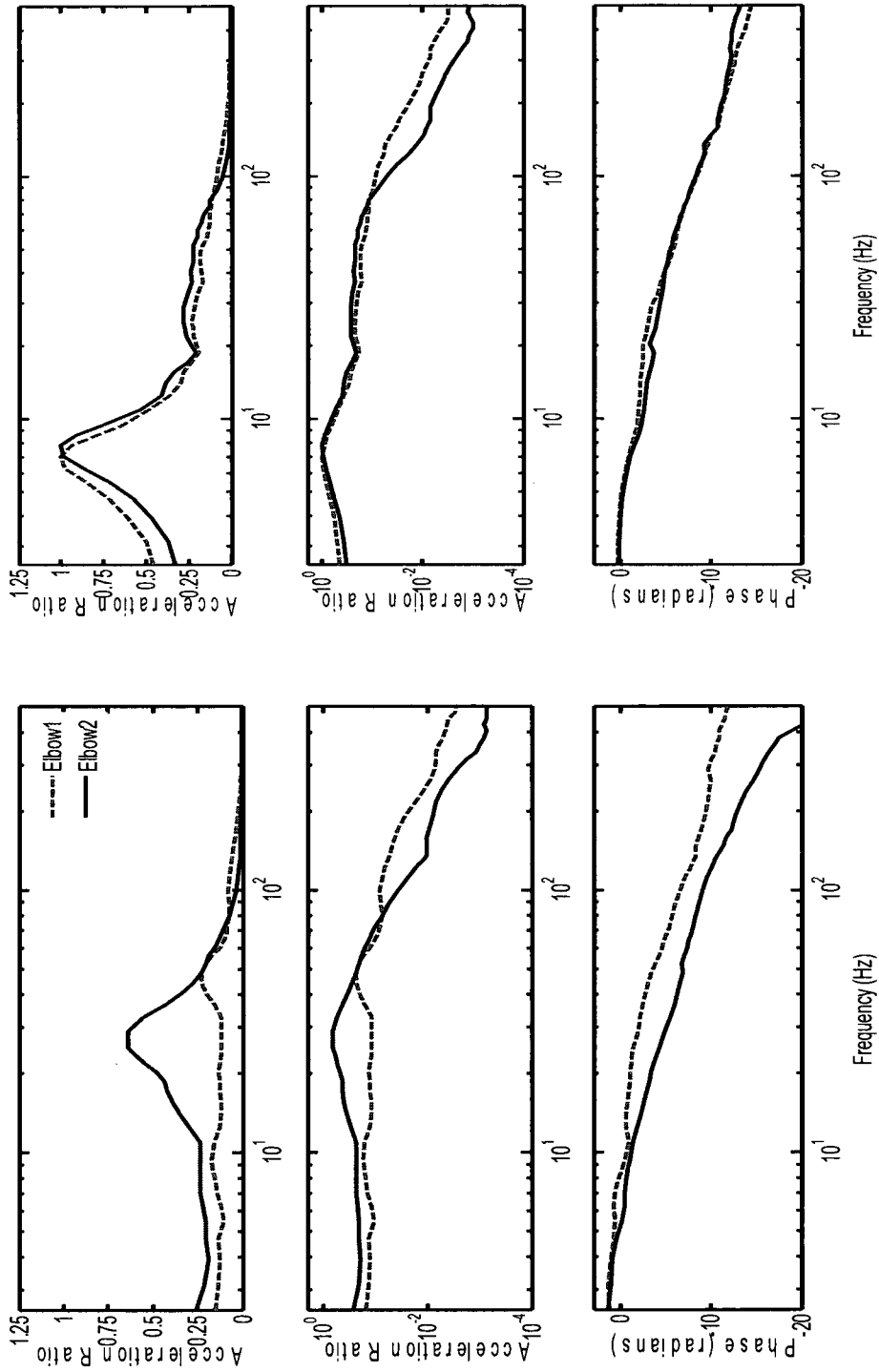
Figure 3.21: Comparisons of x_h-axis mean transmissibility responses measured around the elbow ($F_g = 30$ N, $F_p = 50$ N and $a_{hw} = 5.25$ m/s²): (a) *P1* posture; (b) *P2* posture.

107

posture, the y_h-and x_h-axis magnitudes are in the order of 25 % of the z_h-axis magnitudes, while those corresponding to P2 posture are in the order of 50 %, in the low frequency region.

The transmissibility magnitude at the wrist in both y_h-and x_h-axis are almost the same between 2.5 and 25 Hz for both postures but the magnitudes for the bent-arm posture are greater than those for the extended arm posture above 25 Hz (see Figures 3.25(a) to 3.24(a)). The results therefore show that the human hand-arm system in an extended arm posture amplifies vibration transmitted to the upper-arm below 25 Hz, but it tends to attenuate vibration transmitted to the upper-arm more effectively than the bent-arm posture above 25 Hz. Similar observations have also been reported in [94, 98]. The deviation in the phase responses at all measurement locations also increases with increase in frequency.

3.8 Identification of Resonant Frequencies

The vast majority of the reported studies have identified the human hand-arm resonant frequencies as characteristic frequencies corresponding to peaks in the impedance magnitude response [65, 67, 77, 82]. A few studies, however, refer these to the valleys in the magnitude responses [71, 81], while others have not attempted to relate the peaks or valleys in the DPMI magnitude response to the resonance frequencies [69, 70, 73, 80]. Following the proposed hypothesis in section 3.3, the frequencies of the peaks and valleys in the DPMI magnitude are considered to correspond to the resonant frequencies of the tissues/muscles and bones/structure of the human hand-arm system, respectively. The frequencies corresponding to the peaks and valleys in the mean measured DPMI magnitudes are thus denoted as characteristic frequencies. These

characteristics frequencies for the bent-arm and extended arm postures were identified from the DPMI responses, presented in Figure 3.17(b) and summarized in Tables 3.8 and 3.9, respectively, in decreasing order of prominence. These frequencies are also compared with those obtained from the peaks in the transmissibility magnitudes shown in Figures 3.19 to 3.21. The characteristic frequencies identified from the mean transmissibility responses that are close to those corresponding to the peaks in the mean DPMI magnitudes are under scored in Tables 3.8 and 3.9, while those close to the valleys are italicized. Other transmissibility characteristic frequencies that could not be related to either the peak or the valley in the DPMI magnitudes are presented in the normal font.

The resonant frequencies identified from the mean measured transmissibility responses compare reasonably well with those in the reported studies, as summarized in Table 3.2. It is observed that some of the characteristic frequencies (peaks in the transmissibility magnitudes) for the bent-arm posture are comparable to those corresponding to the valleys (3.9 and 134.4 Hz) and the peaks (28.9, 56.3 and 15.6 Hz) in the DPMI response magnitudes, while others (12.5, 25.0, 71.6 and 146.1 Hz) could not be related to either the valleys or the peaks in the DPMI response. It should be noted that the characteristic frequency in the DPMI valley (89.4 Hz), which is closest to one of the damped frequencies of the 3-DOF hand-arm model reported in ISO 10068 [86], was not observed in the z_h-axis transmissibility magnitudes. However, a comparable frequency, near 99.2 Hz in the y_h- and x_h-axis transmissibility magnitudes at elbow 2 is observed. Furthermore, the most prominent characteristic frequency (12.5 Hz) in the z_h-axis transmissibility magnitude at elbow 1 and 2 and the shoulder, and at elbow 1 and the shoulder in the y_h-axis, is not found in the valleys or peaks of the DPMI magnitude. This

Table 3.8: Characteristic frequencies observed from the DPMI and transmissibility responses under *P1* posture

$$(F_g = 30 \text{ N}, F_p = 50 \text{ N and } a_{hw} = 5.25 \text{ m/s}^2)$$

	WRIST	ELBOW 1	ELBOW 2	SHOULDER	DPMI
x_h-axis		48.4, 99.2, 333.6	26.3, 7.0, 68.0, 216.4		Peaks 28.9, 56.3, 15.6, 110.9, 239.4
y_h-axis	44.5, 68.0, 134.4	12.5, 20.3, 36.7, 56.3, 134.1, 216.4	28.9, 10.9, 99.2, 239.8	12.5, 40.6, 71.9, 239.8	Valleys 3.9, 89.4, 20.3, 48.4, 134.4, 250.0
z_h-axis	28.9, 56.3, 15.6, 134.4	12.5, 28.9, 56.3, 157.8	12.5, 25.0, 56.3, 134.4	12.5, 5.5, 71.6, 146.1	

Table 3.9: Characteristic frequencies observed from the DPMI and transmissibility responses under *P2* posture

$$(F_g = 30 \text{ N}, F_p = 50 \text{ N and } a_{hw} = 5.25 \text{ m/s}^2)$$

	WRIST	ELBOW 1	ELBOW 2	SHOULDER	DPMI
x_h-axis		7.0, 15.6, 25.0, 50.0	7.8, 14.1, 28.9, 64.1, 200.0		Peaks 15.6, 48.4, 3.1, 7.8, 110.9, 216.4
y_h-axis	40.6, 68.0, 99.2	36.7, 134.4, 10.9, 14.1, 28.9, 64.1	6.3, 10.9, 28.9, 64.1, 216.4	8.6, 28.9, 48.4, 64.1	Valleys 75.8, 4.7, 44.5, 10.9, 134.4, 157.8
z_h-axis	12.5, 110.9, 333.6	12.5, 15.6, 4.5, 122.7, 357.0	8.6, 12.5, 15.6, 44.5, 68.0, 79.7, 134.4	7.0, 12.5, 44.5, 79.7, 110.9, 193.0	

suggests that the DPMI and transmissibility responses may characterize different components of the hand-arm system. For example, it seems that transmissibility responses characterize the dynamics of the tissues/muscles better than the DPMI.

Similarly, the impedance responses under the extended arm posture exhibit characteristic frequencies corresponding to the valleys (75.8, 44.5, 10.9 and 134.4 Hz) and the peaks (15.6, 7.8 and 110.9 Hz). These frequencies are also observed among the frequencies corresponding to peaks in the transmissibility responses, while some of the frequencies in the transmissibility responses (12.5, 8.6, 122.7, 357, 68.0 and 193.0 Hz) could not be related to frequencies corresponding to either the valleys or the peaks in the DPMI magnitude. However, some of the characteristic frequencies in the y_h- and x_h-axis transmissibility magnitudes for both postures could be related to those observed from the DPMI magnitudes.

The results thus further support the hypothesis that the resonant frequencies of the muscles/tissues and the bones/structure of the human hand-arm system correspond, respectively, to the peaks and the valleys in the DPMI magnitude. The results also suggest that transmissibility response characterizes the dynamics of the muscles/tissues better than the DPMI response, which seems to better characterize the dynamics of the bones/structure of the hand-arm system.

3.9 Influences of Primary Contributing Factors

The effects of the main factors, namely the grip force, push force, hand-arm posture and excitation level on the measured biodynamic responses are investigated through analyses of important trends in the mean responses and Analysis of Variance (ANOVA) using the Statistical Product and Service Solutions (SPSS).

111

3.9.1 Hand forces and posture effects on biodynamic responses

Figure 3.22(a) illustrates the influence of variation in the grip force on the mean impedance response for both postures, while the push force was kept constant around 50 N. In a similar manner, Figure 3.23(b) shows the effect of variation in push force under a constant grip force of 30 N. The results show that an increase in the grip force tends to shift the peaks in the DPMI magnitude for both postures to a higher frequency and a higher magnitude, while a negligible effect is observed in the magnitudes and frequencies of the valleys. On the other hand, an increase in the push force increases the characteristic frequencies and magnitudes corresponding to both the peaks and the valleys. It should be noted that an increase in the hand grip force stiffens the tissues/muscles of the hand-arm system, particularly the muscles of the hand and the forearm, while an increase in the push force stiffens both the tissues/muscles and bone joints. The effects of the grip force on the DPMI magnitude are relatively small at frequencies above 200 Hz, for both postures, while the effect of the push force is negligible above 400 Hz, irrespective of the posture. For the bent-arm posture, the grip force has negligible effect below 20 Hz and around the valleys near 4.5 and 90 Hz, but it shows significant effects at all other frequencies below 200 Hz, particularly around the peaks. The push force, on the other hand, yields negligible effect in the 5 - 25 Hz frequency range and above 200 Hz, but it affects both the peaks and valleys in the DPMI magnitudes at frequencies below 200 Hz. For the extended arm posture, the grip force has negligible effect below 7 Hz and around the valley near 90 Hz, while the push force has significant effect in the 2.5 - 400 Hz frequency range.

The changes in the characteristic frequencies and magnitudes of the DPMI
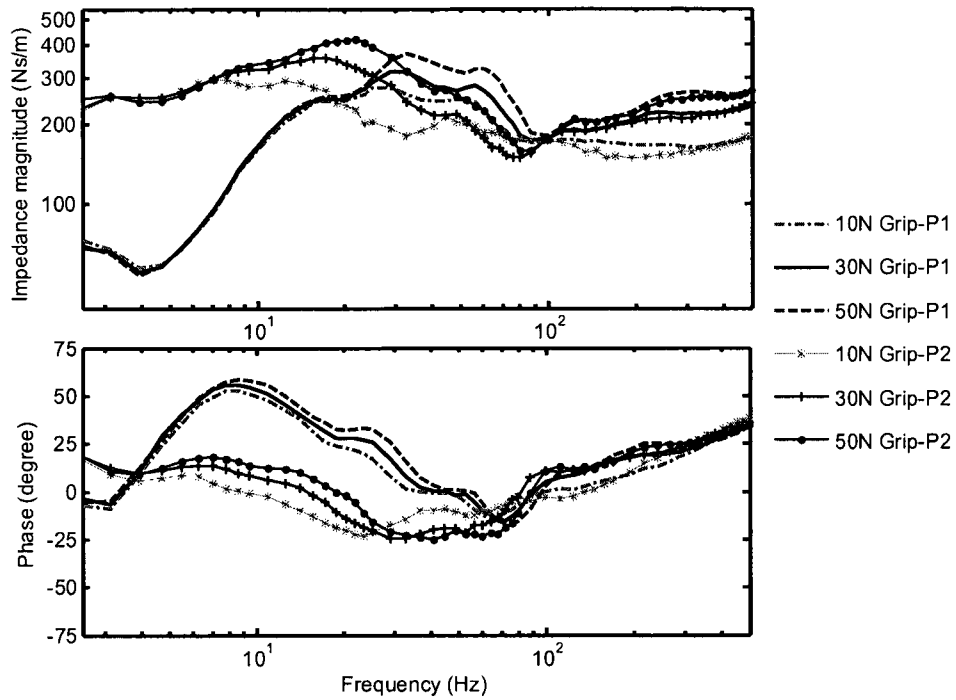
(a)
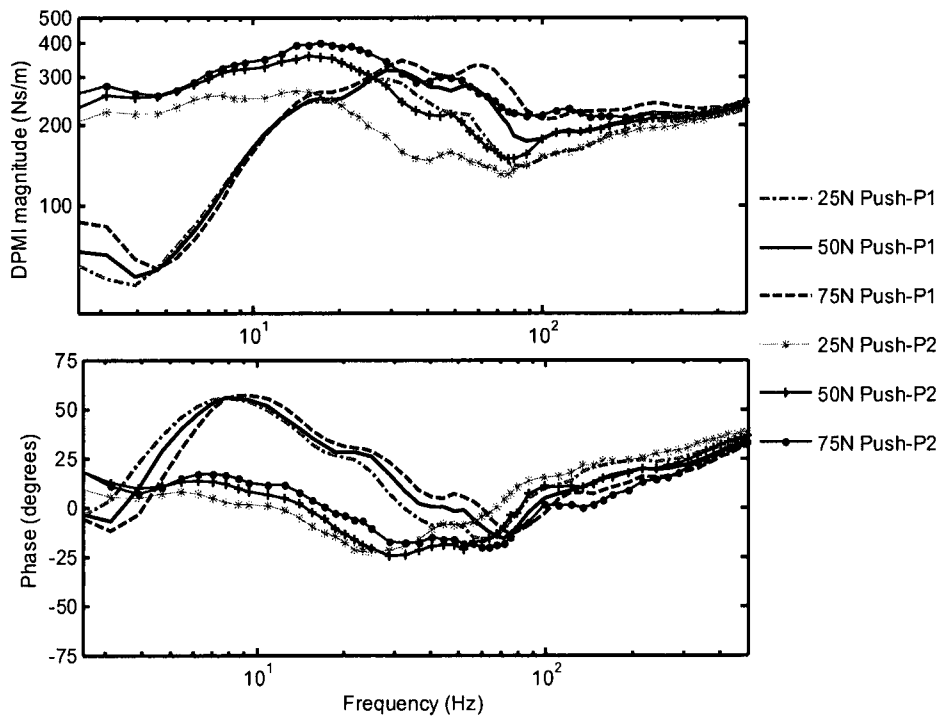
(b)

Figure 3.22: Effects of hand forces and posture on the mean DPMI responses under $a_{hw} = 5.25$ m/s^2: (a) different F_g when $F_p = 50$ N; (b) different F_p when $F_g = 30$ N.

Table 3.10: Effects of hand forces on the DPMI characteristic frequencies and magnitude ($P1$ posture; $a_{hw} = 5.25$ m/s^2)

Hand Forces (N)	Peaks		Valleys	
	Frequency (Hz)	Magnitude Ns/m	Frequency (Hz)	Magnitude Ns/m
$F_g = 10$, $F_p = 50$	*26.6*, 52.3	*277.7*, 248.1		
$F_g = 30$, $F_p = 50$	*29.7*, 56.3, 118.8, 235.9	*322.4*, 279.6, 191.1, 221.1		
$F_g = 50$, $F_p = 50$	*34.4*, 60.2, 134.4, 267.2	*372.4*, 324.4 207.6, 260.5		
Maximum change (Percentage)	7.8 (29.30%)	94.7 (34.10%)		
$F_g = 30$, $F_p = 50$	*28.1*, 52.3, 110.9, 235.9	*298.9*,218.9, 156.9, 206.5	3.91, *87.5*	51.0, *139.7*
$F_g = 30$, $F_p = 50$	*29.7*, 56.3 110.9, 251.6	*322.4*, 279.6 187.5, 221.3	3.91, *87.5*	54.6, *172.9*
$F_g = 30$, $F_p = 75$	*34.4*, 60.2, 134.4, 235.9	*347.6*, 332.7, 224.8, 240.9	4.7, *108.1*	58.5, *209.3*
Maximum change (Percentage)	**6.3 (22.40%)**	**48.7 (16.30%)**	**15.6 (17.80%)**	**69.6 (49.80%)**

response due to increase in the hand forces are summarized in Table 3.10 for the bent-arm posture. The values used in determining the percentage changes are shown in italics. The results show that an increase in the grip force from 10 N to 50 N (400 %) yields an increase of 7.8 Hz (29.3 %) in the most prominent characteristic frequency and 94.7 Ns/m (34.1 %) in the most prominent peak magnitude, while no appreciable change was observed around the valleys. Similarly, an increase from 25 N to 75 N in the push force (200 %) yields an increase of 6.3 Hz (22.4 %) in the characteristic frequency corresponding to the most prominent peak and 48.7 Ns/m (16.3 %) in the peak magnitude. This further resulted in an increase in the frequency corresponding to the

most prominent valley of 15.6 Hz (17.8 %) and 69.6 Ns/m (49.8 %) in the corresponding

valley. The observed trends in the effects of grip and push forces therefore support the

hypothesis that the resonant frequencies of the muscles/tissues and the bones/structure of

the human hand-arm system correspond, respectively, to the peaks and the valleys in the

DPMI magnitude.

Figures 3.23 – 3.25 show the influence of the grip force and posture on

transmitted vibration magnitudes in the z_h- and y_h-axis at the wrist, elbow and shoulder.

The figures show that an increase in the grip force increases transmissibility magnitude

and characteristic frequencies for both postures. An increase in the grip force yields

negligible effect on the z_h- axis wrist transmissibility under the *P1* posture in the 2.5 – 15

Hz frequency range, while it increases the magnitude and the characteristic frequencies

for both postures above 15 Hz. The increases in the response magnitudes for the bent-arm

posture are higher than those for the extended arm above 15 Hz, particularly along the z_h-

axis. This may be due to the partial stiffening of the muscles/tissues and the joints in the

extended arm posture, which tends to increase the damping effect of the hand-arm

system. In the y_h-axis (Figure 3.23(b)), the effect is more prominent in the 15 – 80 Hz

frequency range for both postures, while the response magnitudes are higher for the *P1*

posture.

The effect of the grip force on the z_h- axis vibration transmitted to elbow 1

location is similar to those observed at the wrist, as shown in Figure 3.24(a). In the y_h-

axis, however, the effect is prominent below 50 Hz for both postures (Figure 3.24(a)),

while the magnitudes are greater for the *P2* posture compared to the *P1* posture. The

effect of grip force is more prominent on the z_h- axis shoulder transmissibility under *P2*

Table 3.11: Effect of hand forces on the z_h-axis vibration transmissibility magnitudes and characteristic frequencies (P1 posture; $a_{hw} = 5.25$ m/s²)

Hand forces (N)	Wrist		Elbow 1		Elbow 2		Shoulder	
	Frequencies (Hz)	Magnitudes	Frequencies (Hz)	Magnitudes	Frequencies (Hz)	Magnitudes	Frequencies (Hz)	Magnitudes
$F_g = 10, F_p = 50$	15.6, 25.0, 56.3	1.349, 1.232, 0.807	15.6, 25.0, 56.3	1.566, 1.212, 0.270	12.5, 25.0, 56.3	1.388, 0.766, 0.159	5.5, 12.5, 56.3	0.674, 1.094, 0.049
$F_g = 30, F_p = 50$	14.8, 29.7, 56.3	1.287, 1.472, 1.067	14.8, 26.6, 56.3	1.494, 1.404, 0.362	13.3, 25.0, 56.3	1.500, 0.813, 0.187	5.5, 12.5, 56.3	0.649, 1.146, 0.048
$F_g = 50, F_p = 50$	16.4, 31.3, 56.3	1.315, 1.544, 1.142	16.4, 29.7, 60.2	1.498, 1.532, 0.387	14.1, 25.0, 56.3	1.480, 0.794, 0.225	5.5, 13.3, 56.3	0.683, 1.210, 0.028
Maximum change (Percentage)	6.3 (25.00%)	0.312 (25.30%)	4.69 (18.76%)	0.32 (26.40%)	1.6 (12.80%)	0.092 (6.63%)	0.8 (6.40%)	0.116 (10.60%)
$F_g = 30, F_p = 25$	15.6, 26.6, 52.3	1.370, 1.390, 0.860	12.5, 25.0, 56.3	1.550, 1.300, 0.269	11.7, 25.0, 65.3	1.393, 0.810, 0.161	5.5, 10.9, 40.6	0.698, 1.135, 0.064
$F_g = 30, F_p = 50$	14.8, 29.7, 56.3	1.290, 1.470, 1.070	14.5, 26.6, 56.3	1.494, 1.404, 0.362	13.3, 25.0, 56.3	1.500, 0.813, 0.187	4.5, 12.5, 31.3	0.645, 1.146, 0.088
$F_g = 30, F_p = 75$	16.4, 31.3, 56.3	1.290, 1.370, 1.127	15.6, 28.1, 64.1	1.471, 1.382, 0.354	15.6, 26.6, 56.3	1.436, 0.863, 0.231	5.5, 14.1, 34.4	0.645, 1.143, 0.134
Maximum change (Percentage)	4.69 (17.66%)	-0.02 (-1.44%)	7.8 (13.86%)	0.085 (31.60%)	3.9 (33.30%)	0.043 (3.09%)	3.2 (29.36%)	0.008 (0.71%)

116
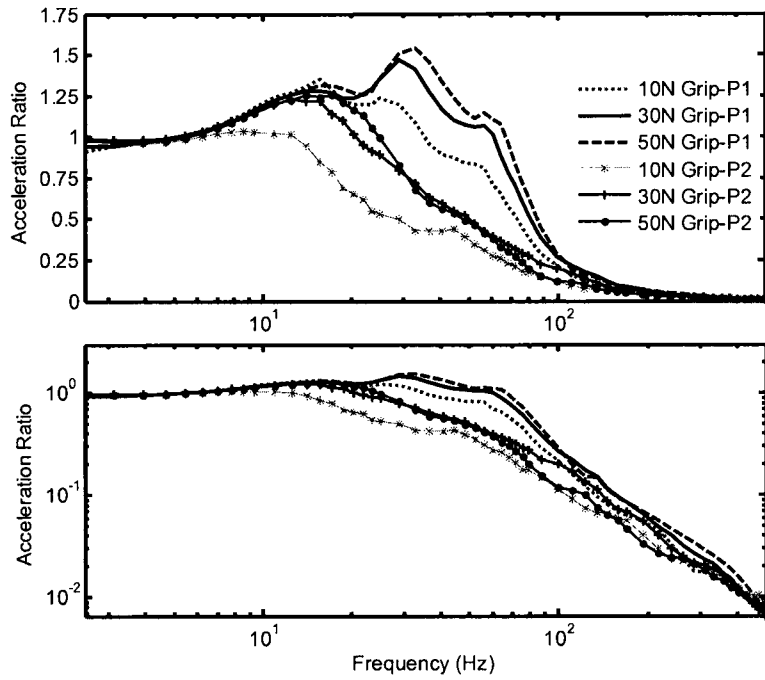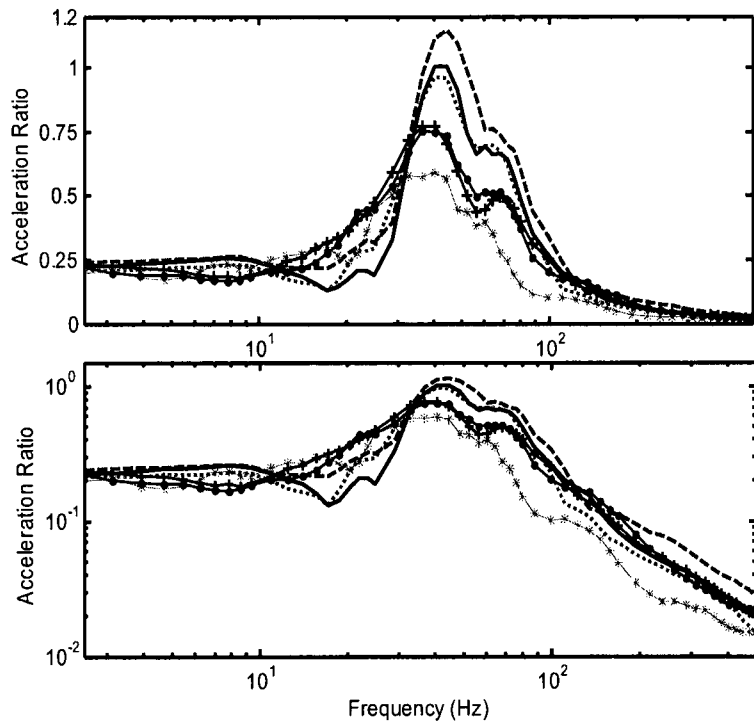
Figure 3.23: Effects of grip force and posture on the vibration transmissibility at the wrist (F_p = 50 N, a_{hw} = 5.25 m/s^2): (a) z_h-axis; (b) y_h-axis.
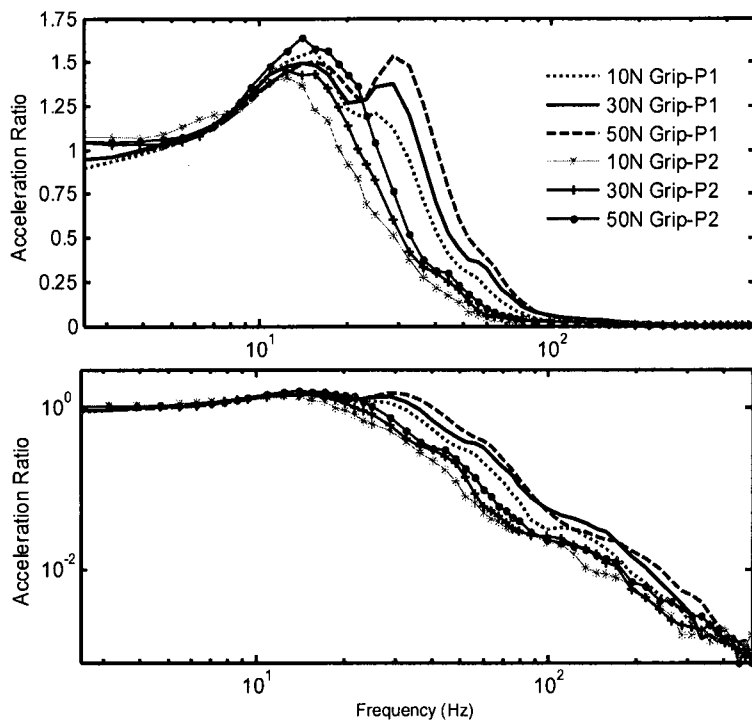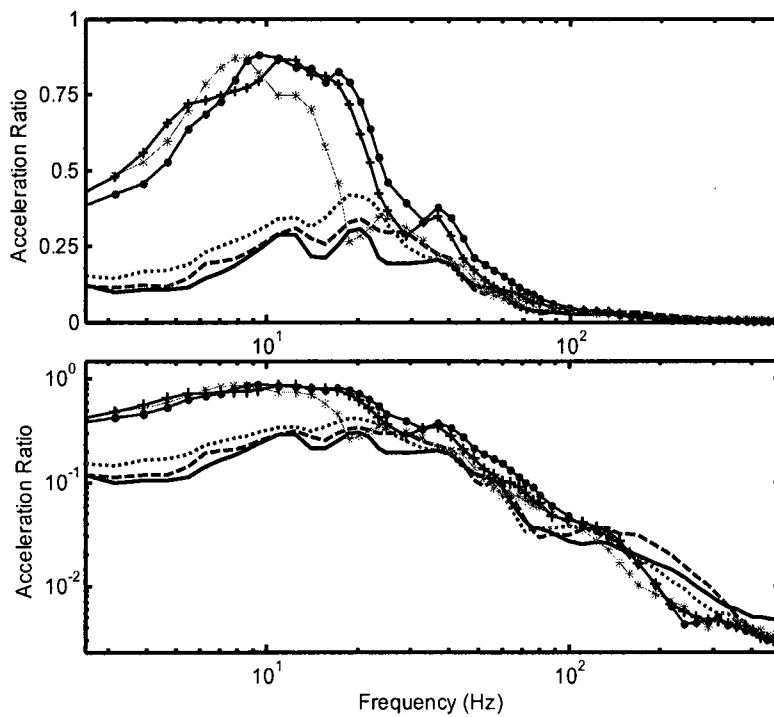
Figure 3.24: Effects of grip force and posture on the vibration transmissibility at elbow 1 $(F_p = 50$ N, $a_{hw} = 5.25$ m/s^2): (a) z_h-axis; (b) y_h-axis.

118
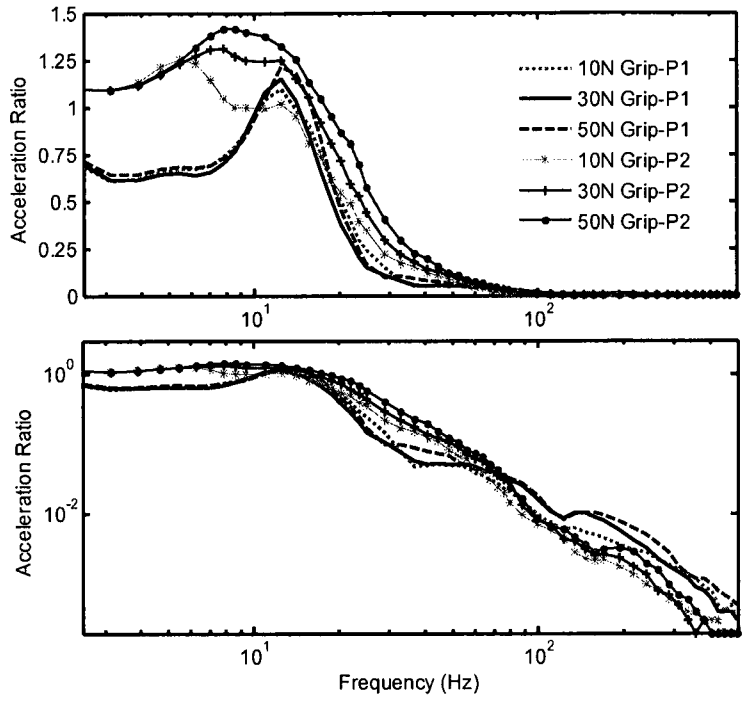
(a)
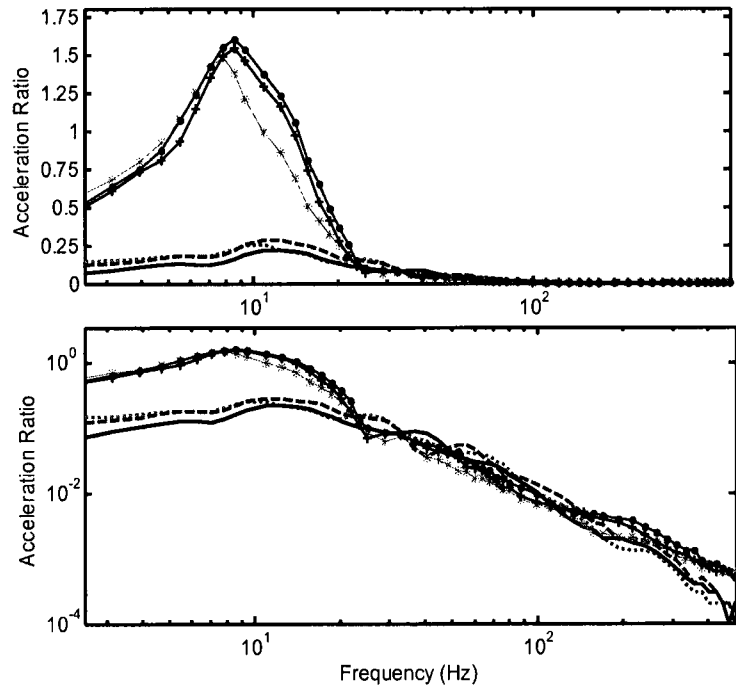
(b)

Figure 3.25: Effects of grip force and posture on the vibration transmissibility at the shoulder ($F_p = 50$ N, $a_{hw} = 5.25$ m/s^2): (a) z_h-axis; (b) y_h-axis.

posture in the 5 – 80 Hz frequency range, while the effect in the y_h- axis is small for both postures. The changes in the prominent characteristic frequencies and z_h- axis transmissibility magnitudes under different hand forces, for the $P1$ posture, are determined and summarized in Table 3.11. The results suggest that an increase in the grip force from 10 N to 50 N (400 %) yields an increase of 6.3 Hz (25.0 %) in the characteristic frequency at the wrist, and 0.32 (26.4 %) in the transmissibility magnitude at elbow 2.

Figures 3.26 - 3.28 illustrate the influence of the push force and posture on the z_h- and y_h-axis transmissibility responses at the wrist, elbow and shoulder, for a constant grip force of 30 N. Similar to the effect of the grip force, an increase in the push force generally yields higher transmissibility magnitudes and characteristic frequencies for both postures. The influences of variations in the push force on the z_h- and y_h-axis transmitted vibration at the wrist and elbow are similar to those observed under grip force variations. However, unlike the grip force, the push force significantly affects the transmissibility magnitude and characteristic frequencies at the shoulder in both axes for the $P2$ postures (Figure 3.28). This could be attributed to a higher reaction force developed in the upper-arm structure under a greater push force. The changes in characteristic frequencies and peak magnitudes with push force variations are summarized in Table 3.11. The results suggest that an increase in the push force from 25 N to 75 N (200 %) yields a maximum increase of 3.9 Hz (33.3 %) in the characteristic frequencies at elbow 2 and 0.085 (31.86 %) in the transmissibility magnitude at elbow 1.

The influence of the hand forces on the transmissibility show that the grip force mostly affects the dynamic characteristics of the forearm, while the push force
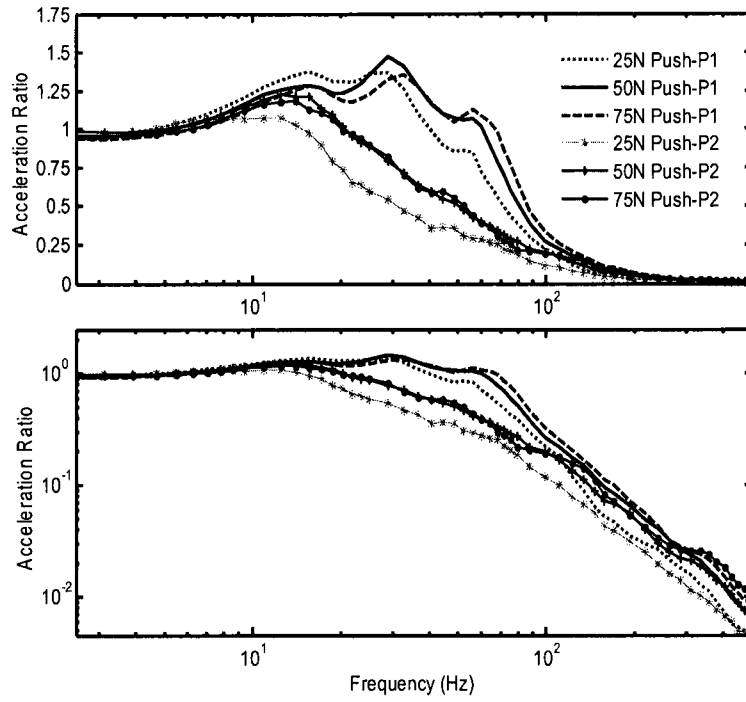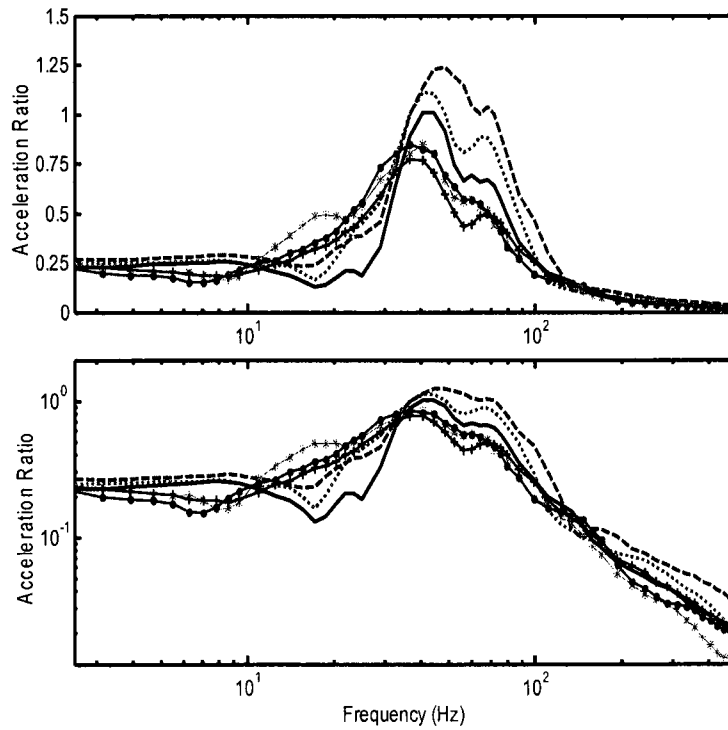
Figure 3.26: Effects of push force and posture on the vibration transmissibility at the wrist ($F_g = 30$ N, $a_{hw} = 5.25$ m/s^2): (a) z_h-axis; (b) y_h-axis.
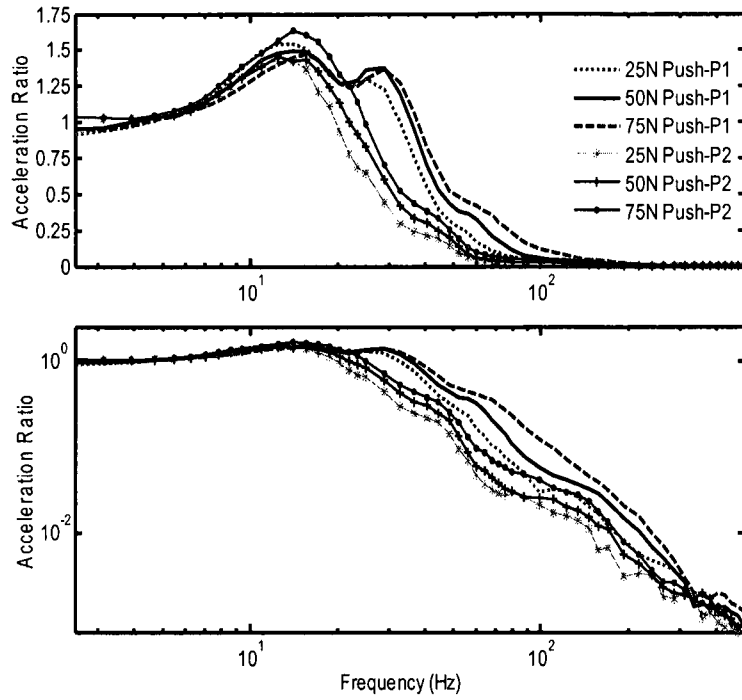
(a)
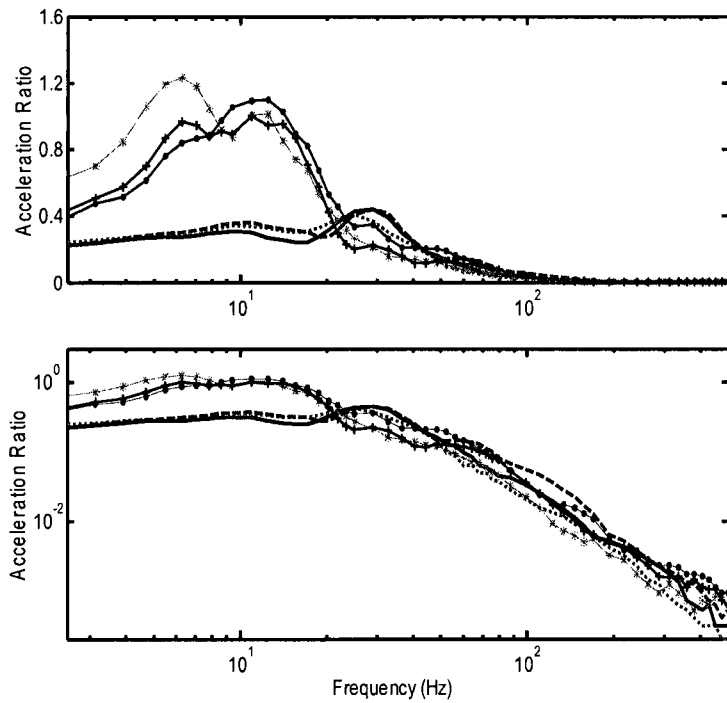
(b)

Figure 3.27: Effects of push force and posture on the vibration transmissibility at elbow 2 ($F_g = 30$ N, $a_{hw} = 5.25$ m/s^2): (a) z_h-axis; (b) y_h-axis.
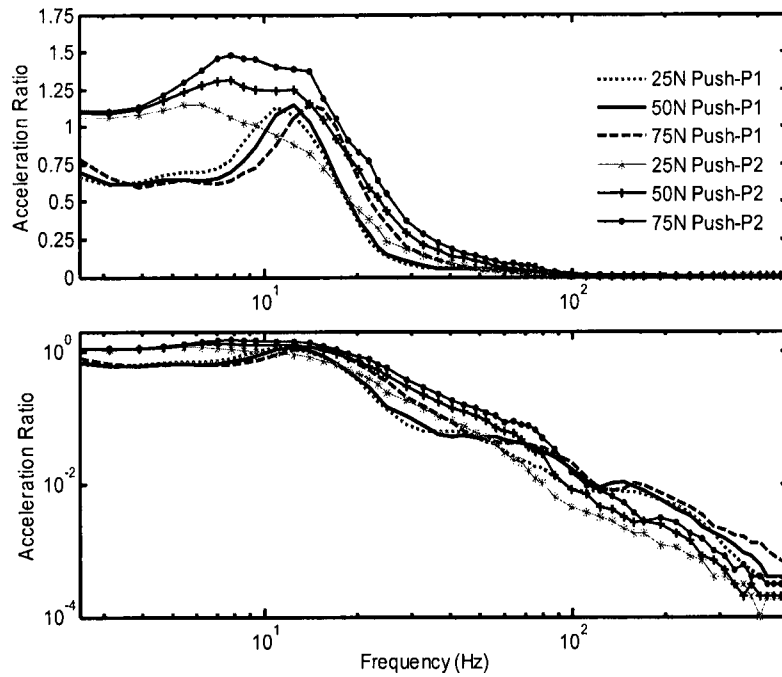
(a)
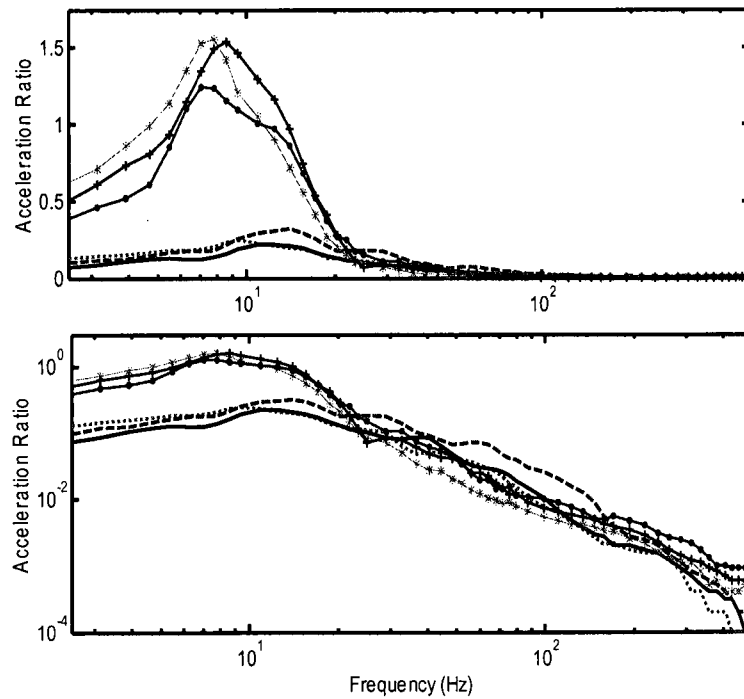
(b)

Figure 3.28: Effects of push force and posture on the vibration transmissibility at the shoulder ($F_g = 30$ N, $a_{hw} = 5.25$ m/s^2): (a) z_h-axis; (b) y_h-axis.

significantly affects the characteristics of the entire hand-arm system. This observation corroborates with the results obtained from the effect of hand forces on the DPMI responses.

3.9.2 Effects of excitation magnitude and posture

The influence of excitation magnitude on the DPMI response of the hand-arm in the bent-arm ($P1$) and extended arm ($P2$) postures is illustrated in Figure 3.29. The figure shows that excitation level has negligible effect on the DPMI response except around 110 Hz for the $P1$ posture and around 12.5 Hz for the $P2$ posture. The peak standard deviation of the DPMI magnitudes obtained under both excitations was found to be 26.24 Ns/m for the $P1$ posture (Table 3.12), which is lower than the peak SDs observed from the data acquired during the repeatability tests (31.28 Ns/m), and the reproducibility test (48.14 Ns/m), and inter-subject variability (67.50 Ns/m). Moreover, the peak SDs occurred in the vicinity of peak responses. It may thus be deduced that other factors, such as unsteadiness in the hand forces and variations in the hand-arm orientation contribute to the observed influence of the excitation level on the DPMI responses. The effect of excitation level on the DPMI phase is also very small, as seen in Figure 3.29. The effect of excitation magnitude on the DPMI responses may thus be considered to be relatively small to negligible. Some of the reported studies have also concluded that excitation magnitude has negligible effect on the DPMI magnitude response [67, 70, 73, 78, 84].

Figures 3.30 to 3.32 present the influences of excitation magnitude on the z_h- and y_h-axis transmissibility responses for the two postures. The results show that excitation level effects on the transmissibility magnitudes measured with the $P2$ posture are greater than those observed for the $P1$ posture. Table 3.12 summarizes the peak standard
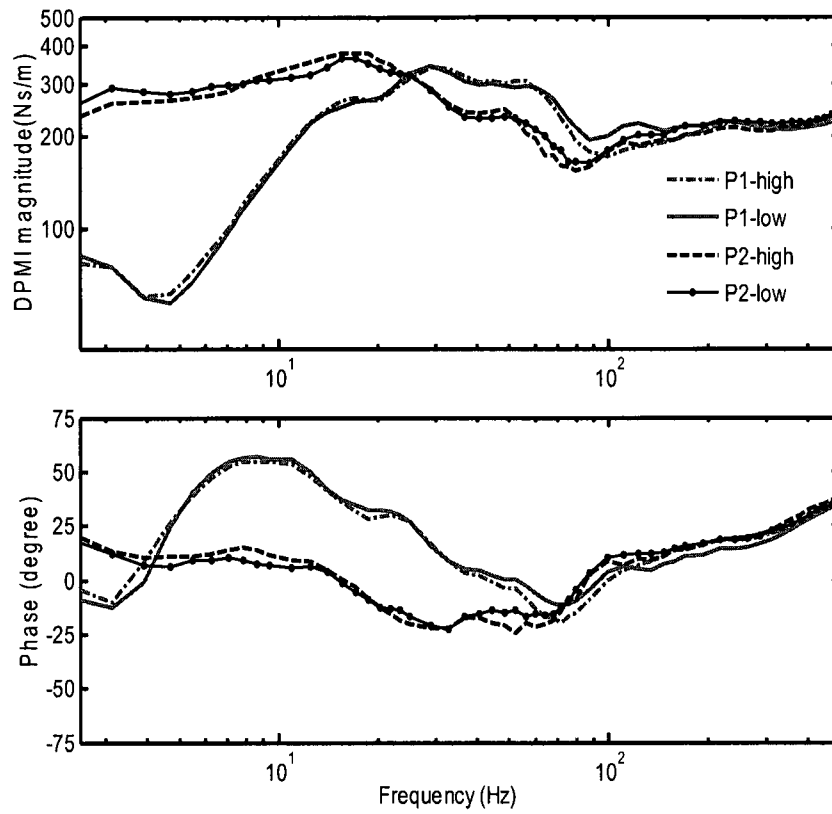
Figure 3.29: Effects of excitation magnitude and posture on the mean DPMI response
$(F_g = 30$ N, $F_p = 50$ N).

Table 3.12: Maximum standard deviation due to different excitation levels
$(F_g = 30$ N, $F_p = 50$ N)

Biodynamic response	Measurement Location_axis	P1 posture		P2 posture	
		Peak standard deviation	Corresponding frequency (Hz)	Peak standard deviation	Corresponding frequency (Hz)
DPMI	Driving-point	26.26	110.94	23.87	12.50
Transmis-sibility	Wrist_y_h	0.16	79.69	0.21	56.25
	Wrist_z_h	0.14	32.81	0.20	56.25
	Elbow1_x_h	0.08	32.81	0.22	10.94
	Elbow1_y_h	0.11	28.91	0.12	6.25
	Elbow1_z_h	0.11	32.81	0.12	12.50
	Elbow2_x_h	0.13	10.94	0.16	5.47
	Elbow2_y_h	0.11	36.72	*0.36*	*12.50*
	Elbow2_z_h	*0.18*	*15.63*	0.18	12.50
	Shoulder_y_h	0.09	25.00	0.21	9.38
	Shoulder_z_h	0.14	10.94	0.28	12.50

125

deviations of transmissibility magnitudes measured under the two excitation levels at each measurement location and the corresponding frequencies. The results suggest peak standard deviation of 0.36 in the y_h-axis transmissibility at elbow 2 under $P2$ posture, and 0.18 in the z_h-axis transmissibility at elbow 2 under the $P1$ posture. The observed peak SD for the $P1$ posture is lower than those obtained from the data acquired during repeatability test (0.23) and reproducibility test (0.35), and the inter-subject variability (0.38) for comparable hand forces. This suggests that the effect of excitation level on the z_h-axis vibration transmissibility under the $P1$ posture is small. The effect, however, is significant for the $P2$ posture. The effects of excitation magnitude on the y_h-axis vibration transmissibility are also evident under both postures. These suggest nonlinearity of the hand-arm system, which is not clearly evident from the responses measured at the driving-point. These further suggest that localized vibration transmissibility responses describe the dynamics of the hand-arm structure more accurately than the driving-point measures.

Somewhat contradictory findings have been reported in the published studies on effects of the excitation magnitudes. Some studies have reported that a 10 dB increase in the excitation magnitude increases the transmissibility magnitude by 8 - 10 dB at all frequencies [94, 98], while Aatola [95] reported negligible influence of excitation magnitude on the wrist transmissibility. A careful examination of the results presented in [95], however, revealed notable effect of excitation magnitude on the imaginary part of the measured vibration transmissibility, particularly around characteristic frequencies. These studies however considered different hand-arm postures involving elbow angle of 120°, 150° and 189°, which are closer to the $P2$ posture used in this study. Unlike the
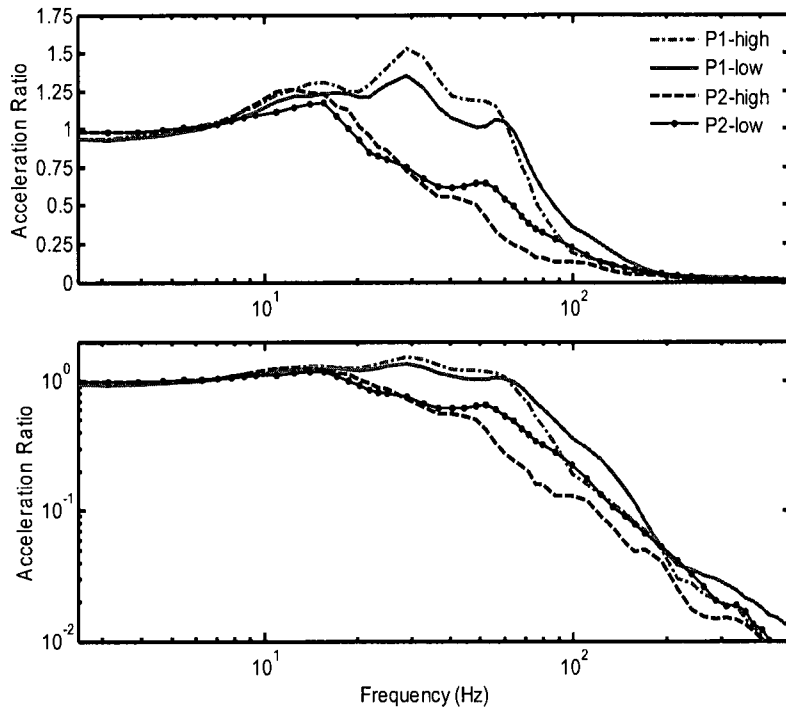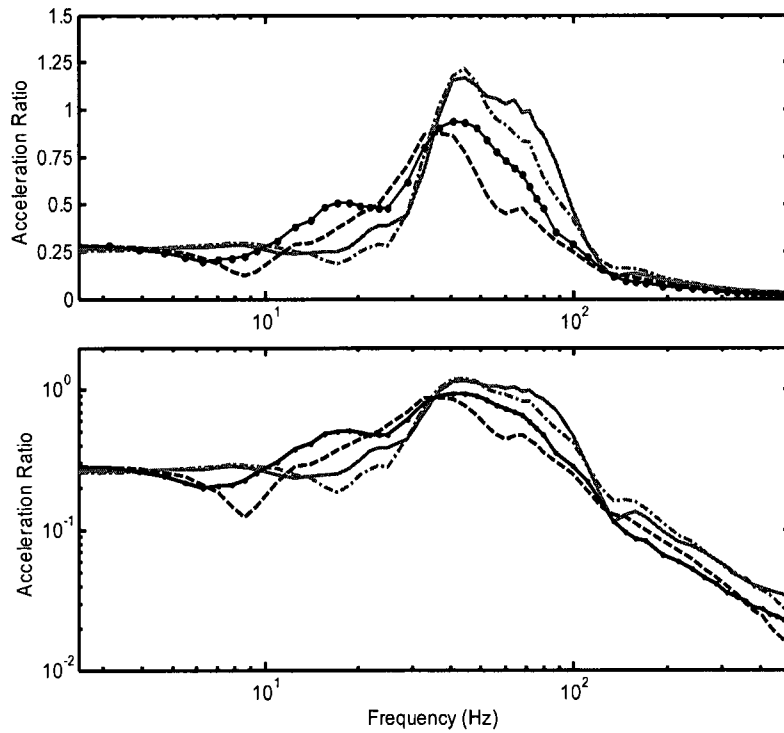
Figure 3.30: Effects of excitation level and postures on the vibration transmissibility at the wrist (F_g = 30 N, F_p = 50 N): (a) z_h-axis; (b) y_h-axis.
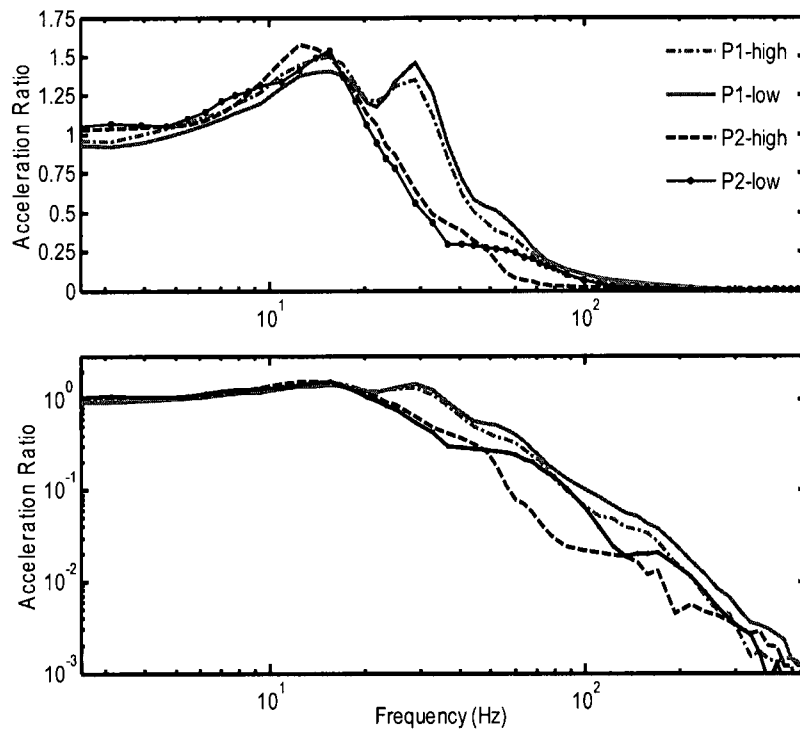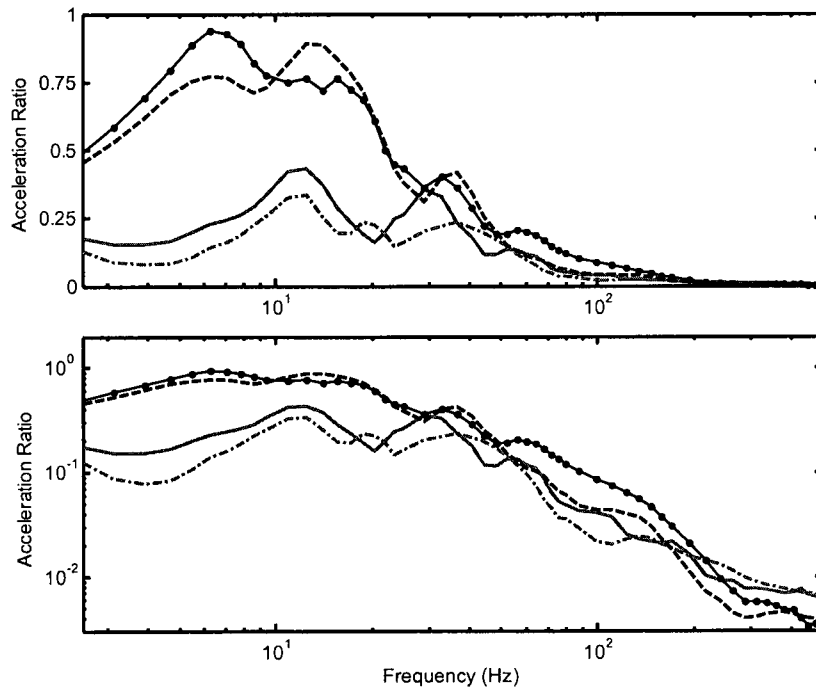
Figure 3.31: Effects of excitation level and posture on the vibration transmissibility at elbow 1 (F_g = 30 N, F_p = 50 N): (a) z_h-axis, (b) y_h-axis.
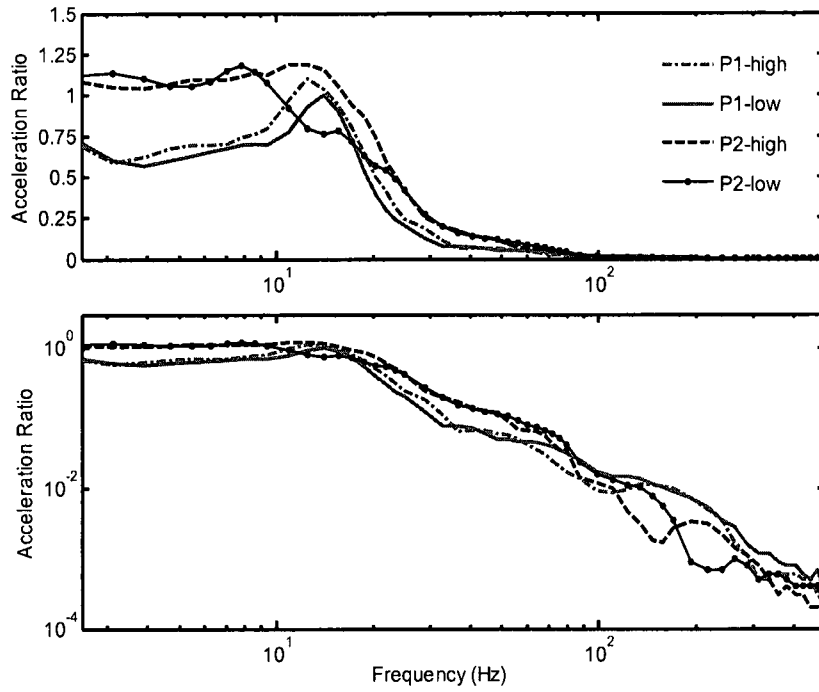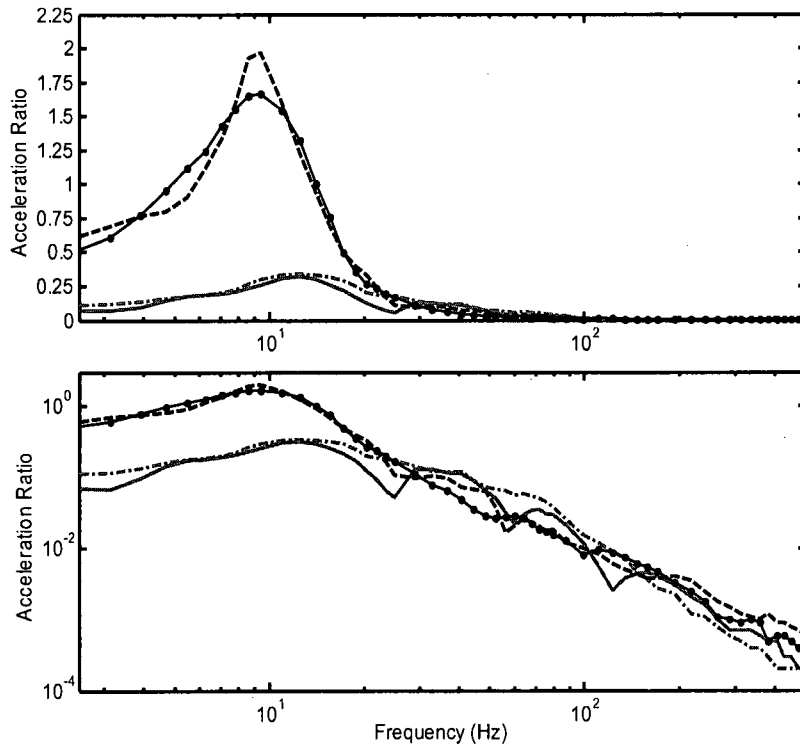
Figure 3.32: Effects of excitation level and posture on the vibration transmissibility at the shoulder (F_g = 30 N, F_p = 50 N): (a) z_h-axis; (b) y_h-axis.

results reported in [94] and [98], Aatola [95] investigated the effect of excitation level on the transmitted vibration through analysis of only the imaginary part of the transmissibility response, obtained for only one subject. The differences in the methodology used in the reported studies account for the different observations in view of excitation level effects. The results of the present study exhibit only partial agreements with the findings reported in [94] and [98], that the variations in the excitation level affect the transmissibility magnitudes, but disagree that the increase in transmissibility magnitude is the same in the entire frequency range. The results presented in Figures 3.30 - 3.32 show pronounced effects in the vicinity of the characteristic frequencies, which were also observed from the data reported in [95].

3.10 Statistical Analyses

3.10.1 Driving-point mechanical impedance

Analysis of Variance (ANOVA) with Statistical Product and Service Solutions (SPSS) software was used to analyze the experimental data for the two experiment designs that were discussed in section 3.4.2, using 95 % confidence intervals corresponding to significance level (alpha) of 0.05. The analyses were performed on the DPMI magnitudes at eleven selected frequencies in the vicinity of the identified important resonant frequencies of the human hand-arm system, as discussed in section 3.8. The main factors included the posture, grip and push forces, and the excitation level. The results illustrating the main factors effects and their 2-way interactions in terms of p-values are presented in Table 3.13. The results obtained for the two different postures are summarized in Table 3.14. The influence of a factor is considered to be significant if its p-value is less or equal to 0.05, which are italicized in Tables 3.13 and 3.14.

130

The influences of the main factors on the DPMI responses presented in Tables 3.13 and 3.14 generally agree very well with the trends observed in the mean DPMI responses illustrated in Figures 3.22 and 3.29. The effect of the posture (P) on the DPMI magnitude is most significant below 100 Hz, which is also evident in Figure 3.22. The results show that the effects of grip and push forces are mostly significant in the 28.9 - 300 Hz and 14.8 - 300 Hz ranges, respectively, with a few exceptions, which also conform with the trends of the mean data of Figure 3.22. It is interesting to note that the effect of grip force near 4.7 and 100 Hz, the prominent valleys in the DPMI magnitude response, are insignificant ($p > 0.05$). This further supports the observation that the effect of grip force on the valleys in the DPMI magnitude is negligible. The valleys are believed to be related to the resonant frequencies of the bones/structure of the hand-arm system. The results attained across the two postures (Table 3.13) suggest that the effect of push force (F_p) is significant in the 14.8 – 300 Hz frequency range. The results attained for individual postures, however, show significant frequency ranges as 28.9 – 134.4 Hz for the *P1* posture and 7.8 – 134.4 Hz for the *P2* posture (Table 3.14). These suggest that the push force effect is insignificant at frequencies above 200 Hz when individual postures are considered. The variations in the mean data, presented in Figures 3.22 (b), also confirm the insignificant push force effect. The difference in the results above 200 Hz is thus attributable to the influence of the posture. Considering the significant posture effects, it is essential to consider the individual posture effect in the ANOVA experimental design.

Table 3.13: Statistical significance of the main factors on DPMI magnitude

Factors	4.7 Hz	7.8 Hz	14.8 Hz	28.9 Hz	48.4 Hz	64 Hz	78.9 Hz	100 Hz	134.4 Hz	200 Hz	300 Hz
P	0.00	0.00	0.00	0.00	0.00	0.00	0.00	0.16	0.29	0.46	0.24
F_g	0.93	0.80	0.00	0.00	0.00	0.00	0.00	0.50	0.00	0.00	0.00
F_p	0.22	0.15	0.00	0.00	0.00	0.00	0.00	0.00	0.00	0.04	0.02
a_{hw}	0.20	0.62	0.46	0.05	0.47	0.56	0.90	0.40	0.00	0.33	0.11
$P * a_h$	0.09	0.47	0.28	0.68	0.51	0.41	0.12	0.03	0.21	0.79	0.61
$P * F_g$	0.85	0.40	0.00	0.00	0.90	0.01	0.00	0.08	0.79	0.64	0.95
$a_{hw} * F_g$	0.93	0.12	0.52	0.86	0.27	0.67	0.80	0.56	0.77	0.79	0.85
$P * F_p$	0.25	0.01	0.00	0.00	0.51	0.19	0.07	0.52	0.88	0.94	0.76
$a_{hw} * F_p$	0.96	0.94	0.87	0.50	0.60	0.99	0.84	0.94	0.64	0.99	0.91
$F_g * F_p$	0.96	0.97	0.94	0.33	0.27	0.39	0.95	0.70	0.92	0.94	0.89

Table 3.14: Statistical significance of the main factors on DPMI magnitude for each posture

Factors	4.7 Hz		7.8 Hz		14.8 Hz		28.9 Hz		48.4 Hz		64 Hz		78.9 Hz		100 Hz		134.4 Hz		200 Hz		300 Hz	
	P1	P2	P1	P2	P1	P2	P1	P2	P1	P2	P1	P2	P1	P2	P1	P2	P1	P2	P1	P2	P1	P2
F_g	0.89	0.89	0.81	0.49	0.98	0.00	0.00	0.00	0.00	0.00	0.00	0.04	0.00	0.92	0.19	0.21	0.00	0.00	0.00	0.00	0.00	0.00
F_p	0.99	0.22	0.44	0.01	0.47	0.00	0.02	0.00	0.00	0.00	0.00	0.00	0.00	0.00	0.00	0.00	0.00	0.00	0.17	0.24	0.09	0.24
a_{hw}	0.34	0.13	0.83	0.47	0.83	0.13	0.35	0.03	0.36	0.96	0.28	0.87	0.21	0.33	0.05	0.27	0.01	0.21	0.39	0.61	0.47	0.11
$a_{hw} * F_g$	1.00	0.92	0.93	0.09	0.96	0.22	0.88	0.52	0.87	0.19	0.88	0.31	0.97	0.80	0.73	0.76	0.92	0.81	0.86	0.91	0.93	0.91
$a_{hw} * F_p$	0.99	0.96	0.96	0.95	0.83	0.81	0.82	0.29	0.60	0.93	0.97	0.94	0.99	0.81	0.94	0.66	0.75	0.80	0.96	0.98	0.85	0.83
$F_g * F_p$	1.00	0.96	1.00	0.95	1.00	0.69	0.42	0.70	0.13	0.99	0.20	0.95	0.86	0.91	0.97	0.23	0.95	0.98	0.98	0.98	0.93	0.94

The influence of excitation magnitude is observed to be significant near 134.4 Hz and only marginally significant near 28.9 Hz when the ANOVA design involved both postures (Table 3.13). The analyses of the data attained for individual postures, however, suggest that excitation magnitude effect near 134.4 Hz is significant ($p < 0.05$) only for the $P1$ posture and near 28.9 Hz ($p < 0.05$) for the $P2$ posture only. These two frequencies are the prominent characteristics frequencies for the respective postures, as seen in Figure 3.29. The analysis based on the standard deviation of the mean, however, suggested negligible effect of the excitation magnitude.

The results attained for the two individual posture further show insignificant two-way interactions between the main factors over the entire frequency range. The results attained from the data across the two postures, however, show interactions that involve the posture at a few frequencies, notably below 100 Hz, as seen in Table 3.13.

3.10.2 Vibration transmissibility

The first ANOVA design was used to investigate the influence of all the main factors (posture P, measurement direction D_h, grip force F_g, push force F_p, and excitation level a_{hw}) on the transmissibility magnitudes at the wrist, elbow 1, elbow 2 and the shoulder. The results are summarized in Table 3.15. The second design was used to study the effects of the three main factors (F_g, F_p, and a_{hw}) on the z_h-axis and y_h-axis transmissibility magnitudes for each posture, as shown in Tables 3.16 and 3.17, respectively. The number of frequency points at which the main factors are significant were determined for each posture, measurement direction, and measurement location. The corresponding percentages, relative to the eleven selected frequencies points, were calculated and summarized in Table 3.18.

The results presented in Table 3.15 show significant effects of the hand-arm posture, measurement direction and their interactions on the hand-arm vibration transmissibility at nearly all the frequencies considered. The influences of the grip and push forces are also significant between 14.8 and 300 Hz, as observed from the DPMI data, while the effect of the excitation magnitude is significant only at very few frequencies. These results agree with the trends observed in the mean transmissibility magnitude data presented in section 3.9, except that the posture effect on the wrist transmissibility was not evident near 7.8 Hz.

Tables 3.16 to 3.18 show that the effect of the grip force is significant on the transmissibility magnitudes in both measurement directions and both postures at some of the frequencies and insignificant at other frequencies in the vicinity of the valleys in the DPMI responses. The statistical analysis results agree with the observations in the trends in Figures 3.23 – 3.25. The results further reveal the most significant effect of grip force on the forearm vibration for both postures, since the number of frequency points at which the effect of the grip force (F_g) is significant are higher at the wrist and elbow 1 (Table 3.18). This agrees with the inference derived from the DPMI response magnitudes and the observation of the subjects that the effect of grip force was mostly felt on the forearm. However, the effect of F_g in the z_h-axis direction is more prominent in the bent-arm posture than the extended arm posture, while the effect is more prominent for the extended arm posture in the y_h-axis.

Unlike the grip force, the main effect of the push force in the z_h-axis is significant for all measurement locations for both postures and measurement directions, as shown in Table 3.18. The effect of F_p is more prominent at the upper-arm in the y_h-axis

Table 3.15 Statistical significance of the main factors on transmissibility magnitudes

Factors	Locations	4.7 Hz	7.8 Hz	14.8 Hz	28.9 Hz	48.4 Hz	64 Hz	78.9 Hz	100 Hz	134 Hz	200 Hz	300 Hz
P	Wrist	0.09	0.00	0.16	0.00	0.00	0.00	0.00	0.00	0.05	0.13	0.01
	Elbow1	0.00	0.00	0.00	0.00	0.00	0.00	0.00	0.04	0.45	0.00	0.00
	Elbow2	0.00	0.00	0.00	0.00	0.22	0.01	0.00	0.00	0.00	0.00	0.00
	Shoulder	0.00	0.00	0.00	0.00	0.11	0.88	0.96	0.02	0.00	0.00	0.49
D_h	Wrist	0.00	0.00	0.00	0.00	0.00	0.05	0.00	0.00	0.17	0.00	0.00
	Elbow1	0.00	0.00	0.00	0.00	0.00	0.00	0.00	0.37	0.01	0.22	0.00
	Elbow2	0.00	0.00	0.00	0.00	0.24	0.00	0.00	0.01	0.12	0.00	0.00
	Shoulder	0.00	0.00	0.00	0.00	0.00	0.00	0.01	0.44	0.00	0.00	0.00
F_g	Wrist	0.69	0.08	0.12	0.15	0.10	0.00	0.00	0.00	0.05	0.49	0.02
	Elbow1	0.37	0.28	0.43	0.44	0.41	0.00	0.00	0.00	0.04	0.00	0.00
	Elbow2	0.80	0.30	0.24	0.00	0.06	0.16	0.66	0.71	0.27	0.52	0.00
	Shoulder	0.16	0.74	0.25	0.01	0.23	0.13	0.19	0.01	0.00	0.11	0.84
F_p	Wrist	0.49	0.32	0.57	0.01	0.00	0.00	0.00	0.00	0.00	0.00	0.00
	Elbow1	0.58	0.92	0.00	0.00	0.00	0.00	0.00	0.00	0.00	0.00	0.00
	Elbow2	0.81	0.30	0.00	0.00	0.05	0.00	0.00	0.00	0.00	0.00	0.14
	Shoulder	0.84	0.08	0.00	0.00	0.00	0.03	0.02	0.03	0.00	0.00	0.10
a_{hw}	Wrist	0.92	0.52	0.86	0.10	0.00	0.00	0.00	0.00	0.00	0.03	0.00
	Elbow1	0.12	0.19	0.00	0.00	0.00	0.00	0.00	0.00	0.00	0.00	0.23
	Elbow2	0.23	0.83	0.00	0.00	0.00	0.00	0.00	0.00	0.00	0.00	0.00
	Shoulder	0.43	0.17	0.00	0.00	0.00	0.00	0.00	0.00	0.00	0.00	0.00
$P * D_h$	Wrist	0.00	0.04	0.00	0.00	0.00	0.00	0.01	0.20	0.03	0.42	0.28
	Elbow1	0.00	0.00	0.00	0.00	0.00	0.00	0.00	0.00	0.00	0.08	0.14
	Elbow2	0.00	0.00	0.00	0.00	0.05	0.41	0.06	0.36	0.91	0.13	0.05
	Shoulder	0.00	0.02	0.00	0.00	0.00	0.00	0.00	0.00	0.00	0.00	0.00
$P * F_g$	Wrist	0.96	0.59	0.36	0.51	0.29	0.04	0.27	0.53	0.82	0.88	0.68
	Elbow1	0.76	0.09	0.00	0.00	0.67	0.53	0.42	0.34	0.66	0.62	0.33
	Elbow2	0.83	0.10	0.00	0.47	0.92	0.55	0.03	0.17	0.06	0.00	0.50
	Shoulder	0.84	0.06	0.00	0.00	0.31	0.50	0.83	0.85	0.92	0.44	0.35
$P * F_p$	Wrist	0.75	0.60	0.08	0.08	0.63	0.09	0.20	0.20	0.96	0.98	0.86
	Elbow1	0.95	0.04	0.00	0.01	0.08	0.05	0.07	0.21	0.50	0.58	0.74
	Elbow2	0.97	0.30	0.05	0.40	0.92	0.43	0.19	0.04	0.19	0.02	0.03
	Shoulder	0.87	0.01	0.15	0.51	0.03	0.19	0.30	0.40	0.37	0.99	0.97
$D_h * F_g$	Wrist	0.04	0.51	0.00	0.00	0.05	0.01	0.58	0.04	0.36	0.11	0.10
	Elbow1	0.63	0.34	0.01	0.00	0.02	0.48	0.14	0.29	0.55	0.82	0.95
	Elbow2	0.40	0.30	0.00	0.08	0.84	0.47	0.54	0.54	0.83	0.24	0.63
	Shoulder	0.34	0.64	0.74	0.01	0.32	0.72	0.67	0.90	0.48	0.00	0.24
$D_h * F_p$	Wrist	0.01	0.37	0.73	0.12	0.52	0.78	0.69	0.48	0.02	0.52	0.97
	Elbow1	0.03	0.09	0.01	0.02	0.01	0.01	0.02	0.16	0.82	0.72	0.06
	Elbow2	0.01	0.03	0.00	0.11	0.19	0.02	0.01	0.55	0.47	0.52	0.19
	Shoulder	0.00	0.00	0.78	0.27	0.01	0.01	0.02	0.90	0.35	0.32	0.45
$F_g * F_p$	Wrist	0.87	0.99	0.65	0.16	0.23	0.85	0.98	0.99	0.79	0.89	0.94
	Elbow1	0.98	0.85	0.00	0.00	0.96	0.82	0.49	1.00	0.69	0.84	0.08
	Elbow2	0.86	0.99	0.00	0.81	0.29	0.11	0.19	0.41	0.91	0.69	0.23
	Shoulder	0.95	0.89	0.97	0.94	0.91	1.00	0.91	0.99	0.89	0.84	0.33

Table 3.16: Statistical significance of the main factors on transmissibility magnitudes in the z_h-axis for each posture

Factors	Location	4.7 Hz		7.8 Hz		14.8 Hz		28.9 Hz		48.4 Hz		64 Hz		78.9 Hz		100 Hz		134.4 Hz		200 Hz		300 Hz	
		P1	P2	P1	P2	P1	P2	P1	P2	P1	P2	P1	P2	P1	P2	P1	P2	P1	P2	P1	P2	P1	P2
F_g	Wrist	0.27	0.83	0.07	0.58	0.75	0.00	0.00	0.00	0.00	0.01	0.00	0.00	0.00	0.05	0.05	0.36	0.05	0.47	0.45	0.80	0.01	0.95
	Elbow1	0.30	0.35	0.03	0.33	0.05	0.00	0.00	0.00	0.00	0.00	0.01	0.40	0.01	0.23	0.08	0.47	0.11	0.01	0.17	0.00	0.00	0.13
	Elbow2	0.76	0.75	0.34	0.75	0.00	0.00	0.00	0.00	0.88	0.27	0.14	0.07	0.01	0.66	0.02	0.35	0.04	0.68	0.00	0.54	0.80	0.11
	Shoulder	0.99	0.58	0.94	0.56	0.82	0.00	0.75	0.17	0.73	0.18	0.38	0.02	0.07	0.01	0.19	0.24	0.00	0.07	0.00	0.00	0.45	0.24
F_p	Wrist	0.00	0.93	0.00	0.47	0.08	0.00	0.40	0.00	0.01	0.01	0.00	0.00	0.00	0.00	0.00	0.01	0.00	0.03	0.13	0.24	0.07	0.04
	Elbow1	0.35	0.10	0.01	0.25	0.10	0.00	0.00	0.00	0.00	0.00	0.00	0.05	0.00	0.09	0.00	0.07	0.08	0.24	0.07	0.81	0.00	0.74
	Elbow2	0.03	0.18	0.01	0.73	0.00	0.00	0.00	0.00	0.23	0.01	0.00	0.00	0.00	0.00	0.00	0.00	0.00	0.00	0.00	0.06	0.01	0.32
	Shoulder	0.22	0.19	0.10	0.74	0.26	0.00	0.00	0.03	0.01	0.02	0.01	0.00	0.00	0.00	0.00	0.00	0.14	0.00	0.13	0.00	0.02	0.16
a_{hw}	Wrist	0.13	0.41	0.32	0.32	0.03	0.60	0.60	0.19	0.20	0.14	0.00	0.00	0.28	0.03	0.11	0.04	0.10	0.23	0.83	0.68	0.02	0.19
	Elbow1	0.00	0.05	0.02	0.95	0.14	0.66	0.94	0.95	0.89	0.12	0.20	0.01	0.53	0.79	0.11	0.04	0.10	0.26	0.02	0.04	0.00	0.81
	Elbow2	0.95	0.91	0.85	0.49	0.64	0.21	0.02	0.01	0.34	0.13	0.52	0.24	0.26	0.46	0.45	1.00	0.87	0.03	0.95	0.36	0.00	0.18
	Shoulder	0.01	0.38	0.19	0.26	0.08	0.09	0.07	0.17	0.47	0.57	0.09	0.10	0.26	0.46	0.13	0.67	0.00	0.02	0.26	0.28	0.63	0.68

Table 3.17: Statistical significance of the main factors on transmissibility magnitudes in the y_h-axis for each posture

Factors	Location	4.7 Hz		7.8 Hz		14.8 Hz		28.9 Hz		48.4 Hz		64 Hz		78.9 Hz		100 Hz		134.4 Hz		200 Hz		300 Hz	
		P1	P2	P1	P2	P1	P2	P1	P2	P1	P2	P1	P2	P1	P2	P1	P2	P1	P2	P1	P2	P1	P2
F_g	Wrist	0.14	0.62	0.22	0.00	0.59	0.00	0.05	0.67	0.19	0.53	0.30	0.77	0.21	0.18	0.03	0.09	0.03	0.00	0.18	0.00	0.14	0.02
	Elbow1	0.45	0.56	0.32	0.76	0.31	0.00	0.23	0.02	0.38	0.00	0.01	0.00	0.06	0.00	0.42	0.03	0.01	0.00	0.12	0.00	0.07	0.12
	Elbow2	0.82	0.46	0.76	0.13	0.15	0.00	0.18	0.00	0.30	0.45	0.19	0.66	0.07	0.22	0.32	0.31	0.11	0.68	0.01	0.91	0.23	0.54
	Shoulder	0.90	0.24	0.89	0.08	0.04	0.01	0.41	0.00	0.09	0.15	0.40	0.37	0.47	0.45	0.73	0.46	0.80	0.12	0.42	0.02	0.17	0.59
F_p	Wrist	0.00	0.72	0.01	0.18	0.35	0.74	0.42	0.19	0.01	0.12	0.00	0.08	0.02	0.07	0.01	0.10	0.97	0.41	0.79	0.61	0.61	0.27
	Elbow1	0.00	0.29	0.00	0.29	0.82	0.00	0.37	0.03	0.01	0.00	0.00	0.00	0.01	0.00	0.06	0.00	0.04	0.00	0.69	0.03	0.40	0.57
	Elbow2	0.82	0.05	0.72	0.15	0.25	0.00	0.42	0.00	0.00	0.00	0.01	0.03	0.00	0.21	0.00	0.05	0.00	0.02	0.00	0.02	0.00	0.02
	Shoulder	0.40	0.00	0.89	0.00	0.00	0.00	0.00	0.00	0.00	0.00	0.00	0.00	0.00	0.00	0.00	0.05	0.02	0.00	0.05	0.00	0.03	0.00
a_{hw}	Wrist	0.26	0.60	0.26	0.72	0.27	0.75	0.11	0.03	0.99	0.73	0.97	0.33	0.56	0.18	0.39	0.58	0.35	0.89	0.81	0.66	0.49	0.32
	Elbow1	0.11	0.60	0.02	0.16	0.02	0.34	0.29	0.16	0.61	0.55	0.02	0.00	0.16	0.00	0.80	0.00	0.56	0.00	0.25	0.00	0.02	0.37
	Elbow2	0.49	0.13	0.43	0.65	0.01	0.44	0.53	0.00	0.01	0.64	0.11	0.21	0.03	0.00	0.50	0.04	0.97	0.82	0.53	0.11	0.00	0.01
	Shoulder	0.40	0.08	0.17	0.26	0.79	0.38	0.12	0.03	0.00	0.48	0.40	0.34	0.77	0.49	0.07	0.22	0.61	0.00	0.00	0.00	0.00	0.73

136

Table 3.18: Percentage of discrete frequencies illustrating significance of the main factors

Factors	Measurement Location	z_h-axis		y_h-axis	
		P1	P2	P1	P2
F_g	Wrist	63.6	45.5	27.3	45.5
	Elbow1	63.6	45.5	18.2	72.7
	Elbow2	54.5	18.2	9.1	18.2
	Shoulder	18.2	36.4	9.1	27.3
F_p	Wrist	63.6	72.7	54.5	0.0
	Elbow1	63.6	36.4	54.5	72.7
	Elbow2	90.9	63.6	63.6	81.8
	Shoulder	54.5	72.7	81.8	100
a_{hw}	Wrist	54.5	27.3	0.0	9.1
	Elbow1	36.4	45.5	36.4	45.5
	Elbow2	18.2	18.2	36.4	36.4
	Shoulder	18.2	9.1	27.3	27.3
$a_{hw} * F_g$	Wrist	0.0	9.1	0.0	0.0
	Elbow1	9.1	9.1	0.0	9.1
	Elbow2	0.0	0.0	0.0	0.0
	Shoulder	0.0	0.0	18.2	0.0
$a_{hw} * F_p$	Wrist	0.0	0.0	0.0	0.0
	Elbow1	0.0	0.0	0.0	0.0
	Elbow2	0.0	0.0	18.2	0.0
	Shoulder	0.0	0.0	0.0	0.0
$F_g * F_p$	Wrist	0.0	9.1	0.0	0.0
	Elbow1	18.2	27.3	9.1	18.2
	Elbow2	9.1	27.3	0.0	0.0
	Shoulder	0.0	0.0	9.1	0.0

for both postures. The ANOVA results agree with the trends observed in the mean measured transmissibility responses presented in Figures 3.27 to 3.29. The effect of the interaction between the grip and push forces occurred in the z_h-axis at elbow 1 and 2 for the extended arm posture, although the effect of the interaction of the hand forces is small compared with their main effect. In general, the main effect of the grip force is more significant on the forearm in both directions and for both postures, while the significance of the push force is prominent at nearly all the locations hence it affects the entire hand-arm system. The effect of the excitation level is most significant at the wrist for the bent-

arm posture in the z_h-axis. Excitation level in the y_h-axis is significant at elbow 1 and 2, and the shoulder for both postures. The significance of the acceleration level (a_{hw}) is the least compared with the hand forces. The ANOVA results corroborate the trends shown in Figures 3.30 to 3.32.

3.11 Summary

The results of the analyses of simultaneously measured driving-point mechanical impedance (DPMI) and acceleration transmissibility responses of the human hand-arm system suggest that the DPMI characterizes the dynamics of the entire hand-arm system with emphasis around the driving-point and the bones/structure, while the acceleration transmissibility emphasizes the dynamic responses of the tissues/muscles of the human hand-arm system. Some of the characteristic frequencies obtained from the peaks in the mean transmissibility magnitudes are comparable with characteristic frequencies corresponding to valleys and peaks in the DPMI magnitudes, while some could not be related to either the valley or the peak. The influences of the hand forces show that the grip force mostly affects the peaks in the DPMI magnitude and transmissibility magnitudes measured on the forearm, while the push force affect both the valleys and peaks in the DPMI magnitude, and transmissibility magnitudes measured on the forearm and the upper-arm. Therefore, the experimental results support the hypothesis that was derived from the results of the analysis of dynamic characteristics of the 3-DOF hand-arm model reported in ISO 10068 (1998), namely: the peaks and valleys in the DPMI magnitude correspond to the resonant frequencies of the tissues/muscles and bones/structure of the human hand-arm system, respectively.

The main factors (grip and push forces, posture and excitation magnitude)

influence transmissibility responses in both the z_h- and y_h-axis directions and in the bent-arm and the extended arm postures. However, the effect of excitation magnitude on the DPMI magnitude is negligible, while other main factors have significant influence. The mean measured transmissibility magnitudes show that the human hand-arm system in an extended arm posture amplifies vibration transmitted to the upper-arm below 25 Hz, but it tends to attenuate vibration transmitted to the upper-arm more effectively than the bent-arm posture above 25 Hz, which limits greater vibration to the hand and the wrist.

The frequency weightings defined in ISO 5349-1 (2001) emphasize the assessment of vascular and neurological components of the hand-arm vibration syndrome, which are high frequency phenomenon since vibration at high frequencies (above 200 Hz) is mostly confined to the hand, even though the frequency weightings in ISO 5349-1 is maximum around 12.5 Hz. It has also been shown that the vibration of some hand-held power tools are predominant in the low frequency range (12.5 – 31.5 Hz), which is lower than the low frequency band in the medium-spectrum defined in ISO 10819 (1996). Considering the significant differences in the response of the human hand-arm to vibration in the bent-arm and extended arm postures at low frequencies, and the fact that musculoskeletal disorders have been associated with low frequency vibration, it may therefore be more appropriate to have two sets of standardized guidelines for assessment of potential injury risks. The first guideline for high frequency power tools for assessment of vascular and neurological disorder for high frequency hand-held power tools. The second guideline for low frequency power tools and assessment of musculoskeletal disorders.

CHAPTER 4

THE HUMAN HAND-ARM MODELS

4.1 Introduction

The human hand-arm responses to vibration exhibit extensive variations in the data and thus pose considerable complexities in interpretations. Apart from possible contributions due to anthropometric differences, such variabilities are attributed to variations in experimental conditions, as shown in chapter 3. The primary motivations for developing mechanical-equivalent models of the human hand-arm system arise from many potential applications. These include: (i) characterization of vibration amplitude and power flow in a coupled hand-arm and tool system; (ii) analyses of potential performance benefits of vibration-attenuation devices in an efficient manner; and (iii) development of a hand-arm simulator for assessing vibration transmission characteristics of different tools and vibration attenuation devices with minimal variability in the data. A number of biodynamic models of the hand-arm system have been proposed, which have been described in chapter one (section 1.2.2). The vast majority of the reported models do not consider the anatomical structure of the human hand-arm system. Furthermore, the shoulder is invariably assumed fixed, although considerable vibration of the shoulder was observed during the measurements. Moreover, considerable vibration of the shoulder and the head has been reported under an extended arm posture [93, 98]. This raises a major concern on the validity of the reported biodynamic models of the hand-arm system.

Only a few studies have proposed biomechanical models with consideration of the masses and physical dimensions of different structures of the human hand-arm [92, 99].

These models represented the hand by two masses representing the tissue/muscle/skin and the bones of the fingers and the palm-wrist structure. In both studies, the masses of the tissues/muscles and bones of the forearm and upper-arm were combined. Cherian et al. [92] obtained the model parameters by using the measured transmissibility responses on only one subject, while a poor agreement was observed between the model response and the measured data. On the other hand, Fritz [99] used the compliance data measured at the driving-point by Reynolds and Falkenberg [79] for model parameter identification, and compared the transmissibility responses of the resulting model with those reported by Reynolds and Angevine [93] and Pyykko et al. [94]. There was poor agreement between the measured compliance and transmissibility data and the model responses.

A recent study has proposed a bi-directional model of the hand for simulating the driving-point biodynamic responses distributed at the fingers and palm of the hand under excitation in the z_h-axis, using experimental DPMI data measured at the two driving-points (fingers-handle and palm-wrist-handle interfaces) [128]. The hand was represented by a clamp-like structure, in which the tissue/muscle/skin and bones of the fingers and the palm-wrist-forearm were separated. Although anthropometric masses were considered in the study, the dimensions of the forearm and the upper-arm were not considered since rotational degree-of-freedom was neglected. The comparison of the measured and model DPMI responses was satisfactory but combining palm, wrist and forearm as a single lumped mass did not permit analyses of the localized vibration properties of the hand-arm substructures.

In this dissertation research, a mechanical-equivalent model of the hand-arm system is proposed on the basis of the simultaneously measured DPMI and vibration

transmissibility responses, while anthropometric data are applied for constructing the model. Furthermore, the shoulder constraint employed in all of the reported models is relaxed by considering a lumped mass due to the trunk. The rationale for including the trunk into the model evolved from the observation made during the experiments, which clearly confirmed vibration of the upper body, particularly under the extended arm posture. Owing to the significant posture effect observed in the experimental data, two different models corresponding to the bent-arm and extended arm postures are proposed. The parameters of the models are obtained by minimizing the errors between the measured and the model DPMI and transmissibility responses. Sensitivity analyses were performed to identify parameters that greatly affect the biodynamic responses of the hand-arm system. In addition to matching the biodynamic responses of the models with the measured data, attempts were made to obtain reasonable agreement between the damped frequencies of the model and the characteristic frequencies obtained from the measured responses.

4.2 Biomechanical Models of the Hand-arm System

The measured biodynamic responses of the hand-arm system exposed to z_h-axis vibration revealed most important influence of the hand-arm posture, particular at low frequencies (below 25 Hz). It is thus essential to incorporate the postural variations as a variable in the model formulation. The reported hand-arm models, however, did not consider the effect of posture [51, 56, 68, 72, 79, 86, 100, 102, 103, 104]. Moreover, the structure of these models does not permit variation in the posture. The biomechanical model structures reported by Cherian et al. [92] and Fritz [99] could be applied to consider the postural variation in terms of the elbow angle, although the parameters of

these models were determined for fixed elbow angles of 90° and 120°, respectively. The consideration of elbow angle variations in the model is quite complex, since it would necessitate characterization of biodynamic responses and identification of biomechanical properties as a function of the elbow angle.

Alternatively, different models may be defined for different fixed elbow angles for which the target biodynamic responses are known. In this dissertation, two different models of the hand-arm system are formulated, corresponding to the two postures used in the experimental studies, namely: the bent-arm posture (elbow angle = 90°) and the extended arm posture (elbow angle = 180°).

4.2.1 Hand-arm model with 90° elbow angle

Figure 4.1 illustrates the structure of the proposed hand-arm system model corresponding to the bent-arm posture with 90° elbow angle. The hand is represented by a clamp-like structure, representing the bones of the fingers m_f and palm-wrist m_p, as proposed in [128]. The masses due to the tissues and skin covering the fingers and the palm-wrist contacting the handle are represented by m_{tf} and m_{tp}, respectively. The visco-elastic properties of the tissues are assumed to be linear and are designated by c_1 and k_1 for the fingers, and c_2 and k_2 for the palm. The masses due to the fingers (m_f) and the palm-wrist (m_p) are coupled through a visco-elastic element (c_3 and k_3), representing the visco-elastic properties of the carpals and metacarpals. The masses of the bones, tissues and skin of the forearm are lumped as m_{fa} and their linear visco-elastic properties are lumped at the wrist (c_w and k_w) and elbow (c_e and k_e). The masses due to the bone, tissues and skin of the upper-arm are also lumped as m_{ua}, and the linear visco-elastic
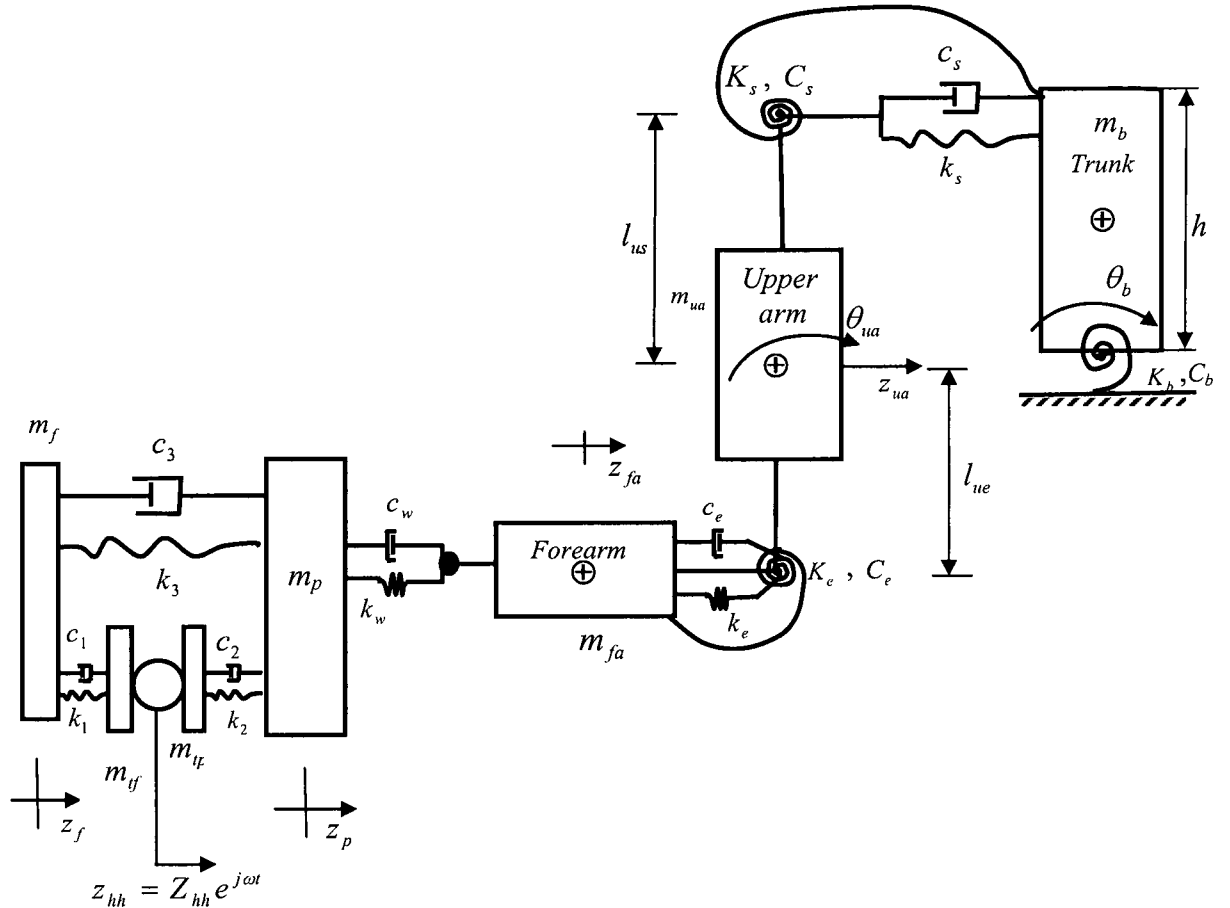
Figure 4.1: The biomechanical model of the hand-arm system with 90° elbow angle posture.

properties of the upper-arm structure are lumped at the elbow and shoulder (c_s and k_s). The rotation at the wrist is neglected, while the rotational visco-elastic properties at the elbow and shoulder joints are represented by C_e and K_e, and C_s and K_s, respectively. The trunk is also represented by a lumped mass m_b and with height h, coupling to the shoulder joint. The visco-elastic properties of the entire trunk structure are lumped at the pelvic joint and are represented by rotational stiffness K_b and viscous damping C_b.

In the model, z_{hh} is the displacement of the handle and z_i represents the motion of the masses of different substructures along the z_h-axis, where $i = f$, p, fa, ua,

corresponding to the masses of the fingers, palm-wrist, forearm and upper-arm, respectively. The rotational degrees-of-freedom (DOF) of the upper-arm and the trunk are represented by θ_{ua} and θ_b, respectively.

The equations of motion of the 6-DOF planar model of the hand-arm system are derived assuming that the measured responses represent the combined responses of the bone and muscle/tissue/skin of the human hand-arm structure. The hand and forearm structures are assumed to move along the z_h-axis, while the upper-arm structure undergoes general plane motion. The angular motion of the forearm is thus considered negligible when the hand exerts grip and push forces on the handle. The upper-arm, however, undergoes an angular motion about its center of mass. The trunk motion is assumed to be predominantly along the rotational direction, while the magnitudes of all angular motions are assumed to be small. The generalized coordinates of the model are chosen as the motions of the fingers mass m_f along the axis of vibration (z_f), palm-wrist mass m_p along z_h-axis (z_p), forearm mass m_{fa} along z_h-axis (z_{fa}), upper arm mass m_{ua} along z_h-axis (z_{ua}) and rotation about its center of mass (θ_{ua}), and the trunk mass m_b rotation about the pelvic joint (θ_b).

The equations describing the motions of the masses due to the fingers, palm-wrist and forearm are formulated as:

$$m_f \ddot{z}_f + c_1\left(\dot{z}_f - \dot{z}_{hh}\right) + c_3\left(\dot{z}_f - \dot{z}_p\right) + k_1\left(z_f - z_{hh}\right) + k_3\left(z_f - z_p\right) = 0 \tag{4.1}$$

$$m_p \ddot{z}_p + c_2\left(\dot{z}_p - \dot{z}_{hh}\right) + c_3\left(\dot{z}_p - \dot{z}_f\right) + c_w\left(\dot{z}_p - \dot{z}_{fa}\right) + k_2\left(z_p - z_{hh}\right) + \\ k_3\left(z_p - z_f\right) + k_w\left(z_p - z_{fa}\right) = 0 \tag{4.2}$$

$$m_{fa} \ddot{z}_{fa} + c_w \left(\dot{z}_{fa} - \dot{z}_p \right) + c_e \left(\dot{z}_{fa} - \dot{z}_{ua} + l_{ue} \dot{\theta}_{ua} \right) + k_w \left(z_{fa} - z_p \right) +$$
$$k_e \left(z_{fa} - z_{ua} + l_{ue} \theta_{ua} \right) = 0 \tag{4.3}$$

The equations describing the z_h-axis and rotational motion of the upper-arm mass are formulated as:

$$m_{ua} \ddot{z}_{ua} + c_e \left(\dot{z}_{ua} - l_{ue} \dot{\theta}_{ua} - \dot{z}_{fa} \right) + c_s \left(\dot{z}_{ua} + l_{us} \dot{\theta}_{ua} - h \dot{\theta}_b \right) +$$
$$k_e \left(z_{ua} - l_{ue} \theta_{ua} - z_{fa} \right) + k_s \left(z_{ua} + l_{us} \theta_{ua} - h \theta_b \right) = 0 \tag{4.4}$$

$$J_{ua} \ddot{\theta}_{ua} + C_e \dot{\theta}_{ua} + C_s \left(\dot{\theta}_{ua} - \dot{\theta}_b \right) + K_e \theta_{ua} + K_s \left(\theta_{ua} - \theta_b \right) +$$
$$\left[c_e \left(\dot{z}_{ua} - l_{ue} \dot{\theta}_{ua} - \dot{z}_{fa} \right) + k_e \left(z_{ua} - l_{ue} \theta_{ua} - z_{fa} \right) \right] l_{ue} + \tag{4.5}$$
$$\left[c_s \left(\dot{z}_{ua} + l_{us} \dot{\theta}_{ua} - h \dot{\theta}_b \right) + k_s \left(z_{ua} + l_{us} \theta_{ua} - h \theta_b \right) \right] l_{us} = 0$$

where J_{ua} is the mass moment of inertia of the upper-arm about the center of mass , l_{ua} is the upper-arm length, and l_{ue} and l_{us} define the distances from the upper-arm mass center to the elbow and shoulder joints, respectively. The equation of motion describing the rotational motion of the trunk is derived as:

$$J_b \ddot{\theta}_b + C_b \dot{\theta}_b + C_s \left(\dot{\theta}_b - \dot{\theta}_{ua} \right) + K_b \theta_b + K_s \left(\theta_b - \theta_{ua} \right) -$$
$$\left[c_s \left(\dot{z}_{ua} + l_{us} \dot{\theta}_{ua} - h \dot{\theta}_b \right) + k_s \left(z_{ua} + l_{us} \theta_{ua} - h \theta_b \right) \right] h = 0 \tag{4.6}$$

where J_b is the mass moment of inertia of the trunk about the pelvic joint. Two additional equations of motion are also derived for the masses m_{tf} and m_{tp} in order to derive the DPMI responses at the two interfaces:

$$m_{tf} \ddot{z}_{hh} + c_1 \left(\dot{z}_{hh} - \dot{z}_f \right) + k_1 \left(z_{hh} - z_f \right) = f_f$$
$$m_{tp} \ddot{z}_{hh} + c_2 \left(\dot{z}_{hh} - \dot{z}_p \right) + k_2 \left(z_{hh} - z_p \right) = f_p \tag{4.6a}$$

where f_f and f_p are the forces developed at the driving-points formed by the fingers-handle and palm-handle interfaces.

4.2 2 Hand-arm model with 180° elbow angle

The biomechanical model of the hand-arm system with an extended arm posture is formulated in a similar manner by considering elbow angle of 180°, as shown in Figure 4.2. The measured y_h-axis vibration responses at the elbow and shoulder of the hand-arm with an extended arm posture were observed to be significantly higher than those with the bent-arm posture, particularly up to 25 Hz. This suggested greater angular motion of the forearm under the extended arm posture, which is partly caused by the upper body serving as a constraint to the z_h-axis motion. Unlike the bent-arm posture, the extended arm model is thus formulated upon consideration of an additional degree-of-freedom associated with angular motion of the forearm (θ_{fa}), as shown in Figure 4.2. The equations of motion for the model are formulated using the assumptions outlined for the bent-arm model. The generalized coordinates of the model are chosen as the z_h-axis motions of the fingers mass m_f (z_f), palm-wrist mass m_p (z_p), forearm mass (z_{fa}),
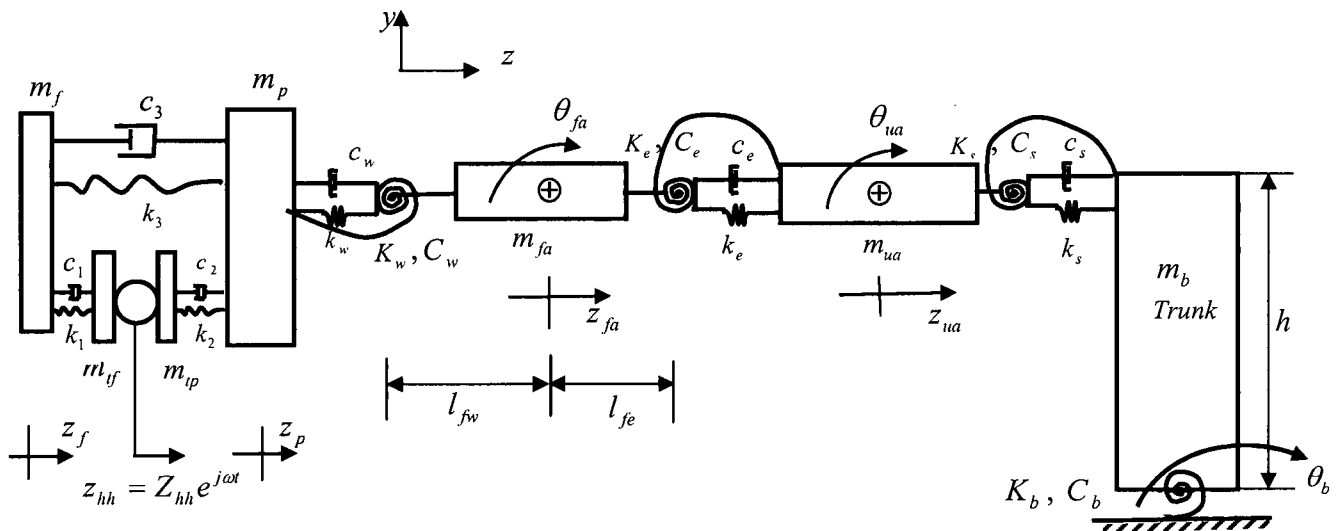
Figure 4.2: The biomechanical model of the hand-arm system with an extended arm posture.

upper arm mass m_{ua} (z_{ua}), and angular motions of the forearm (θ_{fa}) and upper-arm (θ_{ua}) about their respective mass centers, and angular motion of the trunk (θ_b) about the pelvic joint.

The stiffness of the hand-arm structure along the y_h-axis is assumed to be very large, although the rotation of the forearm and the upper-arm masses could yield their motions along the y_h - axis. The y_h - and z_h - axis motions at the wrist joint (y_w, z_w) are related to the forearm rotation θ_{fa} through the following kinematic relations:

$$z_w = z_{fa} + l_{fw}\left(1 - \cos\theta_{fa}\right)$$
$$y_w = l_{fw}\sin\theta_{fa}$$

where l_{fw} is the distance between the wrist joint and the forearm mass center. The y_h - and z_h - axis motions at the elbow joint (y_e, z_e) are also related to the forearm rotation, such that:

$$z_e = z_{fa} - l_{fe}\left(1 - \cos\theta_{fa}\right)$$
$$y_e = -l_{fe}\sin\theta_{fa}$$

where l_{fe} is the distance between the elbow joint and the forearm mass center. The assumption of small magnitude rotation of the forearm yields:

$$z_w = z_e = z_{fa}$$
$$y_w = l_{fw}\theta_{fa} \tag{4.7}$$
$$y_e = -l_{fe}\theta_{fa}$$

The equations describing the motion of the fingers and palm-wrist masses are identical to those derived for the bent-arm posture in Eqs. (4.1) and (4.2). The equations describing the z_h-axis and angular motions of the forearm are derived as:

$$m_{fa}\ddot{z}_{fa} + c_w\left(\dot{z}_{fa} - \dot{z}_p\right) + c_e\left(\dot{z}_{fa} - \dot{z}_{ua}\right) + k_w\left(z_{fa} - z_p\right) + k_e\left(z_{fa} - z_{ua}\right) = 0 \tag{4.8}$$

$$J_{fa}\ddot{\theta}_{fa} + C_w\dot{\theta}_{fa} + C_e\left(\dot{\theta}_{fa} - \dot{\theta}_{ua}\right) + K_w\theta_{fa} + K_e\left(\theta_{fa} - \theta_{ua}\right) +$$
$$\left[c_w\left(\dot{z}_{fa} - \dot{z}_p\right) + k_w\left(z_{fa} - z_p\right)\right]_{fw}\theta_{fa} + \left[c_e\left(\dot{z}_{fa} - \dot{z}_{ua}\right) + k_e\left(z_{fa} - z_{ua}\right)\right]_{fe}\theta_{fa} = 0 \tag{4.9}$$

The second order terms involving products of small motions could be neglected considering small motions. Equation (4.9) thus reduces to the following linear form:

$$J_{fa}\ddot{\theta}_{fa} + C_w\dot{\theta}_{fa} + C_e\left(\dot{\theta}_{fa} - \dot{\theta}_{ua}\right) + K_w\theta_{fa} + K_e\left(\theta_{fa} - \theta_{ua}\right) = 0 \tag{4.9a}$$

Equations (4.8) and (4.9a) suggest that the z_h-axis and rotational motions are uncoupled, while the y_h-axis motion at the wrist and elbow joints are related to the forearm rotation, as seen in Eq. (4.7). The equations describing the upper-arm motions are obtained in a similar manner assuming small magnitude rotation θ_{ua} and negligible contributions due to second order terms, such that:

$$m_{ua}\ddot{z}_{ua} + c_e\left(\dot{z}_{ua} - \dot{z}_{fa}\right) + c_s\left(\dot{z}_{ua} - h\dot{\theta}_b\right) + k_e\left(z_{ua} - z_{fa}\right) + k_s\left(z_{ua} - h\theta_b\right) = 0 \tag{4.10}$$

$$J_{ua}\ddot{\theta}_{ua} + C_e\left(\dot{\theta}_{ua} - \dot{\theta}_{fa}\right) + C_s\left(\dot{\theta}_{ua} - \dot{\theta}_b\right) + K_e\left(\theta_{ua} - \theta_{fa}\right) + K_s\left(\theta_{ua} - \theta_b\right) = 0 \tag{4.11}$$

The y_h-axis motion of the elbow joint on the upper-arm side (y_e^{ua}) and the shoulder joint (y_s) are related to the upper arm rotation as:

$$y_e^{ua} = l_{ue}\theta_{ua}$$
$$y_s = -l_{us}\theta_{ua} \tag{4.12}$$

The equation of motion for the trunk rotation is derived in a similar manner as:

$$J_b\ddot{\theta}_b + C_s\left(\dot{\theta}_b - \dot{\theta}_{ua}\right) + C_b\dot{\theta}_b + K_s\left(\theta_b - \theta_{ua}\right) + K_b\theta_b$$
$$+ \left[c_s\left(h\dot{\theta}_b - \dot{z}_{ua}\right) + k_s\left(h\theta_b - z_{ua}\right)\right]h = 0 \tag{4.13}$$

4.3 Analyses of Biodynamic Responses

The equations of motion derived for the two postures are analyzed to derive the

biodynamic responses of the hand-arm system subject to z_h-axis vibration. The responses are obtained in terms of driving-point mechanical impedance (DPMI) and vibration transmitted to different locations of the hand-arm model. The differential equations of motion of the two models can be expressed in the matrix form in the following manner:

$$[M]\{\ddot{\xi}_{ea}\} + [C]\{\dot{\xi}_{ea}\} + [K]\{\xi_{ea}\} = \{F_{ea}\} \tag{4.14}$$

where $[M]$, $[C]$ and $[K]$ are $(n \times n)$ inertial, damping and stiffness matrices, respectively, $\{F_{ea}\}$ is $(n \times 1)$ force vector and $\{\xi_{ea}\}$ is $(n \times 1)$ generalized displacement coordinate vector of the model, where n refers to the DOF of the model and ea designates elbow angle (90° or 180°). The displacement vectors for the 6- and 7- DOF models corresponding to the bent-arm and extended arm postures are defined as:

$$\{\xi_{90^\circ}\} = \{z_f \quad z_p \quad z_{fa} \quad z_{ua} \quad \theta_{ua} \quad \theta_b\}' \text{ for the bent-arm model; and}$$

$$\{\xi_{180^\circ}\} = \{z_f \quad z_p \quad z_{fa} \quad \theta_{fa} \quad z_{ua} \quad \theta_{ua} \quad \theta_b\}' \text{ for the extended arm model.}$$

where "'" designates the transpose. Assuming harmonic solutions $z_{hh} = Z_{hh}e^{j\omega t}$ and $\xi_{ea} = \chi_{ea}e^{j\omega t}$, the force vectors for the models are obtained as:

$$\{F_{90^\circ}\} = \{k_1 + j\omega c_1 \quad k_2 + j\omega c_2 \quad 0 \quad 0 \quad 0 \quad 0\}' Z_{hh}e^{j\omega t}$$

$$\{F_{180^\circ}\} = \{k_1 + j\omega c_1 \quad k_2 + j\omega c_2 \quad 0 \quad 0 \quad 0 \quad 0\}' Z_{hh}e^{j\omega t}$$

Equation (4.14) is then solved to determine the transmitted vibration responses in the frequency domain as:

$$\{\chi_{ea}(j\omega)\} = [[K] - \omega^2[M] + j\omega[C]]^{-1}\{F_{ea}\} \tag{4.15}$$

The z_h-axis vibration transmissibility responses of different segments of the hand-arm models are subsequently defined as:

$$T_{wz}(j\omega) = \frac{Z_p(j\omega)}{Z_{hh}(j\omega)} \qquad (4.16a)$$

$$T_{ez}(j\omega) = \frac{Z_{fa}(j\omega)}{Z_{hh}(j\omega)} \qquad (4.16b)$$

$$T_{sz}(j\omega) = \frac{Z_s(j\omega)}{Z_{hh}(j\omega)} \qquad (4.16c)$$

where T_{wz} refers to vibration transmissibility of the wrist joint along the z_h-axis, which is considered to be identical to that of the wrist-palm mass, T_{ez} refers to the vibration transmissibility of the elbow joint on the forearm side, and T_{sz}, in a similar manner, refers to the vibration transmissibility at the shoulder joint. It should be noted that the z_h-axis motion of the shoulder joint (Z_s), in the case of the extended arm posture, is identical to Z_{ua} for small rotation of the upper-arm, in a similar manner that has been demonstrated for the elbow joint on the forearm side in Eq. (4.7). The z_h-axis response of the shoulder, Z_s, for the bent-arm posture, is defined as:

$$Z_s(j\omega) = Z_{ua}(j\omega) + l_{us}\theta_{ua}(j\omega) \qquad (4.17)$$

The y_h-axis responses at the joints for the extended arm posture are derived from the angular motions of the fore- and upper-arm, together with the kinematic relations, such that:

$$T_{wy}(j\omega) = \frac{l_{fw}\theta_{fa}(j\omega)}{Z_{hh}(j\omega)} \qquad (4.18a)$$

$$T_{ey}(j\omega) = \frac{l_{ue}\theta_{ua}(j\omega) - l_{fe}\theta_{fa}(j\omega)}{Z_{hh}(j\omega)} \qquad (4.18b)$$

$$T_{sy}(j\omega) = \frac{l_{us}\theta_{ua}(j\omega)}{Z_{hh}(j\omega)} \qquad (4.18c)$$

The DPMI responses distributed at the fingers and palm sides of the handle are derived as:

$$DPMI_f(j\omega) = \frac{f_f(j\omega)}{j\omega Z_{hh}} = \frac{-\omega^2 Z_{hh} m_{tf} + (k_1 + j\omega c_1)(Z_{hh} - Z_f(j\omega))}{j\omega Z_{hh}} \qquad (4.19a)$$

$$DPMI_p(j\omega) = \frac{f_p(j\omega)}{j\omega Z_{hh}} = \frac{-\omega^2 Z_{hh} m_{tp} + (k_2 + j\omega c_2)(Z_{hh} - Z_p(j\omega))}{j\omega Z_{hh}} \qquad (4.19b)$$

where the subscripts 'f' and 'p' refer to the DPMI at the fingers- and palm-side interface, respectively. The total DPMI of the hand-arm system for both the bent-arm and extended arm models is derived as:

$$DPMI(j\omega) = DPMI_f(j\omega) + DPMI_p(j\omega) \qquad (4.20)$$

4.4 Identification of Model Parameters

The vast majority of the reported models of the human-arm have been derived on the basis of DPMI response alone, by curve fitting the model response with the measured DPMI data, where the anatomical structure and anthropometry were ignored [51, 56, 68, 72, 79, 86, 100, 102, 103, 104]. Thus, the resulting solution cannot be considered unique. This is evident from the large differences in the reported model parameters [65]. The biomechanical models reported in [92, 99] considered both the anthropometric masses and dimensions of the human hand-arm system, while those in [128] considered only the anthropometric masses. The model parameters were derived using "to-the-hand" biodynamic response in [99 and 128], while "through-the-hand" responses were used in [92]. Although a reasonably good agreement between the model and the measured DPMI data was presented in [128], poor agreements in compliance [99] and transmitted vibration [92] responses were obtained. The model prediction ability and uniqueness

could be enhanced by considering the hand-arm anthropometry, together with the measured DPMI and localized vibration responses, and the identified characteristic frequencies. The ranges of the model parameters identified through the available anthropometric data are described below, together with the model parameters to be determined.

4.4.1 Inertia, geometric and visco-elastic parameters

The hand-arm biodynamic models corresponding to the bent-arm and extended arm posture involve identification of 25 and 27 parameters, respectively. The parameter vectors comprising inertia and visco-elastic parameters are given by:

$$\{X_{90°}\} = [m_f \quad m_{tf} \quad m_p \quad m_{tp} \quad m_{fa} \quad m_{ua} \quad m_b \quad c_1 \quad c_2 \quad c_3 \quad c_w \quad c_e \quad c_s \quad C_e \quad C_s \quad C_b$$
$$k_1 \quad k_2 \quad k_3 \quad k_w \quad k_e \quad k_s \quad K_e \quad K_s \quad K_b]'$$
(4.21a)

$$\{X_{180°}\} = [m_f \quad m_{tf} \quad m_p \quad m_{tp} \quad m_{fa} \quad m_{ua} \quad m_b \quad c_1 \quad c_2 \quad c_3 \quad c_w \quad c_e \quad c_s \quad C_w \quad C_e \quad C_s \quad C_b$$
$$k_1 \quad k_2 \quad k_3 \quad k_w \quad k_e \quad k_s \quad K_w \quad K_e \quad K_s \quad K_b]'$$
(4.21b)

The inertia and geometric parameters are estimated from the human anthropometry defined in [107]. The mean body mass of the subjects was estimated as 72.2 kg, while the mean lengths of the forearm and the upper-arm were 26.0 and 20.5 cm, respectively (Table 3.4). The anthropometric masses of the hand M_h, forearm M_{fa}, upper-arm M_{ua} and the trunk M_b have been estimated as 0.65 %, 1.9 %, 3.3 % and 45.5 %, respectively, of the mean body mass [107]. Considering the mean body mass of 72.2 kg, masses and dimensions of different segments of the hand-arm system and the trunk are evaluated and summarized in Table 4.1. The table also shows the mass and dimensional model parameters that are either related to or estimated from the nominal anthropometric parameters. The stiffness and damping parameters of the models were identified through

minimization of composite error function of the measured data and the model responses.

Table 4.1: Inertial and dimensional data for the hand-arm models

Substructure description	Anthropometric values	Model parameters
Hand-arm mass M_{ha}	4.224 kg	$m_f + m_{tf} + m_p + m_{tp} + m_{fa} + m_{ua} = M_{ha}$
Hand mass M_h	0.469 kg	$m_f + m_{tf} + m_p + m_{tp} = M_h$
Forearm mass M_{fa}	1.372 kg	m_{fa}
Forearm length l_{fa}	26.0 cm	$J_{fa} = \dfrac{m_{fa} l_{fa}^2}{12}$
Forearm center of mass to wrist l_{fw}	14.8 cm	
Forearm center of mass to elbow l_{fe}	11.2 cm	
Upper-arm mass M_{ua}	2.383 kg	m_{ua}
Upper-arm length l_{ua}	20.5 cm	$J_{ua} = \dfrac{m_{ua} l_{ua}^2}{12}$
Upper-arm center of mass to elbow l_{ue}	8.94 cm	
Upper-arm center of mass to shoulder l_{us}	11.56 cm	
Trunk mass M_b	33.2 kg	$m_b,\ J_b = \dfrac{m_b h^2}{3}$
Trunk length h	52.0 cm	

4.4.2 Optimization formulation and solution methodology

The model parameters were determined by minimizing a composite squared error function between the model and the measured biodynamic responses. The objective or error function $E(X_{ea})$ is formulated upon considerations of errors between the DPMI and the localized transmitted vibration responses, such that:

$$E(X_{90^\circ}) = \alpha_1 \left[\sum_{r=1}^{N} \sum_{i=1}^{3} \left\{ \beta_{1i} \left(T_{mi}(\omega_r) - T_i(\omega_r) \right)^2 + \gamma_{1i} \left(\phi_{mi}(\omega_r) - \phi_i(\omega_r) \right)^2 \right\} \right] +$$
$$\alpha_2 \left[\sum_{r=1}^{N} \left\{ \beta_2 \left(DPMI_m(\omega_r) - DPMI(\omega_r) \right)^2 + \gamma_2 \left(\phi_m(\omega_r) - \phi(\omega_r) \right)^2 \right\} \right]$$

(4.22a)

$$E(X_{180^\circ}) = \alpha_1 \left[\sum_{r=1}^{N} \sum_{i=1}^{3} \left\{ \begin{matrix} \beta_{1i}\left(T_{mi}(\omega_r) - T_i(\omega_r)\right)^2 + \gamma_{1i}\left(\phi_{mi}(\omega_r) - \phi_i(\omega_r)\right)^2 + \\ \beta_{1yi}\left(T_{myi}(\omega_r) - T_{yi}(\omega_r)\right)^2 + \gamma_{1yi}\left(\phi_{myi}(\omega_r) - \phi_{yi}(\omega_r)\right)^2 \end{matrix} \right\} \right] +$$

$$\alpha_2 \left[\sum_{r=1}^{N} \left\{ \beta_2 \left(DPMI_m(\omega_r) - DPMI(\omega_r)\right)^2 + \gamma_2\left(\phi_m(\omega_r) - \phi(\omega_r)\right)^2 \right\} \right] \qquad (4.22b)$$

where $E(X_{ea})$ is the composite error function corresponding to elbow angle "ea" (90° and 180°) and $\{X_{ea}\}$ is the parameter vector. Each error function comprises two components: a weighted error between the measured and model DPMI responses, and a weighted error between the measured vibration transmissibility and model responses of different segments.

In the above formulation, $T_{mi}(\omega_r)$ and $\phi_{mi}(\omega_r)$ refer to the measured z_h-axis vibration transmissibility magnitude and phase, respectively, at a location i (wrist, elbow or shoulder). $T_i(\omega_r)$ and $\phi_i(\omega_r)$ are the model z_h-axis vibration transmissibility magnitude and phase from the model. Similarly, T_{myi} and T_{yi}, are the measured and model vibration transmissibility magnitudes along the y_h–axis, and ϕ_{myi} and ϕ_{yi} are the corresponding phase responses. In a similar manner, $DPMI_m$ and $DPMI$, are the DPMI magnitudes of the measured and model responses, and the ϕ_m and ϕ are the corresponding phase responses. The error functions are computed at 56 different discrete frequencies in the 2.5 – 500 Hz range ($r = 1, 2, 3,...N; N = 56$). The coefficients α_1 and α_2 are weighting factors imposed on the transmissibility and the DPMI errors, respectively, while β_j and γ_j are the weighting factors imposed on the magnitude and phase errors, respectively ($j = 1$ for transmissibility, and $j = 2$ for DPMI).

The composite error functions are minimized subject to the following inequality constraints:

$$c_l > 0; \quad k_l > 0 \quad (l = 1,2,3,w,e,s)$$

$$C_v > 0; \quad K_v > 0 \quad \begin{pmatrix} v = e,s,b & for & the & bent-arm & and \\ v = w,e,s,b & for & the & extended & arm & model \end{pmatrix} \tag{4.23}$$

Apart from the above, the minimization problem is solved subject to a number of limit constraints. The segment masses and the hand-arm masses are permitted to vary about the nominal masses, estimated from the anthropometric data (Table 4.1), by defining the following limit constraints:

$$(1-\eta)M_{fa} < m_{fa} < (1+\eta)M_{fa}$$
$$(1-\eta)M_{ua} < m_{ua} < (1+\eta)M_{ua}$$
$$(1-\eta)M_b < m_b < (1+\eta)M_b \tag{4.24}$$
$$(1-\eta)M_h < m_f + m_{tf} + m_p + m_{tp} < (1+\eta)M_h$$
$$(1-\eta)M_{ha} < m_f + m_{tf} + m_p + m_{tp} + m_{fa} + m_{ua} < (1+\eta)M_{ha}$$

where η defines the permissible variation about the nominal anthropometric masses.

4.4.3 Solution of the minimization problem

The constrained optimization toolbox in MATLAB was used to solve the minimization problem defined in Eqs. (4.22) to (4.24). The solutions were attained for three different functions: (i) minimization of DPMI error by letting $\alpha_1 = 0$; (ii) minimization of transmissibility error by letting $\alpha_2 = 0$; (iii) minimization of the combined error functions. The solutions were attained for different values of the weighting functions β_{1i}, γ_{1i}, β_2, γ_2, β_{1yi} and γ_{1yi} for the first two cases, while the final case further involved different values of α_1 and α_2. The weights were selected to achieve minimum errors in the responses, while the solution were obtained for a wide range of the starting vector, which generally converged to comparable solutions.

Furthermore, sensitivity analyses were performed to identify the parameters that

greatly affect the biodynamic responses of the hand-arm models by: (1) observing the effects of (± 5, 10, 15 and 20 %) variations in each parameter on the DPMI and transmissibility responses; and (2) logarithmic sensitivity analysis in the frequency domain as proposed in [129], when each parameter was varied by 20 %. The logarithmic sensitivity function is defined as:

$$S_{X_{ea}^k}^{\chi_{ea}^{k,r}} = \frac{\partial \ln \chi_{ea}^{k,r}}{\partial \ln X_{ea}^k} \approx \mathrm{Re}\left[\frac{\Delta\chi_{ea}^{k,r}/\chi_{ea}^r}{\Delta X_{ea}^k/X_{ea}^k}\right] \tag{4.25}$$

where 'Re' denotes the real part of the complex logarithmic sensitivity expression. $S_{X_{ea}^k}^{\chi_{ea}^{k,r}}$ is the logarithmic sensitivity index of the responses of the model masses due to a change in parameter k (X_{ea}^k) at frequency r. $\Delta\chi_{ea}^{k,r}$ is the change in the response vector determined from Eq. (4.15) at a frequency r due to a change in parameter k, χ_{ea}^r is the response vector at a frequency r corresponding to the nominal parameter vector. The nominal parameter vector is taken as that obtained upon minimization of the DPMI and transmissibility response errors, as defined in Eqs. (4.22a) or (4.22b). The results of the sensitivity analysis were used to reduce the number of parameters to be identified through solution of the minimization problems.

4.4.4 The target functions

The minimization problems are solved using the measured target response function of DPMI and vibration transmissibility. The measured biodynamic responses of the human hand-arm to vibration, however, revealed dependence on the hand-arm forces and posture, while the effect of excitation magnitude was marginally significant on the transmissibility responses and insignificant on the DPMI response. For the purposes of

determining the model parameters, the mean measured DPMI and transmissibility responses corresponding to 30 N grip force, 50 N push force and excitation level of 5.25 m/s^2, presented in Figures 3.17(b), 3.19 and 3.20, are considered as the target functions for the two different postures. The selected hand forces are identical to those recommended in ISO 10819 [117] for the assessment of anti-vibration gloves. Moreover, this hand forces combination was judged as the most comfortable and easily controllable for relatively long periods by all the subjects. The sensitivity analysis was performed on the target functions corresponding to the same experimental conditions. The responses corresponding to other hand forces combinations (10 and 50 N grip, and 25 and 75 N push forces) were also considered as target functions, in order to study the effect of hand forces on the model parameters.

The identified characteristic frequencies from the mean measured biodynamic responses presented in Tables 3.8 and 3.9 are also considered as target functions for the modal parameters of the models. Therefore, attempts were made to match the responses of the proposed models with the mean measured biodynamic responses and the identified characteristic frequencies of the human hand-arm system.

4.5 Biodynamic Responses of the Models and Identified Parameters

4.5.1 Responses of the bent-arm model

Figures 4.3 and 4.4 present comparisons of the measured and the model DPMI and transmissibility response magnitudes with those of the model, respectively, derived upon minimization of the DPMI ($\alpha_1 = 0$) and transmissibility ($\alpha_2 = 0$) errors. The comparisons of the transmissibility responses are presented in linear as well as logarithmic scales, in order to highlight the prediction abilities in the low and high

frequency ranges, respectively. The target responses are designated as "Measured" in the figures. The model derived on the basis of the DPMI response error alone resulted in very good agreement in the DPMI responses (Figure 4.3(a)) but considerable errors in all the transmissibility responses (Figure 4.4(a)). The minimization of the transmissibility error alone, on the other hand, resulted in reasonably good agreement between the mean measured and the model transmissibility responses (Figure 4.4(b))), while the agreement between the measured and the model DPMI responses was poor (Figure 4.3(b)). The results suggest the models identified on the basis of either DPMI or transmissibility errors would yield poor prediction of the biodynamic responses of the hand-arm system to z_h-axis vibration. Moreover, a rapid convergence of the solution was attained when the DPMI response alone was considered compared with the transmissibility error function. The corresponding errors in the transmissibility responses were substantial in most of the frequency range. Since the reported models are vastly based on measured DPMI response alone, these models may not be considered applicable for predicting transmitted vibration. Furthermore, all attempts to match the model transmissibility phase with the measured data proved to be futile, hence the transmissibility phase responses are not presented.

Figure 4.5 presents comparison of the responses of the measured data with the biodynamic responses of the model derived upon minimization of composite error function of the DPMI and transmissibility responses. The solutions represent a compromise between the responses of the model obtained through minimization of individual biodynamic response errors. The comparisons reveal relatively smaller errors in the transmissibility responses, while the error in the DPMI response is larger.
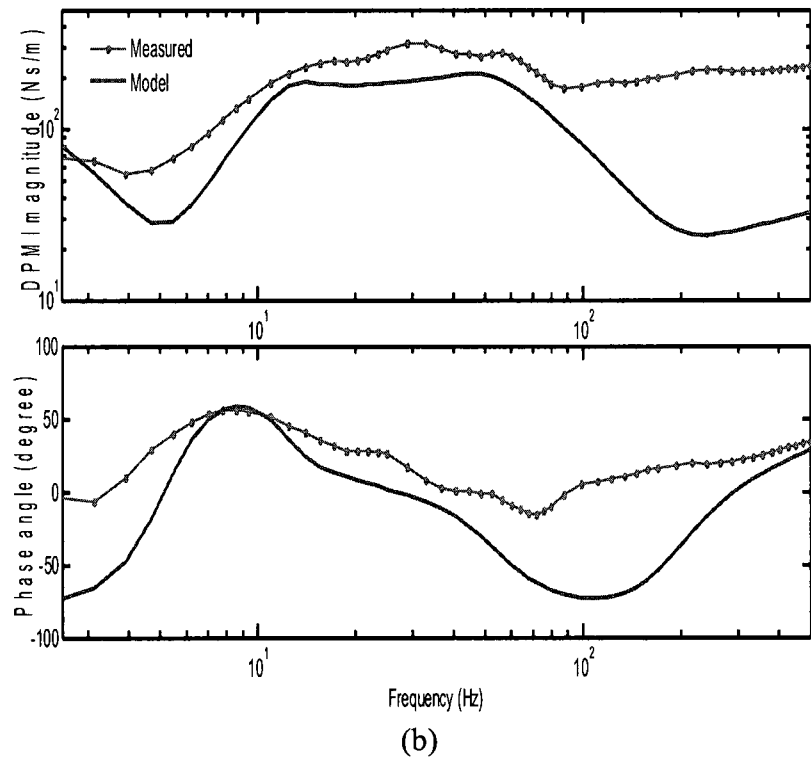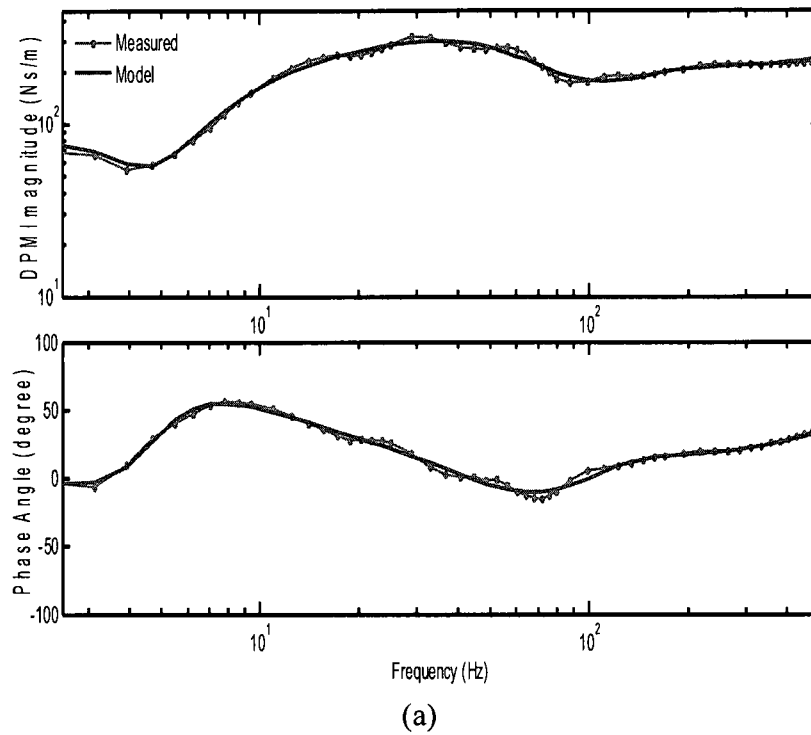
Figure 4.3: Comparison of the measured DPMI magnitude and phase responses with those of the model derived through minimization of errors in: (a) DPMI only; (b) transmissibility only.

160
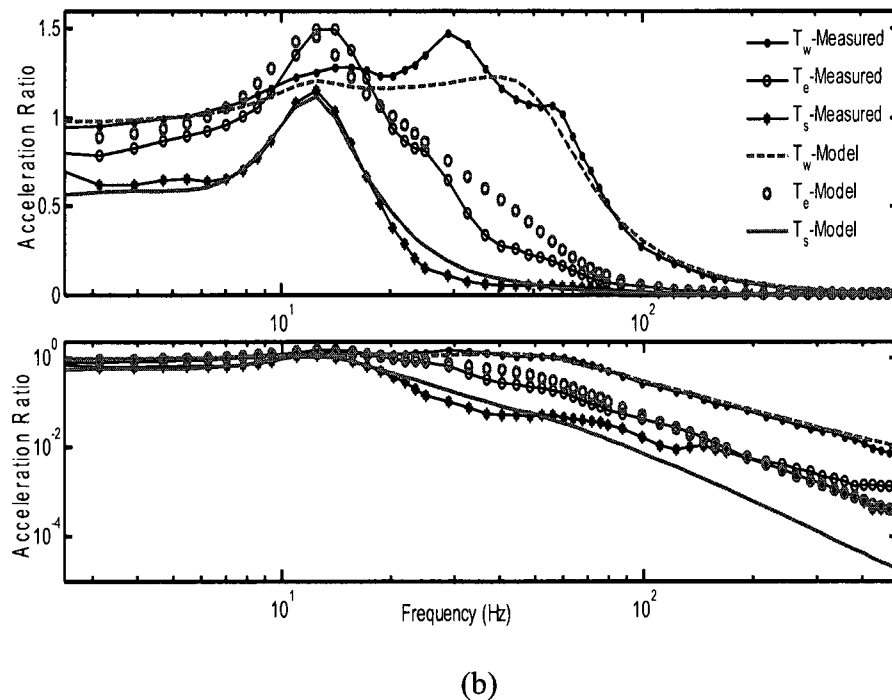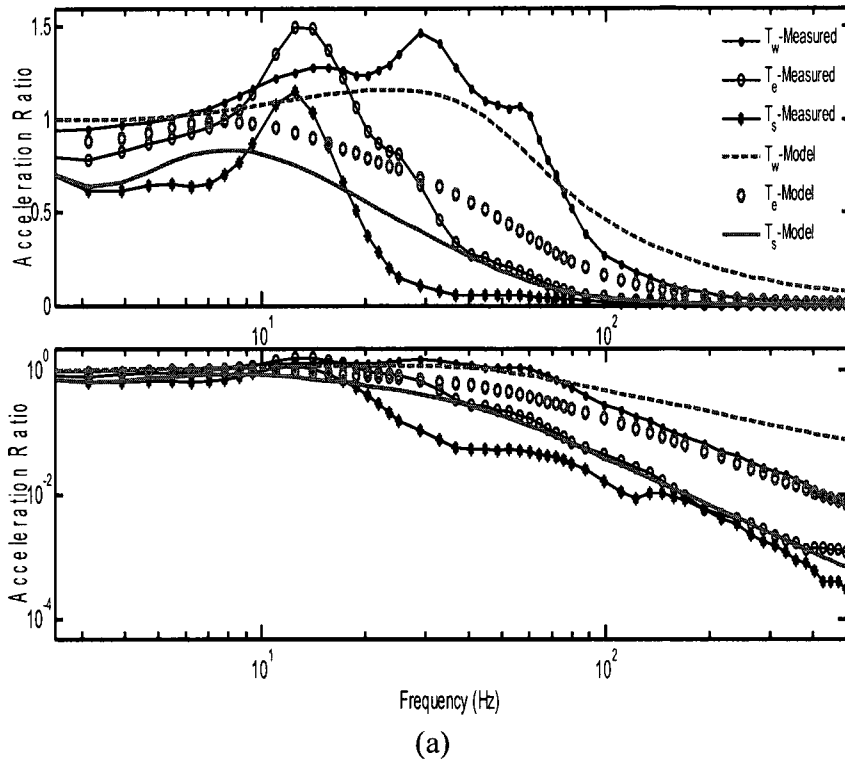
Figure 4.4: Comparison of the measured transmissibility magnitudes with those of the model derived through minimization of errors in: (a) DPMI only; (b) transmissibility only.
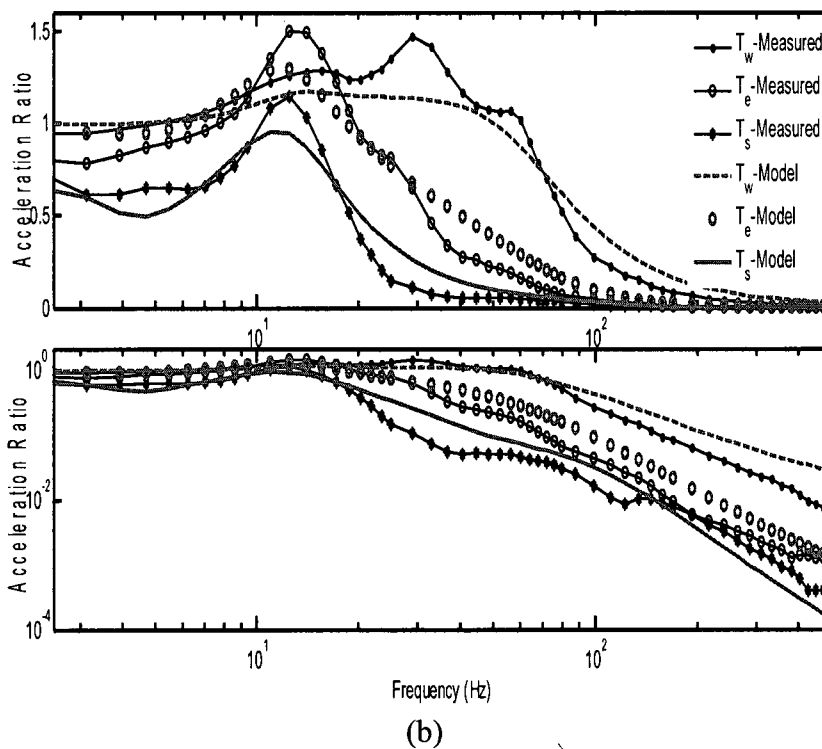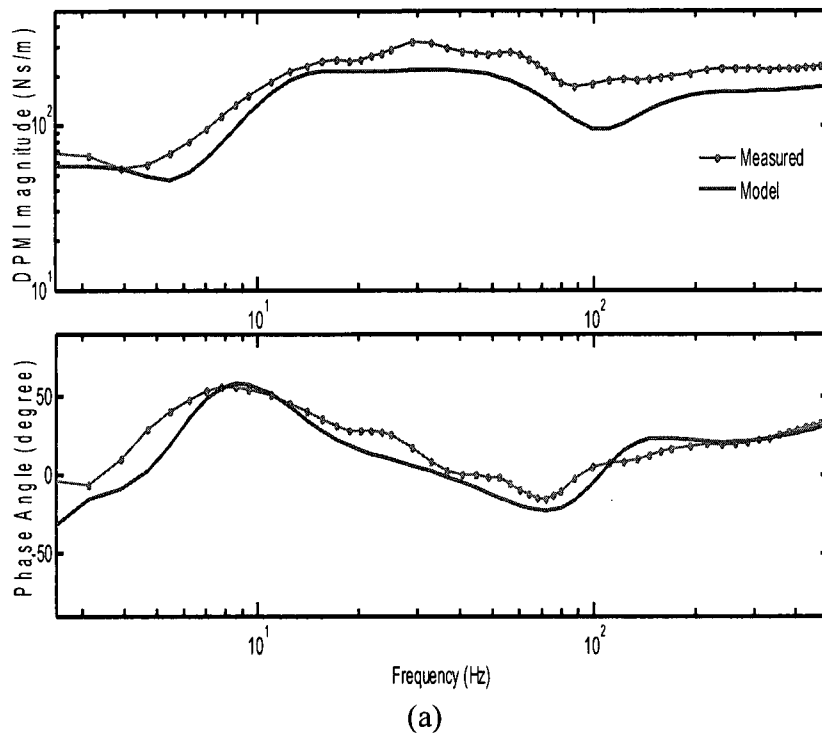
Figure 4.5: Comparison of the measured responses with those of the model derived through minimization of errors in DPMI and transmissibility responses: (a) DPMI; (b) z_h-axis transmissibility.

4.5.2 Sensitivity analyses results

The solutions of the minimization problems corresponding to different combinations of weightings and starting vectors revealed negligible changes in some of the model parameters, suggesting that the biodynamic responses was insensitive to variations in some of the parameters. Consequently, sensitivity analyses were performed to identify the parameters that have the most influence on the biodynamic responses using the two techniques discussed in section 4.4.3. The results were applied to refine the minimization problem with reduced parameters vector, which was achieved by fixing the values of the parameters that have negligible influence on biodynamic responses. The parameters vector, corresponding to Figure 4.5, identified through minimization of the composite error function was used as the nominal parameters for the sensitivity analyses.

Figures 4.6 to 4.9 show the variations in logarithmic sensitivity indices due to 20 % change in the model parameters on the responses at the fingers, palm-wrist, forearm and upper-arm in the entire frequency range. The results clearly suggest strong influences of some of the model parameters on the biodynamic responses, while the effect of changes in other parameters is small. This is evident from the summary of sensitivity analyses presented in Table 4.2. The table presents the frequency regions in which the changes in model parameters significantly affect the DPMI and transmissibility responses, together with transmissibility response location. The results suggest that m_{if} (finger skin mass), c_3 (damping of the hand back), C_e (elbow angular damping), C_s (shoulder angular damping), k_3 (stiffness of the hand back) and K_s (shoulder angular stiffness) parameters have negligible influence on both the DPMI and transmissibility responses. These suggest that changes in the visco-elastic properties of the shoulder joint

and the carpal and metacarpal joints do not influence either biodynamic response. The results also show that model parameters c_s, K_e and K_b have negligible influence on the DPMI response, which suggest that angular stiffness of the elbow and the upper-body, and the damping at the shoulder joint do not contribute to the biodynamic forces developed at the driving-point. These parameters influence the localized vibration responses of the hand-arm models. Variation in some of the model parameters in the vicinity of the driving-point have negligible effect on transmissibility responses, namely m_f, m_{tp}, c_1, and k_1.

On the basis of the results attained from the sensitivity analysis, six additional equality constraints on the parameters m_{tp}, k_3, c_3, K_3, C_s and C_e, were defined in the solution of the minimization problem in Eq. (4.22a). The resulting solutions were further evaluated in terms of characteristic frequencies through eigen analysis of the model. A sensitivity analysis of the damped eigen values of the model to changes in the model parameters (Table 4.3) revealed that variations in above-mentioned parameters could slightly influence the characteristic frequencies, although the effect on the biodynamic responses is nearly negligible. The model parameters obtained through minimization of error function of DPMI alone, transmissibility alone and combined DPMI and transmissibility, are summarized in Table 4.4. A trial and error approach was subsequently adopted in choosing the values of the parameters summarized in Table 4.3 to minimize the deviations between the model damped frequencies and those identified from the mean measured DPMI and transmissibility magnitudes (Table 3.8).

The final model responses attained from solution of the minimization problems formulated after the findings of the sensitivity analyses are presented in Figure 4.10,
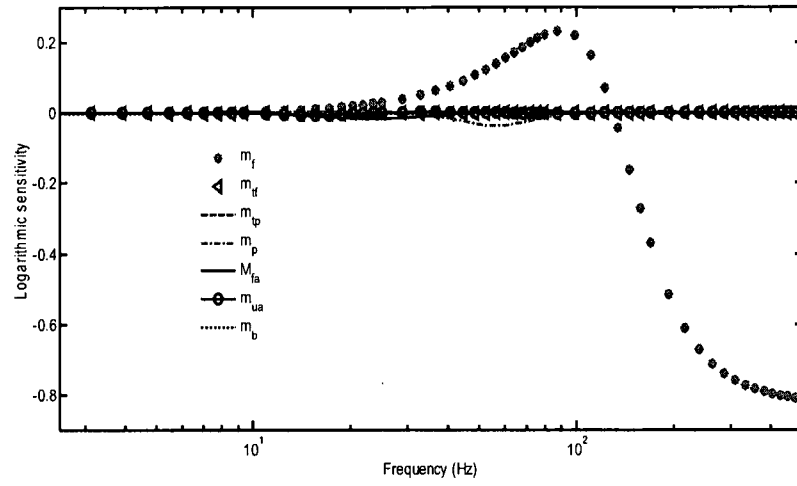
(a)
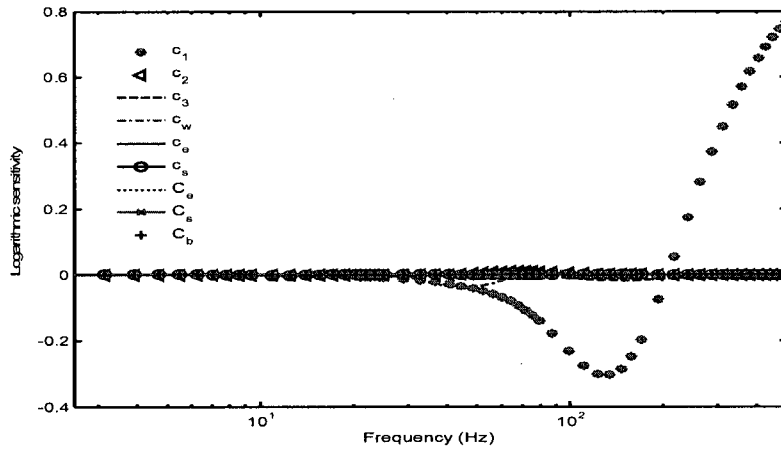
(b)
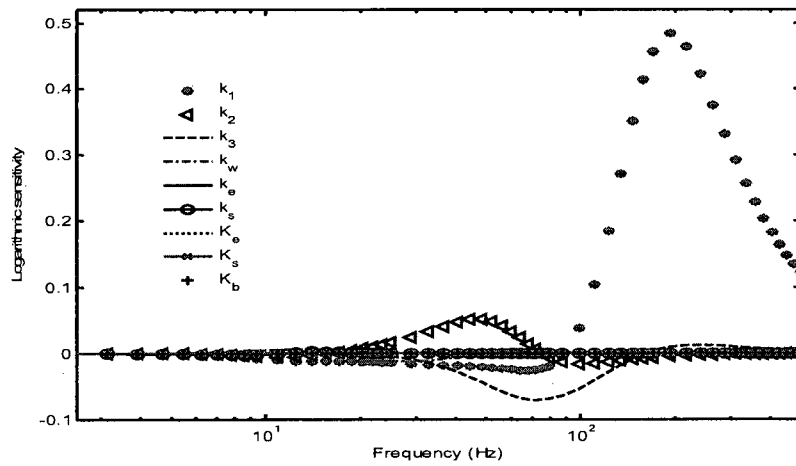
(c)

Figure 4.6: Logarithmic sensitivity of fingers' response to 20 % change in: (a) mass; (b) damping; and (c) stiffness parameters.
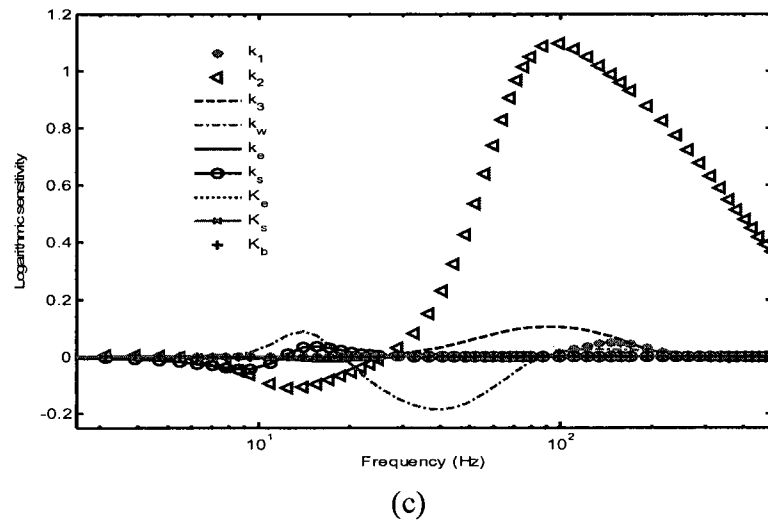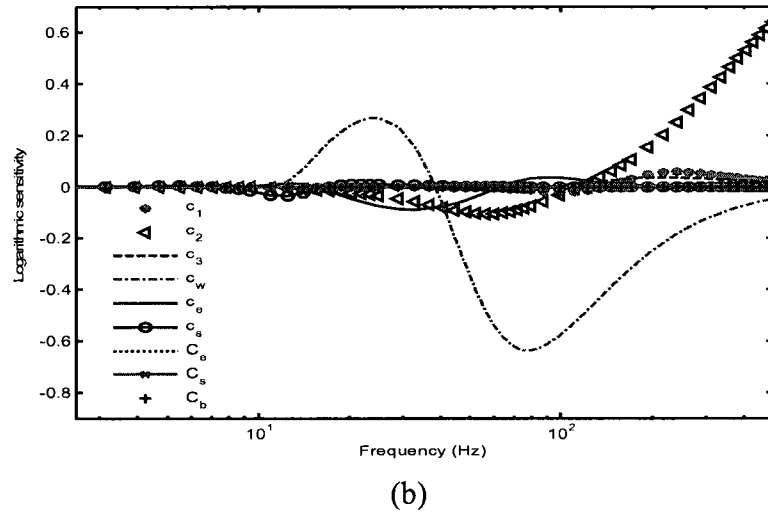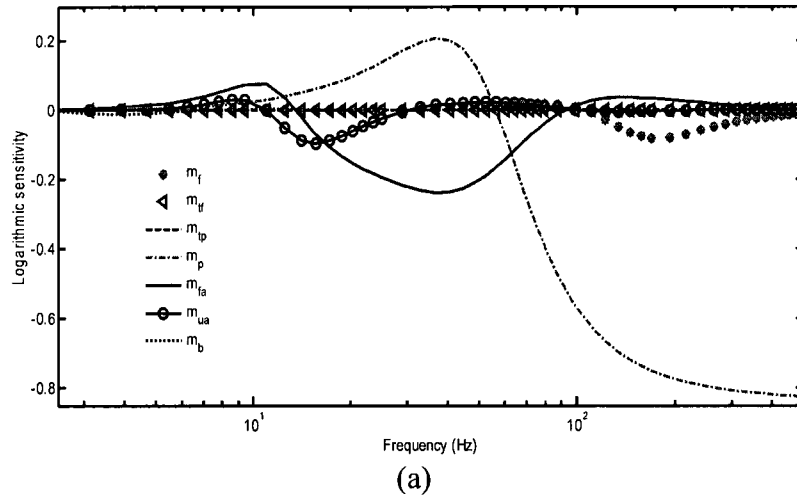
Figure 4.7: Logarithmic sensitivity of palm-wrist response to 20 % change in: (a) mass; (b) damping; and (c) stiffness parameters.

(a)

(b)

(c)
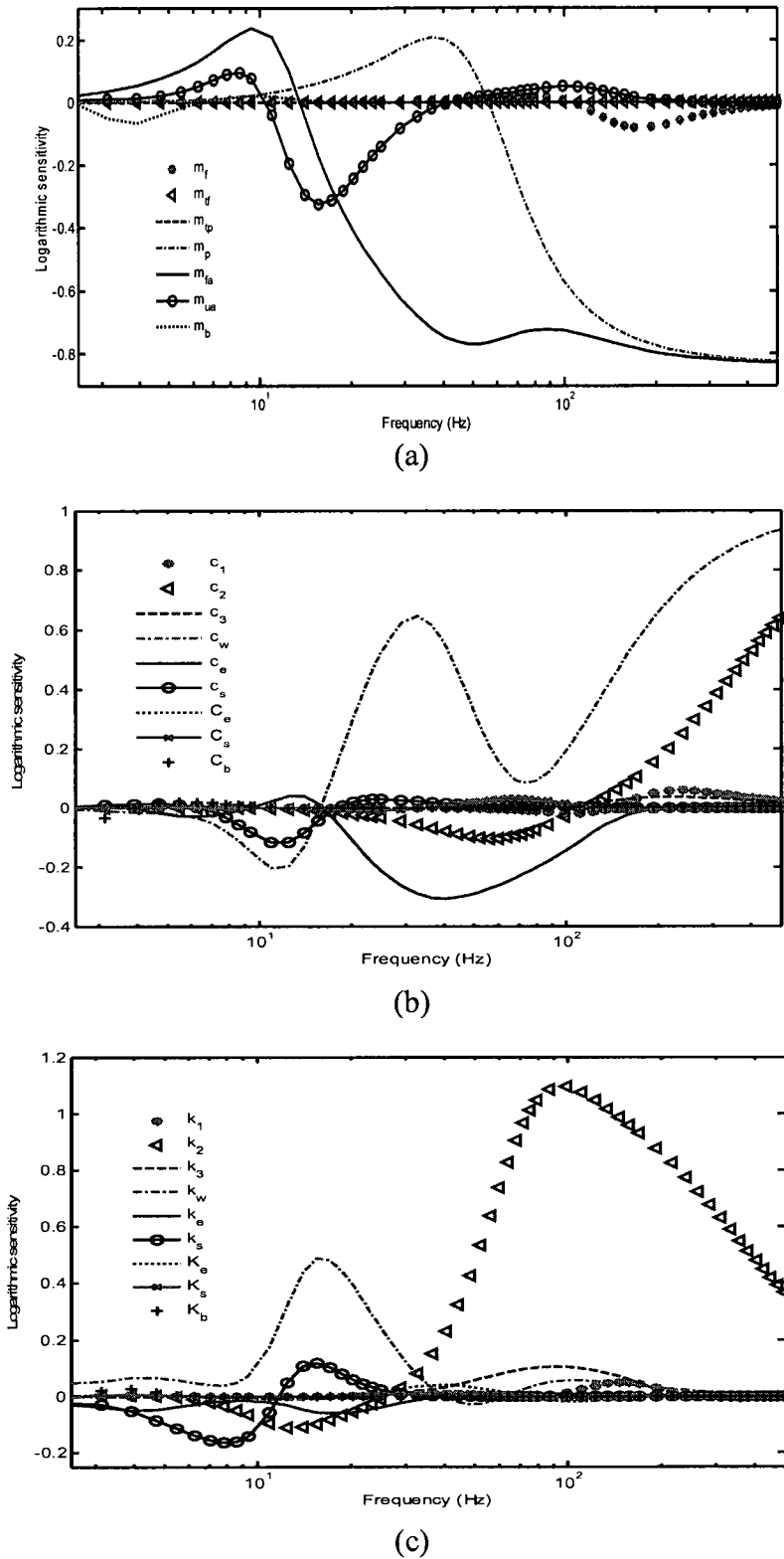
Figure 4.8: Logarithmic sensitivity of forearm response to 20 % change in: (a) mass; (b) damping; and (c) stiffness parameters.
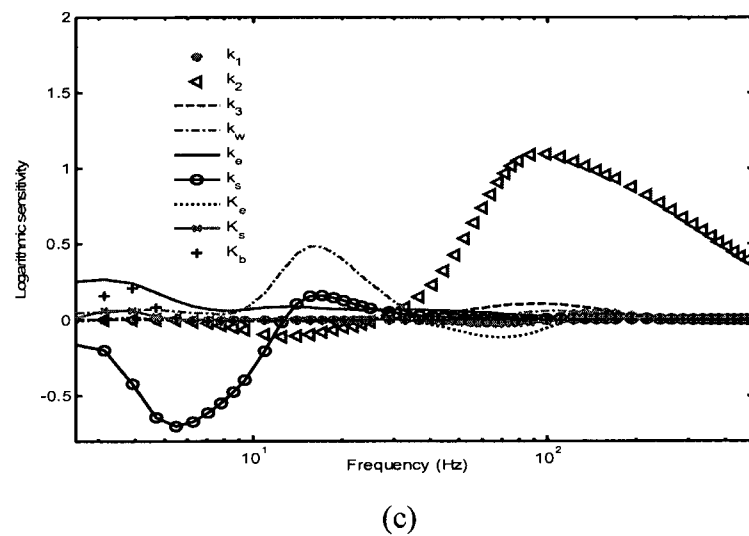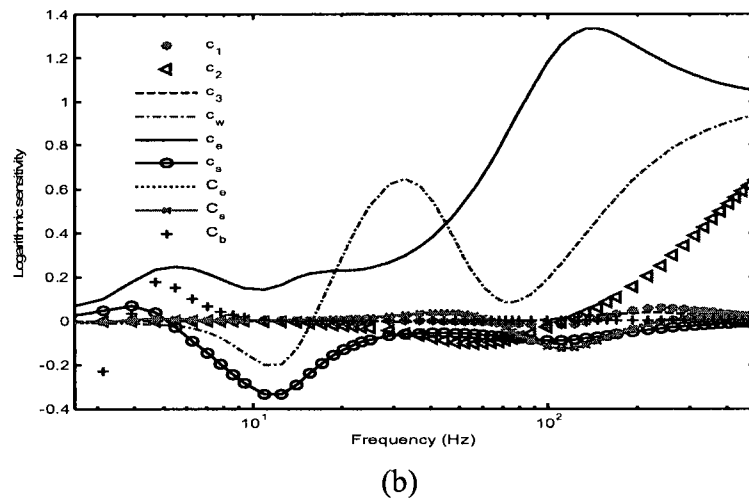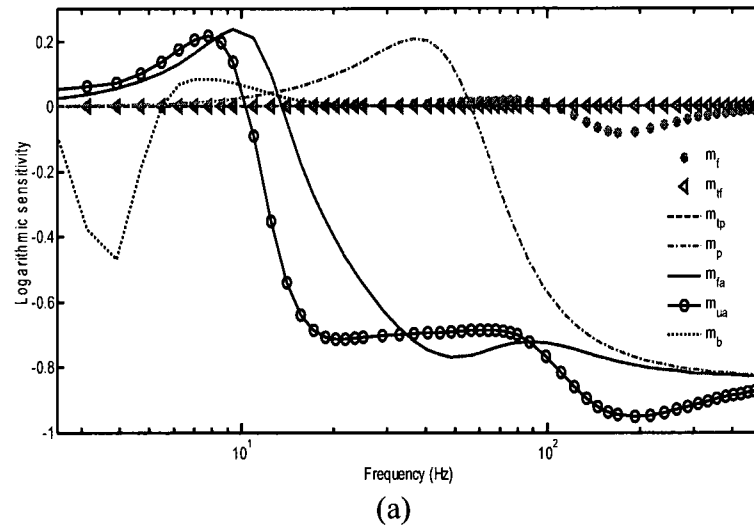
Figure 4.9: Logarithmic sensitivity of upper-arm response to 20 % change in: (a) mass; (b) damping; and (c) stiffness parameters.

Table 4.2: Summary of parameters that mostly influenced biodynamic responses of the model

Parameters	DPMI response	Transmissibility responses
m_f	80 < f < 250 Hz	-
m_{tf}	-	-
m_{tp}	100 < f < 500 Hz	-
m_p	10 < f < 100 Hz	T_w (10 < f < 500 Hz) and T_e
m_{fa}	3 < f < 80 Hz	T_w; (T_e and T_s) (20 < f < 500 Hz)
m_{ua}	3 < f < 20 Hz	T_e ; (T_s) (10 < f < 500 Hz)
m_b	2.5 < f < 6 Hz	T_s
c_1	100 < f < 500 Hz	-
c_2	100 < f < 500 Hz	T_w, T_e and T_s
c_3	-	-
c_w	20 < f < 60 Hz	T_w, T_e and T_s
c_e	2.5 < f < 100 Hz	T_w, T_e and T_s
c_s	-	T_s (2.5 < f < 20 Hz)
C_e	-	-
C_s	-	-
C_b	2.5 < f < 6 Hz	T_s
k_1	150 < f < 400 Hz	-
k_2	30 < f < 150 Hz	T_w, T_e and T_s
k_3	-	-
k_w	10 < f < 40 Hz	T_w, T_e and T_s (30 < f < 150 Hz)
k_e	2.5 < f < 6 Hz	T_s
k_s	2.5 < f < 20 Hz	T_e and T_s
K_e	-	T_s (2.5 < f < 15 Hz)
K_s	-	-
K_b	-	T_s (2.5 < f < 5 Hz)

Table 4.3: Summary of parameters that mostly influenced characteristic frequencies of the model

Characteristic frequency mode	Parameters
1st	k_1, k_3, k_w, c_1, c_3, c_w
2nd	k_e, K_s, K_e, c_e, C_s, C_e
3rd	k_1, k_3, k_w, c_1, c_3, c_w
4th	k_w, c_w
5th	m_{ua}
6th	K_b, C_b

while the corresponding parameters are summarized in Table 4.4. The table also lists the model parameters obtained from solution of the minimization problems formulated prior to and after the findings of the sensitivity analysis. The solutions based on minimization of DPMI alone provided excellent agreement of the model DPMI response with the target response, with considerably large error in transmissibility responses, as observed in Figure 4.3. In a similar manner, minimization of the transmissibility error alone resulted in good agreement in transmissibility with large error in the DPMI response. The solution based on DPMI error alone generally converged to higher values of viscous damping and mass parameters, since the DPMI response resembles that of a well-damped dynamic system. The solutions based on the transmissibility error alone, however, converge towards lower damping and mass parameter values in order to match the resonant peaks in target data, while some the stiffness parameters are higher. The solution attained through minimization of errors in both responses are considered to provide a better compromise in both the responses (Figure 4.10) although considerable deviation in the responses could be observed. The results also resulted in reasonably good agreements in the damped characteristic frequencies of the model with those identified from the measured data.

The comparisons (Figure 4.10(a)) show noticeable deviations between the DPMI response magnitudes around the valley near 100 Hz. The comparison of the mean measured and model transmissibility responses (Figure 4.10(b)) also show reasonably good agreement except in the 10 to 40 Hz frequency range, where the wrist responses show considerable deviations, and in the 10 to 20 Hz frequency range, where the deviations in the shoulder responses are evident. These discrepancies are mostly
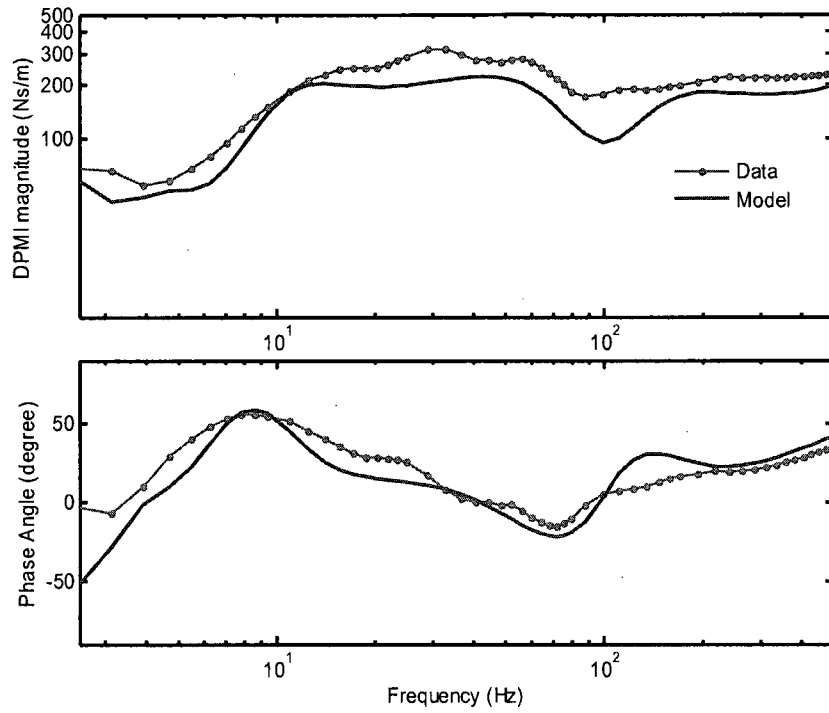
(a)
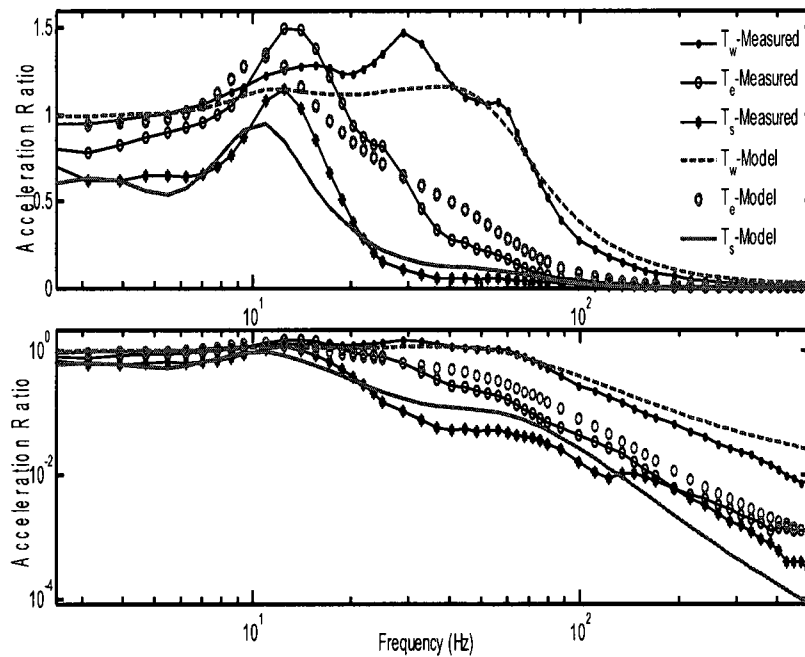
(b)

Figure 4.10: Comparisons of the measured responses with those of the model derived
after sensitivity analyses through minimization of errors in both the biodynamic
responses functions: (a) DPMI; (b) z_h – axis transmissibility.

attributed to well-damped character of the DPMI response, and lumped representation of tissues/muscles and bones in the model formulation. The deviations in the transmissibility responses, however, are noticeable only in the low frequency range, as evidenced in the linear scale presentation of the transmissibility responses. The deviations at higher frequencies are relatively small, as seen in the logarithmic scale.

4.5.3 The bent-arm model parameters

The bent-arm model parameters identified from solutions of different minimization problems are also compared with those reported in previous studies [92, 99 and 128] in Table 4.4. It needs to be emphasized that the proposed model structure differs significantly from the reported models. Consequently, only a few of the model parameters could be compared. The model masses, particularly those derived from the DPMI response, compare reasonably well with those reported by Cherian et al. [92] and Fritz [99]. Some of the mass parameters differ from those reported in [128]. The masses due to palm (m_p) and upper-arm (m_{ua}) were found to be considerably smaller than those reported in [128], where the mass due to palm-wrist-forearm are combined, while the upper-arm comprised a portion of the trunk mass. There are significant differences in the model parameters obtained when DPMI and transmissibility responses were separately used for parameter identification. The mass and damping parameters that were derived from transmissibility responses are generally lower than those derived from the DPMI response, while the stiffness elements are generally higher. Considering that the transmissibility measures described localized responses, the model parameters may be considered to reflect the properties of tissues/muscles of individual segments. The DPMI, on the other hand, emphasizes the global response of the hand-arm structure at the

driving-point. This perhaps explains the rapid convergence of the solution when the

DPMI target function alone was considered. Therefore, separating the mass of the

Table 4.4: Comparisons of model parameters derived from minimization of error functions of different biodynamic responses with those reported in previous studies

Posture:	90° Elbow Angle (EA)				60° EA	90° EA	90° EA 50N G,
Hand forces: Response	30N grip (G) force and 50N push (P) force				DPMI⁻¹	25 N G Transmissibility	50N P DPMI
	DPMI	Transmissibility	DPMI & Transmissibility				
Author:			Before Sensitivity Analysis	After Sensitivity Analysis	Fritz [99]	Cherian et al. [92]	Dong et al [128]
Parameter							
m_f (kg)	0.11	0.019	0.11	*0.11*	-	-	0.08
m_{tf} (kg)	0.02	0.003	0.02	*0.02*	-	-	0.01
m_{tp} (kg)	0.03	0.004	0.01	*0.03*	0.05	-	0.03
m_p (kg)	0.31	0.466	0.36	*0.47*	0.41	0.45	1.42[1]
m_{fa} (kg)	1.19	1.09	1.19	*1.09*	1.15	1.15	-
m_{ua} (kg)	1.92	1.15	1.25	*1.73*	1.96	1.90	6.09
m_b (kg)	32.98	29.51	29.51	*29.51*	-	-	-
c_1 (Ns/m)	118.22	23.85	118.22	*103.14*	-	-	120.60
c_2 (Ns/m)	69.53	6.39	25.22	*33.68*	-	-	118.40
c_3 (Ns/m)	20.07	2.09	2.09	*2.09*	-	-	38.00
c_w (Ns/m)	354.34	109.35	173.95	*147.86*	178.00	202.80	-
c_e (Ns/m)	241.36	50.31	103.99	*103.99*	103.00	500.00	77.00
c_s (Ns/m)	37.41	32.11	32.11	*28.90*	90.00	164.60	97.50
C_e (Nms/rad)	24.86	2.24	2.24	*2.24*	60.00	6.14	-
C_s (Nms/rad)	8.06	2.65	2.65	*2.52*	100.00	4.90	-
C_b (Nms/rad)	31.52	97.47	44.84	*53.49*	-	-	-
k_1 (Ns/m)	100290.0	9216.0	81650.0	*94714.0*	-	-	208489.0
k_2 (N/m)	88354.0	41261.0	56319.0	*53750.0*	-	-	57535.0
k_3 (N/m)	5371.8	6478.0	5371.8	*6478.0*	-	-	6347.0
k_w (N/m)	6727.8	13480.0	13480.0	*14155.0*	66500.0	23600.0	-
k_e (N/m)	2763.6	4123.3	2763.6	*2763.6*	14000.0	444600.0	5382.0
k_s (N/m)	2369.3	4467.0	3685.3	*4467.0*	3500.0	415400.0	9425.0
K_e (Nm/rad)	1342.9	128.2	1262.9	*537.1*	3800.0	2.0	-
K_s (Nm/rad)	308.8	1210.5	308.8	*605.3*	5300.0	2.0	-
K_b (Nm/rad)	257.6	2530.6	603.6	*1353.3*	-	-	-

[1]-mass of palm-wrist-forearm structure

tissues/muscles and the bones of the arms (as in the case of fingers and the palm) may yield improved model responses as opposed to the combined lumped masses considered in the present model.

The modal parameters of the model for different parameter identification techniques are summarized in Table 4.5. The natural frequencies and frequencies of damped oscillations, together with the damping ratios, were obtained through eigen analysis of the models derived on the basis of DPMI, transmissibility, and combined biodynamic responses. Similar to Table 4.4, Table 4.5 shows differences in the modal parameters of the models derived using the three composite error functions. The table also illustrates the modal properties prior to and after application of the results of the sensitivity analyses. The results show that the model based on DPMI alone yields relatively higher modal damping and greater number of over-damped modes compared to those based on transmissibility alone. These support the inference derived from the model parameters reported in Table 4.4 and that the DPMI tends to characterize the entire human hand-arm system at the driving-point (the hand), while transmissibility measures tend to characterize the localized tissues/muscles responses.

The normalized eigen vectors of the model derived on the basis of both the biodynamic responses and the sensitivity analysis are also evaluated to study the dominant modes of vibration. The results presented in Table 4.6 suggest that the higher frequency of 153.9 Hz corresponds to the resonance of the fingers mass, while the lower frequencies 4.2 Hz, 10.0 Hz and 18.4 Hz correspond to those of the trunk mass, upper-arm and forearm, respectively. These further support the widely reported finding that higher frequency vibrations are generally retained to the hand, while the low frequency

vibrations are transmitted to the upper arm and the body.

A comparison of the damped frequencies of the model with the characteristic frequencies identified from the measured biodynamic responses revealed reasonably good agreements among some of the frequencies. For example, the damped frequency of 133.08 Hz (corresponding to the natural frequency of 153.9 Hz of the fingers) that was derived from the model is close to 134.4 Hz, which is associated with the valley observed in the measured DPMI magnitude and peaks in the measured transmissibility magnitudes at the wrist and elbow 2 (Table 3.8). Furthermore, the mode corresponding to the damped frequency of 57.65 Hz (the natural frequency of the palm-wrist, 63.6 Hz) derived from

Table 4.5: Modal parameters for the bent-arm model

Modal parameters	DPMI Response	Transmissibility Responses	DPMI & Transmissibility responses	
			Before Sensitivity Analysis	After Sensitivity Analysis
Natural Frequencies (Hz)	157.31	143.58	142.77	*153.92*
	91.18	91.06	73.31	*63.90*
	78.36	56.88	99.09	*69.06*
	14.47	19.51	17.72	*18.39*
	7.43	12.12	11.22	*10.03*
	2.50	5.22	3.31	*4.17*
Damped Frequencies (Hz)	119.41	96.06	112.08	*133.08*
	-[†]	28.71	76.21	*57.65*
	33.38	46.83	42.39	*47.66*
	-[†]	16.796	-[†]	*10.14*
	2.54	11.84	11.04	-[†]
	2.25	4.32	2.94	*3.82*
Damping Ratio	0.646	0.740	0.619	*0.502*
	-[†]	0.951	0.718	*0.674*
	0.733	0.439	0.697	*0.529*
	-[†]	0.571	-[†]	*0.358*
	0.931	0.292	0.444	-[†]
	0.520	0.566	0.480	*0.427*

[†] over-damped

Table 4.6: Eigen vectors and values showing predominant modes of the bent-arm model.

	153.92 Hz	63.90 Hz	69.06 Hz	18.39 Hz	10.03 Hz	4.17 Hz
z_f	*-1.000*	-0.077	0.000	0.014	-0.004	0.001
z_p	0.018	*-1.000*	0.002	0.209	-0.060	0.014
z_{fa}	0.000	0.089	-0.002	*1.000*	-0.305	0.073
z_{ua}	0.000	-0.001	0.000	-0.172	*-1.000*	0.412
θ_{ua}	0.000	0.177	*-1.000*	0.419	*0.727*	0.475
θ_b	0.000	0.000	0.002	0.002	0.234	*1.000*

the model is close to the 56.3 Hz characteristic frequency, identified from the peaks in the measured DPMI magnitude and peaks in transmissibility magnitude at the wrist, elbow 1 and elbow 2. The model damped frequency of 47.66 Hz (corresponding to 69.1 Hz, the rotational mode natural frequency of the upper-arm) is close to the 48.4 Hz characteristic frequency, identified as the valley in the measured DPMI response magnitude. The damped frequency of 10.0 Hz (corresponding to 18.4 Hz, the natural frequency of the forearm) of the model may be related to the peak in the measured transmissibility magnitudes occurring near 12.5 Hz at the elbow. Finally, the damped frequency of 3.82 Hz (corresponding to 4.17 Hz, the rotational mode natural frequency of the trunk) of the model is close to 3.9 Hz obtained from the valley in the measured DPMI magnitude response and peak in the measured transmissibility response at the shoulder near 5.5 Hz.

The resonant frequency of 28.9 Hz observed from the measured transmissibility magnitudes at the wrist and elbow 1 and the peak in the measured DPMI response, which has been widely reported as the resonant frequency of the human hand-arm system, could not be identified from the model response when the parameters were derived on the basis of both biodynamic responses. This is probably caused by the over-damped mode associated with the wrist mass of the model, as evident in Figure 4.13. This frequency,

however, was noted in the model response and modal parameters, when the model parameters were derived on the basis of transmissibility responses alone (Table 4.5). This further supports the hypothesis that the resonant frequencies related to the peaks in the DPMI response are the resonant frequencies of the tissues/muscles of the human hand-arm system. For the 3-DOF hand-arm model reported in ISO 10068 [86], it was shown that the damped frequencies of 4.19 and 102.83 Hz correspond to the valleys in the model's DPMI response (section 3.3). It is deduced that the model could yield better agreements between the measured and model biodynamic responses when both the DPMI and transmissibility responses are used for parameters identification, and when the bones and muscles of the forearm and upper-arm are represented by different masses, as it is done for the fingers and palm. Such a hand-arm model could combine the two simple mechanical models (free-free and free-fixed supports), whose responses have been presented in Figure 3.6.

4.5.4 Responses of the extended arm model

Figure 4.11 and 4.12 respectively illustrate comparisons of DPMI and z_h-axis transmissibility responses of the extended arm model with the mean measured data, when the model parameters were separately derived on the basis of DPMI alone and on the transmissibility responses alone. Figure 4.13 shows comparisons of the y_h-axis transmissibility responses of the model with the measured responses. The results suggest trends similar to those observed for the bent-arm posture model for the three different methods used for model parameter identification. However, unlike the z_h-axis transmissibility responses, which show reasonably good agreements with the measured data, as seen in Figure 4.12(b), a poor agreement is observed in the y_h-axis

177

transmissibility responses (Figure 4.13). The extended arm model shows negligible responses in the y_h-axis, which can be attributed to two factors: (i) negligible compliances in the y_h-axis; and (ii) the assumption that the measured transmissibility responses are those of the bones and tissues/muscles combined. While the latter assumption seems to be reasonable for the z_h-axis responses, the y_h-axis responses of the model are perhaps better predicted by considering the tissues/muscles to have independent motion in the y_h-axis. This may also explain the better results obtained when each biodynamic response was separately used for parameter identification, compared to the case when both biodynamic responses were combined. Moreover, the poor agreement in y_h-axis responses of the model may also in-part be attributable to simplification of equations of motion involving nonlinear coupling terms, as seen in Eqs. (4.9) and (4.11).

Figures 4.14 and 4.15 show comparisons between the measured and model responses, when the parameters were derived on the basis of both biodynamic responses. The figures correspond to the responses obtained after the results of the sensitivity analyses and the characteristic frequencies identified from the mean measured responses were utilized in parameter identification. The DPMI response of the model agrees reasonably well with mean data above 15 Hz, as seen in Figure 4.14(a). The z_h-axis transmissibility responses of the model also agree reasonably well with the mean measured responses, although some deviations are evident at frequencies above 50 Hz. The comparisons also suggest deviations between the mean measured and model transmissibility responses at the elbow and the shoulder in the 10 − 20 Hz and 4.5 − 10 Hz frequency ranges, respectively, although these are not noticeable in the logarithmic scale. The comparison of the y_h-axis responses revealed poor agreements between the
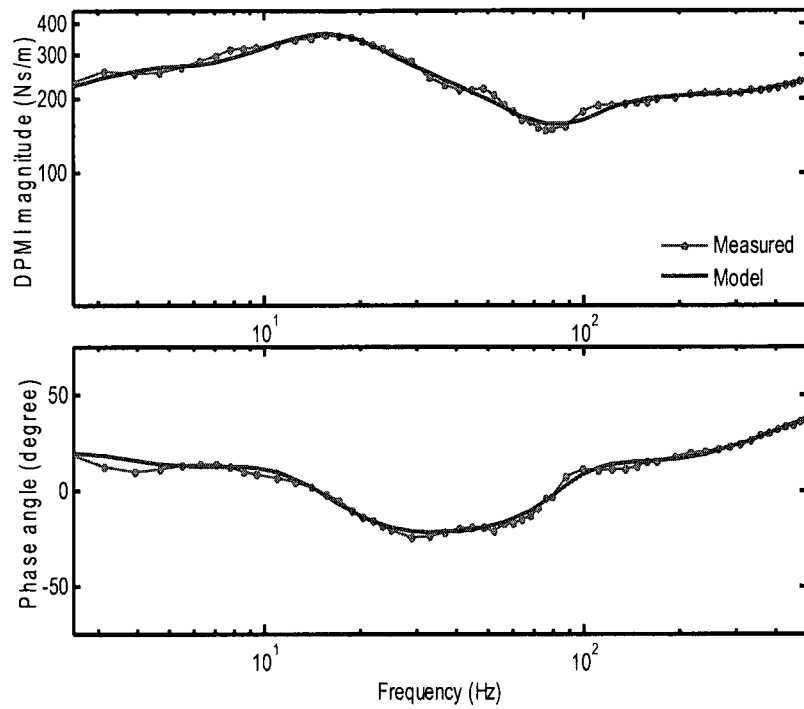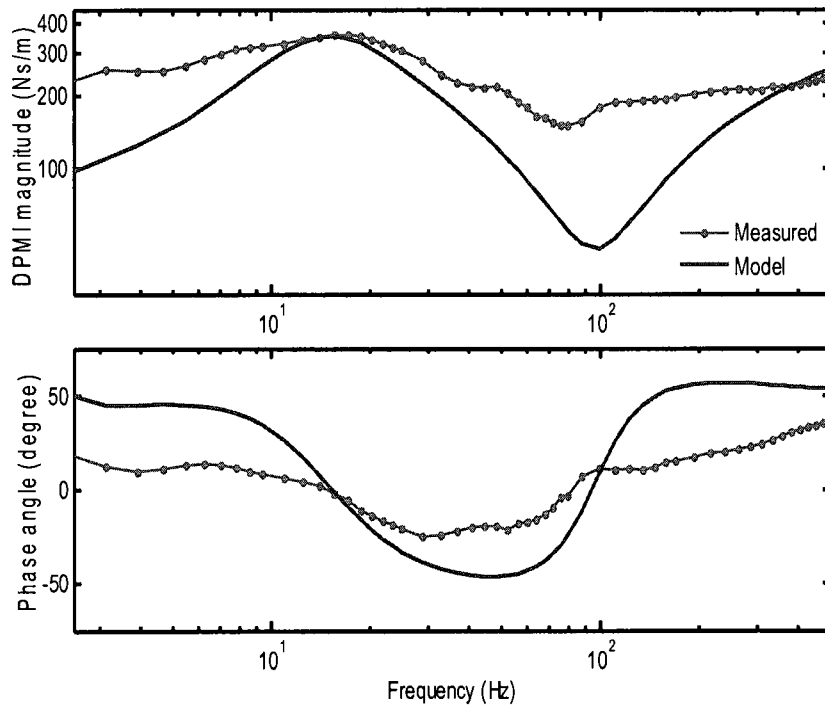
Figure 4.11: Comparisons of mean measured DPMI response with those of the extended arm model derived using: (a) DPMI only; (b) transmissibility only.
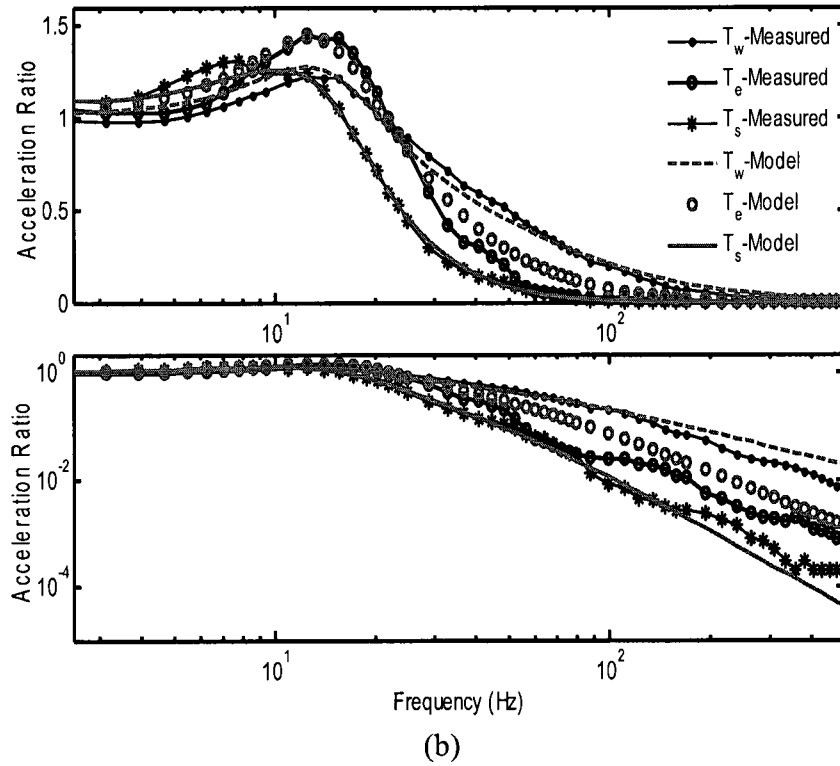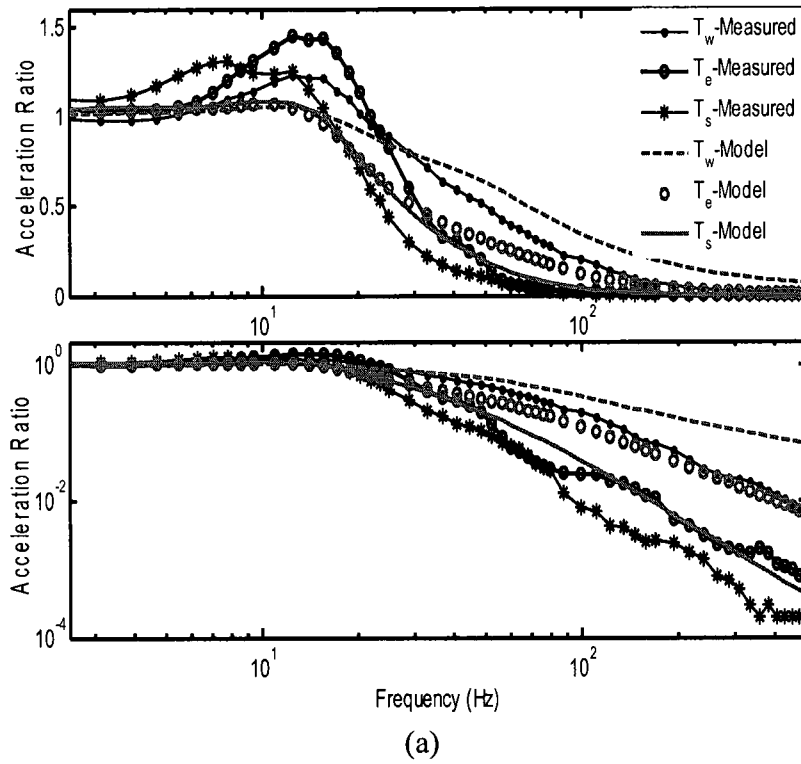
Figure 4.12: Comparisons of mean measured z_h-axis transmissibility responses with those of the extended arm model derived using: (a) DPMI only; (b) transmissibility only.
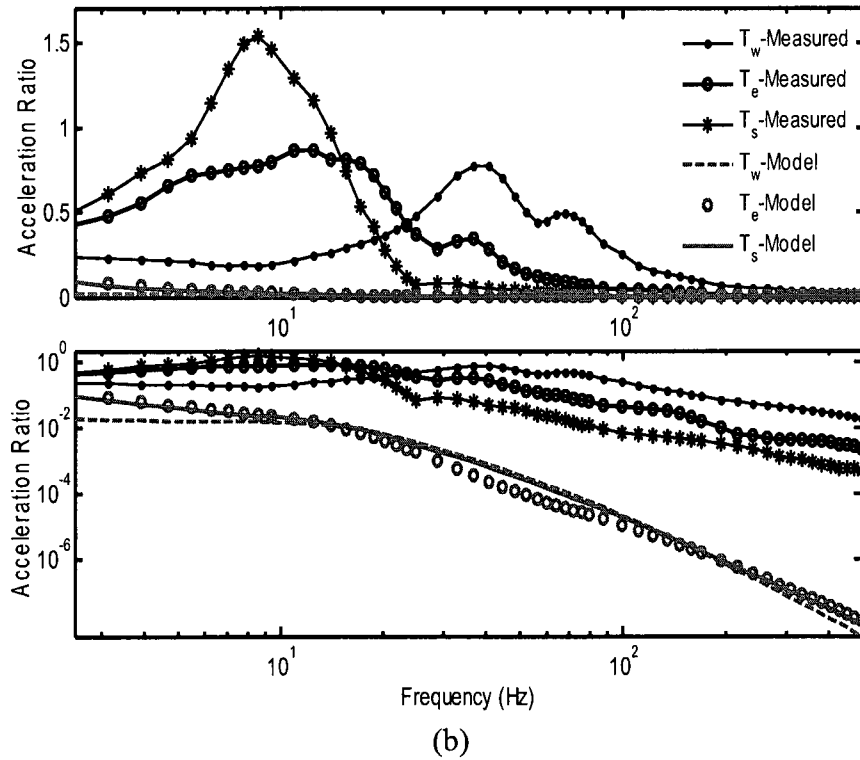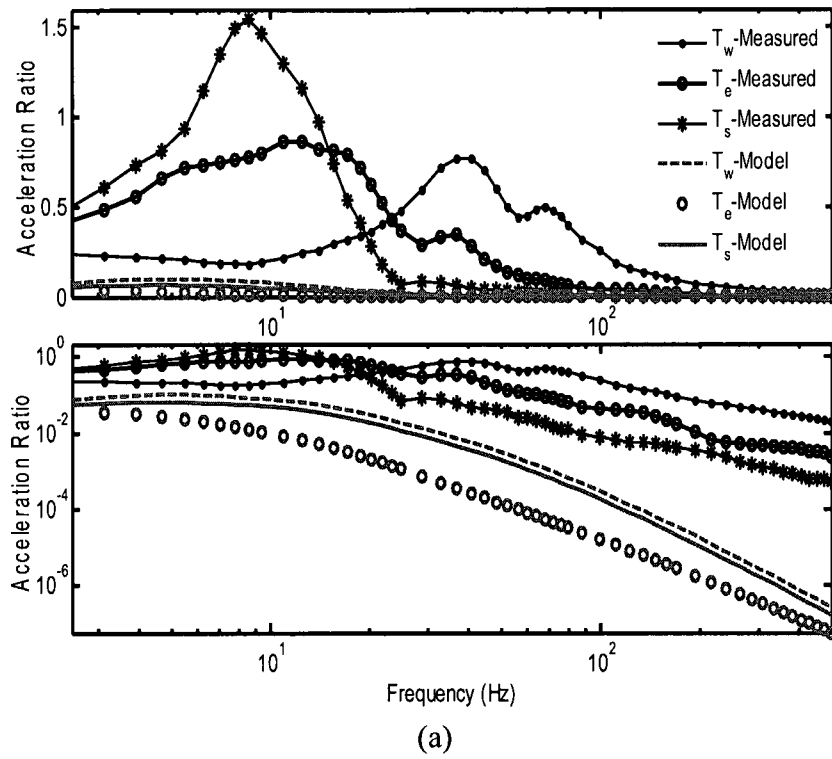
Figure 4.13: Comparisons of mean measured y_h-axis transmissibility responses with those of the extended arm model derived using: (a) DPMI only; (b) transmissibility only
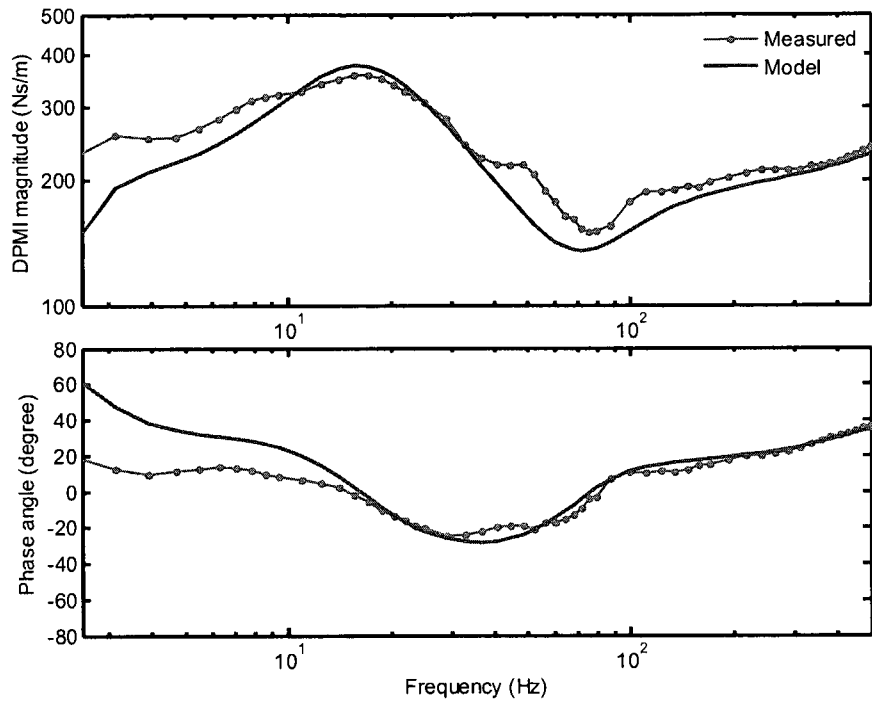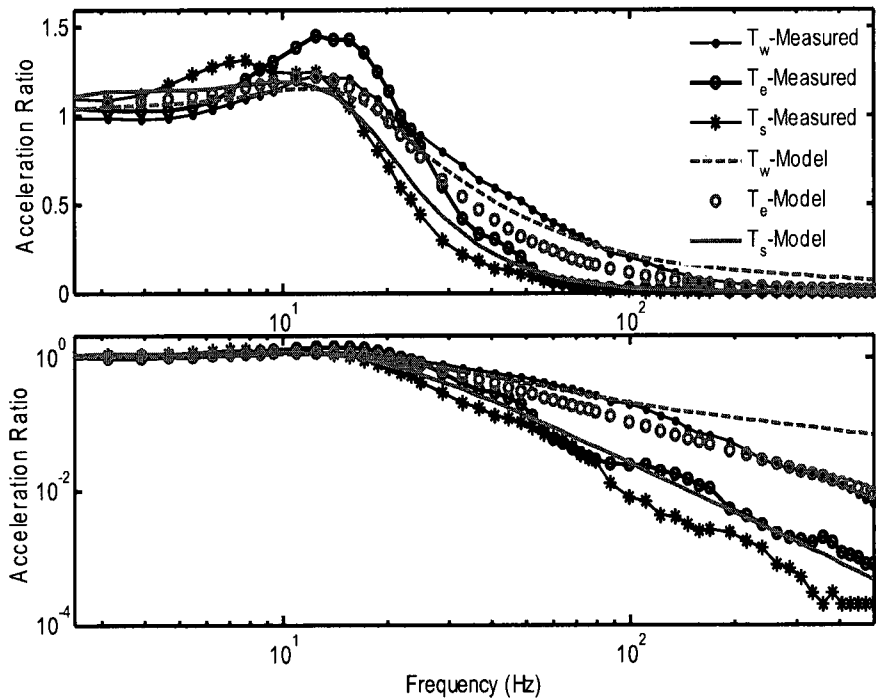
Figure 4.14: Comparisons of the mean measured data with those of the responses of the extended arm model derived using combined biodynamic responses: (a) DPMI; (b) z_h-axis transmissibility
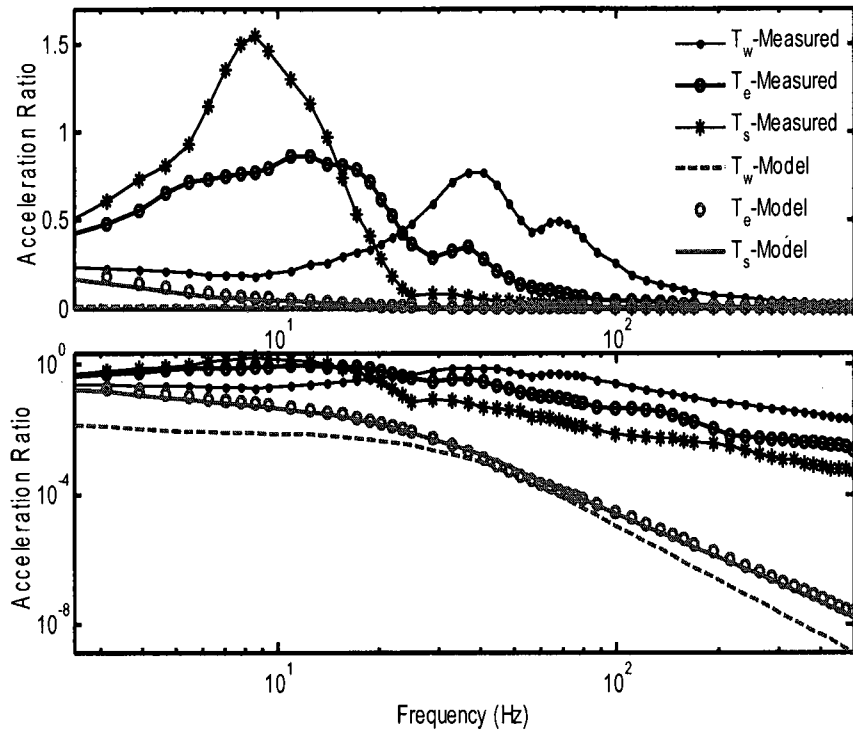
Figure 4.15: Comparisons of the mean measured y_h-axis transmissibility with those of the responses of the extended arm model derived using combined biodynamic responses.

model and measured responses, as it was observed in Figure 4.13.

4.5.5 Extended arm model parameters

The parameters of the extended arm model corresponding to the three different identification methods are summarized in Table 4.7. Unlike the bent-arm model parameters, which showed significant differences in the parameters obtained on the basis of DPMI and transmissibility responses, the differences in the masses of the extended arm model are not very significant. Most of the mass parameters derived from the transmissibility responses are only slightly smaller than those derived from the DPMI response. The values of the angular stiffness parameters of the model are particularly very small, when the parameters are identified using DPMI alone. The angular viscous damping parameters, on the other hand, are generally small when the transmissibility

function alone is employed in parameters identification. These suggest that the biodynamic responses of the extended arm posture are most likely not very sensitive to rotational joint properties.

Table 4.7: Summary of the extended arm model parameters derived from different biodynamic responses

Parameters	DPMI response	Transmissibility response	DPMI & Transmissibility responses
m_f (kg)	0.13	0.09	0.13
m_{tf} (kg)	0.02	0.02	0.02
m_{tp} (kg)	0.03	0.02	0.02
m_p (kg)	0.32	0.34	0.31
m_{fa} (kg)	1.33	1.27	1.27
m_{ua} (kg)	2.24	2.03	2.14
m_b (kg)	28.14	28.14	28.14
c_1 (Ns/m)	114.1	212.0	112.9
c_2 (Ns/m)	71.1	13.9	78.4
c_3 (Ns/m)	4.0	4.0	1.5
c_w (Ns/m)	408.7	288.4	549.4
c_e (Ns/m)	444.2	199.1	331.2
c_s (Ns/m)	189.3	63.3	136.1
C_w (Nms/rad)	2.0	2.0	1.6
C_e (Nms/rad)	84.2	6.0	1.1
C_s (Nms/rad)	17.5	28.2	1.2
C_b (Nms/rad)	28.0	2.1	2.1
k_1 (Ns/m)	65097.0	1042.4	42376.0
k_2 (N/m)	79286.0	41390.0	54683.0
k_3 (N/m)	439.0	2234.5	439.0
k_w (N/m)	55337.0	58157.0	95627.0
k_e (N/m)	68536.0	8635.0	25751.0
k_s (N/m)	5183.1	297.4	983.3
K_w (Nm/rad)	827.8	710.8	710.8
K_e (Nm/rad)	4.4	30.6	30.6
K_s (Nm/rad)	1.2	1.2	207.7
K_b (Nm/rad)	1.2	225.8	225.8

Table 4.8: Modal parameters of the extended arm model derived from different biodynamic responses

Modal parameters	DPMI response	Transmissibility response	DPMI & Transmissibility responses
Natural Frequencies (Hz)	114.56	90.62	117.81
	105.46	30.16	88.28
	49.33	24.67	2.23
	15.35	1.74	12.86
	3.35	8.90	35.39
	4.24	10.44	28.28
	53.07	51.26	51.28
Damped Frequencies (Hz)	_†	_†	_†
	87.19	_†	53.52
	35.25	12.49	2.05
	12.67	9.42	16.77
	_†	1.71	7.60
	2.64	_†	13.02
	_†	_†	37.39
Damping Ratio	_†	_†	_†
	0.648	_†	0.795
	0.781	0.974	0.512
	0.589	0.554	0.922
	_†	_†	0.975
	0.766	0.397	0.607
	_†	_†	0.487

† over-damped

Table 4.9: Eigen values and vectors showing predominant modes of the extended arm model

	117.8 Hz	88.3 Hz	2.23 Hz	12.9 Hz	35.4 Hz	28.3 Hz	51.3 Hz
z_f	0.056	*1.000*	0.000	-0.010	0.023	0.000	0.000
z_p	*-0.985*	0.020	-0.007	-0.272	0.554	0.000	0.000
z_{fa}	0.164	-0.006	-0.011	-0.426	*0.792*	0.000	0.000
θ_{fa}	0.000	0.000	-0.027	0.001	0.000	0.059	*0.998*
z_{ua}	-0.004	0.000	-0.025	*-0.862*	-0.257	0.000	0.000
θ_{ua}	0.000	0.000	*-0.661*	0.030	-0.002	*0.998*	-0.057
θ_b	0.000	0.000	*-0.750*	0.027	0.001	-0.003	0.000

The modal parameters of the hand-arm model in the extended arm posture are summarized in Table 4.8, while Table 4.9 presents the normalized eigen-vectors of the model derived on the basis of both biodynamic responses. The predominant vibration modes are italicized in Table 4.9. The results suggest that the higher frequency (88.3 and 117.8 Hz) modes are associated with the finger and palm masses, while the lower frequency modes (2.2 and 12.9 Hz) are attributed to the upper arm and the trunk masses. Similar to the results obtained for the bent-arm model, there are considerable differences in the modal parameters when different biodynamic measures are employed in parameter identification. The model parameters obtained when transmissibility measures alone were used are generally smaller than those derived from the DPMI measure with a few exceptions. The following damped frequencies of the extended arm model 13.0, 16.8, 7.6 and 2.02 Hz could be respectively related to the characteristic frequencies of 12.5, 15.6, 7.8 or 8.6 or 7.0, and 3.1 Hz, identified from the mean measured transmissibility and DPMI response magnitudes and summarized in Table 3.9.

4.6 Effects of Hand Forces on the Model Parameters

The measured biodynamic responses of the hand-arm system exposed to z_h-axis vibration clearly revealed nonlinear effects of the hand grip and push forces. The model parameters, presented in the previous section, are considered valid for hand grip and push forces in the vicinity of 30 N and 50 N, respectively. The linear hand-arm vibration models could be applied for alternate hand forces by considering the appropriate target functions in parameter identification. The model parameters corresponding to different combinations of hand forces are identified using the appropriate target functions in DPMI and transmissibility responses. The model parameters derived on the basis of both

biodynamic responses for 30 N grip and 50 N push forces were applied as the baseline parameters in the parameter identifications. The mass inertia parameters of the models were held at the baseline values, the remaining parameters were permitted to vary within ±50 % of the baseline values for different combinations of the hand forces. Subsequently, the lower or/and upper bound values of sensitive parameters (Table 4.2) were further relaxed when they converge to either the lower or upper bound. The parameters of the resulting models corresponding to different combinations of hand forces are presented in the following sub-sections, where superscripts "L" and "U" are used to indicate the convergence of a particular parameter to the respective lower and upper bound even after several relaxations. These parameters were considered insensitive to hand forces and were not considered in the assessment of the effect of the hand forces.

4.6.1 Effects of hand forces on the bent-arm model parameters

Tables 4.10 to 4.12 illustrate the visco-elastic parameters of the model derived on the basis of DPMI only, transmissibility responses only, and the combined measures, respectively, corresponding to different hand forces combinations. The results show that changes in the hand forces strongly influence the visco-elastic parameters of the model, irrespective of the parameter identification method used. The effects of the hand forces on the model parameters are, however, strongly nonlinear. While some of the parameters increased with increase in the hand forces, others decreased or revealed increasing/decreasing patterns. The same trend was also observed in the modal parameters, which can be attributed to nonlinearity in the hand-arm system. From the measured data, it was observed that an increase in the grip force and push force yields a decrease in the transmissibility magnitudes in the low frequencies region (Figures 3.24

and 3.27). Owing to the varied trends in the parameters due to changes in hand forces, the

percentage change in each parameter for successive increase in hand forces relative to the

baseline values were calculated in order to identify the substructure of the hand-arm

model that is most affected by changes in the grip and push forces.

The model parameters derived using the DPMI responses alone (Table 4.10) show

that an increase in the grip force yields higher values of the parameters associated with

the hand substructure (c_1, c_2, k_1, k_2 c_w) and the elbow stiffness k_e. These parameters

directly contribute to the dynamic forces developed at the hand-tool interface. The

remaining parameters initially increased and then decreased or vice-versa. The damping

Table 4.10: Effects of hand forces on visco-elastic parameters of the bent-arm model
when DPMI response was used for parameter identification.

| Parameters | 50 N push force | | | 30 N grip force | | |
	10 N grip force	30N grip force	50N grip force	25 N push force	50 N push force	75 N push force
c_1 (Ns/m)	93.49	118.22	142.40	124.59	118.22	121.01
c_2 (Ns/m)	38.66	69.53	86.56	50.30	69.53	78.66
c_3 (Ns/m)	30.11^U	20.07	10.04^L	30.11^U	20.07	10.04^L
c_w (Ns/m)	272.90	354.34	386.94	334.75	354.34	354.21
c_e (Ns/m)	141.49	241.36	128.82	120.68	241.36	198.76
c_s (Ns/m)	56.11^U	37.41	43.50	48.23	37.41	40.07
C_e (Nms/rad)	12.43^L	24.86	37.29^U	37.29^U	24.86	8.08^L
C_s (Nms/rad)	4.03^L	8.06	4.03^L	4.03^L	8.06	4.03^L
C_b (Nms/rad)	126.97	31.52	37.74	81.48	31.52	57.59
k_1 (Ns/m)	86608.0	100290.0	117540.0	111620.0	100290.0	104340.0
k_2 (N/m)	78491.0	88354.0	110940.0	64164	88354.0	127150.0
k_3 (N/m)	2685.9^L	5371.8	2685.9^L	2685.9^L	5371.8	2685.9^L
k_w (N/m)	20512.0	6727.8	29411.0	21487.0	6727.8	16184.0
k_e (N/m)	301.6	2763.6	1463.3	345.4^L	2763.6	756.1
k_s (N/m)	3617.6	2369.3	2889.4	2795.4	2369.3	3554.0
K_e (Nm/rad)	2014.3^U	1342.9	671.4^L	671.4^L	1342.9	671.4^L
K_s (Nm/rad)	154.4^L	308.8	154.4^L	395.11	308.8	154.4^L
K_b (Nm/rad)	135.0	257.6	236.7	203.02	257.6	128.8^L

L and U-indicate lower and upper bound value, respectively.

parameters in decreasing order of the influence of grip force, based on percentage

change, was C_b, c_2, c_w and c_1, while the order for the stiffness parameters was k_w, k_e,

k_s, K_b, k_2 and k_1. On the other hand, an increase in the push force caused increase in

c_2 and k_2, while the damping and stiffness parameters in decreasing order of the

influence of the push force was C_b, c_e, c_w, c_s, c_2, c_1 and k_w, k_s, k_2, k_1, respectively.

The changes in the stiffness parameters of the model, that were derived from

transmissibility responses alone, are presented in Table 4.11. The table shows that an

increase in the grip force increased k_2 but decreased c_s, while other parameters initially

Table 4.11: Effects of hand forces on visco-elastic parameters of the bent-arm model
when transmissibility responses were used for parameter identification.

Paramters	50 N push force			30 N grip force		
	10 N grip force	30N grip force	50N grip force	25 N push force	50 N push force	75 N push force
c_1 (Ns/m)	32.00	23.85	2.98^L	19.05	23.85	20.63
c_2 (Ns/m)	0.79^L	6.39	0.79^L	1.60^L	6.39	1.60^L
c_3 (Ns/m)	1.04^L	2.09	1.04^L	1.04^L	2.09	1.04^L
c_w (Ns/m)	143.42	109.35	128.07	133.42	109.35	129.63
c_e (Ns/m)	98.40	50.31	75.46	64.01	50.31	86.24
c_s (Ns/m)	36.47	32.11	22.34	22.25	32.11	44.32
C_e (Nms/rad)	1.12^L	2.24	1.12^L	1.12^L	2.24	1.12^L
C_s (Nms/rad)	1.33^L	2.65	1.33^L	1.33^L	2.65	1.33^L
C_b (Nms/rad)	94.32	97.47	74.84	69.22	97.47	95.34
k_1 (Ns/m)	4608.0^L	9216.0	4608.0^L	4608.0^L	9216.0	4608^L
k_2 (N/m)	33328.0	41261.0	49865.0	33302.0	41261.0	51982
k_3 (N/m)	8983.3	6478.0	3239.0^L	5863.3	6478.0	5319.6
k_w (N/m)	12645.0	13480.0	12983.0	10480.0	13480.0	18052
k_e (N/m)	5891.2	4123.3	5305.9	3865.1	4123.3	7926.1
k_s (N/m)	4946.3	4467.0	5183.4	3975.2	4467.0	6258.2
K_e (Nm/rad)	32.0^L	128.2	32.0^L	32.05^L	128.2	32.05^L
K_s (Nm/rad)	1146.6	1210.5	1161.4	940.0	1210.5	1480.9
K_b (Nm/rad)	2828.9	2530.6	3591.1	3202.5	2530.6	1530.3

L and U-indicate lower and upper bound value, respectively.

increased but later decreased with further increase in the grip force or vice-versa. The influence of the grip force on the percentage change in the damping parameters in decreasing order is c_e, c_w, c_s and C_b; the order for stiffness parameters is k_e, K_b, k_2, k_s, k_w and K_s. An increase in the push force affected the damping and elastic parameters in the following decreasing order c_e, c_s, C_b, c_w, c_1; and k_e, k_s, K_b, k_w, k_2, K_s, respectively. Table 4.11 also shows that an increase in push force results in higher values of c_s, k_2, k_w, k_e, k_s and K_s.

The parameters attained when combined DPMI and transmissibility responses were used for parameter identification (Table 4.12) suggest that an increase in the grip force increased k_1 and k_w, while other sensitive parameters initially increased then decreased or vice-versa. The percentage change in the parameters relative to the baseline values yields the following damping and stiffness parameters in decreasing order: c_2, c_w, c_1, C_b; and K_b, k_1, k_s, k_2, k_w, respectively. The percentage change in the parameters due to an increase in the push force in decreasing order are respectively: c_e, c_w, C_s, c_2, C_b, c_1; and K_b, k_s, k_2, k_1, k_w, while an increase in the push force increased k_1, k_2 and k_w, as evident in Table 4.12.

In general, the results suggest that an increase in the hand forces tends to increase the parameters in the vicinity of the driving-point, regardless of the biodynamic measure used for parameter identification. Furthermore, the ranking of the percentage changes in the model parameters relative to the baseline parameters show that an increase in the grip force has more pronounced effect on the damping and stiffness parameters in the vicinity of the driving-point, when the trunk damping and stiffness parameters are ignored. On the

Table 4.12: Effects of hand forces on visco-elastic parameters of the bent-arm model when DPMI and transmissibility responses were used for parameter identification.

Parameters	50 N push force			30 N grip force		
	10 N grip force	30N grip force	50N grip force	25 N push force	50 N push force	75 N push force
c_1 (Ns/m)	66.21	103.14	134.91	105.81	103.14	109.10
c_2 (Ns/m)	50.84	33.68	33.80	37.24	33.68	50.48
c_3 (Ns/m)	1.05^L	2.09	1.05^L	1.05^L	2.09	1.05^L
c_w (Ns/m)	216.22	147.86	199.73	211.94	147.86	217.91
c_e (Ns/m)	194.98^U	103.99	179.82	154.93	103.99	207.25
c_s (Ns/m)	16.40	28.90	9.03^L	9.03^L	28.90	13.85
C_e (Nms/rad)	3.36^U	2.24	1.23	0.70^L	2.24	3.36^U
C_s (Nms/rad)	1.80	2.52	3.78^U	3.47	2.52	2.52
C_b (Nms/rad)	69.07	53.49	66.50	60.09	53.49	74.59
k_1 (Ns/m)	43378.0	94714.0	123020.0	71319.0	94714.0	96342.0
k_2 (N/m)	53969.0	53750.0	76632.0	50723.0	53750.0	86729.0
k_3 (N/m)	3239.0^L	6478.0	3239.0^L	3239.0^L	6478.0	3239.0^L
k_w (N/m)	13669.0	14155.0	14775.0	11762.0	14155.0	18566.0
k_e (N/m)	898.17^L	2763.6	863.6^L	863.6	2763.6	449.1^L
k_s (N/m)	5893.8	4467.0	6380.8	4925.4	4467.0	7804.4
K_e (Nm/rad)	1007.1^U	537.1	1980.2	1394.8	537.1	1812.7^U
K_s (Nm/rad)	846.1	605.3	302.7^L	189.2^L	605.3	828.7
K_b (Nm/rad)	2413.3	1353.3	3295.8	2624.5	1353.3	3007.7

L and U-indicate lower and upper bound value, respectively.

other hand, an increase in the push force affected the forearm, upper-arm and the trunk parameters more than the parameters of the hand (the driving-point). These observations are similar to those obtained from the influences of hand forces on the mean measured transmissibility responses. The results further show that an increase in the grip force yields the highest percentage change in the stiffness of the trunk K_b, followed by that of the fingers k_1. The highest percentage change in the damping parameters due to variations in the grip force occurred at the palm c_2, followed by the wrist c_w. The push force also resulted in the highest change in the stiffness of the trunk K_b followed by that

191

at the shoulder k_s. The highest effect of the push force on damping parameters occurred at the elbow c_e followed by that of the wrist c_w. It is interesting to note that the hand forces significantly affected visco-elastic parameters of the trunk at the pelvic. This suggests a strong coupling between the hand-arm and whole-body. The results further reveal the inadequacy of the reported models that assume the shoulder as a fixed support.

The strong influence of the grip force, on the elastic parameters of the hand-arm model near the fixed support, has been illustrated in a single study [68]. The study reported a grip force dependent 3-DOF lumped-mass model of the hand-arm system in the bent-arm posture, which showed the highest stiffness near the fixed support representing the shoulder followed by the elastic element close to the driving-point for different values of the grip force. The lumped-mass model also showed the highest damping at the driving-point followed by that of the middle mass, while the damping near the fixed support was the lowest.

4.6.2 Effects of hand forces on the extended arm model parameters

The effects of grip and push forces on the visco-elastic parameters of the extended arm model, obtained using both the biodynamic responses are presented in Table 4.13. The results show that an increase in the hand forces has negligible influence on the rotational visco-elastic parameters. Furthermore, the rotational parameters are generally small suggesting that the rotational motion of the forearm and the upper-arm in the extended arm posture is negligible, and that the biodynamic responses are less sensitive to such parameters. The damping and stiffness parameters in decreasing order, based on the percentage change in the parameters due to an increase in the grip force are respectively c_1, c_2, c_s, c_e; and k_w, k_1, k_2, k_e. An increase in the grip force increase

Table 4.13: Effect of variations in hand forces on the parameters of the extended arm model

Parameters	50 N push force			30 N grip force		
	10 N grip force	30 N grip force	50 N grip force	25 N push force	50 N push force	75 N push force
c_1 (Ns/m)	34.5	112.9	137.2	107.1	112.9	68.4
c_2 (Ns/m)	102.9	78.4	94.0	70.6	78.4	130.7
c_3 (Ns/m)	1.7^L	3.3	1.7^L	1.7^L	3.3	1.7^L
c_w (Ns/m)	824.2^U	549.4	824.2^U	484.8	549.4	824.2^U
c_e (Ns/m)	321.9	331.2	321.2	230.1	331.2	314.1
c_s (Ns/m)	165.0	136.1	131.4	121.4	136.1	131.4
C_w (Nms/rad)	0.8^L	1.6	0.8^L	0.8^L	1.6	0.8^L
C_e (Nms/rad)	1.6^U	1.1	0.5^L	0.5^L	1.1	0.5^L
C_s (Nms/rad)	0.6^L	1.2	0.6^L	0.6^L	1.2	0.6^L
C_b (Nms/rad)	7.1^U	2.1	1.1^L	1.1^L	2.1	1.1^L
k_1 (Ns/m)	14005.0	42376.0	37992.0	22050.0	42376.0	17224.0
k_2 (N/m)	34172.0	54683.0	62335.0	31106.0	54683.0	64815.0
k_3 (N/m)	219.5^L	439.0	219.5^L	219.5^L	439.0	219.5^L
k_w (N/m)	169780.0	95627.0	201860.0	106120.0	95627.0	183060.0
k_e (N/m)	23522.0	25751.0	26098.0	10789.0	25751.0	30085.0
k_s (N/m)	1846.9	983.3	491.6^L	887.2	983.3	122.9^L
K_w (Nm/rad)	7552.3^U	710.8	355.4^L	355.4^L	710.8	355.4^L
K_e (Nm/rad)	15.3^L	30.6	15.3^L	15.3^L	30.6	15.3^L
K_s (Nm/rad)	2207.2^U	207.7	175.0	222.6	207.7	137.6
K_b (Nm/rad)	112.9^L	225.8	112.9^L	112.9^L	225.8	112.9^L

L and U-indicate lower and upper bound value, respectively.

the values of c_1, k_2, k_w and k_e, while all other parameters initially increased then decreased or vise-versa, with successive increase in the grip force, as seen in Table 4.13.

An increase in the push force caused increase of parameters c_2, k_2 and k_e. The damping and elastic parameters in decreasing orders, based on the percentage change in the parameters due to an increase in the push force were c_2, c_1, c_e, c_s and k_w, k_1, k_e, k_2, K_s, respectively. Unlike the bent-arm model, for the extended arm model, increase in hand forces mostly affected the parameters of the hand and the forearm substructures.

Since hand forces had significant effect on the elastic parameter of the bent-arm model near the fixed support, it was expected that an increase in the push force would yield a significant influence on the parameters of the extended arm model near the shoulder and the fixed support, the pelvic joint. Table 4.13, however, shows significant decrease in shoulder stiffness k_s when hand forces were increased. This trend shown by k_s may be attributed to nonlinearity of the hand-arm system. Similar to the effect of higher grip force on the bent-arm model parameters, an increase in the grip force resulted in increase in the extended arm model parameters around the vicinity of the driving-point.

4.6.3 Effects of hand forces on biodynamic responses of the models

The influences of the hand forces on the model parameters are further examined through analyses of the biodynamic responses of the bent-arm (*P1*) and extended arm (*P2*) models. Figure 4.16(a) illustrates the influence of grip force on the DPMI responses of both the bent-arm and extended arm models. The figure shows that an increase in the grip force generally increased the DPMI magnitude and phase responses above 10 Hz, and the characteristic frequencies corresponding to peaks in the DPMI magnitude. The effect of the grip force is more evident in the responses of the extended arm model. The influence of grip force around valleys in the DPMI magnitude is very small, while it is significant around the peaks. Figure 4.16(b) shows the influence of push force. An increase in the push force increased the magnitude and characteristic frequencies around the peaks and the valleys in the DPMI response. The observed trends in Figure 4.19 are similar to those in the mean measured data presented in Figure 3.22.
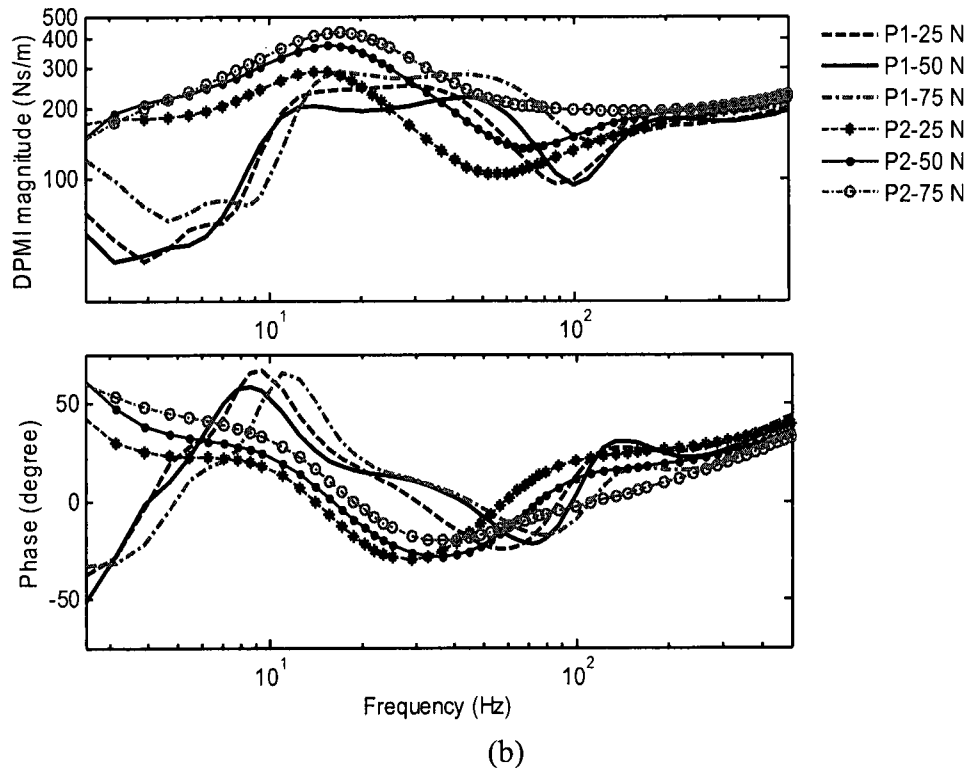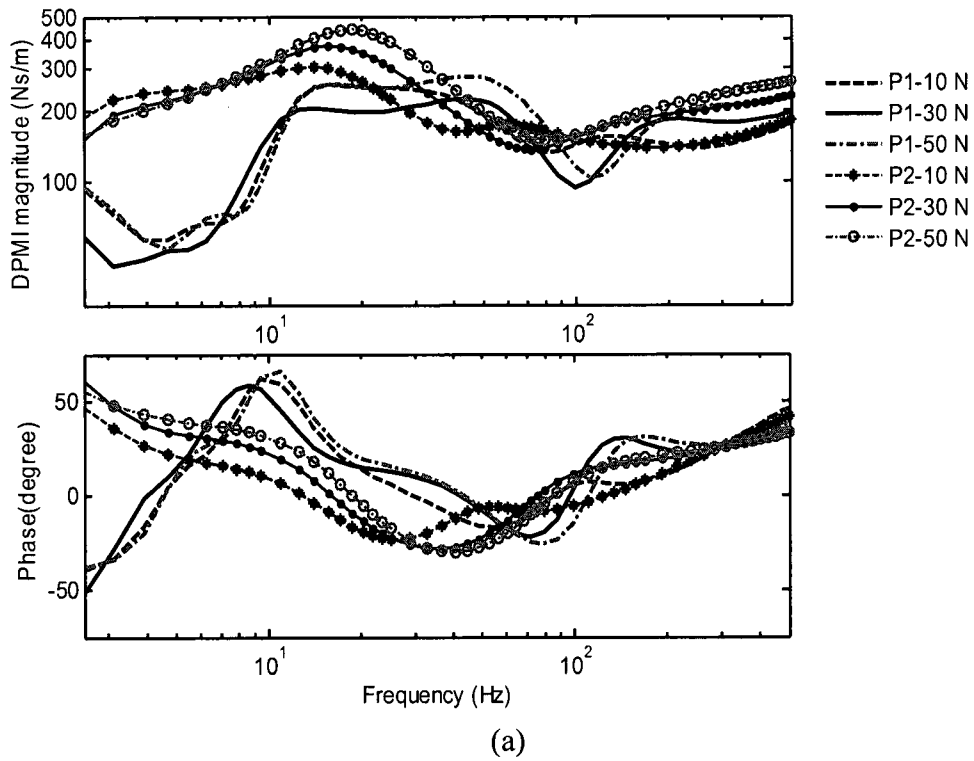
Figure 4.16: Effects of hand forces on the DPMI responses of the models: (a) constant push force; (b) constant grip force.

Figures 4.17 to 4.19 illustrate the effects of the grip and push forces on the z_h-axis transmissibility magnitudes of the bent-arm and extended arm models, at the wrist, elbow and the shoulder, respectively. The effects are presented in both the linear and logarithmic scales in order to emphasize responses in the low and high frequency regions. The influences of variations in hand forces on the z_h-axis transmissibility responses at the wrist (Figure 4.17) show trends similar to those observed in the mean measured data presented in Figures 3.23(a) and 3.26(a) for grip and push force, respectively. Considerable differences in the measured and model responses due to different hand forces, however, could be observed above 200 Hz. The transmissibility magnitude responses of the extended arm model are greater than those of the bent-arm model above 200 Hz, whereas the mean measured responses showed larger responses of the bent-arm posture at frequencies above 25 Hz.

The trends observed in the influences of hand forces on the z_h-axis transmissibility responses at the elbow and the shoulder (Figures 4.18 and 4.19) are generally similar to those observed in the mean measured data. An increase in the hand forces increased the transmissibility magnitudes and characteristic frequencies. The measured data showing the effects of grip force on the elbow and shoulder responses were presented in Figures 3.24(a) and 3.25(a), respectively, while Figures 3.27(a) and 3.28(a) illustrated the effects of the push force on the mean measured z_h-axis transmissibility responses. The results, however, suggest differences in the elbow and shoulder responses of the models and the mean measured data under different hand forces. For example, the extended arm model response magnitudes are higher than those of the measured responses in almost entire frequency range, except between 40 and 60 Hz for the elbow responses, and 60 to 200 Hz
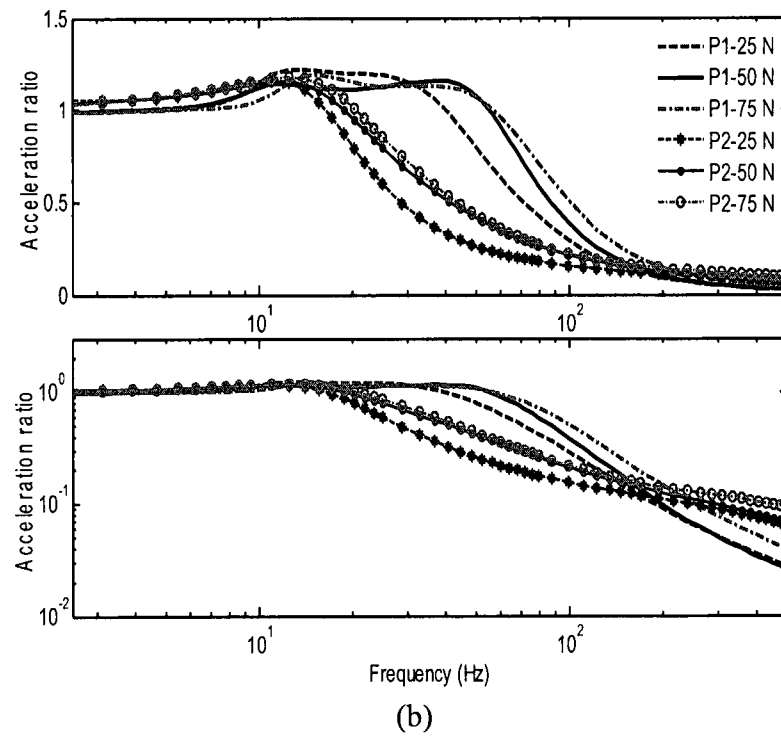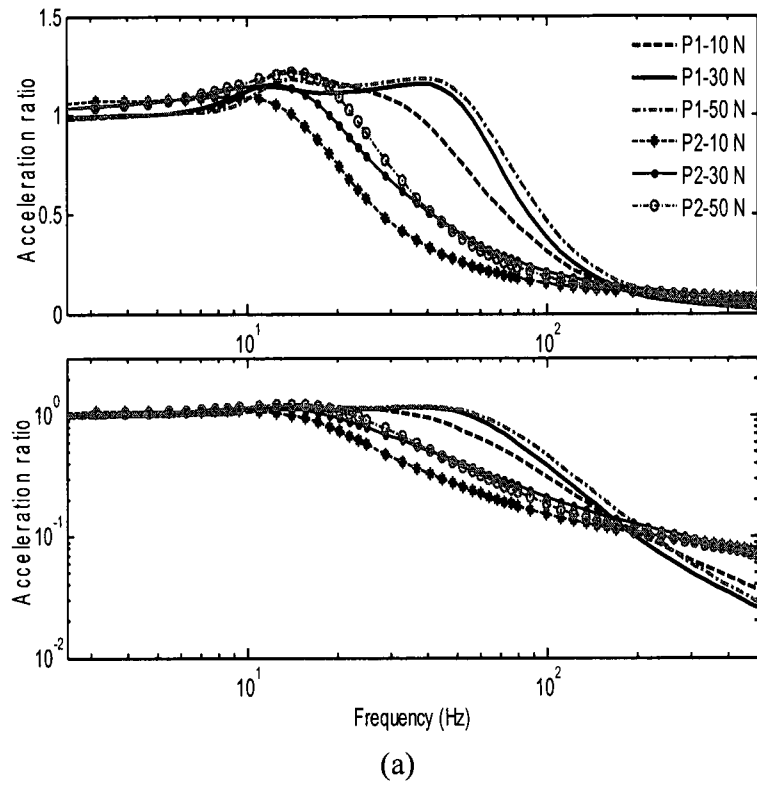
Figure 4.17: Effects of hand forces on the z_h-axis wrist transmissibility magnitude responses of the models: (a) constant push force; (b) constant grip force.

197
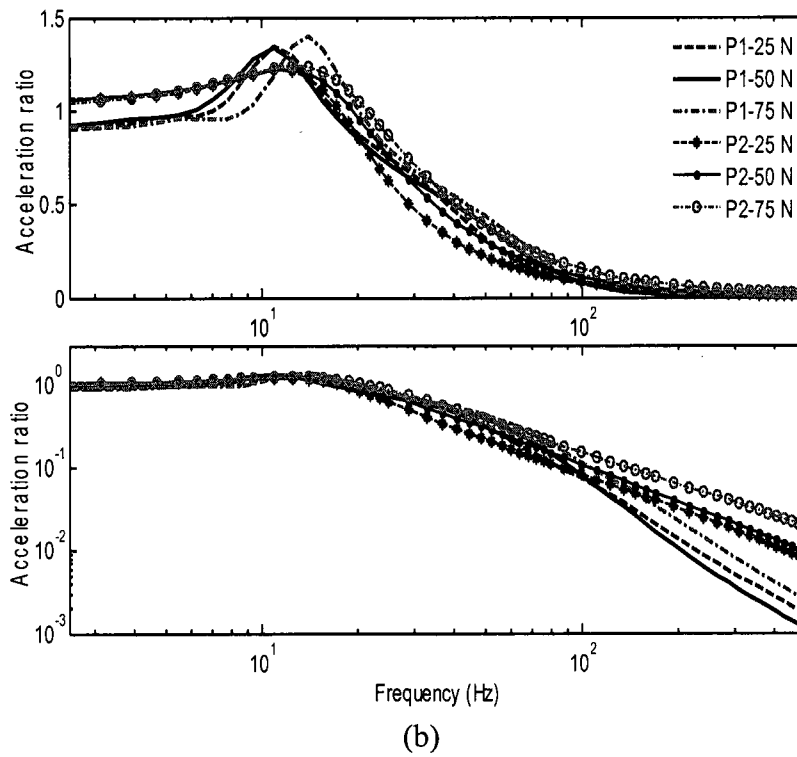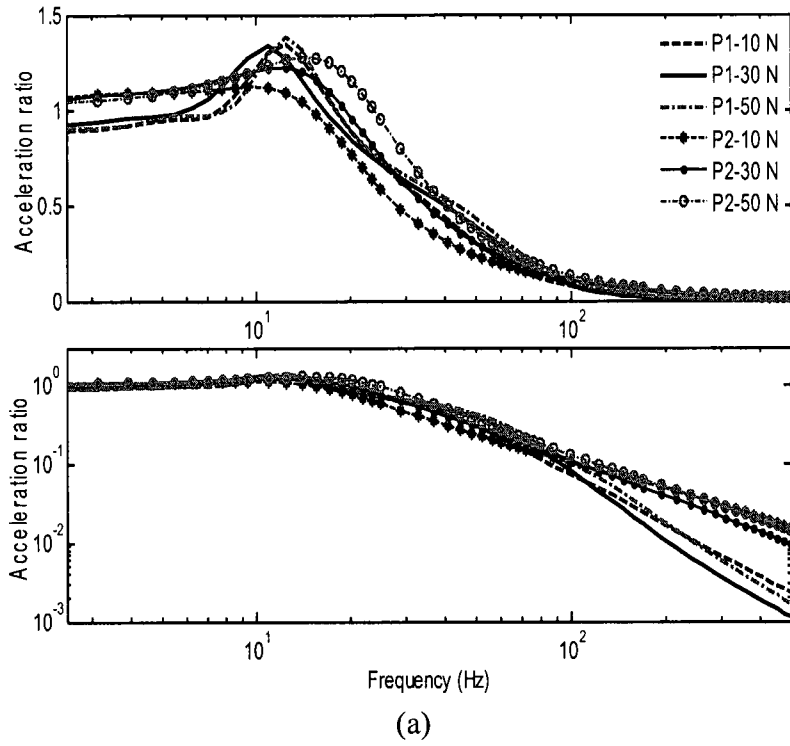
Figure 4.18: Effects of hand forces on the z_h-axis elbow transmissibility magnitude responses of the models: (a) constant push force; (b) constant grip force.
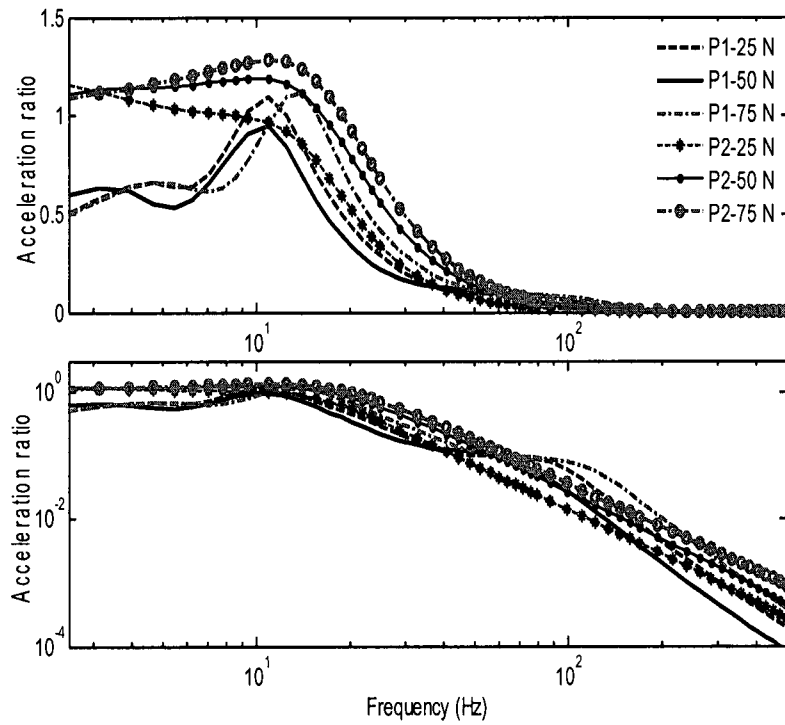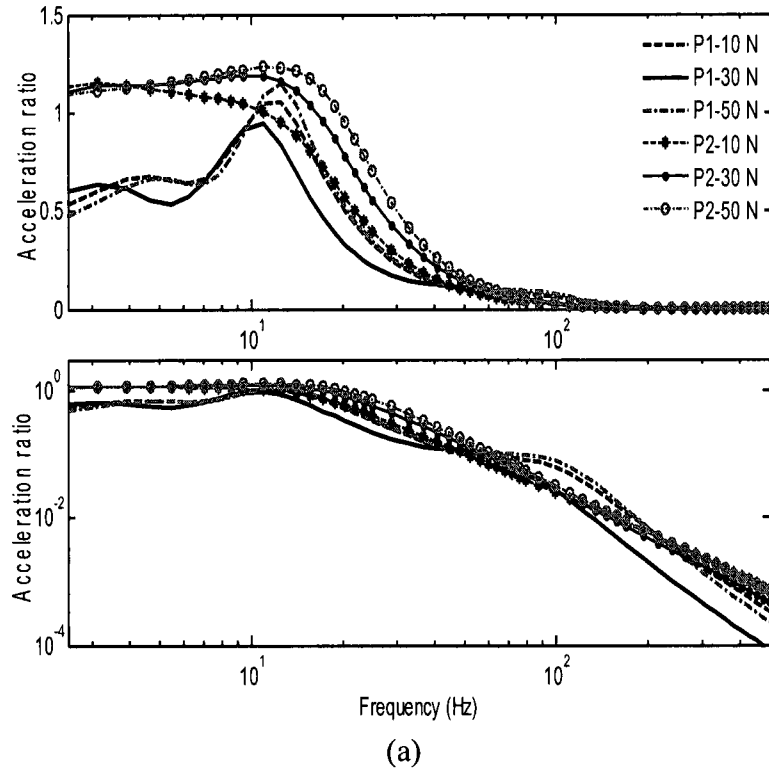
Figure 4.19: Effects of hand forces on the z_h-axis shoulder transmissibility magnitude responses of the models: (a) constant push force; (b) constant grip force.

frequency range for the responses at the shoulder. Whereas the mean measured data showed that the bent-arm transmissibility magnitudes are greater than those of the extended arm above 25 Hz at the elbow, and above 80 Hz for the shoulder responses.

4.7 Summary

Biomechanical models of the human hand-arm in the bent-arm and extended arm postures were developed. The parameters of the models were derived by minimizing the errors between the model and measured driving-point mechanical impedance (DPMI) and transmissibility responses, and characteristic frequencies coupled with the sensitivity analyses. The effects of changes in the hand forces on the parameters and biodynamic responses of the models were studied. The results showed that the parameters of the models are strongly dependent on the type of target biodynamic measure. The parameters derived on the basis of transmissibility responses alone were smaller in values than those derived using the DPMI response and the combined biodynamic measures. This suggests that transmissibility responses characterize the dynamics of the tissues/muscle of the human hand-arm at different locations, while the DPMI characterizes the entire hand-arm system with emphasis around the driving-point.

An increase in the grip force revealed the highest effect on the parameters of the models around the driving-point (fingers, palm and wrist) and forearm, while the push force affected the parameters of the entire system. Similar trends were observed in the mean measured biodynamic responses. The majority of the rotational visco-elastic parameters of the extended arm model appeared to be redundant; the responses were observed to be relatively insensitive to changes in these parameters. Furthermore, the y_h-axis responses of the models resulted in very low magnitude, which was attributed to lack

of consideration of y_h-axis compliance of the joints and substructures, and linearization of the models. The consideration of individual masses due to tissues/muscles and the bones of the forearm and the upper-arm together with the visco-elastic properties may be more appropriate. The proposed hand-arm vibration models are further applied to study the distribution of absorbed power within the and-arm system in the subsequent chapter.

CHAPTER 5

VIBRATION POWER DISTRIBUTION IN THE HAND-ARM SYSTEM

5.1 Introduction

The severity of the hand-arm vibration exposure is most strongly related to the intensity of vibration and exposure duration. The measured biodynamic responses, particularly the DPMI, show only marginal influence of excitation magnitude, while exposure duration is not considered. The biodynamic responses are mainly used to characterize the dynamic properties of the hand-arm system, and thus cannot be used as an exposure assessment tool. While the ISO-5349-1 weighted acceleration is mainly used to assess vibration exposure, the overall vibration power absorption (VPA) of the hand-arm system has been suggested as a better measure for assessing the health effects of vibration exposure [133, 134]. Mathematically, the VPA is proportional to the real part of DPMI and to the square of the vibration velocity. Furthermore, it has been shown that VPA is also approximately proportional to the square of excitation acceleration magnitude [84, 134]. Considering the direct relationship between the VPA and vibration magnitude, a number of studies have focused on characterization of localized VPA distribution in the human hand-arm exposed to vibration [128, 133]. Whereas the VPA could provide important information on possible injury risks of different substructures of the human hand-arm system, the measurement of distributed VPA is generally complex since it requires the measurement of dynamic force. It is difficult to measure the dynamic force of hand-held power tools in the field, even though it could easily be measured in the

laboratory via instrumented simulated handles. Although the total VPA at the driving-point could be obtained indirectly from DPMI response, the determination of distributed VPA of different substructures of the hand-arm system requires the use of mechanical-equivalent models, which exhibit large differences in their types and parameters [65]. Subsequently, there are large variations in the reported VPA distribution due to its dependence on excitation type and hand-arm model, in addition to other factors like hand forces, subject anthropometry and hand-arm posture. The localized response of different substructures of the hand-arm can be obtained by vibration transmissibility measurement at different segments of the human hand-arm system, as demonstrated in chapter 3. Furthermore, VPA is vibration excitation-specific; it has also been shown that VPA cannot be directly compared with frequency-weighted acceleration for assessment of potential injury, but the square root of VPA showed good correlation with frequency-weighted acceleration defined in ISO 5349-1 [134].

The knowledge of VPA distribution at different substructures of the human hand-arm could yield significant insight into injury mechanism of different substructures. In this chapter, the VPA distributions in the substructures of the two hand-arm models, that were developed in chapter 4, are evaluated. Laboratory experiments were performed to measure the acceleration of the handle of a chipping hammer under different working conditions. The accelerations measured on different hand-held power tools were applied to the bent-arm model to estimate the VPA distribution of the hand-arm system.

5.2 Characterization of Hand-arm Responses to a Chipping Hammer Vibration

The hand-transmitted vibration due to the operation of a chipping hammer was measured when a subject operated the tool. The effects of hand forces and speed (blows per minute) of the power tool on hand-transmitted vibration are investigated. The measured acceleration on the tool's handle and those reported for other power tools are used to estimate the VPA distributions in the bent-arm hand-arm model.

5.2.1 Experimental setup

A uni-axial accelerometer (B&K type 4393) was mounted on the handle of a chipping hammer using a mechanical filter (B&K WA-0224). The tool was operated in a steel ball energy dissipater, as in ISO 8662-2 [139], and the setup is shown in Figure 5.1(a). The experiments were conducted using one subject. Figure 5.1(b) shows the posture of the subject. The selected electric percussion chipping hammer (BOSCH 11313 EVS) comprises a variable electric drive capable of delivering 1300 – 2600 blows per minute (BPM) or revolution per minute (RPM) under no load. The amperage rating of the 115 V AC drive is 8.8 A. Using the six speed control dial positions, the motor speed could be varied in the 1300 - 2600 RPM speed range. A built-in internal electronic feedback system maintains the pre-selected impact rate almost constant, irrespective of the load or no-load operating conditions. The measurements were obtained for two speeds corresponding to settings 3 and 6 of the speed dial, which were designated as "low speed" and "high speed", respectively. The subject applied two push forces of 78 N and 118 N while assuming 90° elbow angle and about 30° abduction angle as shown in Figure 5.1(b). The push force was measured using a force plate and digitally displayed to the subject for maintaining the force at a desired level. The grip force imparted on the handle,

however, was not measured. The hand-transmitted vibration was measured at four locations on the subject's hand-arm using Velcro mounted tri-axial accelerometers (PCB - ICP) in a manner similar to that described for the experiments in chapter 3. The posture that was assumed by the subject did not permit a direct relationship between the direction of the measured acceleration and the basicentric coordinate defined in ISO 5349-1 [31], as used with the simulated handle experiments. The measured acceleration direction is thus related to the axis of the accelerometers. Although the tool was guided in the energy dissipater, multi-axis vibration at the handle was expected, unlike the simulated handle vibration generated by the electro-dynamic shaker, whose excitation is predominantly uni-axial. Three measurement trials were performed for each condition and the coherence of the measurements was also considered to monitor the reliability of the measured data.
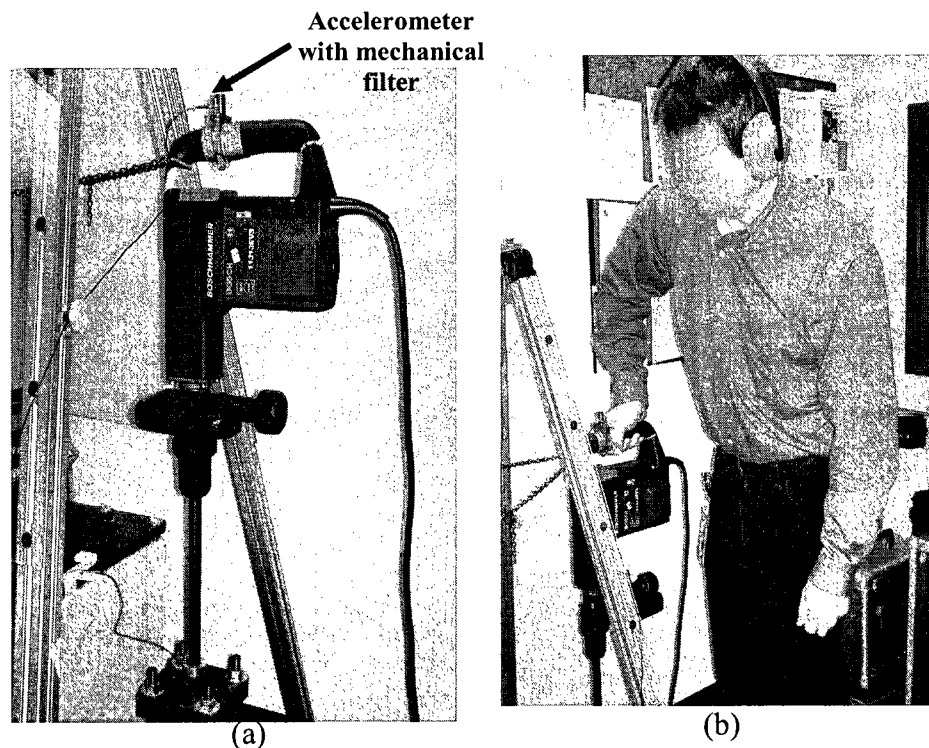
Figure 5.1: Experimental setup for the measurement of the hand tool vibration: (a) Bosch chipping hammer showing accelerometer location; (b) posture adopted by an operator.

5.2.2 Acceleration spectrum of the chipping hammer

The mean acceleration spectra of the tool handle vibration along the dominant axis (z-axis of accelerometer) for different experimental conditions together with the constant power spectral density (PSD) acceleration used in the simulated handle experiments, corresponding to 30 N grip and 50 N push forces (a_{hw} = 5.25 m/s^2), are compared in Figure 5.2. The experimental conditions of the chipping hammer presented in Figure 5.2 are low- and high-speed acceleration spectra corresponding to two different push forces: 78 N and 118 N. The figure shows the operating frequencies of the tool corresponding to low and high speeds, which are approximately 30.5 Hz and 43.75 Hz,
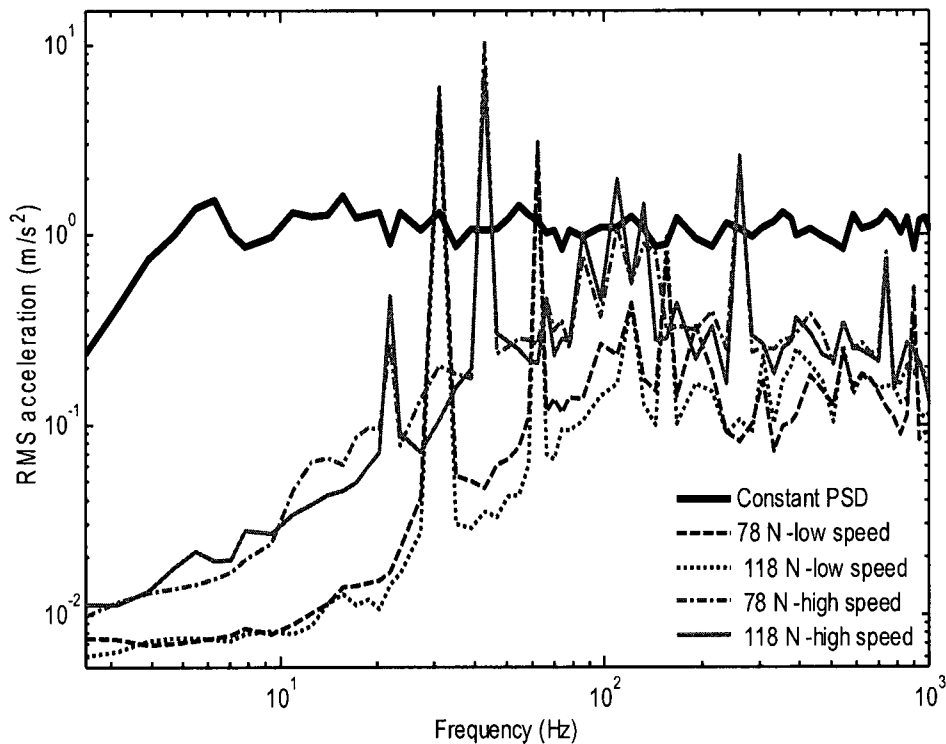
Figure 5.2: Comparison of acceleration spectra of the chipping hammer under different operating conditions with the constant PSD acceleration.

respectively. The tool's acceleration spectra show sub-harmonics and harmonics of the dominant operating frequencies. It is evident that the effect of the operating speed on the hand tool vibration is more significant than that of the push force, whose effect is marginal. There is considerable difference between the constant PSD acceleration used in the simulated handle experiments and the chipping hammer tool acceleration spectra, particularly in the low frequency region. The overall un-weighted (a_{rms}) and frequency-weighted (a_{hw}) rms acceleration values of the spectra presented in Figure 5.2 are summarized in Table 5.1. The table shows that a higher operating speed yields higher a_{rms} and a_{hw}, while an increase in the push force yields lower acceleration magnitudes. The observed decrease in acceleration magnitudes due to an increase in the push force may be attributed to increased restriction on the contacting parts of the chipping hammer.

Table 5.1: Un-weighted and frequency-weighted rms acceleration values of the chipping hammer under different operation conditions

Excitation type	a_{rms} (m/s^2)	a_{hw} (m/s^2)
Electro-dynamic exciter		
Constant PSD, 30 N grip, 75 N push	31.95	5.25
Chipping hammer		
78 N push, low speed (30.5 Hz)	23.49	4.55
118 N push, low speed (30.5 Hz)	21.37	3.80
78 N push, high speed (43.75 Hz)	41.33	8.84
118 N push, high speed (43.75 Hz)	37.69	6.53

5.2.3 Transmissibility responses due to chipping hammer vibration

The repeatability of the hand-arm transmissibility response measurements was examined before the data were averaged. The repeatability of the measurements was observed to be reasonably good, considering that the hand grip force and hand-arm posture could not be precisely controlled. As an example, Figure 5.3 compares the z-axis
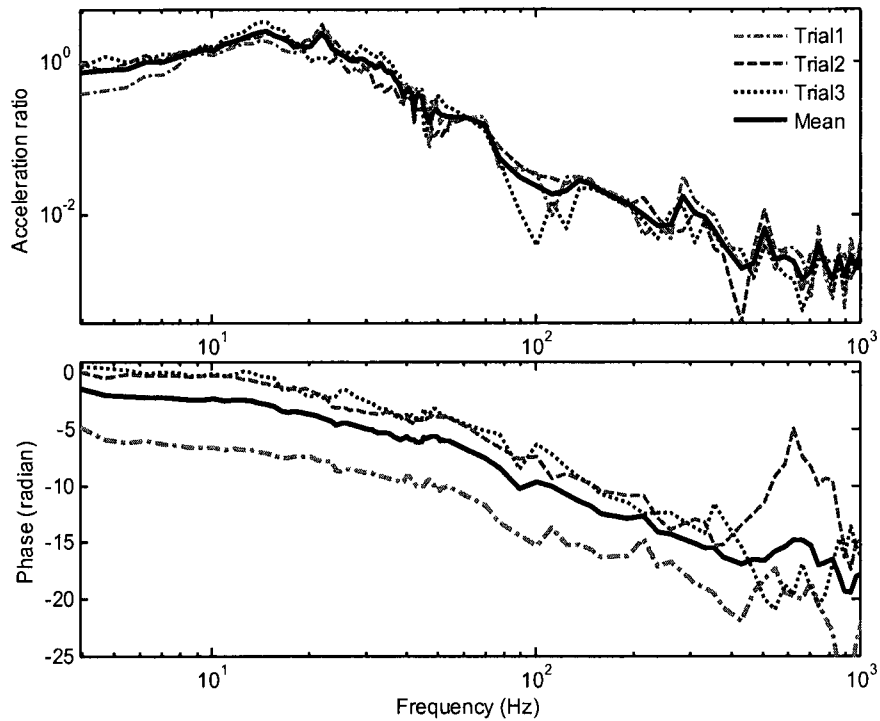
Figure 5.3: Repeatability of measurements at elbow 1 along the z-axis (F_p = 78 N, speed = 2600 rpm)

Table 5.2: Maximum standard deviation in transmissibility responses at different measurement locations

Location and direction	Peak standard deviation	Mean	Frequency of peak deviation (Hz)
Wrist, y-axis	2.25	2.42	22.66
Wrist, z-axis	0.64	1.54	21.88
Elbow1, x-axis	1.81	2.99	3.13
Elbow1, y-axis	1.60	1.10	2.34
Elbow1, z-axis	1.06	2.38	21.88
Elbow2, x-axis	1.39	2.61	3.13
Elbow2, y-axis	1.94	1.86	2.34
Elbow2, z-axis	1.15	2.29	13.28
Shoulder, y-axis	2.08	2.11	2.34
Shoulder, z-axis	0.91	1.99	14.06

vibration transmissibility measured at the elbow during the three trials. The figure also

shows the mean response corresponding to a push force of 78 N and tool speed of 2600

208

rpm. The results suggest reasonably good repeatability of measurements in terms of the transmissibility magnitude, while some differences are evident in the phase response. The coherence of the measurements, however, was generally poor below 5 Hz and above 200 Hz, which was attributed to low signal to noise ratio due to dominance of tool's vibration around its operating speed of 2600 rpm (43.75 Hz). The peak standard deviations (SDs) in the transmissibility response magnitudes for all measurement locations and directions are summarized in Table 5.2, together with the frequency at which the peak deviation occurred and the corresponding mean value. The table shows that the highest deviation in measurements occurred at the wrist along the y-axis, while a deviation of 1.15 (mean value = 2.29) occurred at elbow 2 at 13.28 Hz in the z-axis. The deviations in the phase responses were considerably greater than those in the transmissibility magnitudes. Such variations were attributed to possible variations in the subject posture, which affected the orientation of the accelerometers in a considerable manner. The measurements along the dominant z-axis alone are thus considered for further analysis, since the peak deviations in this direction were considerably lower than those in the x- and y-axis magnitudes.

The mean z-axis transmissibility response measured at the wrist, elbow and the shoulder are presented in Figure 5.4. The transmissibility magnitudes are presented in both the linear and logarithmic scales to emphasize responses at low and high frequency regions, respectively. The responses can be divided into two frequency regions, namely: (1) below 25 Hz, where the responses around the elbow and shoulder are higher than the response at the wrist; and (2) above 25 Hz, where the transmissibility response magnitude decreases from the wrist to the shoulder. The trend above 25 Hz is similar to that observed in Figure 3.19 for the hand-arm posture with zero abduction angle exposed to
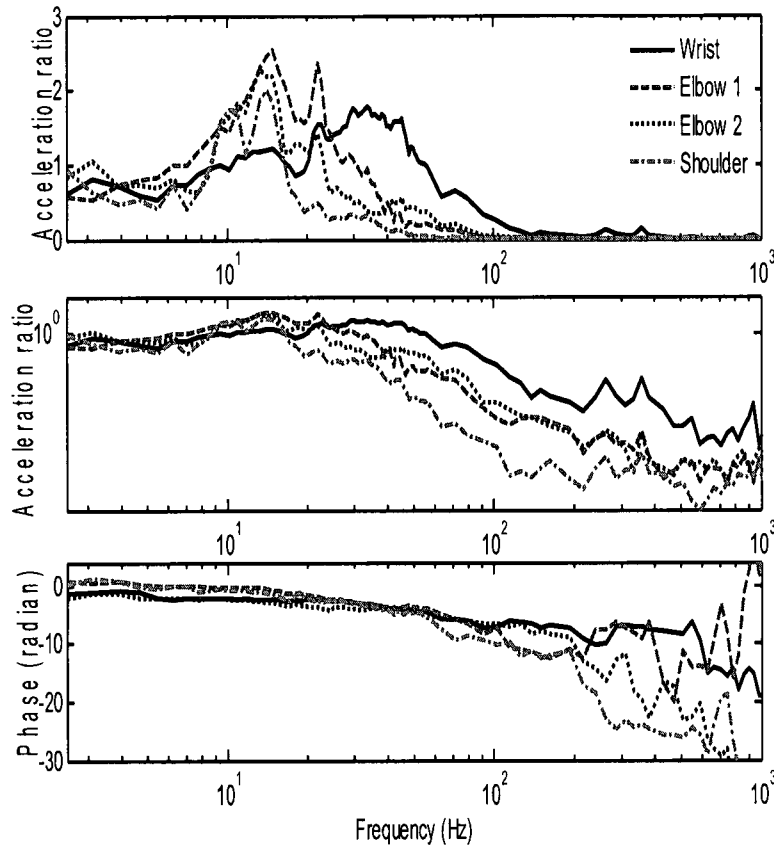
Figure 5.4: Mean z-axis acceleration transmissibility responses measured at different locations (F_p = 78 N, speed = 2600 rpm)

z_h-axis constant spectrum excitation. The results show that the wrist and elbow 1 response magnitudes at low frequency (≈ 2.5 Hz) are well below 1.0, which was believed to be caused by error in the orientation of the accelerometers due to somewhat awkward posture assumed during the experiments. Furthermore, the low magnitude vibration of the chipping hammer in the low-frequency region, as evident in Figure 5.2, may also be a contributing factor. The results suggest that the prominent characteristic frequencies of the z-axis vibration are in the vicinity of 10.2, 14.8, 21.9, 33.0, 71.9, 263.3 and 357 Hz.

5.2.4 Effects of push force and tool speed on transmissibility responses

The influences of push force as well as the impact rate or the operating speed of the power tool on vibration transmitted along the z-axis at the wrist, elbow 1 and the shoulder are illustrated in Figures 5.5 through 5.7, respectively. The figures show that the impact rate of the hand-held power tool has more pronounced effect on the wrist transmissibility response of the human hand-arm than the push force. This is similar to the trend observed in the hand tool un-weighted and frequency-weighted acceleration values, as shown in Table 5.1. In general, an increase in the tool speed and push force tend to increase transmissibility magnitude, particularly in the low frequency region.

The low frequency transmissibility magnitudes measured at the wrist for all conditions were lower than 1.0, as shown in Figure 5.5. The highest magnitude occurred
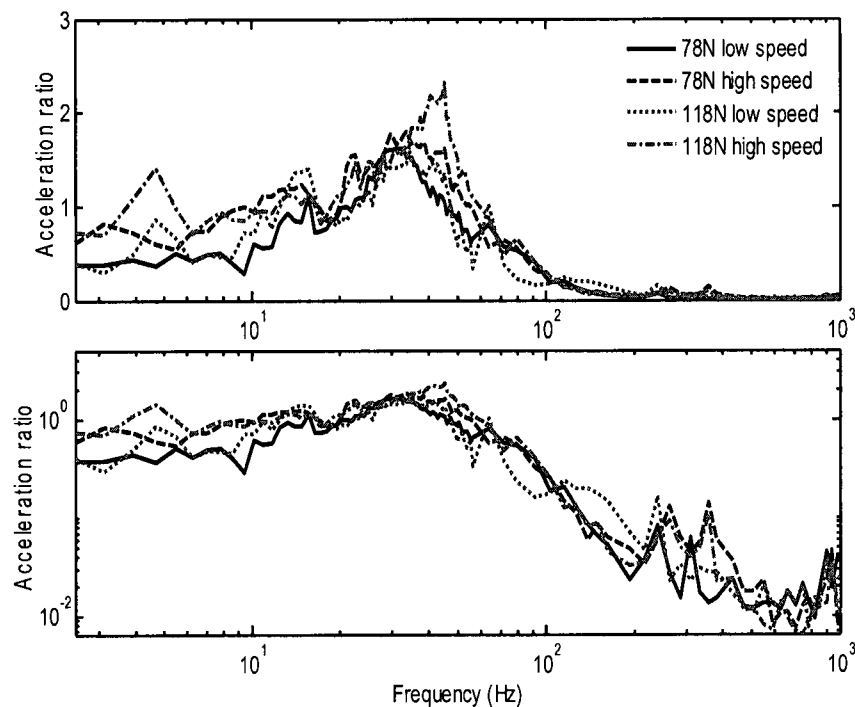
Figure 5.5: Effects of push force and tool speed on the mean z-axis transmissibility at the wrist
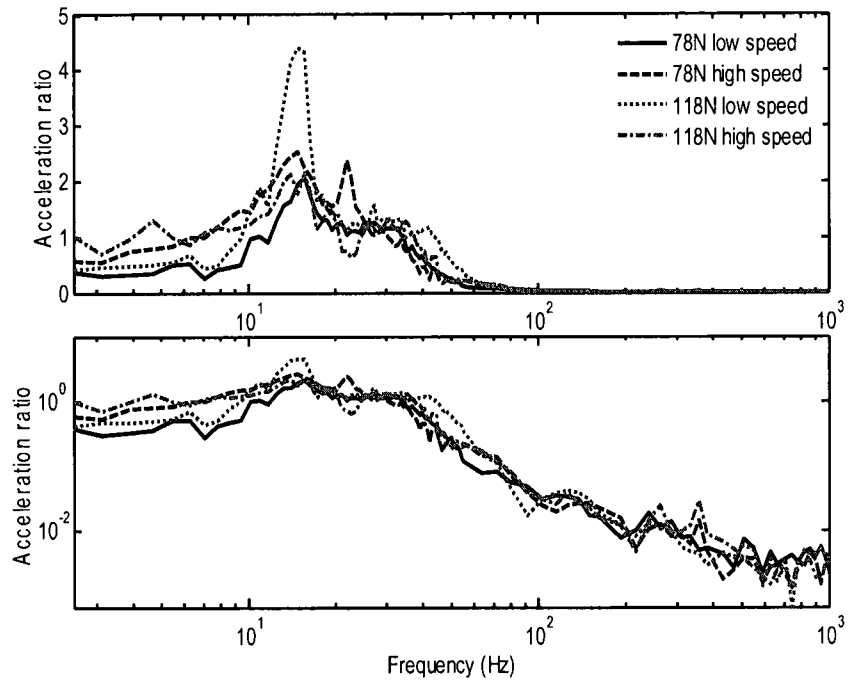
Figure 5.6: Effects of push force and tool speed on the mean z-axis transmissibility at elbow 1
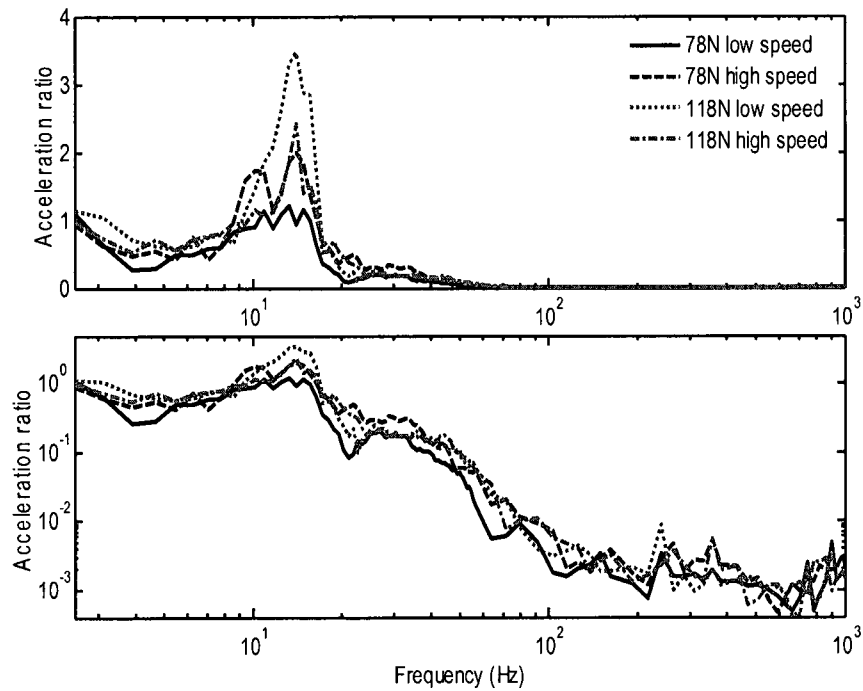
Figure 5.7: Effects of push force and tool speed on the mean z-axis transmissibility at the shoulder

around 45.3 Hz in the wrist response, corresponding to 118 N push force and high tool speed (43.8 Hz). The highest elbow 1 transmissibility magnitude occurred around 14.8 Hz, corresponding to 118 N push force and low tool speed. The shoulder response corresponding to 118 N push force and low tool speed (30.5 Hz) revealed the highest magnitude at 14.1 Hz.

5.2.5 Comparison of transmissibility magnitudes of the model with mean responses due to simulated handle and power tool vibrations

The VPA of different substructures of the hand-arm system is highly dependent on the type of excitation [128] and the response magnitudes across different substructures of the hand-arm model. Considering that the vibration transmissibility is far less sensitive to excitation magnitude, the transmissibility responses of the human hand-arm system are compared with those of the model under different excitations. It should be noted that neither the bent-arm nor extended arm postures would represent the hand-arm posture assumed in experiments with the tool. This posture, however, was considered closer to the bent-arm than the extended arm. The responses of the bent-arm model are thus considered for comparisons. Figures 5.8 to 5.10 illustrate comparisons of the mean z_h-axis transmissibility magnitudes of the bent-arm hand-arm model, derived in chapter 4 and the mean measured responses due to constant PSD excitation of the simulated handle and the chipping hammer at the wrist, elbow 1 and the shoulder, respectively. The excitation acceleration for the model and the measured responses correspond to 30 N grip force, 75 N push force and weighted acceleration level (a_{hw}) of 5.25 m/s^2. The chipping hammer responses correspond to a push force of 78 N, a frequency-weighted acceleration a_{hw} of 4.55 m/s^2, and an operating speed of 30.5 Hz or about 1830 blows per minute. It was not possible to measure the grip force on the chipping hammer. Apart from the low
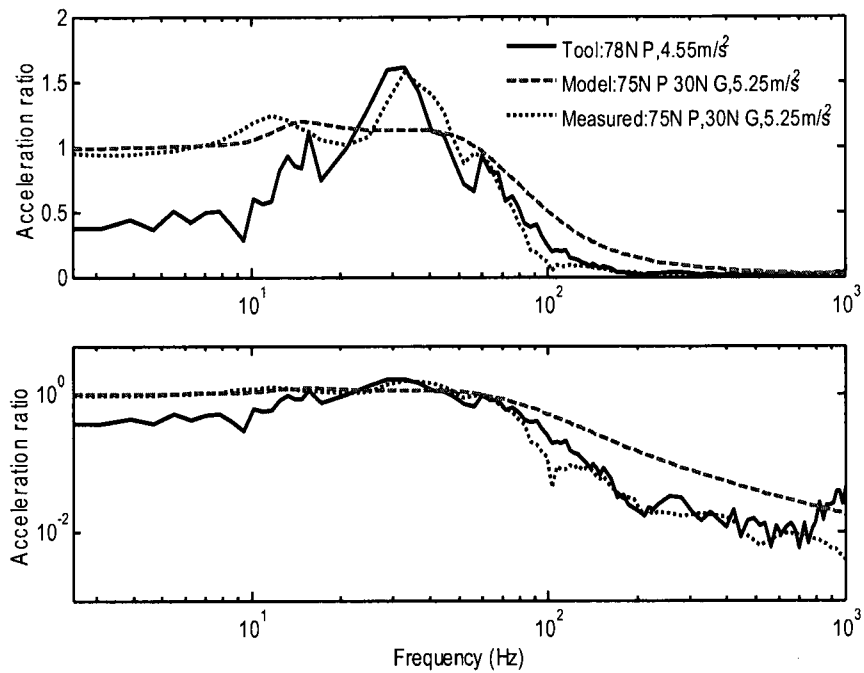
Figure 5.8: Comparison of the mean z-axis wrist transmissibility magnitudes due to model response and measured responses due to shaker and hand tool excitations.
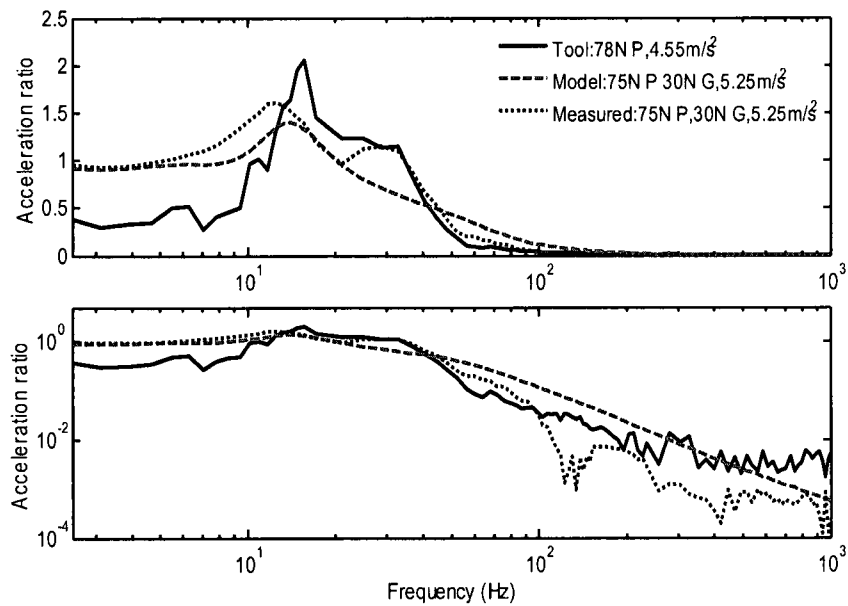
Figure 5.9: Comparison of the mean z-axis elbow 1 transmissibility magnitudes due to model response and measured responses due to shaker and hand tool excitations.
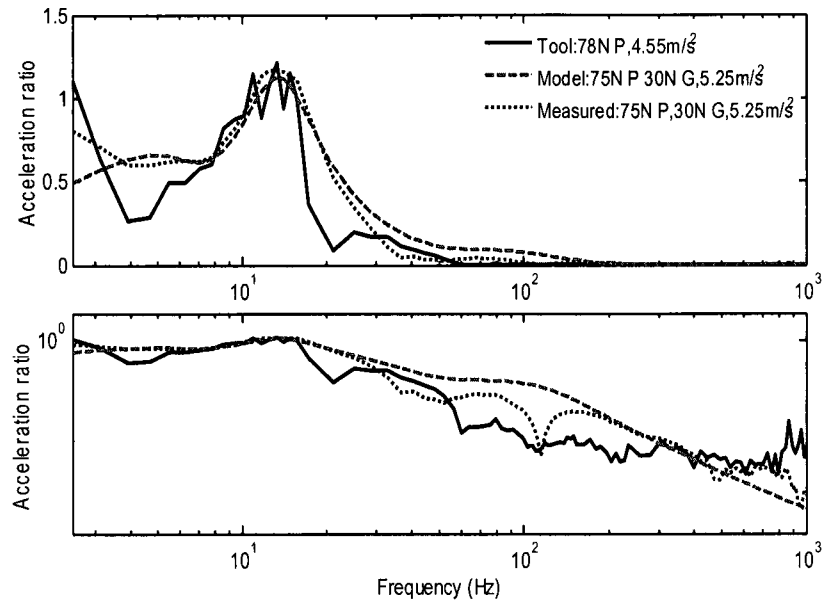
Figure 5.10: Comparison of the mean z-axis shoulder transmissibility magnitudes due to model response and measured responses due to shaker and hand tool excitations.

transmissibility magnitudes, which could be attributed to low signal to noise ratio, at low frequency region, at the wrist and elbow 1 for the responses due to hand tool excitation, the trends in transmissibility responses of the human hand-arm are comparable for the two excitations considered. In general, the trends of the transmissibility responses obtained in the laboratory with excitation from an electro-dynamic exciter and the hand-arm model are also similar to the responses obtained from the excitation from the impact tool. Similar observations were also reported in [77] and [95].

5.3 Method of Analyses of Vibration Power Absorption

The VPA distribution in substructure k ($k = 1, \ldots, 7$) P_k and the total VPA distribution P_{total} of the hand-arm system are estimated from energy dissipated per second in the damping elements as follows [133]:

$$P_k(f) = c_k[\Delta v_k(f)]^2 + C_k[\Delta\Omega_k(f)]^2 \qquad (5.1)$$

$$P_{total}(f) = \sum_{k=1}^{7} P_k(f) \qquad (5.2)$$

where f is the frequency in Hz, Δv_k and $\Delta\Omega_k$ are relative translational and rotational rms

velocities across the damping element at joint k, respectively. The coefficients c_k and

C_k are, respectively, the linear and rotational damping coefficients of the hand-arm

models components derived in chapter 4. The parameters Δv_k and $\Delta\Omega_k$ can be obtained

by re-writing Eq. (4.15) as:

$$\{\chi_{ea}(j\omega)\} = [[K] - \omega^2[M] + j\omega[C]]^{-1}\{f_{ea}\}Z_{hh} \qquad (5.3)$$

$$\begin{aligned}\Delta v_k(f) &= j2\pi f(Z_{k+1} - Z_k)\\ \Delta\Omega_k(f) &= j2\pi f(\theta_{k+1} - \theta_k)\end{aligned} \qquad (5.4)$$

where $\{f_{ea}\}Z_{hh} = \{F_{ea}\}$. It should be noted that χ_{ea} is a vector containing translational

Z_i ($i = 1,\ldots, n$) and angular θ_i displacement coordinates, where n is the number of DOF

of the model. The handle excitation Z_{hh} in Eq. (5.3) represents the displacement of the

handle held by the hand-arm system. However, the handle excitation is usually measured

in terms of acceleration. The corresponding displacement spectra is derived from the

acceleration PSD S_x, as:

$$Z_{hh(rms)}(f) = \sqrt{\frac{1}{B}S_x(f)\Delta f} \qquad (5.5)$$

where Δf is the frequency resolution and B is the noise equivalent bandwidth constant

and its value depends on the type of window. For the hanning window used in the data

analysis, $B = 1.5$.

Furthermore, the total VPA distribution of the hand-arm system could also be estimated from the measured DPMI response ($P_{measured}$) by using Eq. (1.3). The total VPA distribution obtained from Eqs. (5.2) and (1.3) are compared to validate the VPA distribution derived from the hand-arm models. Finally, the overall VPA (P) is obtained from VPA distributions in the frequency range of interest such that:

$$P = \int_{f_1}^{f_2} P_k(f)\,df \tag{5.6}$$

where f_1 and f_2 define the lower and upper limits of the frequency range of interest.

5.4 Vibration Power Absorption due to a Constant PSD Acceleration and Model Validation

The distributed VPA properties of the two hand-arm models were determined under constant power spectral density (PSD) acceleration excitation of the simulated handle. Although VPA is excitation specific, excitation with a constant PSD has been used to evaluate VPA [84, 135]. The VPA due to handle acceleration with constant PSD would facilitate the validation of the total VPA distribution derived from the hand-arm model (Eq. (5.2)) by comparing the total VPA distribution of the model with the VPA distribution derived from the mean measured DPMI (Eq. (1.3)).

The comparison of the total VPA distributions of the human hand-arm system in the bent-arm and extended arm postures, that were obtained using different estimation methods, are illustrated in Figure 5.11. The experimental conditions correspond to a grip force (F_g) of 30 N, push force (F_p) of 50 N and random acceleration with constant PSD (a_{hw} = 5.25 m/s^2). The model parameters that were derived from combined DPMI and transmissibility responses are used. The VPA is presented in logarithmic scale. The results show that the VPA decreases with increase in frequency, the same trend that has

217

been observed in the transmissibility responses (see Figure 5.7, the logarithmic scale). The figure shows that the VPA estimated from the two models, using Eq. (5.3), are comparable with those obtained from the model and measured DPMI responses, using Eq. (1.3).

For the bent-arm posture (Figure 5.11(a)), the VPA estimated from the model DPMI is greater than those derived from the measured DPMI. In addition, the summation of dissipated energy are slightly lower below 12.5 Hz and in the 12.5 – 70 Hz frequency range. The VPA derived from the measured DPMI is quite comparable with that obtained from the dissipated energy of the damping elements (P_{total}), except in the 70 – 160 Hz frequency range, where the later is slightly lower. On the other hand, all the VPAs for the extended arm posture (Figure 5.1(b)) show reasonably good comparison except in the low frequency range. For example, the VPA derived from the measured DPMI ($P_{measured}$) is lower in the 2.5 – 10 Hz frequency range. Also, the VPA estimated from the damping elements P_{total} is slightly higher in the 7 - 20 Hz range. The deviations in the VPA in the low frequency range may be attributed to relatively high deviation between the measured and the extended arm model DPMI responses, as seen in Figure 4.14(a). The DPMI characterizes the hand-arm responses in the high frequency region better than the transmissibility responses, which show better hand-arm characteristics in the low frequency region. The hand-arm models were derived based on compromise between the DPMI and transmissibility responses. Figure 5.11 shows that the total VPA (P_{total}) estimated from the damping elements in the hand-arm model is comparable to that obtained from the measured DPMI ($P_{measured}$). The subsequent analyses of VPAs are thus performed on the basis of dissipated energy using Eqs. (5.1) and (5.2).
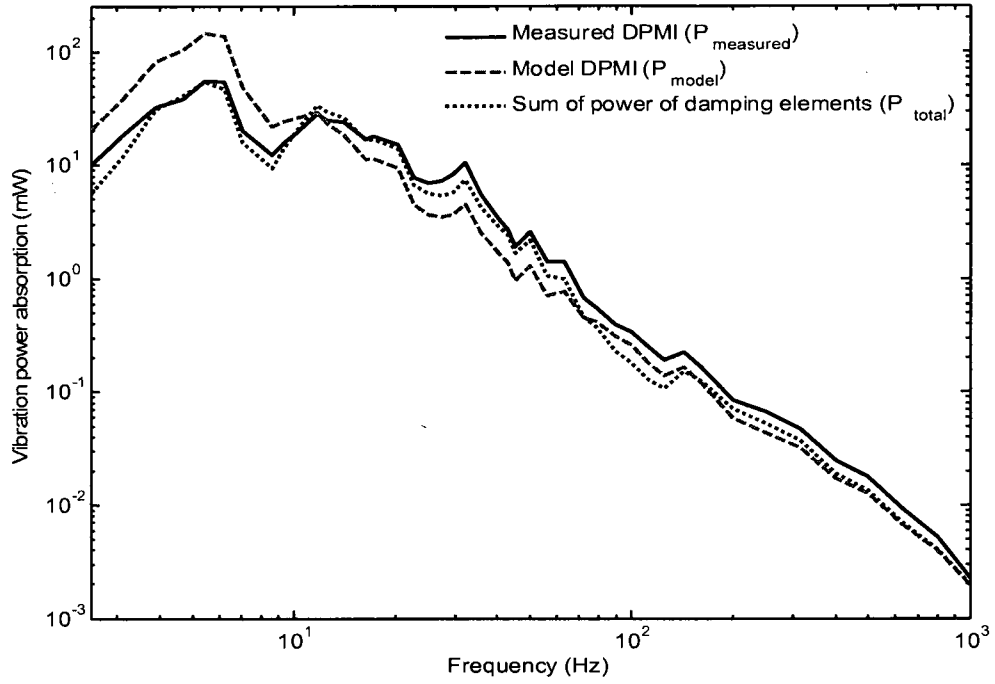
(a)
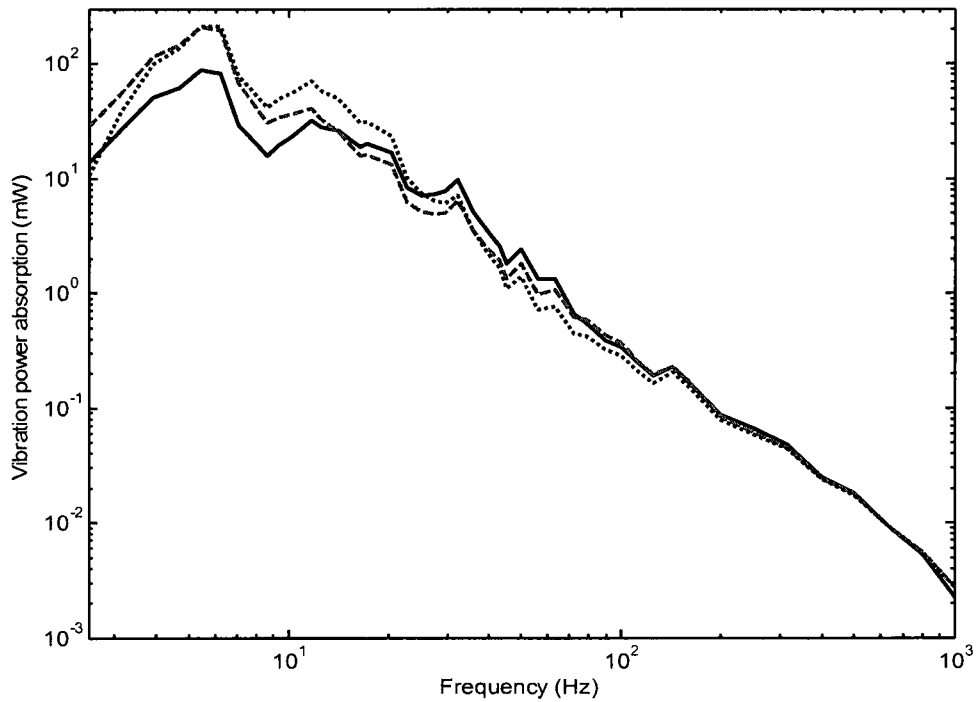
(b)

Figure 5.11: Comparisons of VPA estimated using three different methods (F_g = 30 N, F_p = 50 N and constant PSD excitation with a_{hw} of 5.25 m/s^2): (a) bent-arm posture; (b) extended arm posture.

The effect of the method of parameter identification of the hand-arm model on the VPA distribution of different substructures is further investigated by considering the bent-arm model parameters derived from DPMI alone and those derived from transmissibility responses alone. It should be noted that the parameters that were derived from transmissibility responses are lower than those derived from the DPMI response; hence the corresponding overall VPAs are also lower, as shown in Table 5.3. The percentage error between the overall VPA obtained from the model and the measured DPMI is in the order of 3 % for the case when the model parameters were derived from DPMI response alone, and nearly 32 % when the parameters were derived from the transmissibility responses. The results further show that about 3.2 % of the overall power is absorbed in the hand (fingers, palm and hand back) for parameters derived from transmissibility responses, compared with 10.7 % for the model derived from the DPMI response. For both cases, maximum VPA occurred at the wrist and greater proportion of the power is absorbed in the arms and the trunk of the body than the hand.

Table 5.3: Comparisons of distributed and total VPA of the bent-arm hand-arm model derived from different biodynamic measures ($a_{hw} = 5.25$ m/s^2; $F_g = 30$ N; $Fp = 50$ N).

Location	DPMI response only		Transmissibility responses only	
	Overall Power (mW)	Percentage of power	Overall Power (mW)	Percentage of power
Fingers	21.87	2.39	6.81	1.12
Palm	60.96	6.67	10.80	1.78
Hand back (c_3)	14.78	1.62	1.66	0.27
Wrist	388.89	42.55	257.83	42.55
Elbow	208.56	22.82	143.33	23.66
Shoulder	185.80	20.33	123.54	20.39
Trunk	33.18	3.63	61.93	10.22
P_{total}	914.03		605.90	
$P_{measured}$	886.94		886.94	

The total VPA distributions that were obtained from the three different estimation methods are also compared when the model parameters were derived from different biodynamic measures. The VPA distributions that were obtained when the parameters were derived from the DPMI response alone are similar to those illustrated in Figure 5.11(a), which correspond to the case when the model parameters were derived from both the DPMI and the transmissibility responses.

Figure 5.12 shows the comparisons of the VPA estimated from DPMI and dissipated energy of the model based on the transmissibility responses alone, and the measured DPMI ($P_{measured}$). The results show that the VPA estimated from the DPMI and dissipated energy of the model are lower than that obtained from the measured DPMI except in the 12.5 – 50 Hz frequency region, where the dissipated-based VPA is quite comparable with that derived from the measured DPMI. This may also be attributed to the observation deduced in chapter 4, that is, the hand-arm model based on transmissibility responses alone tends to emphasize the dynamics of tissues/muscles, while that based on DPMI response characterizes the entire hand-arm with emphasis on the driving-point responses. The results suggest that the hand-arm models based on vibration transmissibility responses alone under-estimate the VPA of the human hand-arm system, while those on the basis of DPMI yield good estimate of VPA distribution, particularly at the driving-point. It should however be noted that the DPMI response alone cannot adequately characterize localized dynamics of different substructures of the hand-arm system, while the total VPA evaluated from the DPMI gives a better description of the dynamics of the entire hand-arm system. The results shown in Figure 5.11(a) show that the overall VPA estimated from the dissipated energy of the bent-arm

hand-arm model is comparable with the VPA estimated from the measured DPMI response. It may thus be deduced that the bent-arm model derived on the basis of both biodynamic functions can provide good estimates of total as well as distributed VPA.
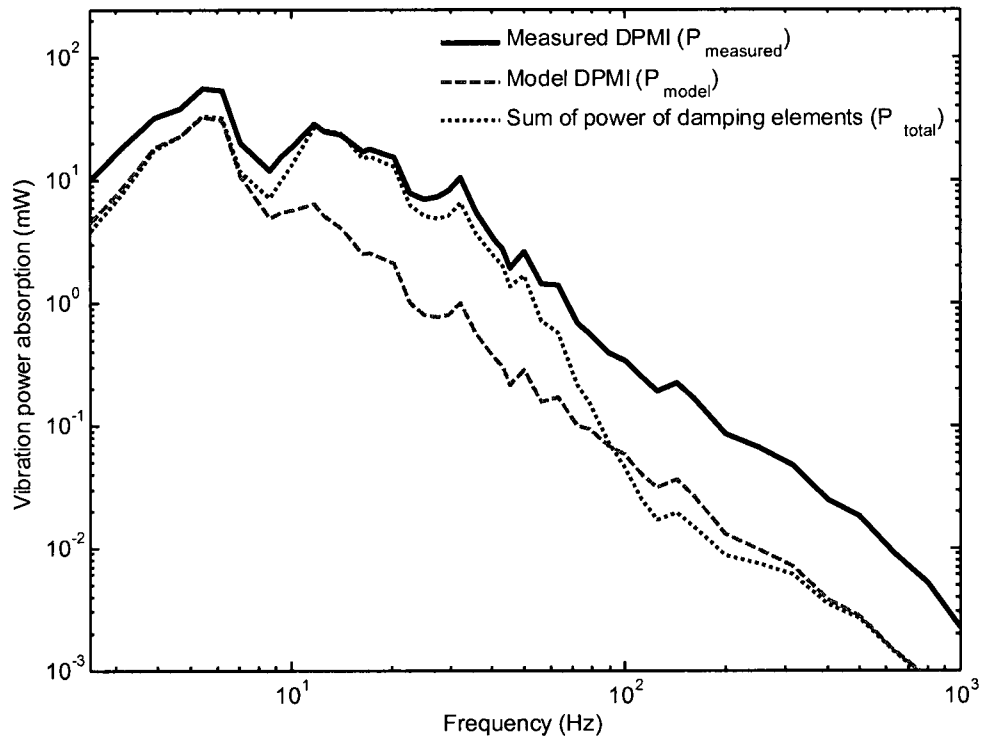
Figure 5.12: Comparison of total VPA distributions estimated using three different methods when the bent-arm model parameters are derived from transmissibility responses ($F_g = 30$ N, $F_p = 50$ N and constant spectrum acceleration of $a_{hw} = 5.25$ m/s^2).

The VPA distribution in different substructures of the hand-arm system are computed for the bent-arm and extended arm postures and presented in Figure 5.13. The figure shows that the VPA values in the vicinity of the driving-point (fingers, palm and the back of the hand with carpal and metacarpals bones connected by c_3) are lower than those for the arms (wrist, elbow and shoulder) and the trunk below 25 Hz for both postures. However, the VPA of the fingers is greater than those of other substructures
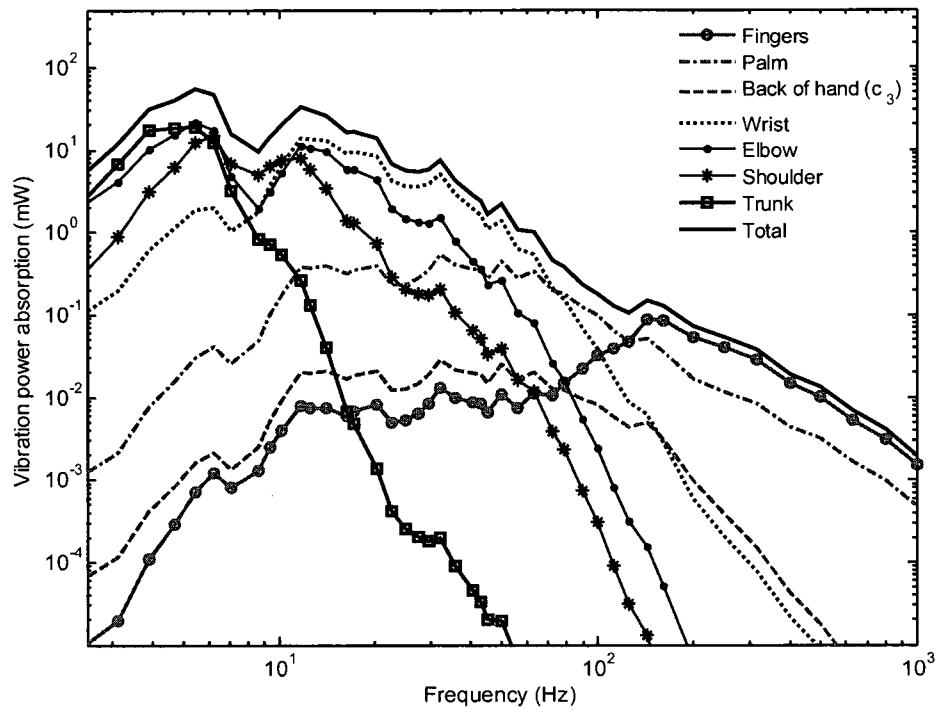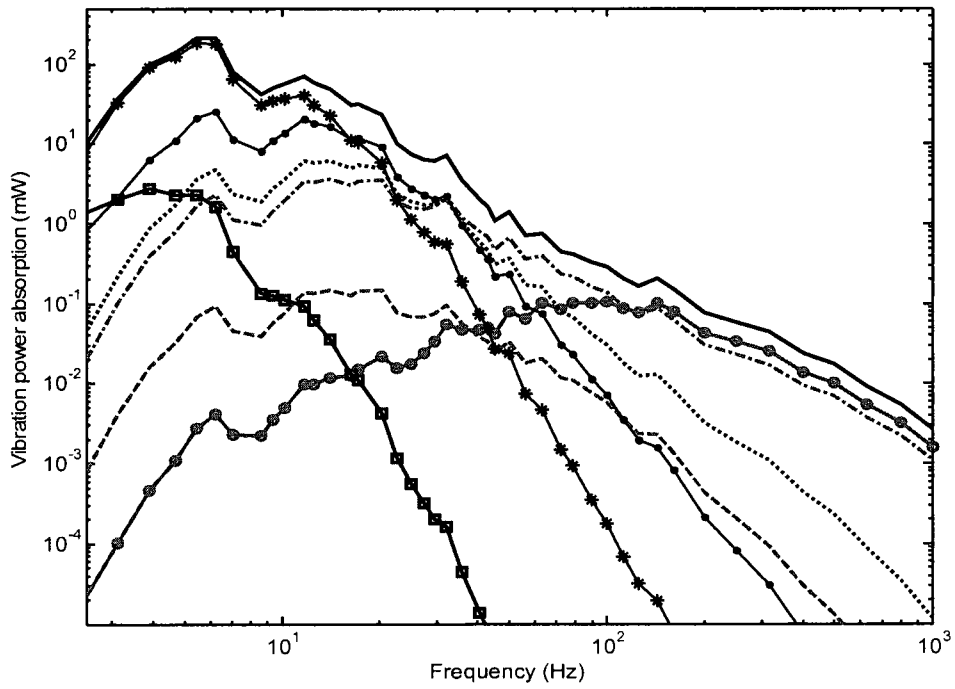
Figure 5.13: Comparison of VPA distribution of different segments of the hand-arm system (F_g = 30 N, F_p = 50 N and constant spectrum vibration with a_{hw} of 5.25 m/s^2): (a) bent-arm posture; (b) extended arm posture.

above 100 Hz. However, the magnitude of VPA at high frequencies is generally lower than that observed in the low frequency region. The VPAs of the hand-arm substructures initially increase with increase in frequency, but later decrease with increase in frequency, for acceleration with a constant PSD at the driving-point. The observed trends are similar to those reported in ref. [133], in which VPA of the hand-arm substructures were obtained under vibration spectra of hand-held power tools coupled to lumped-mass hand-arm model. The trends in Figure 5.13 buttress the conclusions and the results obtained from the transmissibility responses in chapter 3, namely: high frequency vibration is confined to the hand, while low frequency vibration is transmitted to the arms and the trunk of operators of the hand-held power tools. The frequencies corresponding to peaks in the total VPA distribution are similar to the characteristic frequencies observed in the DPMI response. The results show peak VPA around 5 Hz, which is close to the characteristic frequency of the whole-body represented by the trunk in the model. It was reported that subjects exposed to vertical whole-body vibration showed greatest absorbed power around 5 Hz [135].

The overall VPA of each substructure, obtained by summing the VPA distribution in the 2.5 – 1000 Hz frequency range, and the percentage of the power that is absorbed in each substructure relative to the overall total power are summarized in Table 5.4. The results also compared reasonably well with the overall VPA obtained from the measured DPMI ($P_{measured}$). The results suggest that the posture has significant influence on the VPA of different substructures of the human hand-arm system, and greater power is absorbed in the hand-arm system in the extended arm posture than in the bent-arm posture. Furthermore, the percentage of the total power absorbed in the hand (fingers,

Table 5.4: Comparisons of distributed and total VPA of the hand-arm models in the 2.5 – 1000 Hz region under constant spectrum acceleration (a_{hw} = 5.25 m/s^2; F_g = 30 N; Fp = 50 N).

Location	Bent-arm		Extended arm	
	Overall Power (mW)	Percentage of power	Overall Power (mW)	Percentage of power
Fingers	22.06	2.76	29.61	1.63
Palm	43.06	5.39	140.69	7.75
Hand back (c_3)	2.55	0.32	5.78	0.32
Wrist	301.83	37.80	155.66	8.58
Elbow	228.57	28.62	375.32	20.68
Shoulder	117.06	14.66	1093.80	60.28
Trunk	83.42	10.45	13.76	0.76
P_{total}	798.56		1814.62	
$P_{measured}$	886.94		1051.95	

back of the hand and the palm) is relatively small compared with that absorbed in the arms. This may be attributed to the presence of more muscles/tissues and larger joints on the arm structure, which account for damping.

It should be noted that the acceleration transmissibility magnitudes also show that greater vibration is transmitted to the arms and shoulder in the extended arm posture, particularly at low frequencies. The percentage errors between the overall VPA obtained from the models and the measured DPMI are about 10 % and 72 % for the bent-arm and extended arm postures, respectively. The high percentage error for the extended arm posture can be attributed to high discrepancy between the VPA of the model and that derived from the measured data below 20 Hz as shown in Figure 5.11(b). Subsequent VPAs are evaluated using the bent-arm model, which is perhaps more representative of the hand-arm posture adopted while operating the chipping hammer.

5.5 VPA distribution due to Vibration from Hand-Held Power Tools

The VPA due to hand-transmitted vibration is strongly dependent on the frequency contents and magnitude of handle vibration. Thus, the VPA responses attained under control acceleration spectrum cannot be generalized for assessing the potential injury risks arising from different tools, since it does not take into account the differences in vibration levels encountered with real tools and the impulsiveness of their time signals (i.e. high crest factor for impact tools). The vibration spectrum of different tools considerably differs depending on the tool type, tool size, nature of task, hand forces, etc. The VPA due to a particular tool vibration may be effectively evaluated from a proven model and measured handle vibration. Considering the complexities associated with measurement of forces with the hand-held power tools, the field studies are mostly limited to tool vibration and hand-arm transmissibility responses measurement. A validated mechanical-equivalent model of the human-arm system is thus needed for evaluation of VPA distribution to different hand-arm substructures due to hand-held power tool vibration.

5.5.1 VPA distribution due to chipping hammer vibration

The VPA distributions in different substructures of the bent-arm hand-arm model under excitation from the percussion chipping hammer, when operated at 2600 rpm and pushed with a force of 78 N, are presented in Figure 5.14. The results show trends that are similar to those observed in Figure 5.13(a) for the constant spectrum excitation, although the magnitudes of the VPA are considerably different due to differences in the excitation. The responses consistently exhibit peak VPA value near the operating frequency of the tool. Furthermore, the VPA values in Figure 5.14 are considerably

smaller in the low frequency region compared with those observed under constant acceleration spectrum. This is attributed to low intensity of tool's vibration in the low frequency region, as seen in the Figure 5.2. The overall VPAs in the substructures and the corresponding percentages relative to the total VPA are summarized in Table 5.5.
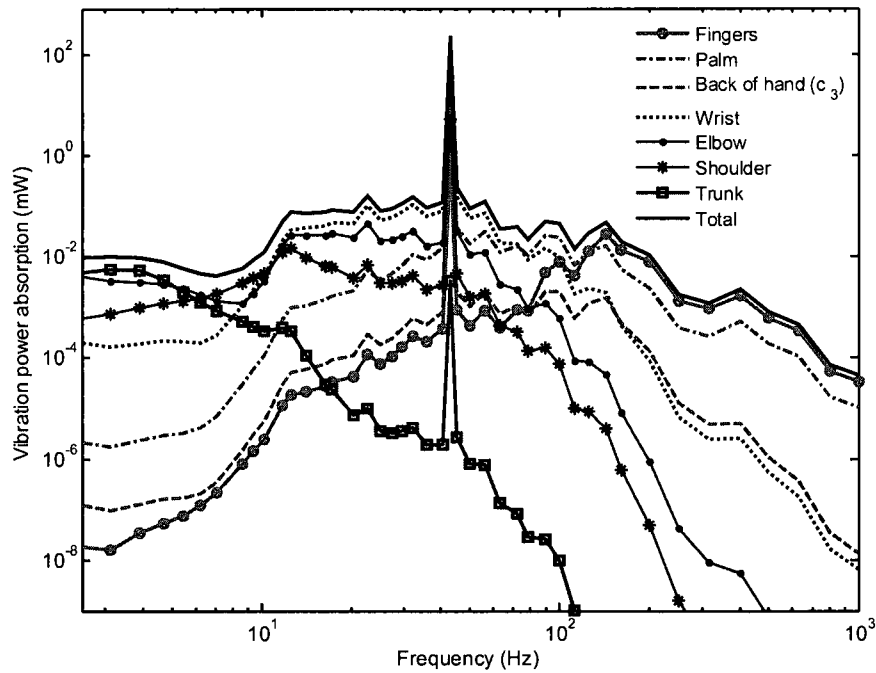
Figure 5.14: VPA distribution due to vibration from chipping hammer (78 N push force and 2600 rpm speed, a_{hw} = 8.84 m/s^2).

Table 5.5: Overall VPA in the 2.5 – 1000 Hz region due to vibration from chipping hammer (78 N push force and 2600 rpm speed, a_{hw} = 8.84 m/s^2)

Location	Overall Power (mW)	Percentage of power
Fingers	79.56	5.43
Palm	307.37	20.99
Hand back (c_3)	20.09	1.37
Wrist	853.90	58.31
Elbow	177.88	12.15
Shoulder	25.65	1.75
Trunk	0.04	0.00
P_{total}	1464.48	

Similar to the results presented in Table 5.4, the results show that greater power is absorbed in the arms' components than in the components of the hand (fingers, palm and c_3). The wrist substructure tends to absorb the highest proportion of the total power (58 %) . It is expected that the overall VPA of the hand substructures (fingers, palm and hand back) should be greater than those of other substructures since it is generally believed that vibration white finger syndrome (VWF) is the most severe and common form the hand-arm vibration syndrome (HAVS) disorders. However, the overall VPAs due to both the constant PSD acceleration and chipping hammer vibration have shown that greater power is absorbed in the arms than the hand. It may be speculated that the obstruction of blood flow in the hand due to high localized contact pressure may be a contributing factor to the development of VWF. Furthermore, the results raise question about the rationale behind the use of the frequency-weightings defined in ISO 5349-1 [31] for assessment of VWF. The weighting has maximum weight around 12.5 Hz, while several studies have shown that high frequency (above 100 Hz) vibration are confined to the hand, while low frequency (below 25 Hz) vibration are transmitted to the upper-arm and causes musculoskeletal disorder.

The VPA distributions of the bent-arm hand-arm model corresponding to different operating conditions of the percussion chipping hammer are compared with the VPA corresponding to a constant acceleration spectrum excitation in Figure 5.15. The acceleration spectra of the chipping hammer have been presented in Figure 5.2. The overall VPA of the hand-arm substructures in the 2.5 – 1000 Hz frequency range and the overall un-weighted and frequency-weighted rms values of the excitations are summarized in Table 5.6. Similar to the results in Figure 5.2, the results in Figure 5.15
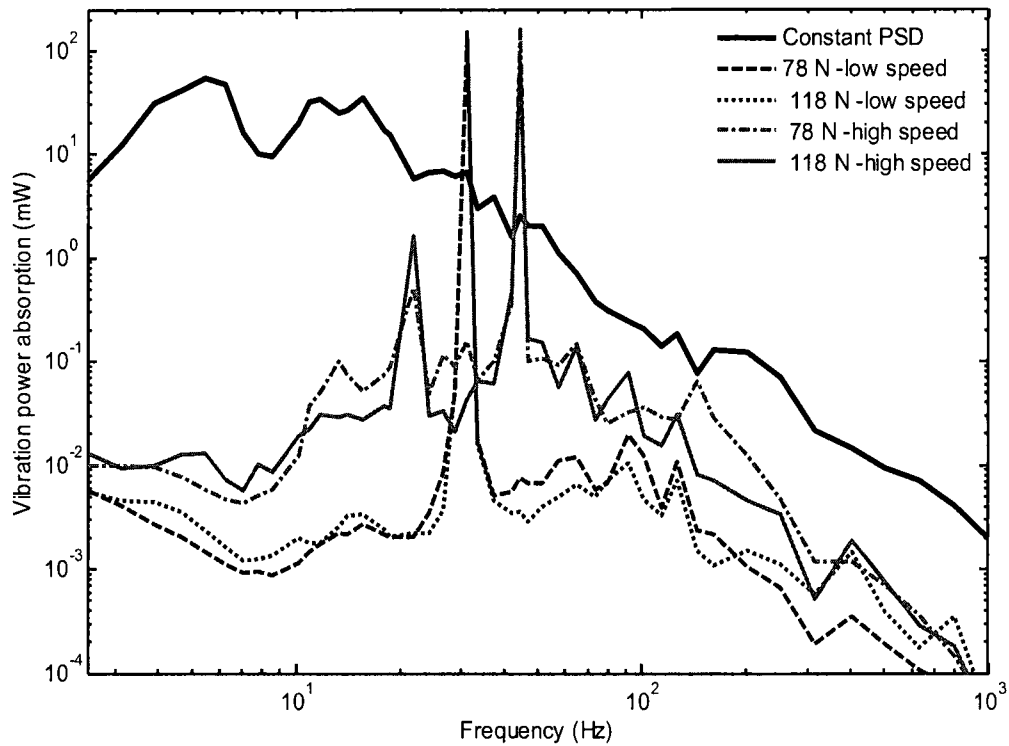
Figure 5.15: Comparison of total VPA distributions due to the chipping hammer vibration under different operating conditions.

Table 5.6: Overall VPA in the 2.5 – 1000 Hz region due to vibration from percussion tool under different push forces and operating speeds.

Location	Overall VPA (mW)				
	Constant spectrum 50 N push	Low speed (30.50 Hz)		High speed (43.75 Hz)	
		78 N push	118 N push	78 N push	118 N push
Fingers	22.06	31.21	27.02	79.56	88.52
Palm	43.06	61.58	40.24	307.37	168.30
c_3	2.55	4.61	2.95	20.09	11.97
Wrist	301.83	184.27	135.03	853.90	390.71
Elbow	228.57	52.79	39.33	177.88	81.54
Shoulder	117.06	7.10	5.29	25.65	11.78
Trunk	83.42	0.02	0.01	0.04	0.04
P_{total}	798.56	341.56	249.87	1464.48	752.86
Excitation magnitude					
a_{hw} (m/s^2)	5.25	4.55	3.80	8.84	6.53
a_{rms} (m/s^2)	31.95	23.49	21.27	41.33	37.69

229

and Table 5.6 show that the VPA is more strongly dependent on the operating speed of the power tool than the applied push force. Figure 5.15 further shows that an increase in the operating speed of the tool yields higher total VPA, while the VPA spectra exhibit a conspicuous peak in the vicinity of the operating speed. Kihlberg [77] has also reported that the maximum absorbed power occurs around the operating frequency of the power tools. The figure also reveal that the VPA corresponding to low speed (30.5 Hz) tends to slightly increase with an increase in the push force below 20 Hz, while an increase in the push force did not show a discernable trend in the VPA distributions corresponding to high tool speed (43.75 Hz). Table 5.6, however, shows that an increase in the push force decreased the overall VPA, while an increase in the tool speed increased both the overall VPA and acceleration rms values.

It should be noted that Figures 5.8 to 5.10 showing the transmissibility responses of the hand-arm system subject to tool vibration and constant acceleration spectra do not show the dominant frequency of the excitation. The characteristic frequencies in transmissibility responses correspond to hand-arm resonant frequencies. The VPA of the hand-arm system due to constant PSD excitation show characteristic frequencies believed to be the resonant frequencies of the hand-arm system, while the VPA distributions due to hand-tool vibration show prominent peak near the tool operating frequency, in addition to resonant frequencies of the hand-arm system. This suggests the strong dependence of VPA on the nature of excitation, unlike the DPMI and transmissibility responses. Furthermore, the VPA of the hand-arm due to constant spectrum excitation is concentrated in the forearm, upper-arm and the trunk substructures. While that due to the chipping hammer is concentrated near the wrist and the palm of the hand for high

operating speed of the tool, and near the wrist and elbow for the low tool speed, as seen in Table 5.6.

5.5.2 VPA due to vibration of different power tools

The total and distributed VPA of the hand-arm substructures would differ considerably for different tools due to wide variations in their vibration spectra. The vibration spectra of different hand-held power tools (impact wrench, zip gun, sander, die grinder and air rachet) that were measured during field operations by IRSST [137] are applied to the bent-arm model to study the VPA of different substructures of the hand-arm system coupled with different power tools. Although the exact operating conditions of the tools are not reported, the overall frequency-weighted rms acceleration and the operating speeds could be estimated from the reported vibration spectra of the tools. Table 5.7 summarizes the estimated operating frequencies, un-weighted and frequency-weighted rms acceleration and the total VPA of different segments of the hand-arm system model.

The rms acceleration spectra of the tools are presented in Figure 5.16(a), which varied greatly in magnitudes and spectral components. Unlike the acceleration spectra of the chipping hammer (Figure 5.2), which revealed relatively low acceleration magnitudes $(0.004 - 0.03 \text{ m/s}^2)$ in the 2.5 – 10 Hz frequency range, the tools' spectra in Figure 5.16(a) exhibit relatively higher values $(0.1 - 1 \text{ m/s}^2)$ in the same frequency range. The observed differences in the hand-held power tools acceleration spectra at low frequencies compared with those presented in Figure 5.1, despite the use of mechanical filter, may be attributed to the very high measurement range (5000 g) of the accelerometer used. The differences may also be partly due to the design of the tools, mode of vibration
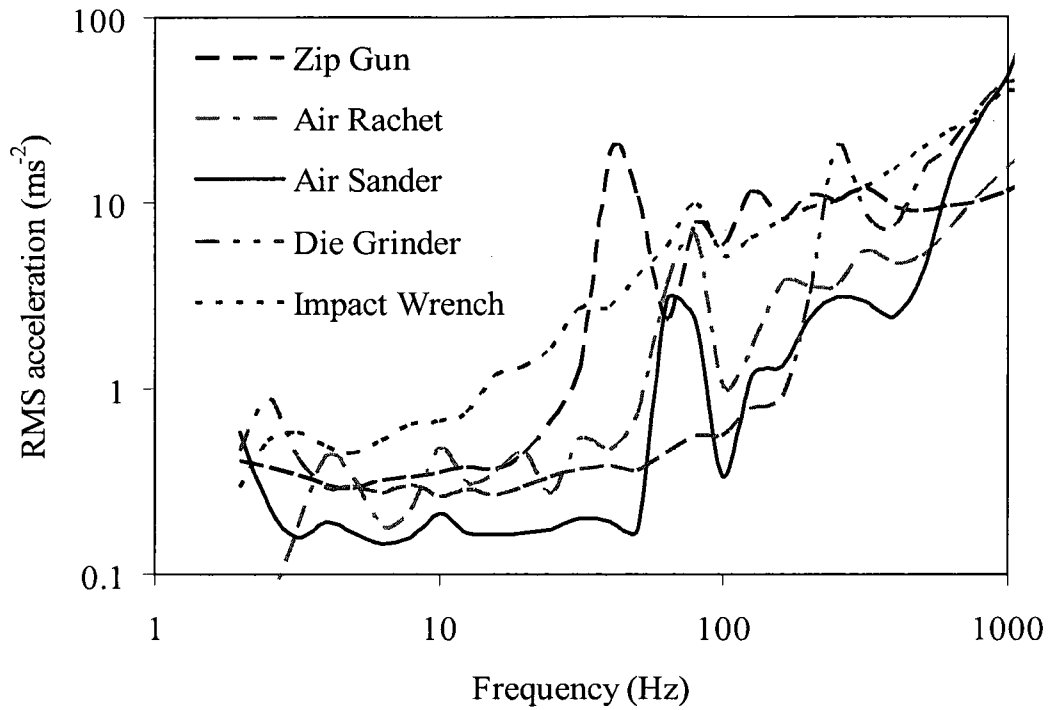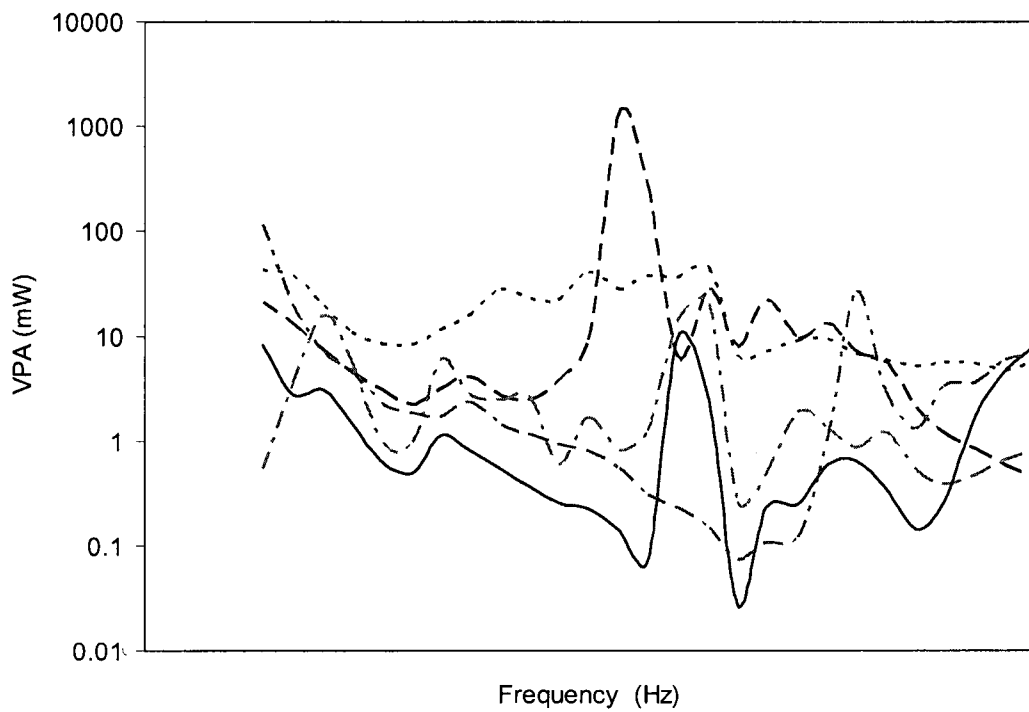
Figure 5.16: Comparison of responses of different power tools: (a) handle rms
acceleration spectrum; (b) overall VPA distribution.

Table 5.7: Overall VPA of substructures of the hand-arm system in the 2.5 – 1000 Hz
frequency region due to vibration from different hand-held power tools

Location	VPA (mW)				
	Impact Wrench	Zip Gun	Sander	Die Grinder	Air Rachet
Fingers	49.83	48.71	10.21	35.54	8.37
Palm	76.58	262.05	7.62	11.14	22.24
c_3	4.59	15.10	0.31	0.25	1.39
Wrist	184.08	1035.13	8.16	9.00	33.65
Elbow	116.24	233.98	24.28	79.60	21.86
Shoulder	35.05	36.97	4.89	15.70	7.79
Trunk	73.89	8.93	25.69	93.13	17.89
P_{total}	540.27	1640.88	81.16	244.34	113.20
Excitation magnitude					
a_{hw} (m/s^2)	4.71	8.68	1.31	1.85	2.19
a_{rms} (m/s^2)	59.42	39.91	47.71	55.64	22.71
Operating Frequency (Hz)	43.75	78.13	68.16	264.80	72.16

generation, and operating conditions. While the majority of the acceleration spectra of

hand-held power tools reported in the literature are similar to those in Figure 5.2, a few

studies have reported tool spectra with high values in the low frequency region. For

examples, the reported spectrum of a road breaker revealed very high acceleration PSD of

3 (m/s^2)^2/Hz at 10 Hz [88], and a rock drill was reported to have 2 m/s^2 rms acceleration

at 10 Hz [133].

Figure 5.16(b) shows that the VPA generally decreases with increase in frequency

for all tools. The observed trends in the VPA distributions are similar to those obtained

under a constant acceleration spectrum excitation, with the exception of the presence of

the dominant tool operating frequencies. The overall frequency-weighted rms

acceleration and the total VPA of the zip gun are the highest (Table 5.7). The air rachet

with a_{hw} of 2.19 m/s^2 (a_{rms} = 22.71 m/s^2) yields an overall VPA of 0.113 Watts, while the die grinder with a lower a_{hw} of 1.85 m/s^2 (a_{rms} = 55.64 m/s^2) yields a relatively higher VPA (0.224 Watts). The lower a_{hw} and the higher VPA of the die grinder may be due to the high operating frequency (about 265 Hz) since the frequency weighting defined in ISO 5349-1 [31] exhibits the highest weight near 12.5 Hz and rapidly attenuates vibration magnitude at higher frequencies. The weighting thus under-estimates the overall weighted rms acceleration of tools with high operating frequency, as seen in the a_{hw} of the die grinder. Although it has been reported that VPA is approximately proportional to the square of a_{hw} [84], the observed results in the VPA, a_{hw} and a_{rms} for the die grinder and air rachet suggest VPA is also related to a_{rms}.

5.5.3 Relationship between VPA and acceleration magnitude

It has been reported that the overall VPA is approximately proportional to the square of the overall frequency-weighted rms acceleration [84, 133, 135] and that it is excitation specific [133]. Attempts are made to verify this assertion by finding a relationship between the overall VPA and the overall frequency-weighted (a_{hw}) and un-weighted (a_{rms}) rms accelerations of the chipping hammer and different tools, as illustrated in Figure 5.17.

The results presented in Figure 5.17(a) show that the overall VPA is indeed approximately proportional to the square of a_{hw} ($VPA = 0.014 a_{hw}^{2.12}$) since the correlation coefficient is approximately unity, the correlation coefficient is about 0.94 with a_{rms} ($VPA = 0.0002 a_{rms}^{2.34}$) when un-weighted rms accelerations were used for the chipping hammer. Figure 5.17(b) shows the relationship between VPA and the rms acceleration of
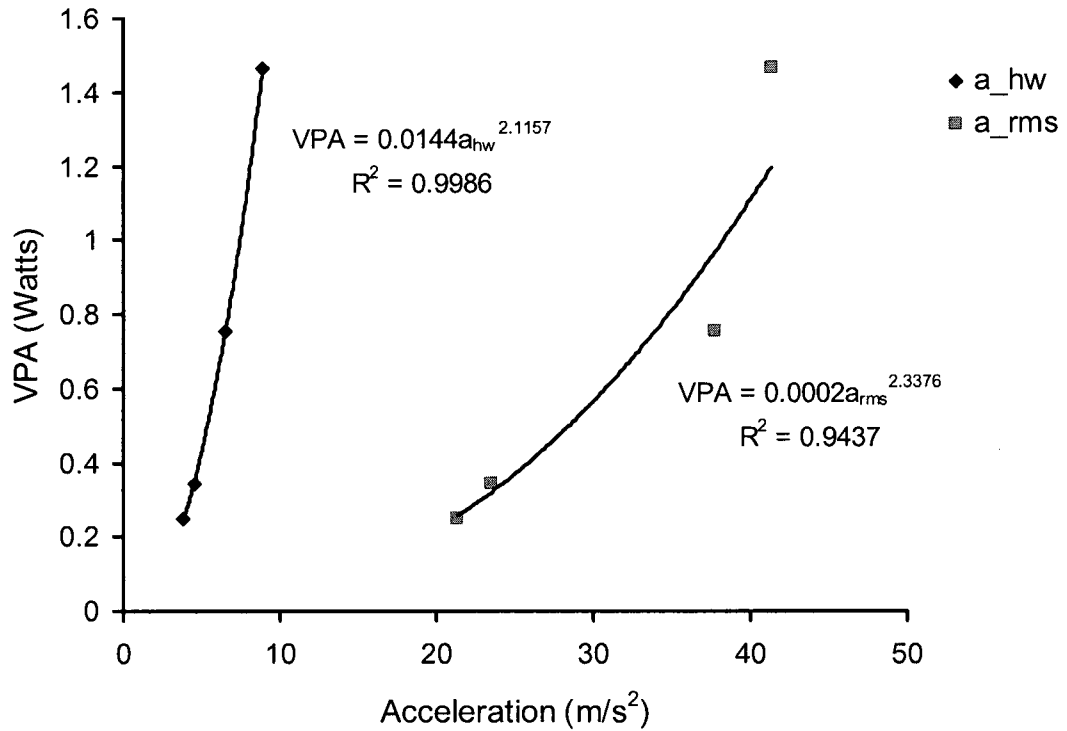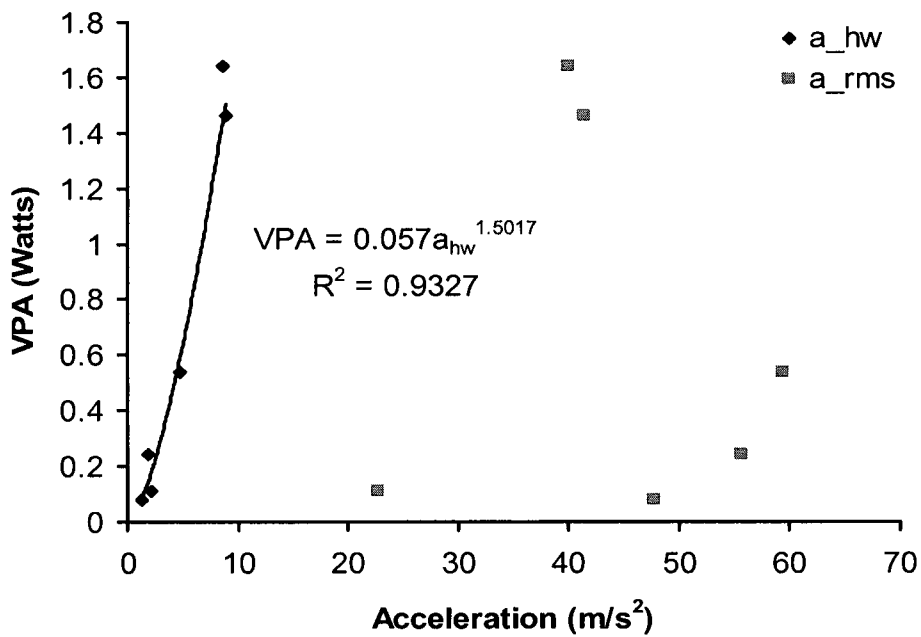
Figure 5.17: Relationship between overall VPA and rms acceleration in the 2.5 – 1000 Hz frequency range for: (a) chipping hammer; (b) different hand-held power tools.

different tools (impact wrench, zip gun, sander, die grinder, air rachet and the chipping hammer). While there is a relationship between the VPA and frequency-weighted rms acceleration ($VPA = 0.057a_{hw}^{1.50}$) with correlation coefficient around 0.93, no relationship could be established between the VPA and the unweighted rms acceleration, as seen in Figure 5.17(b). The results suggest that the relationship between the total VPA and rms acceleration could be dependent on the tool type, tool size, nature of the task, nature of tool's vibration generation and hand forces. While the current ISO 5349-1 [31] frequency-weighting may be considered appropriate for low frequency power tools, it grossly underestimates the weighted rms acceleration of tools with high operating frequency, as seen in Table 5.7. Alternatively, two different frequency-weightings may be defined for low and high frequency tools for assessing musculoskeletal and vibration induced white finger disorders, respectively. It was also shown in [134] that the total VPA is highly correlated with the ISO frequency-weighted rms acceleration for different tools.

5.5.4 Comparisons of the total VPA with those in the reported studies

The segmental and total VPA of the chipping hammer with overall frequency-weighted rms acceleration of 8.84 m/s^2 are compared with those of a grinder with a carborundum wheel having an overall frequency-weighted rms acceleration of 13.62 m/s^2, reported in [133]. It is recognized that the VPA strongly depends on the acceleration magnitudes and tool operating frequency. The comparisons are thus discussed in light of differences in frequency-weighted acceleration of the tools. It should also be noted that the localized VPA is also dependent on the type of hand-arm model and model parameters in addition to the nature of excitation. The hand-arm model that is

236

developed in this study is a biomechanical model, which considers anatomical structure of the human hand-arm system and whose parameters were derived from both the DPMI and the transmissibility responses. On the other hand, the model developed in [133] is a lumped-mass model whose parameters were derived from the DPMI response alone. In order to minimize the sources of possible differences in the two datasets, the VPA obtained from the bent-arm model parameters that were derived from DPMI response alone are calculated and summarized in Table 5.8 for the purpose of comparison. The substructure names in the parenthesis are for the hand-arm model developed in the present study.

Table 5.8 shows that the overall VPA of the hand-arm substructures for the two datasets are different except for the shoulder substructure. Furthermore, the results in the present study show that greater power is absorbed in the wrist, while the reported study suggests that most of the power is absorbed in the palm-wrist substructure. However, if the VPAs of the palm and wrist in the present study are added together, the results of the two studies become comparable. Different studies reporting overall VPA have employed different excitations, hand forces, ranges of vibration excitation and method of analysis, as seen in Table 5.9.

The VPA reported by these studies thus differ considerably. The reported results would suggest that the VPA does not depend only on the excitation type and magnitude but also on the type of the hand-held power tool involved. For example, two different tools, an impact hammer and a grinder, with the same overall frequency-weighted acceleration of about 8.8 m/s^2 yield overall VPA of 4.1 and 2.5 Watts, respectively, in a similar frequency range and with similar hand forces and posture [77]. Similarly, a

Table 5.8: Comparisons of total VPA of the chipping hammer in the 10 – 1000 Hz range with that of grinder with a carborundum wheel [133].

Location	Chipping hammer VPA (W)	Chipping hammer Perce-ntage	Grinder [133] VPA (W)	Grinder [133] Perce-ntage
Fingers	0.084	4.20	0.53	14.32
Palm and wrist (Palm)	0.426	21.44	2.06	55.68
Hand back and metacarpo-phalangeal joints (c_3)	0.115	5.82	0.50	13.51
(Wrist)	0.993	49.93	-	-
Forearm and upper arm (Elbow)	0.351	17.67	0.60	16.22
Shoulder, neck and head (shoulder)	0.019	0.95	0.01	0.27
Trunk	0.000	0.00	-	-
P_{total}	1.988	-	3.70	-
Excitation values				
$a_{h,w}$ (m/s^2)	8.84	-	13.62	-
a_{rms} (m/s^2)	41.33	-	-	-

straight grinder and a hammer yield the same total VPA but different weighted rms acceleration values [138]. The overall VPA of the tools obtained in the present study are lower than those reported with comparable weighted rms acceleration values. This may be due to differences in the operating conditions and design of the tools involved. The VPA values due to excitation with constant spectrum reported in [84] are comparable with those obtained in the present study, as shown in Table 5.9. The VPA obtained in the present study under a constant spectrum acceleration of 4.99 m/s^2 from an electro-dynamic exciter yields a VPA of 0.56 W in the 10 – 1000 Hz frequency range, while 5.0 m/s^2 and 0.46 W in the 8 – 1000 Hz one-third octave frequency region were reported in [84]. This further supports the developed hand-arm models, although further efforts are desired to explore a relation between the VPA and the vibration of different power tools.

Table 5.9: Comparison of overall VPA of the human hand-arm system reported by different investigators

Author	Type	Excitation (m/s²)		Power		Frequency range (Hz)	Hand forces (N)		Posture
		a_{rms}	a_{hw}	(Watts)	Method		Grip	Push	
Present study	Broad-band vibration	31.85	4.99	0.59	$(\mathrm{Re}[DPMI])|v|^2$ and $\sum c_i|\Delta v_i|^2$ of hand-arm model	10 - 1000	30	50	90° elbow angle
	Chipping hammer	41.33	8.84	1.46	$\sum c_i|\Delta v_i|^2$ of hand-arm model		-	78	90° elbow and 30° abduction angles
	Zip gun	39.90	8.67	1.62			-	-	-
	Impact wrench	59.41	4.62	0.39			-	-	-
Aldien et al. [84]	Broad-band vibration	-	5.00	0.46	$(\mathrm{Re}[DPMI])|v|^2$	8 – 1000 ⅓ octave	30	50	90° elbow angle
		-	2.50	0.12					
Dong et al. [133]	Rock drill	-	22.44	12.24	$\sum c_i|\Delta v_i|^2$ of hand-arm model	10 - 1000	30	45	-
	Grinder	-	13.62	3.70					
	Sand rammer	-	22.62	14.77					
Kilberge [77]	Impact hammer	-	8.80	4.10	$(\mathrm{Re}[DPMI])|v|^2$	10– 1000	40	50	110° elbow angle
	Grinder	-	8.80	2.50					
Burstrom et al. [138]	Angle grinder	168.8	5.20	3.10	$\mathrm{Re}[G_{Fv}(j\omega)]$	6 – 1000 ⅓ octave	-	-	-
	Straight grinder	241.4	4.70	6.60					
	Hammer	168.1	12.00	6.60					

239

5.6 Summary

The transmissibility responses of the hand-arm system, while operating a chipping hammer were studied under different push forces and operating speeds. The excitation with a constant power spectral density (PSD) from an electro-dynamic shaker and the vibration of different hand-held power tools were applied to the biomechanical hand-arm models to determine the vibration power absorption (VPA) distributions in different substructures of the human hand-arm system. The results show that the trends in the transmissibility responses due to vibration from the chipping hammer are similar to those due to excitation with a constant PSD. The VPA distributions revealed that greater power is absorbed in the arms at low frequencies than in the hand (fingers, palm and the back of the hand), while the VPA of fingers is greater above 100 Hz although its value is small compared to the VPA of the arms in the low frequency region. The VPA distribution of the hand-arm system depends on the type of excitation. The total VPA distribution due to a constant PSD excitation slightly increased in the low frequency region with increase in the frequency, then rapidly decreased with increase in frequency in a manner similar to the trend observed in the transmissibility response magnitudes.

The trends in the VPA distribution of the majority of the hand-held power tools were similar to those observed under a constant PSD acceleration except for the chipping hammer, which showed a relatively constant VPA in the low frequency region before decreasing with increase in the frequency. Unlike the VPA distribution due to a constant PSD excitation, the DPMI and transmissibility responses, in which there is absence of excitation frequency, the operating frequencies of the power tools were prominent in the VPA distributions based on the power tool excitations. The overall VPA in the 2.5 – 1000

Hz frequency range showed that smaller amount of power was generally absorbed in the hand (fingers, palm and hand back) compared with the wrist and the elbow. An increase in the operating speed of the chipping hammer increased the overall VPA and the overall frequency-weighted rms acceleration (a_{hw}) of the tool vibration, while an increase in the push force decreased both a_{hw} and overall VPA. The relationships between the VPA and the rms accelerations for the chipping hammer were obtained as $VPA = 0.0144a_{hw}^{2.1}$ and $VPA = 0.0002a_{rms}^{2.34}$, respectively, with correlation coefficients of nearly 1.00 for the frequency-weighted acceleration (a_{hw}), and 0.94 for the un-weighted acceleration (a_{rms}). The relationship for different power tools was $VPA = 0.057a_{hw}^{1.50}$ with correlation coefficient around 0.93 for the frequency-weighted acceleration, while no relationship could be established between the VPA and un-weighted rms acceleration.

CHAPTER 6

CONCLUSIONS AND RECOMMENDATIONS

6.1 Major Highlights and Contributions of the Research Work

The overall contribution of this research dissertation was the development of biomechanical models of the human hand-arm system based on measured impedance and localized transmissibility responses, anatomical structure, anthropometric parameters and characteristic frequencies. The models were used to estimate absorbed power in different segments of the hand-arm system for injury risk assessment. The specific contributions can be summarized as follows:

- Identification of sources of discrepancies in the reported human hand-arm DPMI response at frequencies above 500 Hz;

- Relationships between resonant frequencies of the human hand-arm model (eigen-analysis) and the characteristic frequencies observed from measured DPMI and transmissibility magnitudes;

- Simultaneous characterization of DPMI and localized transmissibility responses at the wrist, elbow (on both forearm and upper-arm sides) and the shoulder of the human hand-arm system under different hand forces, postures and excitation levels;

- Biomechanical modeling of the hand-arm in the bent-arm and extended arm postures on the basis of anthropometry and anatomical structure of the hand-arm system, measured DPMI and localized transmissibility responses, and resonant frequencies of the hand-arm system;

- Identification of model parameters for different combinations of the hand force;

- Evaluation of localized vibration power absorption of different components of the human hand-arm system subjected to constant spectrum excitation and vibration from hand-held power tools for potential injury risk assessments.

6.2 Major Conclusions

The following major conclusions were drawn form the dissertation research:

- The discrepancies in the reported impedance responses above 500 Hz were found to be attributable to acceleration measurement location, handle dynamics (handle resonant frequency and flexural deformation) and ineffectiveness of handle inertia correction technique at high frequencies. It is concluded that dynamic responses at the hand-handle interface must be measured in the proximity of the hand, and alternate inertial correction methods must be explored.

- An accurate measurement of the impedance (error ≤ 5 %) of the hand-arm system up to 1000 Hz would require a handle design with natural frequency in the order of 5400 Hz and 2600 Hz, for measurements based upon the base and handle accelerations, respectively.

- The DPMI seems to characterize the dynamic response of the entire hand-arm system with emphasis around the driving-point, while the transmissibility responses emphasize the dynamic responses of the tissues/muscles and joints of the human hand-arm system.

- The peaks in the vibration transmissibility response magnitudes represent resonant frequencies of the two main components of the human hand-arm system, namely the

tissues/muscles and the bones/structure, the resonance frequencies of the tissues/muscles, however, were more prominent.

- The peaks and valleys in the DPMI response magnitude correspond to the resonant frequencies of the tissues/muscles and bone/structure of the human hand-arm system, respectively.

- The grip forces mostly affects the properties of the tissues/muscles of the hand and forearm (flexor and extensor muscles), while the push force affects the stiffness of the entire human hand-arm system.

- The influence of an increase in excitation magnitude on DPMI response is negligible, while it marginally increased transmissibility response magnitudes, particularly around the prominent peaks.

- The influence of the hand-arm posture is most significant on the DPMI response below 100 Hz, while it is most significant below 25 Hz on the transmissibility responses.

- The human hand-arm system in the extended arm posture amplifies vibration transmitted to the upper-arm and the body below 25 Hz but attenuates vibration to the upper-arm more effectively than the bent-arm posture above 25 Hz.

- The results suggest the need for two frequency-weightings for the assessment of: (i) vibration-induced white finger (VWF) since high-frequency (above 100 Hz) vibrations are confined to the hand; and (ii) the musculoskeletal disorder risks, since the low-frequency (below 25 Hz) vibrations are transmitted to the upper-arm and whole-body. The current ISO 5349-1 (2001) frequency-weighting, commonly used for assessment of VWF, has the highest weighting factor near 12.5 Hz.

- The most prominent resonant frequencies at the wrist occurred around 28.9 and 56.3 Hz, while the prominent resonances at the elbow and shoulder were 12.5 and 25.0 Hz, and 12.5 and 5.5 Hz, respectively, for the bent-arm posture. The corresponding values for the extended arm posture were 12.5 Hz and 110.9 Hz at the wrist, 8.6 and 12.5 Hz at the elbow, and 7.0 and 12.5 Hz at the shoulder.

- A hand-arm model derived on the basis of either the impedance or transmissibility response cannot adequately characterize the entire dynamics of the human hand-arm system. A model based on both the impedance and transmissibility responses would be more reliable.

- The vibration power absorption (VPA) in the forearm and upper-arm is greater than that of the hand below 100 Hz for all types of excitations, while the power absorbed in the fingers and palm of the hand is larger at higher frequencies.

- An increase in the operating speed of the percussion chipping hammer increased the overall VPA value and the overall un-weighted and frequency-weighted rms acceleration of the percussion chipping hammer, while an increase in the push force decreased both the VPA and acceleration rms values.

- A relationship between the overall VPA and the overall frequency-weighted rms acceleration of the percussion chipping hammer was established as $VPA = 0.0144a_{hw}^{2.12}$ Watts, while the relationship for other hand-held power tools was attained as $VPA = 0.057a_{hw}^{1.5}$ Watts.

6.3 Recommendations for Future Work

The present study provides comprehensive information about biodynamic responses, localized vibration transmissibility, localized and total vibration power

absorption (VPA) distributions and biomechanical models of the human hand-arm system in the bent-arm and extended arm postures. While the transmissibility response magnitudes and the VPA distributions are very small above 500 Hz and not significantly influenced by the instrumented handle dynamics, the driving-point mechanical impedance (DPMI) is highly influenced by the dynamics of the handle above 500 Hz. Consequently, the DPMI responses in this study are limited to 500 Hz in order to minimize the influence of handle dynamics on the DPMI response. The dynamic characteristics of the human hand-arm at higher frequencies are important and necessary because some power tools, particularly the pneumatic percussion tools, can operate at frequency above 500 Hz. The reported DPMI responses above 500 Hz may not be reliable due to the effect of handle dynamics. Furthermore, vibration-induced white finger syndrome is a high-frequency phenomena.

Consequently, the design of a better simulated handle with primary resonance frequency around or above 2000 Hz is recommended in order to characterize DPMI of the human hand-arm system in the high frequency range.

The hand-arm models proposed in this dissertation could not characterize the y_h-axis transmissibility responses due to lack of consideration of y_h-axis compliance and linearization of the formulation. Furthermore, the mass of the tissues/muscles and bones of the forearm and upper-arm were combined. Biomechanical models in which the masses of the tissues/muscles and bones of the forearm and upper-arm are separated are suggested for future work in order to characterize both the z_h- and y_h-axis transmissibility responses.

Furthermore, the following studies would enhance better understanding of the biodynamic responses of the human hand-arm system to vibration and assessment of injury:

- Three dimensional models of the hand-arm system;

- Multibody dynamic models of the hand-arm system;

- Finite element models of the hand-arm system with active tissues/muscles;

- Measurement of grip force on power tools using pressure sensors;

- More thorough study of VPA distribution of different power tools, and the relationship between the VPA and un-weighted acceleration magnitudes of different types of power tools;

- Identification of separate frequency-weights for assessment of vibration-induced white finger and musculoskeletal disorders.

REFERENCES

1. Gemme G., Pyykko I., Taylor W., and Pelmear P. L., The stockholm workshop scale for the classification of cold-induced Raynaud's phenomenon in the hand-arm vibration syndrome, *Scandinavian J. of Work Environ Health* **13** (1987), pp. 275 – 278.

2. Brammer A. J., Taylor W. and Lundborg G., Sensorineural stages of the hand-arm syndrome, *Scandinavian J. of Work Environ Health* **13** (1987), pp. 279 – 283.

3. Taylor W, Biological effects of the hand-arm vibration syndrome: Historical perspectives and current research, *Journal of Acoustics Society of America* **83** (1988), pp. 415-422.

4. Taylor W., Wasserman D., Behrens V., Reynolds D. and Samueloff S., The effect of the air hammer on the hands of stonecutters. The limestones quarries of Bedford, Indiana revisited, *Br J Ind Med* **41** (1984), pp. 289-295.

5. Brammer A. J., Olssen N., Piercy J. E. and Toole F. E., Noise and vibration of chain saws, *Journal of Acoustics Society of America* **51** (1972), pp. 142.143.

6. Dupuis H. and Gemne G., Hand-arm vibration and the central nervous system, *Int Arch Occup Environ Health* **55** (1985), pp. 185-189.

7. Pyykko I., Korhonen O., Farkkila M., Starck J. Aatola S. and Jantti V., Vibration syndrome among Finnish forest workers, a follow-up from 1972 to 1983, *Scandinavian J. of Work Environ Health* **12** (1986), pp. 307 – 312.

8. Starck J., High impulsive acceleration levels in hand-held vibratory tools, *Scandinavian J. of Work Environ Health* **10** (1984), pp. 171 – 178.

9. Bovenzi M., Petronio L. and DiMarino F., Epidemiological survey of shipyard workers exposed to hand-arm vibration, *Int Arch Occup Environ Health* **46** (1980), pp. 251.266.

10. Brammer A. J. Dose-response relationships for hand-transmitted vibration, *Scandinavian J. of Work Environ Health* **12** (1986), pp. 284 – 288.

11. Hasan J., Biomedical aspects of low-frequency vibration. A selective review, *Work Environ Health* **6** (1970), pp. 19 – 45.

12. Nilsson T., Burstrom L. and Hagberg M., Risk assessment of vibration exposure and white finger among platters, *Int Arch Occup Environ Health* **61** (1989), pp. 473-481.

13. Partanen T. J., Kumlin T. and Karvonen M. J., Subjective symptoms connected with exposure of the upper limbs to vibration, *Work Environ Health* **7** (1970), 80-81.

14. Takeuchi T., Futatsuka M., Imanishi H. and Yamada S., Pathological changes observed in the finger biopsy of patients with vibration-induced white fingers, *Scandinavian J. of Work Environ Health* **12** (1986), pp. 280 – 283.

15. Cannon L. J., Bernacki E. J. and Walter S. D., Personal and occupational factors associated with carpal tunnel syndrome, *Journal of Occupational Medicine* **23** (1981), pp. 255 – 258.

16. Rothfleisch S. and Sherman D., Carpal tunnel syndrome: Biomechanical aspects of occupational occurrence and implications regarding surgical management, *Orthop Rev* **7** (1978), 107-109.

17. Farkkila M., Pyykko I., Korhonen O. and Starck J., Vibration-induced decrease in the muscle force in lumberjacks, *Europe J Applied Physiology* **43** (1980), pp. 1.9.

18. Okada A., Yamashita T., Nagano C., Ikeda T., Yachi A. and Shibati S., Studies on the diagnosis and pathogenesis of Raynaud's phenomena of occupational origin, *Br Ind Med* **28** (1971), pp. 353 – 357.

19. Gemne G. and Saraste H., Bone and joint pathology in workers using hand-held vibrating tools, *Scandinavian J. of Work Environ Health* **13** (1987), pp. 290 –300.

20. Bovenzi M., Fiorito A. and Volpe C., Bone and joint disorders in the upper extremities of chipping and grinding operators, *Int Arch Occup Environ Health* **59** (1987), pp. 189 - 198.

21. Malchaire J., Maldague B., Huberlant J. M. and Crouqet F., Bone and joint changes in the wrists and elbows and their association with hand and arm vibration exposure, *Ann Occup Hyg* 30 (1986), pp. 461 – 468.

22. Iwata H., Effects of rock drills on operators. Part 1: Vibration of rock drills and air temperature at pits, *Jap J Ind Health* **6** (1968), pp. 28 – 36.

23. Iwata H., Effects of rock drills on operators. Part 2: Survey and examination on Raynaud's phenomenon, *Jap J Ind Health* **6** (1968), pp. 37 – 47.

24. Kumlin T., Wiikeri M. and Sumari P., Radiological changes in carpal and metacarpal bones and phalanges caused by chain saw vibration, *Br J Ind Med* **30** (1973), pp. 71 – 73.

25. Laitinen J., Puranen J. and Vuorinen P., Vibration syndrome in lumbermen (working with chain saws), *J Occup Med* **16** (1974), pp. 552 -556.

26. NIOSH, Vibration syndrome in chipping and grinding workers, *J Occup Med* **26** (1984), pp. 765 – 788.

27. Friden J., Vibration damage to the hand: Clinical presentation, prognosis and length and severity of vibration required, *Journal of Hand Surgery* **26B** **(5)** (2001), pp. 471 – 474.

28. Hempstock T. I. and O'connor D. E., Evaluation of human exposure to hand-transmitted vibration, *Applied Acoustics* **8** (1975), pp. 87 – 99.

29. NIOSH, Criteria for a recommended standard: Occupational exposure to hand-arm vibration, *National Institute for Occupational Safety and Health* DHHS 1989, pp. 89 – 106.

30. Bovenzi M., Exposure-response relationship in the hand-arm vibration syndrome: an overview of current epidemiology research, *Int. Archive Occup Environ Health* **71** (1998), pp. 509 – 519.

31. INTERNATIONAL STANDARD ORGANIZATION, ISO/DIS 5349-1, Mechanical vibration – measurement and evaluation of human exposure to hand-transmitted vibration, 2001.

32. Miyashita K., Shiomi S., Itoh N. et al., Epidemiological study of vibration syndrome in response to total hand-tool operating time, *British Journal of Industrial Medicine* **40** (1983), pp. 92 – 98.

33. Brubaker R. L., Mackenzie C. J. G. and Hutton S. G., Vibration-induced white finger among selected underground rock drillers in British Columbia, *Scandinavian J. of Work Environ Health* **13** (1986), pp. 296 –300.

34. Engrostrom K. and Dandanell R., Exposure conditions and Raynaud's phenomenon among riveters in the aircraft industries, *Scandinavian J. of Work Environ Health* **12** (1986), pp. 293 –295.

35. Futatsuka M., Sakurai T. and Ariizumi M., Preliminary evaluation of dose-effect relationships for vibration induced white finger in Japan, *Int. Archive Occup Environ Health* **54** (1984), pp. 201 - 221.

36. Lundstrom R., Effects of local vibration transmitted from ultrasonic devices on vibrotactile perception in the hand of therapists, *Ergonomics* **28** (1985), pp. 793 – 803.

37. Broyde M, Donati P. and Bitsch J., Subjective assessment of the vibration discomfort produced by different hand held machines, *Journal of Low Frequency Noise and Vibration* **8** (1989), pp. 50 – 61.

38. Starck J. and Pyykko I., Impulsiveness of vibration as an additional factor in the hazards associated with hand-arm vibration, *Scandinavian J. of Work Environ Health* **12** (1986), pp. 323 –326.

39. Anderson J. S. and Boughtflower R. A. C., Measurement of energy dissipated in the hand and arm whilst using vibratory tools, *Applied Acoustics* **11** (1978), pp. 219 – 224.

40. Cundiff J. S., Energy dissipation in human hand-arm exposed to random vibration, *Journal of Acoust Soc Am* **59** (1976), pp. 212 – 214.

41. Lindstrom I. M., Vibration injury in rock drillers, chiselers, and grinders. Some views on the relationship between the quantity of energy absorbed and the risk of occurrence of vibration injury. In Wasserman D. E., Taylor W., Curry M. G. (Eds). *The International Occupational Hand-Arm Vibration Conference -1975*, US DHEW (NIOSH), Cincinnati, USA, NIOSH publ 77 – 170 (1977), pp. 77 – 83.

42. Stelling J., Hartung E., Dupuis H., Multi-axial hand-arm vibration simulation and biodynamic responses, *Proceedings of the 6th International Conference on Hand-Arm Vibration* 1993, pp. 483 – 490.

43. Thiede R., Miyashita K., Stelling J., Hartung E., Dupuis H., Subjective equal sensation under sing- or multi-axial vibration response, *Proceedings of the 6th International Conference on Hand-Arm Vibration* 1993, pp. 451 – 460.

44. Maeda S., Multi-axial hand-arm vibration testing and simulation at the national institute of industrial health, Kawasaki, Japan, *1st American Conference on Human Vibration* Morgantown, West Virginia, USA, June 2006, pp. 99 – 100.

45. Rakheja S., Rajalingham C. and Boileau P.-É., Analysis of hand-transmitted vibration of a hand-held percussive tool, *European Journal of Mech. & Env. Eng. M* **47**(3) (2002), pp. 141 – 156.

46. Naslund U., Design problems in the reduction of vibration in chain saws, in: Taylor W. (Ed.), *The vibration syndrome*, Academic Press, London 1974, pp. 61 – 70.

47. Miwa T., Studies on hand protectors for portable vibrating tools. Part 1: Measurements of the attenuation effect of porous elastic materials, *Japan J Ind Health* **2** (1964), pp. 95 – 105.

48. Hiratsukaa H., Reducing the physical strain of pneumatic tools, *Advances in Occupational Ergonomics and Safety* in: Kumar S. (ed.), IOS Press 1998, pp. 428 – 431.

49. Greenslade E. and Larsson T. J., Reducing vibration exposure from hand-held grinding, sanding and polishing power tools by improvement in equipment and industrial processes, *Safety Science* **25**(1.3) (1997), pp. 143 – 152.

50. Abrams C. F. and Suggs C. W., Chain saw vibration, isolation and transmission through the human arm, *Trans Am Soc Agr Eng* (1969), pp. 423 – 425.

51. Miwa T., Yonekawa Y., Nara A., Kanada K., Kaba K., Vibration isolators for portable vibrating tool. Part I: A grinder, *Industrial Health* **17** (1979), pp. 85 – 122.

52. Griffin M. J., *Handbook of human vibration*, Academic Press, London 1990.

53. Broch J. T. *Mechanical vibration and shock measurement*, K. Larsson & Sons, Denmark, 1984.

54. Abrams C. F. and Suggs C. W., Modeling the vibrational characteristics of the human hand by the driving point mechanical impedance method, *Purdue Noise Control Conference* Purdue University, West Lafayette, Indiana, USA 1971.

55. Suggs C. W. and Abrams C. F., Mechanical impedance techniques for evaluating the dynamic characteristics of biological materials, *J Agr Eng Res* **16** (1971), pp. 307 – 315.

56. Abrams C. F. and Suggs C. W., Development of a simulator for use of in the measurement of chain saw vibration, *Applied Ergonomics* **8** (1977), pp. 130 – 134.

57. Lundstrom R., Local vibrations - Mechanical impedance of the human hand's glabrous skin, *Journal of Biomechanics* **17(2)** (1984), pp. 137 – 144.

58. Wittman T. J. and Phillips N. S., Human body non-linearity and mechanical impedance analyses, *Journal of Biomechanics* **2** (1969), pp. 281 – 288.

59. Panzke K-J. and Balasus W., Time dependence and non-linearity of the impedance of the human hand-arm system while exposed to intense vibration, *Int Arch Occup Environ Health* **57** (1985), pp. 35 – 45.

60. Franke E. K., Mechanical impedance of the surface of the human body, *Journal of Applied Physiology* **3** (1951), pp. 582 – 590.

61. Farkkila M., Pyykko I., Korhonen O. and Starck J., Hand-grip forces during chain saw operation and vibration white finger in lumberjacks, *British Journal of Industrial Medicine* **36** (1979), pp. 336 – 341.

62. Hempstock T. I. and O'Connor D. E., Accuracy of measuring impedance in the hand-arm system, *Scandinavian J. of Work Environ Health* **12** (1986), pp. 355 – 358.

63. Hakansson B. and Carlsson P., Bias Errors in mechanical impedance data obtained with impedance heads, *Journal of Sound and Vibration* 113 (1987) pp. 173 – 183.

64. Dong R. G., Rakheja S., Schopper A. W., Han B. and Smutz W. P., Hand-transmitted vibration and biodynamic response of the human hand-arm: A critical review, *Critical Review in Biomedical Engineering* **29**(4) (2001), pp. 391 – 441.

65. Rakheja S., Wu J. Z., Dong R. G. and Schopper A. W., A comparison of biodynamic models of the human hand-arm for applications to hand-held power tools, *Journal of Sound and Vibration*, **249** (1) (2002), pp. 55 – 82.

66. Jahn R. and Hesse M., Applications of hand-arm models in the investigation of the interaction between man and machine, *Scandinavian J. of Work Environ Health* **12** (1986), pp. 343 – 346.

67. Aldien Y., Marcotte P., Rakheja S. and Boileau P.-É., Influence of hand–arm posture on biodynamic response of the hand–arm exposed to z_h-axis vibration, *International Journal of Industrial Ergonomics* **36** (2006), pp. 45 – 59.

68. R. Gurram, S. Rakheja and G. J. Gouw, Mechanical impedance of the human hand–arm system subject to sinusoidal and stochastic excitations, *International Journal of Industrial Ergonomics* **16** (1995), pp. 135 – 145.

69. Burstrom L., Measurement of the impedance of the hand and arm, *International Archive of Occupational Environmental Health* **62** (1990), pp. 431 – 439.

70. Hewitt S. M., Measurement of vibration energy absorption by the hand arm system, M.Sc. Thesis, University of Salford, 1994.

71. Mishoe J. W. and Suggs C. W., Hand-arm vibration Part I: Subjective response to single and multi-directional sinusoidal and non-sinusoidal excitation, *Journal of Sound and Vibration* **35** (1974), pp. 479 – 488.

72. Mishoe J. W. and Suggs C. W., Hand-arm vibration Part II: Vibrational responses of the Human Hand, *Journal of Sound and Vibration* **53**(4) (1977), pp. 545 – 558.

73. Burström L., The influence of biodynamic factors on the mechanical impedance of the hand and arm, *International Archives of Occupational Environmental Health* **69** (1997), pp. 437 – 446.

74. Hartung E., Dupuis H and Scheffer M., Effect of grip and push forces on the acute response of the hand-arm system under vibrating conditions, *International Archives of Occupational Environmental Health* **64** (1993), pp. 463 – 467.

75. Riedel S., Consideration of grip and push forces for the assessment of vibration exposure, 7th *International hand-Arm Vibration Conference*, Prague 1995.

76. Reynolds D. D., Basel R., Wasserman D. E. and Taylor W., A study of hand vibration on chipping and grinding operators. Part III: Power levels into the hands of operators of pneumatic tools used in chipping and grinding operations, *Journal of Sound and Vibration* **95**(4) (1984), pp. 515 – 524.

77. Kihlberg S., Biodynamic response of the hand–arm system to vibration from an impact hammer and a grinder, *International Journal of Industrial Ergonomics* **16** (1995), pp. 1–8.

78. Jandák Z., Driving-point mechanical impedance of the hand–arm system at exposure to stochastic vibration, *Proceedings of the 8th International Conference on Hand–arm Vibration*, Umea, Sweden, June 1998, pp. 369 – 375.

79. Reynolds D. D. and Falkenberg R. J., A study of hand vibration on chipping and grinding operators, Part I: four-degree-of-freedom lumped parameter model of the vibration response of the human hand, *Journal of Sound and Vibration* **95** (1984), pp. 499 – 514.

80. Lundström R. and Burström L., Mechanical impedance of the human hand–arm system, *International Journal of Industrial Ergonomics*, **3** (1989), pp. 235 – 242.

81. Cronjäger L., Hesse M., Hand–arm system response to stochastic excitation, *Proceedings of the 5th Conference on Hand–arm Vibration*, Kanzawa, Japan, 1990.

82. Marcotte P., Aldien Y., Boileau P.-É., Rakheja S., Boutin J., Effect of handle size and hand-handle contact force on the biodynamic response of the hand-arm system under z_h–axis vibration, *Journal of Sound and Vibration*, **283** (2005), pp. 1071 – 1091.

83. Hesse M, Die antwort des hand-arm-systems auf stochastiche erregung und ihre anwendung in scwingunsschutz, Ph.D. Thesis, Universitat Dortmund, 1989.

84. Aldien Y., Marcotte P., Rakheja S. and Boileau P.-É., Influence of hand forces and handle size on power absorption of the human hand-arm exposed to z_h-axis vibration, *Journal of Sound and Vibration* **290** (2006), pp. 1015 – 1039.

85. Bystrom B-O., Nilsson A. and Olsson E., Development of artificial hands for use in chain saw vibration measurement, *Journal of Sound and Vibration* **82** (1982), pp. 111 – 117.

86. INTERNATIONAL STANDARDS ORGANIZATION, ISO 10068, Mechanical vibration and shock - free mechanical impedance of the human hand-arm system at the driving point, 1998.

87. Dong R. G., Rakheja S., Mcdowel T. W, Welcome D. E., Wu J. Z., Warren C., Barklay J, Washington B., Schopper A. W., A method for assessing the effectiveness of anti-vibration gloves using biodynamic responses of the hand-arm system, *Journal of Sound and Vibration* **282** (2005), pp. 1101 – 1118.

88. Rakheja S., Dong R., Welcome D., Schopper A., Estimation of tool-specific isolation performance of antivibration gloves, *International Journal of Industrial Ergonomics* **30** (2002), pp. 71 – 87.

89. Goel V. K. and Kwan R., Role of gloves in reducing vibration: analysis for pneumatic chipping hammer, *Am Ind Hyg J* **48**(1) (1987), pp. 9 – 14.

90. Rens G., Dubrulle P. and Malchaire J., Efficiency of conventional gloves against vibration, *Ann Occup Hyg* **31**(2) (1987) pp. 249 – 254.

91. Dong R. G., Rakheja S., Smutz W. P., Schopper A. W., Caporali S., Dynamic characterization of the simulated tool handle and palm-adapter used for assessment of vibration performance of gloves, *Journal of Testing and Evaluation, American Society of Testing Materials* **31**(3) (2003), pp. 243 – 246.

92. Cherian T., Rakheja S., Bhat R. B., An analytical investigation of an energy flow divider to attenuate hand-transmitted vibration, *International Journal of Industrial Ergonomics* **17** (1996), pp. 455 – 467.

93. Reynolds D. D. and Angevine E. N., Hand-arm vibration. Part II: vibration transmission characteristics of the hand and arm, *Journal of Sound and Vibration*, **51** (1977), pp. 255 – 265.

94. Pyykko I., Farkkila M., Toivanen J., Korhonen O., Hyvarinen J., Transmission of vibration in the hand-arm system with special reference to changes in compression and acceleration, *Scandinavian J. of Work Environ Health* **2** (1976), pp. 87 – 95.

95. Aatola S., Transmission of vibration to the wrist and comparison of frequency response function estimators, *Journal of Sound and Vibration*, **131**(3) (1989), pp. 497 – 507.

96. Hanssson J. E., Attebrant-Eriksson M., Gemne G., Kihlberg S. and Kjellberg A., Vibration-transmission to and effects on the hand-arm system, *United Kingdom Informal Group Meeting on Human Response to Vibration* Shrivenham, 1987.

97. Kattel B. P. and Fernandez J. E., The effect of rivet gun on hand-arm vibration, *International Journal of Industrial Ergonomics* **23** (1999), pp. 595 – 608.

98. Sakakibara H., Kondo T., Miyao M., Yamada S., Nakagawa T., Kobayashi F., Ono Y., Transmission of hand-arm vibration to the head, *Scandinavian J. of Work Environ Health* **12** (1986), pp. 359 – 361.

99. Fritz Martin, An improved biomechanical model for simulating the strain of the hand-arm system under vibration stress, *Journal of Biomechanics* **24**(12) (1991), pp. 1165 – 1171.

100. Reynolds D. D. and Soedel W., Dynamic response of the hand-arm system to a sinusoidal input, *Journal of Sound and Vibration*, **21** (1972), pp. 339 – 353.

101. Reynolds, D. D., Hand-arm vibration: A review of 3 years research, In Wasserman D. E., Taylor W., Curry M. G. (Eds). *The International Occupational Hand-Arm Vibration Conference -1975*, US DHEW (NIOSH), Cincinnati, USA, NIOSH publ 77 – 170 (1977), pp. 99 – 128.

102. Diakoku M. and Ishikawa F., Mechanical impedance and vibration model of hand-arm system, *Proceedings of the 5th International Conference on Hand-Arm Vibration*, Kanazawa, Japan 1990.

103. Gurram R., Rakheja S., Boileau P.-E. and Gouw G. J., Development of a grip force dependent hand-arm vibration model, *Central European Journal of Public Health*, **40** (1996), pp. 65 – 68.

104. Rakheja S., Gurram R. and Gouw G. J., Development of linear and nonlinear HAV models using optimization and linearization techniques, *Journal of Biomechanics* **26** (1993), pp. 1253 – 1260.

105. Wood L. A., Suggs C. W. and Abrams C. F., Hand-arm vibration. Part III: A distributed parameter dynamic model of the human hand-arm system, *Journal of Sound and Vibration*, **57** (1978), pp. 157 - 169.

106. Potts R. O., Chrisman D. A. Jr. and Buras E. M. Jr., The dynamic mechanical properties of human skin *in vivo*, J Biomech **16**(6) (1983), pp. 365 – 372.

107. Chaffin D. B., Andersson G. B. J. and Martin B. J., *Occupational Biomechanics*, 3rd Edition, John Wiley & sons, Inc. Canada 1999.

108. Wirtz D. C., Schiffers T., Pandorf T., Radermacher K., Weichert D. and Forst R., Critical evaluation of known bone material properties to realize anisotropic FE simulation of the proximal femur, *Journal of Biomechanics* **33** (2000), pp. 1325 – 1330.

109. Maganaris C. N. and Paul J. P, In vivo human tendon mechanical properties, *Journal of Physiology* **521**(1) (1999), pp. 307 – 313.

110. Roberts S. G., Hutchinson T. M., Arnaud S. B., Kiratli B. J., Martin R. B. and Steele C. R., Noninvasive determination of bone mechanical properties using vibration response: A refined model and validation, *Journal of Biomechanics* **29**(1) (1996), pp. 91 – 98.

111. http://www-personal.une.edu.au/~pbrown3/skeleton.pdf

112. Griffin M. J., Evaluating the effectiveness of gloves in reducing hazards of hand-transmitted vibration, *Occupational and Environment Medicine* **55** (1998), pp. 340 – 348.

113. Wu X, Rakheja S. and Boileau P.E, Analysis of relationship between biodynamic response functions, *Journal of Sound and vibration* 226(3) (1999), pp. 595 - 606.

114. Wasserman D. E., Hudock S. D., Wasserman J. F., Mullinix L., Wurzelbacher S. J. and Siegfried K. V., Hand-arm vibration in a group of hand-operated grinding tools, *Human Factors and Ergonomics in Manufacturing* **12** (2) (2002), pp. 211 – 226.

115. Dandanell R. and Engstrom K, Vibration measurements and analysis of percussion tools such as riveting hammers and bucking bars, *Journal of the society of environmental engineers* Sept. 1986, pp. 21 – 25.

116. Reynolds D. D., Basel R., Wasserman D. E. and Taylor W., A study of hand vibration on chipping and grinding operators. Part I: Vibration acceleration levels measured on pneumatic tools used in chipping and grinding operations, *Journal of Sound and Vibration* **95**(4) (1984), pp. 479 – 497.

117. INTERNATIONAL STARNDARD ORGANIZATION, ISO 10819, Mechanical vibration and shock – hand-arm vibration – method for the measurement and evaluation of the vibration transmissibility of gloves at the palm of the hand, 1996.

118. AMERICAN NATIONAL STANDARDS INSTITUTE, ANSI S.3.34: Guide for the measurement and evaluation of human exposure to vibration transmitted to the hand, 1986.

119. AMERICAN CONFERENCE OF GOVERNMENT INDUSTRIAL HYGIENISTS, ACGIH-TLV: Threshold limit values for hand-arm vibration, 2001.

120. Batbitsky V. I., Hand-held percussion machine as discrete non-linear converter, *Journal of Sound and Vibration* **214**(1) (1998), pp. 165 – 182.

121. Golycheva E.V., Batbitsky V. I. and Veprik A. M., Dynamic correction of excitation in hand-held electro-pneumatic percussion machines, *Journal of Sound and Vibration* **259**(4) (2003), pp. 829 – 843.

122. Golycheva E.V., Batbitsky V. I. and Veprik A. M., Vibration protection for an operator of a hand-held percussion machine, *Journal of Sound and Vibration* **274**(4) (2004), pp. 351 – 367.

123. Boutin J., Marcotte P., Boileau P.-E. and Jasinski J., Design and validation of a mechanical system simulating hand-arm dynamic properties for use in a test set-up for evaluating the vibration emission values of chipping hammers, *4oth United Kingdom Conference on Human Response to Vibration* Liverpool, England, 13-15 September, 2005.

124. Hansson J. E. and Kihlberg S., A test rig for the measurement of vibration in hand-held power tools, *Applied Ergonomics* **14**(1) (1983), pp. 11 – 18.

125. Batako A.D., Batbitsky V. I. and Halliwell N. A., A self-excited system for percussion-rotary drilling, *Journal of Sound and Vibration* **259**(1) (2003), pp. 97 – 118.

126. Nemani Lakshmi, Vibration analysis of a hand-grinder system under wheel unbalance excitation, M.S Thesis, Concordia University, Montreal, Canada, 2005.

127. Dong R. G., Welcome D. E, McDowell T. W. and Wu J. Z., Measurement of biodynamic response of human hand-arm system. *Journal of Sound and Vibration* **294** (2006), pp. 807 – 827.

128. Dong R. G. Dong J. H., Wu J. Z. and Rakheja S., Modeling of biodynamic responses distributed at the fingers and the palm of the human hand-arm system. *Journal of Biomechanics* **40** (2007), pp 1335 – 2340.

129. Nalecz A. G. and Wicher J., Design sensitivity analysis of mechanical systems in frequency domain. *Journal of Sound and Vibration* **120** (1988), pp. 517 – 526.

130. Devriendt C. and Guillaume P., Identification of modal parameters from measurements, *Journal of Sound and Vibration* (2008). doi:10.1016/j.jsv.2007.12.022.

131. Thomson W. T and Dahleh M. D., Theory of vibration with applications 5th edition, Prentice Hall International Inc. NJ, USA, 1997, Chp 3. pp. 49-65.

132. Ogata K., *Systems Dynamics* 3rd edition, Prentice Hall International Inc. NJ, USA, 1998, Chap. 4, pp. 156-159

133. Dong J. H. Dong R. G., Rakheja S., Welcome D. E., McDowell T. W. and Wu J. Z., A method for analyzing absorbed power distribution in the hand and arm substructures when operating vibration tools, *Journal of Sound and Vibration* **311** (2007), pp 1286 – 1304.

134. Dong R. G., Wu J. Z., Welcome D. E., and McDowell T. W., A discussion on comparing alternative vibration measures with frequency-weighted accelerations defined in ISO standards, *Journal of Sound and Vibration* **317** (2008), pp 1042 – 1050.

135. Mansfield N. J and Griffin M. J., Effect of magnitude of vertical whole-body vibration on absorbed power for the seated human body, *Journal of Sound and Vibration* **215** (1998), pp. 813 – 825.

136. Marcotte P., Comments on "A discussion on comparing alternative measures with frequency –weighted accelerations defined in ISO Standards" [R. G. Dong, J. Z. Wu D. E. Welcome, T. W. McDowell, JSV], *Journal of Sound and Vibration* **317** (2008), pp 1051 – 1056.

137. Marcotte P., Oddo R., Boutin J., Boilley R.,Nélisse H., Boileau, P-E., Drouin P., Sirard C. and Daigle R., Industrie de la réparation automobile Caractérisation du bruit et des vibrations émis par les outils portatifs, http://www.irsst.qc.ca/files/documents/PubIRSST/R-554.pdf

138. Burstrom L., Lundstrom R., Hagberg M., Nilsson T., Comparison of different measures for hand-arm vibration exposure, *Safety Science* **28**(1) (1998), pp. 3- 14.

139. INTERNATIONAL STARNDARD ORGANIZATION, ISO 8662-2, Hand-held portable power tools – measurements of vibrations at the handle – part 2: chipping hammers and riveting hammers, 1992.